THE UNIVERSITY OF MICHIGAN

INDUSTRY PROGRAM OF THE COLLEGE OF ENGINEERING

HEAT TRANSFER AND PRESSURE DROP OF AIR IN FORCED CONVECTION ACROSS TRIANGULAR PITCH BANKS OF FINNED TUBES

by

Dennis J. Ward

A dissertation submitted in partial fulfillment
of the requirements for the degree of
Doctor of Philosophy in the
University of Michigan
1958

January, 1958

IP-261

Doctoral Committee:

Associate Professor Edwin H. Young, Chairman
Professor Donald L. Katz
Professor Frank L. Schwartz
Professor J. Louis York
Assistant Professor Charles M. Thatcher

ACKNOWLEDGMENTS

The author wishes to express his gratitude to a number of individuals for their assistance and advice during the course of this study. In particular he wishes to acknowledge the encouragement and advice given by Professor Edwin H. Young during the entire course of his graduate career. The advice of Professors D. L. Katz, F. L. Schwartz, J. L. York and C. M. Thatcher is also appreciated.

The shop personnel, especially Messrs. Cleatis Bolen, William Hines and George Foster were most helpful in the fabrication of the tube banks and other equipment.

The author is indebted to the Wolverine Tube Division of Calumet and Hecla, Inc. for the tubes and generous financial support which made this work possible.

TABLE OF CONTENTS

		Page
ACKNOWLEDGMENTS		iii
LIST OF TABLES		vii
LIST OF FIGURES		ix
NOMENCLATURE		xv
SUMMARY		xvii
I.	INTRODUCTION	1
II.	LITERATURE REVIEW	7
	A. Fin Efficiency	7
	B. Performance Data for Finned Tube Banks	9
	C. Local Rates of Heat Transfer to Finned Surfaces	15
	D. Heat Transfer Correlations	23
	E. Pressure Drop Correlations	24
III.	EXPERIMENTAL EQUIPMENT	27
	A. Wind Tunnel and Auxiliary Equipment	27
	B. Tube Banks	31
	C. Steam Side Equipment	43
	D. Instrumentation and Measuring Device	46
	E. Modification Employed to Obtain Row-To-Row Performance Data	51
	F. Modification Employed to Obtain Steam Film Condensing Coefficients	54
	G. Modifications Employed for Turbulence Measurements	54
IV.	EXPERIMENTAL PROCEDURE AND DATA	55
	A. Experimental Procedure and Data for the Performance Characteristics of Tube Banks	55
	B. Steam Condensing Coefficients	73
	C. Performance of Individual Rows of Tubes	78
	D. Flow Conditions of Air Approaching the Tube Banks	82

TABLE OF CONTENTS CONT'D

Page

V. QUALITATIVE PREDICTION OF THE RELATIVE IMPORTANCE OF VARIOUS DIMENSIONS 87

A. Effect of Number of Tube Rows on Heat Transfer Performance of Finned Tube Banks 87
B. Effect of Geometry on the Mechanisms of Heat Transfer 94

VI. CORRELATIONS OF EXPERIMENTAL HEAT TRANSFER DATA 127

A. Dimensional Analysis 127
B. Heat Transfer Correlations 133

VII. ANALYSIS OF PRESSURE DROP DATA 146

VIII. CONCLUSIONS 165

IX. RECOMMENDATIONS FOR FUTURE WORK 167

APPENDIX A 169

EXAMPLE CALCULATIONS 169

A. Example Calculations of the Mean Air Film Coefficient of a Finned Tube Bank 169
B. Example Calculation of Steam Condensing Coefficient 173

APPENDIX B 175

DERIVATION OF THE FIN METAL RESISTANCE OF A FINNED TUBE 175

A. Derivation of the True Fin Resistance of a Finned Tube 175
B. Derivation of a Useful Pseudo Fin Resistance 177

APPENDIX C 179

MEASUREMENT OF DEGREE OF TURBULENCE 179

A. Theory 179
B. Apparatus 185
C. Experimental Data 185
D. Analysis of Data 188

TABLE OF CONTENTS CONT'D

	Page
APPENDIX D	189
A. Heat Duty	189
B. Design Conditions	189
C. Trial Number 1	190
1. Air Film Resistance	192
2. Outside Fouling Resistance	193
3. Fin Resistance Using Equation 24	193
4. Aluminum Metal Resistance	193
5. Bond Resistance	195
6. Admiralty Metal Resistance	195
7. Inside Fouling Resistance	196
8. Inside Water Coefficient	196
D. Pressure Drop and Fan Horsepower Requirements	197
APPENDIX E	199
DERIVATION OF AN EQUATION TO PREDICT POINT CONDENSING COEFFICIENTS USING THEORY OF NUSSELT	199
REFERENCES	201

LIST OF TABLES

Table		Page
I.	Dimensions of Tube Banks Investigated.....	32
II.	Diameter of Tube Ends and Tube Sheet Drill Sizes.....	38
III.	Dimensions of Tubes Investigated.....	41
IV.	Data Obtained for Run 709.....	58
V.	Effect of Humidity on the Physical Properties of Dry Air.....	60
VI.	Comparison of Calculated Results From Three Different Outlet Air Temperature Measuring Techniques.....	63
VII.	Variation of Fin Resistance With Air Film Heat Transfer Coefficient for the Tubes Used in Unit Number Seven.....	67
VIII.	Original and Processed Data for Unit Number 1..	68
IX.	Original and Processed Data for Unit Number 2..	69
X.	Original and Processed Data for Unit Number 3..	70
XI.	Original and Processed Data for Unit Number 4..	70
XII.	Original and Processed Data for Unit Number 5..	70
XIII.	Original and Processed Data for Unit Number 6..	71
XIV.	Original and Processed Data for Unit Number 7..	71
XV.	Original and Processed Data for Unit Number 8..	71
XVI.	Original and Processed Data Obtained on Steam Condensing Coefficients.....	76
XVII.	Original and Processed Data Obtained on Individual Rows of Tubes (Unit Number 8).....	79

LIST OF TABLES CONT'D

Table		Page
XVIII.	Original and Processed Data Obtained on Velocity Distribution of the Air at Entrance Section.	83
XIX.	Corrections Used to Convert Heat Transfer Data to Six Row Deep Bank.....	94
XX.	Dimensions of Tube Banks Investigated by Jameson(4).....	97
XXI.	Range of Reynolds Number Investigated Based on Fin Diameter.....	123
XXII.	Results of Least-Mean-Square-Fit of Experimental Data.....	132
XXIII.	Range of Variables Investigated.....	136
XXIV.	Summary of Experimental Data for Turbulence Measuring Sphere.....	186

LIST OF FIGURES

Figure		Page
1	Schematic Illustration of a Helically Finned Tube	2
2	Efficiency of a Straight Annular Fin, After Gardner[7]	10
3	Heat Transfer Curve of Jameson[4], 5/8 inch Root Diameter Tube	12
4	Heat Transfer Curve of Jameson[4], 3/4 inch Root Diameter Tube	13
5	Heat Transfer Curve of Jameson[4], 1 inch Root Diameter Tube	14
6	Heat Transfer Curve of London, Kays, and Johnson[15]	16
7	Heat Transfer Curves from Ref. 7, Units 5 and 6	17
8	Heat Transfer Curves from Ref. 7, Units 3, 4 and 10	18
9	Heat Transfer Curves of T. E. Schmidt[2]	19
10	Pressure Drop Results of T. E. Schmidt[2]	20
11	Variation in Heat Transfer Coefficient With Distance From Tip for a Longitudinal Fin, After Ghai	22
12	Finned Tube Pressure Drop Correlation of Katz, et al	26
13	Overall View of Wind Tunnel With Tube Bank Installed	28
14	Frontal View of Entrance Section	29
15	Side View of Entrance Section	29

LIST OF FIGURES CONT'D

Figure		Page
16	Blower, Motor and Speed Control System.....	31
17	Frontal View of the Eight Tube Banks Investigated. Units 1 and 2.....	33
18	Frontal View of the Eight Tube Banks Investigated. Units 3 and 4.....	34
19	Frontal View of the Eight Tube Banks Investigated. Units 5 and 6.....	35
20	Frontal View of the Eight Tube Banks Investigated. Units 7 and 8.....	36
21	Tube Sheet Layout of Unit Number 8.....	39
22	Top View of Unit Number 3.....	40
23	Comparison of the Tubes Used in the Investigation	42
24	Rear View of Unit Number 6.....	43
25	Flow Diagram of Stream.....	44
26	Micro-manometer Used in Investigation.....	48
27	Vane-type Anemometer Used in Investigation.....	49
28	Calibration Correction of Anemometer (supplied by the Taylor Instrument Company).....	50
29	Modification of Steam Supply Used in Determining the Row to Row Performance.....	53
30	Temperature Profile of Exit Air for Run Number 407.....	62
31	Sum of Steam and Metal Resistances of Tubes Used in Unit Number Seven versus Heat Duty.....	66
32	Heat Transfer Curves Obtained For the Seven Finned Tube Banks.....	72

LIST OF FIGURES CONT'D

Figure		Page
33	Summary of Heat Transfer Data of Plain Tube Bank.....	74
34	Comparison of Plain Tube Heat Transfer Results With Results on Geometrically Similar Units Available in the Literature.....	75
35	Summary of Steam Condensing Coefficient Data....	77
36	Heat Transfer Curves Obtained for the Individual Rows of Unit Number 8.....	80
37	Comparison of Individual Row Heat Transfer Data with Data Appearing in the Literature.....	81
38	Velocity Distribution of Air at Entrance Section V_{avg} of 2270 ft. per min.....	85
39	Velocity Distribution of Air at Entrance Section V_{avg} of 1060 ft. per min.....	86
40	Effect of Turbulence Level on Heat Transfer From a Single Cylinder to Air at Re = 5800.(Ref. 28).	90
41	Effect of Number of Rows on Mean Heat Transfer Coefficient.....	93
42	Type of Fin Studied by Ghai[18] and Wagener[36].	99
43	Effect of Fin Spacing for Longitudinal Fins After Wagener[36].....	100
44	Comparison of Heat Transfer Data for Units Number Six and Seven.....	102
45	Comparison of Data of T. E. Schmidt with Heat Transfer Curves for Units 6 and 7.....	104
46	Data for Unit Number 2 Showing Possible Transition Due to Boundary Layer Interference.....	106
47	Schematic Illustration of Velocity Profiles Over a Fin Surface.....	108

LIST OF FIGURES CONT'D

Figure		Page
48	Radial Variation in Heat Transfer Coefficients After Weiner et al.....	110
49	Local Heat Transfer Coefficients Over a Fin Surface After Weiner et al.....	112
50	Temperature Differences in the Wake of a Heated Cylinder With an Air Velocity of 420 feet per minute after Billman(35).....	115
51	Temperature Differences in the Wake of a Heated Cylinder With an Air Velocity of 760 feet per minute after Billman(35).....	116
52	Schematic Illustration of Streamlines of the Air in Flow Through a Finned Tube Bank.....	118
53	Laminar and Turbulent Boundary Layers on a Flat Plate.....	121
54	Local Heat Transfer Coefficients on a Flat Plate for Various Boundary Layer Zones.....	121
55	Experimental Heat Transfer Coefficients for the Seven Finned Tube Banks. Data for Units 6, 7 and 8 Corrected to Six Rows of Tubes.....	129
56	Comparison of Finned Tube Heat Transfer Data With Least Mean Square Fit Curve.....	134
57	Comparison of Data Appearing in the Literature with Least Mean Square Fit Curve.....	135
58	Comparison of Data With Empirical Dimensional Correlation.....	138
59	Comparison of Data From the Literature With Emperical-Dimensional Correlation.....	139
60	Comparison of Data With Emperical Dimensionless Correlation.....	140
61	Comparison of Data From the Literature With Emperical-Dimensionless Correlation.....	141

LIST OF FIGURES CONT'D

Figure		Page
62	Comparison of Data With Correlation of T. E. Schmidt.....	143
63	Comparison of Data With Dimensionless Correlation of Katz, et al.....	144
64	Comparison of Data With Dimensional Correlation of Katz, et al.....	145
65	Pressure Drop Data of Unit Number 1.....	150
66	Pressure Drop Data of Unit Number 2.....	151
67	Pressure Drop Data of Unit Number 3.....	152
68	Pressure Drop Data of Unit Number 4.....	153
69	Pressure Drop Data of Unit Number 5.....	154
70	Pressure Drop Data of Unit Number 6.....	155
71	Pressure Drop Data of Unit Number 7.....	156
72	Pressure Drop Data of Unit Number 8.....	157
73	Comparison of Pressure Drop Data With Gunter-Shaw Correlation for Air at 100°F.....	159
74	Comparison of Pressure Drop Data With Gunter-Shaw Correlation.....	160
75	Original Data Used for Correlation by Gunter and Shaw Indicating Possible Lowering of Mean Curve.....	161
76	Comparison of Pressure Drop Data With Correlation of Jameson(4)	162
77	Comparison of Pressure Drop Data With Dimensionless Correlation of Katz, et al.(7)	163
78	Comparison of Pressure Drop Data With Dimensional Correlation of Katz, et al.(7)	164

LIST OF FIGURES CONT'D

Figure		Page
79	Drag Coefficient of Spheres as a Function of Reynolds Number.....	180
80	Per Cent Turbulence Versus Critical Reynolds Number for a 5 inch sphere.....	182
81	Details of Turbulence Measuring Sphere.....	183
82	Experimental Pressure Ratios Versus Reynolds Number.....	185
83	Typical Curves for Pressure Measuring Spheres for Three Turbulence Levels.....	187

NOMENCLATURE

A - total heat transfer area, ft^2

A_i - inside heat transfer area per foot of length, $ft^2/ft.$

A_m - metal area transverse to direction of heat flow, ft^2

A_o - finside heat transfer area per foot of length, ft^2/ft

c_p - heat capacity of fluid, Btu/lb-°F

D_e - equivalent diameter of a tube defined by the particular equation, ft.

D_o - outside diameter of tube, feet

D_r - root diameter of tube, feet

D_{vh} - volumetric hydralic diameter of a tube, $\frac{4(\text{free volume})}{\text{external heat transfer area}}$, feet

D_{wh} - wetted perimeter hydraulic diameter, $\frac{A_o}{\pi\,[1 + N(D_o - D_r)\,]}$, feet

d_o - outside diamter of tube, inches

d_r - root diameter of tube, inches

f - friction factor

G_m - mass air flow rate through minimum cross sectional spacing, lb/sq.ft.-hr.

g_c - conversion factor 4.17×10^8 $ft/(hr)^2$.

H - fin height, $\frac{d_o - d_r}{2}$, inches

H' - Humidity of air, lbs/lb of dry air

h - outside heat transfer coefficient, $= \frac{1}{\frac{1}{h_o} + r_o}$, Btu/hr-°F-sq.ft. (exterior surface)

h_i - mean inside heat transfer coefficient, Btu/hr-°F-sq.ft.

$(h_i)_p$ - inside heat transfer coefficient at a particular point, Btu/hr-°F-sq.ft.

h_o - mean outside air film coefficient for a finned tube bank, Btu/hr-sq.ft. (external area)

$(h_o)_i$ - average air film heat transfer coefficient of row i, Btu/hr-°F-sq.ft.

$(h_o)_{mi}$ - average air film heat transfer coefficient of a tube bank containing i rows of heated tubes, Btu/hr-°F-sq.ft.

h_p - mean outside air film coefficient for a plain tube bank, Btu/hr-sq.ft. (external area).

k - thermal conductivity of fluid, Btu/hr-°F-ft.

k_M - thermal conductivity of metal Btu/hr-°F-ft.

L - length of exchanger in direction of flow, ft equals n s_L or for the tube banks studied here equals 0.866 n S_ℓ.

L' - length of condensing path, ft.

N - number of fins per linear inch, fins/inch

n - number of rows in the tube bank

P_r - Prandtl number, dimensionless

Q - heat duty, Btu/hr

Q_a - rate of energy transfer to the air, Btu/hr.

Q_s - rate of energy released by steam, Btu/hr.

Re - Reynolds number, dimensionless

r_f - Psuedo fin resistance, hr-°F-sq.ft./Btu.

r_f' - fin resistance, hr-°F-sq.ft/Btu

r_m - metal wall resistance to heat transfer, hr-°F-sq.ft/Btu.

r_o - outside fouling resistance to heat transfer, hr-°F-sq.ft./Btu.

S - Tube pitch for equalateral spacings, feet.

S_A - average tube pitch, $= \frac{S_L - S_t}{2}$, feet

S_a - average tube pitch, $= \frac{S_l - S_t}{2}$, feet.

S_f - spacing between adjacent spaces of fins, equals $(\frac{1}{N} - Y)$, inches

S_L - longitudinal pitch between adjacent rows of tubes, feet

S_l - longitudinal pitch between adjacent tubes in different rows measured on the diagonal, feet.

S_t - transverse pitch between adjacent tubes in the same row, feet

t_m - outside metal temperature at a point, °F.

t_{mf} - mean outside fin metal temperature, °F.

t_{mr} - mean outside root metal temperature, °F.

t_{om} - mean outside metal temperature, °F.

t_{ps} - mixed mean bulk stream temperature, °F.

t_{ss} - temperature of saturated steam at condensing pressure, °F

V_{max} - maximum air velocity in the tube bank occuring at minimum cross section for air = 0.074, ft/min.

x - linear dimension on section under consideration, feet

Y - mean fin thickness, feet

ΔP - pressure drop of air in flowing across a tube bank, lb/sq.ft.

Δp - pressure drop of air in flowing across a tube bank, inches of water.

μ - viscosity of fluid at bulk stream temperature, lb/ft-hr.

μ_w - viscosity of fluid at the temperature of the wall, lb/ft-hr.

ρ - density of fluid, lb/cu.ft.

φ - fin efficiency, dimensionless

φ' - functional relationship

SUMMARY

A review of the literature on the heat transfer and pressure drop characteristics of banks of finned tubes with air in crossflow indicates that there exists but a meager amount of reliable data. There also exists a general lack of agreement between the investigators as to the effect of some of the variables on finned tube bank heat transfer and pressure drop characteristics.

The heat transfer and pressure drop characteristics of seven triangular pitch finned tube banks and one triangular pitch plain tube bank were investigated. Experimental pressure drop and heat transfer data were obtained for air flowing under forced convection in crossflow outside of the tubes. The air was heated by condensing low pressure steam inside of the vertical tubes. With one tube bank, individual rows of tubes were heated to obtain the relative performance of various rows. The turbulence level and velocity profile of the air approaching the tube banks was also studied.

It was observed that the heat transfer and pressure drop characteristics of the tube banks varied due to the difference in geometry between the banks. Studies of the local variation in heat transfer and fluid flow as reported in the literature indicated that the air film heat transfer coefficient should be expected to be independent of the tube spacing and the spacing of adjacent fins. These studies indicated that the important dimensional characteristics should be the root diameter of the tube, the thickness of the fin, and the diameter over the fin. The importance of these dimensions was predicted

to occur in the order given above.

A dimensional analysis of the systems investigated indicated that the heat transfer coefficient should be a function of the following variables:

$$h_o = \varphi' (c_p, \mu, k, V_m, \rho, D_r, D_o, S_f, Y)$$

The variables were arranged in dimensionless groups and the correlating relationship was assumed to be of the following form:

$$Nu = A\, Re^b \left(\frac{D_o}{D_r}\right)^d \left(\frac{D_o}{S_f}\right)^e \left(\frac{S_f}{Y}\right)^f$$

A least-mean-square-fit of the data for the finned tube banks was made using the IBM 650 regression analysis program available at the University of Michigan Statistical Research Laboratory. This program was designed to give the best statistical values of the exponents and automatically rejected any of the dimensionless groups which had confidence limits below 97.5 per cent. The results calculated by the computer were reduced to :

$$Nu = 0.364\, Re^{0.68} \left(\frac{D_o}{D_r}\right)^{0.45} \left(\frac{Y}{D_o}\right)^{0.3} Pr^{1/3}$$

This relationship indicates the relative order of importance of the dimensions as predicted from the study of the technical literature.

A comparison of the experimental data collected and the relationship obtained from the dimensional analysis indicated an average deviation of $\pm$ 7 per cent from the correlating line. A comparison of the experimental data with relationships recommended in the literature indicates that the data is not well correlated by any of the published correlations.

It was determined that the heat transfer coefficient of a bank of finned tubes is dependent on the number of rows of tubes in the direction of flow. This effect was found to be due to a difference between the performance of the first and the succeeding rows of tubes. The performance of the first row is dependent on the conditions of the air approaching the tube banks. Measurements of the degree of turbulence approaching the tube banks indicated that the turbulence level was below 2 per cent. The velocity profile was found to be constant within 1.5 per cent.

The pressure drop of the air flowing through the finned and plain tube banks were compared with correlations recommended in the literature. The general correlation recommended is:

$$\frac{f}{2} = 0.81\ Re^{-0.145} = \frac{\Delta P g_c\ Dvh\ \rho}{G_M^2 L}\left(\frac{\mu}{\mu_w}\right)^{0.14}\left(\frac{S_t}{S_\ell}\right)^{0.6}\left(\frac{S_t}{D_{vh}}\right)^{0.4}$$

This relationship is a modification of the correlation of Gunter and Shaw which was obtained from a study of the pressure drop characteristics of plain tube banks. Other pressure drop correlations available in the literature were not found to be as satisfactory as that of Gunter and Shaw.

I. INTRODUCTION

A particular type of tubing, especially designed for heat transfer applications, has been playing an increasingly important role in industrial heat exchange equipment in recent years. These tubes, known as "helically finned tubes", have been used in a number of types of heat exchangers, such as; shell and tube exchangers, double pipe exchangers, immersed coil exchangers, air blast units, and others. In these units a fluid, which is to be heated or cooled, flows outside the tube and is called the finside fluid. The other fluid, flowing inside of the tube, either supplies or receives the energy being transferred, and is called the tubeside fluid. In many of the applications all or part of the flow is transverse to the axis of the tubes[1]. Consequently, it is important to the designer to be able to predict the heat transfer and pressure drop performance of finned tubing with fluids in pure crossflow. Figure 1 illustrates a typical helically finned tube of the type used in this investigation.

In contrast to the simple geometrical configuration on the inside of the tubes, where the heat transfer resistance and frictional loses can be predicted with a relatively high degree of precision, the geometry on the finside of a rectangular finned tube bundle are quite complex. In the past one has had to rely on: (1) one of the empirical relationships available in the literature[2,3]; (2) the meager amount of data for specific tubes appearing in the literature[2,4,5,6,7]; or (3) private, unpublished data.

There are some difficulties associated with much of the fin tube bank data appearing in the literature which raises serious

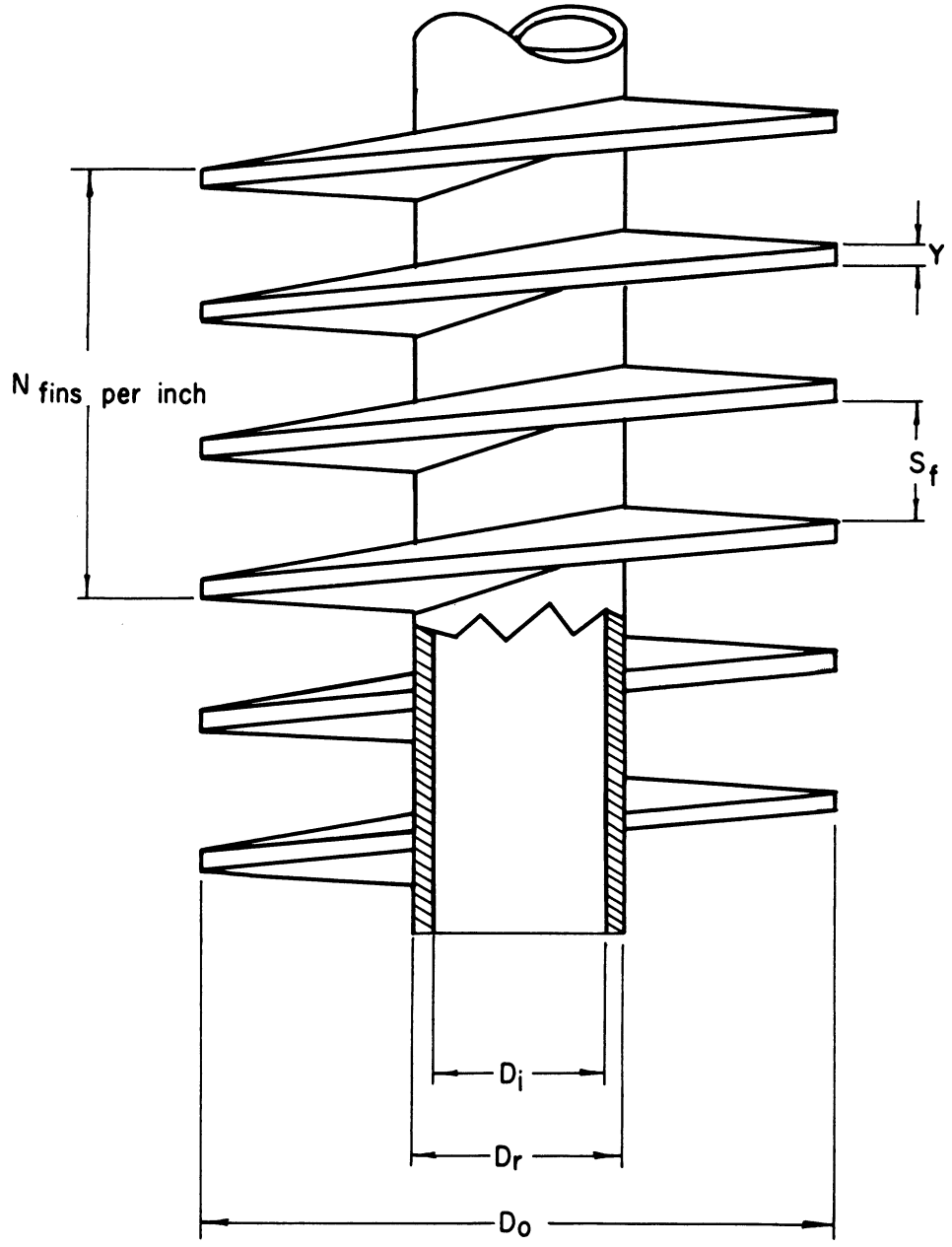

Figure 1. Schematic Illustration of a Helically Finned Tube.

question as to their validity. In some cases there were an insufficient number of rows of tubes to establish good mean heat transfer coefficients.[5] In other cases there existed an additional resistance to heat transfer not taken into account due to incomplete bonds in the metallic surfaces of bi-metallic tubes (2,4,6,7). These difficulties will be discussed in the order given above.

The mean air film coefficient on the fin side of a bank of finned tubes is a function of the number of rows deep in the bank. The dependence of the mean coefficient on the number of rows deep is primarily due to the relatively low performance of the first row of tubes. Since this row is the one primarily affected by the free stream conditions of the air approaching the tube bank, it would be expected that the effect of the number of rows on the mean air film coefficient would depend upon such entering air conditions as, velocity profile and free stream turbulence. Therefore, in order to compare tube banks containing a different number of rows, it is necessary to know the relative heat transfer performance of the first row tested, as compared to subsequent rows or, to have a sufficient number or rows deep in the bank to make the mean heat transfer performance insensitive to the performance of the first row. The latter situation requires tube banks having three or more rows deep in order to compare the heat transfer performance when the inlet conditions are not completely specified.

A second difficulty encountered in comparing finned tube bank heat transfer coefficients reported in the literature is that of a bond resistance encountered in bimetallic tubes. This resistance is primarily due to the methods of duplex tube construction. The three

primary methods of producing finned tubing at the present time consist of; (1) wrapping the fins on the exterior of a plain tube, (2) wrapping of the fins on the plain tube followed by a soldering process to bond the fins to the tube and (3) a mechanical method of extruding the fins from the outer surface of a tube, forming fins which are an integral part of the root metal of the tube.

The difficulties occurring with the wrapped-on finned tubes stem from two sources. The contact area between the fin and the tube can be incompletely filled with the solder causing a partial gap between the two surfaces and consequently an extra heat transfer resistance which is generally not taken into account in the calculation of the air film coefficient from overall heat transfer coefficient data. The second source of difficulty arises in the fact that the fins sometimes tend to vibrate loose from the root metal of the tube. For these reasons, the conditions of the tubes of this type before and subsequent to the investigation should be specified.

The difficulties with the extruded fin tube lie primarily in that for reasons of corrosion or erosion resistance on the inside of the tube, an inner liner of a different metal is sometimes placed inside the finned tube. The bond between the liner tube and the finned tube is purely mechanical and difficulties could be encountered with this bond.

Due to the relatively large ratio of external to internal surface areas of finned tubes, a relatively small bond resistance can appreciably affect the overall heat transfer resistance of the tube. Consequently, the heat transfer results of investigations employing either of these tubes should be viewed with caution unless the contact resistance

in the tube is known.

All of the tubes used in the tube banks reported in the literature have ratios of outside to root diameter values between 1.75 and 2.4, with over 90% of the data having d_o/d_r values between 1.9 and 2.25. This indicates that, except for a difference in fin spacing, the data generally available for design or evaluation purposes is on essentially geometrically similar tubing. The existing heat transfer correlations for banks of finned tubes are based on either some or all of this data.

In view of the paucity of data on the heating of air in crossflow through finned tube banks it was proposed to carry out an experimental investigation of the heat transfer and pressure drop characteristics of finned tube banks containing finned tubes having a wider range of dimensional characteristics than previously studied. This was to be accomplished by heating air flowing in crossflow through the tube bank and condensing steam inside of the tubes. It was felt that with this data, not only could the present correlations be tested for different tube configurations, but possibly some insight as to the effects of the geometry of the tube on the performance characteristics of the tube bank and possibly new correlations of a more general nature might result. It was proposed to eliminate any possible bond resistance in the tube by employing integrally finned-monometallic tubes and to study the effect of the number of rows deep on the mean heat transfer coefficient.

A total of eight tube banks, seven containing finned tubes, one containing plain, were used in this work. Each tube bank contained a number of identical tubes on an equilateral triangular pitch. The finned tubes had root diameters which varied between 0.438 and 1.147

inches, D_o/D_r ratios which varied between 1.18 and 2.04, and fins per inch which varied from 5.13 to 19.5. The tube pitch used for all tube banks equaled the nominal fin diameter of the tube plus a 3/16 inch clearance. The air velocity generally ranged from about 300 feet per minute to about 2000 feet per minute. The upper limit of the velocity was dictated by the capacity of the motor used.

II. LITERATURE REVIEW

The literature concerning finned tubing can be divided into five areas, namely; (1) fin efficiency, (2) performance data of finned tube banks, (3) local heat transfer coefficients for finned surfaces, (4) heat transfer correlations, and (5) pressure drop correlations. The above five types of investigations will be reviewed in the order indicated.

A. Fin Efficiency

For a plain cylindrical tube exchanging heat to a fluid flowing outside of the tube, the rate of heat transfer is considered proportional to the temperature difference between the fluid and metal wall, the area of contact between the fluid and the metal wall, and inversely proportional to the resistances to heat transfer between the wall and the ambient fluid. This can be expressed algebraically as:

$$q = \left[\frac{1}{\frac{1}{h_o} + r_o}\right] A_o \, (t_{bs} - t_{om}) \qquad (1)$$

If fins, such as those used in this investigation, are formed on the outside surface of the tube, it might be expected, for a first approximation, that the rate of heat transfer would increase in proportion to the increase in surface between the fluid and metal interface. However, upon closer examination of the problem, it is realized that not only can the exterior resistance to heat transfer change (due to the change in the geometry of the tubes) but also there is a decrease in the average temperature difference driving force between the ambient

fluid temperature and the skin temperature of the metal surface. This decrease in temperature difference is due to a temperature gradient which must be maintained in the fin metal. The temperature gradient for a two dimensional system is given by the basic Fourier equation

$$q = -k_m A_m \frac{dT}{dx} \qquad (2)$$

In order to solve this differential equation it is necessary to relate the rate of heat transfer and mean metal area to the position "x".

The integrated solution to equation two is generally obtained in terms of a fin efficiency which is defined as:

$$\varphi = \frac{\int_0^{A_f} h(t_{bs} - t_m)\, dA}{h_{mean} A_f (t_{bs} - t_{mr})} \qquad (3)$$

However, in the solution of equation two it is generally assumed that the outside heat transfer resistance is constant, so that equation 3 reduces to:

$$\varphi = \frac{t_{bs} - t_{mf}}{t_{bs} - t_{mr}} \qquad (4)$$

where the term "t_{mf}" denotes the integrated mean fin temperature.

A number of papers have been presented relating the fin efficiency to the geometry of the tube and the heat transfer conditions outside of the fin[8-14]. The most definitive work to date was presented in a paper by Gardner which both summarizes previous work in this field and gives the solution for many fin shapes of practical

interest[14]. The fin efficiency for a circular fin of constant thickness as obtained by Gardner is reproduced in Figure 2.

Kayan[15] studied the efficiency of a particular fin by use of an electrical resistance model for the purpose of studying the validity of some of the assumptions made by Gardner in his derivation. He concluded that the assumptions were essentially valid for the shapes tested.

Dusinberre has recently given a simple, approximate relationship for Gardner's fin efficiency curves, valid down to fin efficiencies of 75%[16].

The use of the fin efficiency is illustrated in a recent article by Young and Ward[17] and will be further discussed in the analysis of the data.

B. Performance Data For Finned Tube Banks

All of the data appearing in the literature on the heat transfer and pressure drop performance of finned tube banks involve the heating or cooling of air flowing in crossflow outside of the tubes. The heating medium used inside the tubes was commonly steam, but occasionally hot water was used, whereas the cooling medium always involved cold water flowing in the tubes.

The first data appearing in the literature on the heat transfer and pressure drop of air flowing through finned tube banks was presented by Katz, Beatty and Foust[13]. The two tube banks studied contained integrally finned, helical finned tubes. Steam was condensed inside the tubes to heat the air which flowed over the tubes from a blower placed upstream of the tube bank. One of the tube banks studied

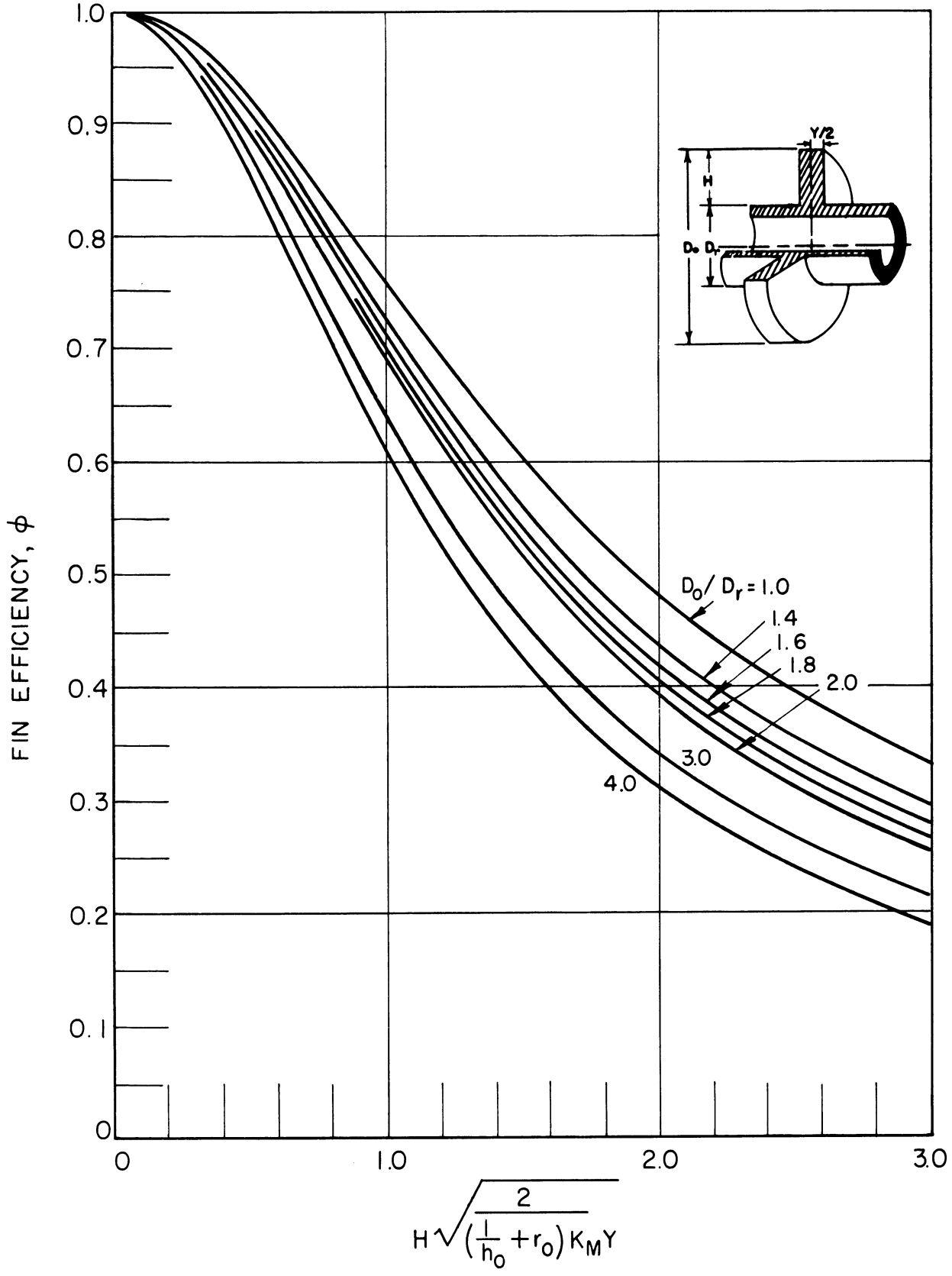

Figure 2. Efficiency of a Straight Annular Fin, After Gardner[7].

contained only a single row of tubes, while the second contained two rows of tubing. As will be subsequently shown, it is difficult to compare tube banks containing less than three rows of tubing. Consequently, this data is of limited value in preparing heat transfer correlations.

At the same time that the above article appeared, Jameson[4] presented the results of an investigation of the heat transfer and pressure drop performance of a number of triangular pitch finned tubes. The finned tubes used in this investigation consisted of fins wrapped around and soldered to the exterior surface of circular tubes. As indicated earlier, this method of fabrication of the finned tubing raises the question of a possible bond resistance to heat transfer in the tube.

Jameson's study was primarily concerned with the effect of the tube spacing in finned tube banks. He also included the effects of number of rows on heat transfer and two different fin spacings. His primary conclusions were that the effect of tube spacing on heat transfer are small, within the range of his investigation. There did exist a measurable effect of tube spacing on the pressure drop across finned tube banks.

Jameson's heat transfer curves are presented in Figures 3, 4, and 5.

London, Kays and Johnson[6] published the results of an investigation of four different finned tube banks. Three of the tube banks were made up from bimetallic finned tubes which were subsequently found to have relatively high bond resistance values. The results on these tubes will not be considered here. The fourth tube bank was made from monometallic integrally finned tubes. The heat transfer performance of

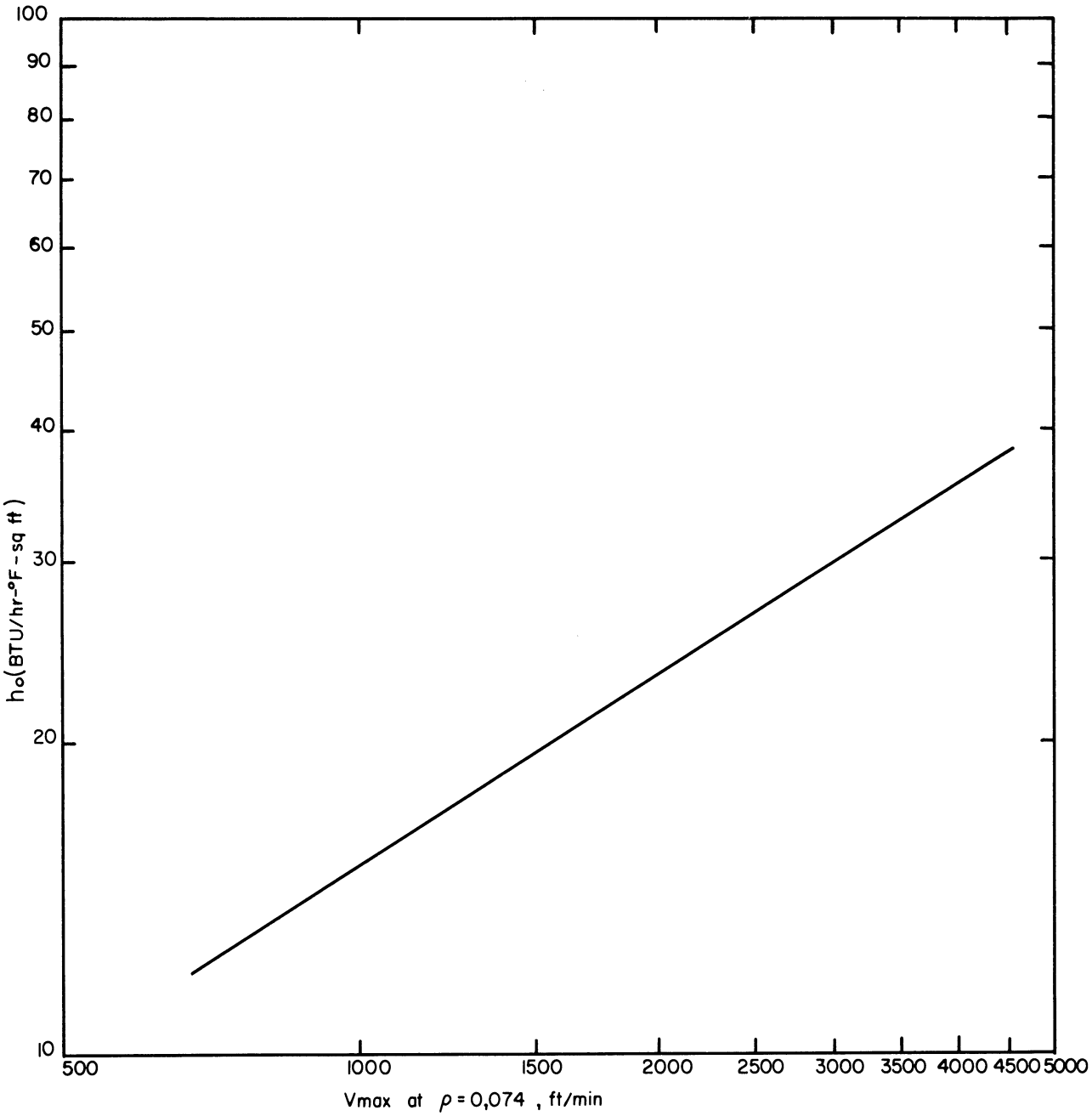

Figure 3. Heat Transfer Curve of Jameson[4], 5/8 inch Root Diameter Tube.

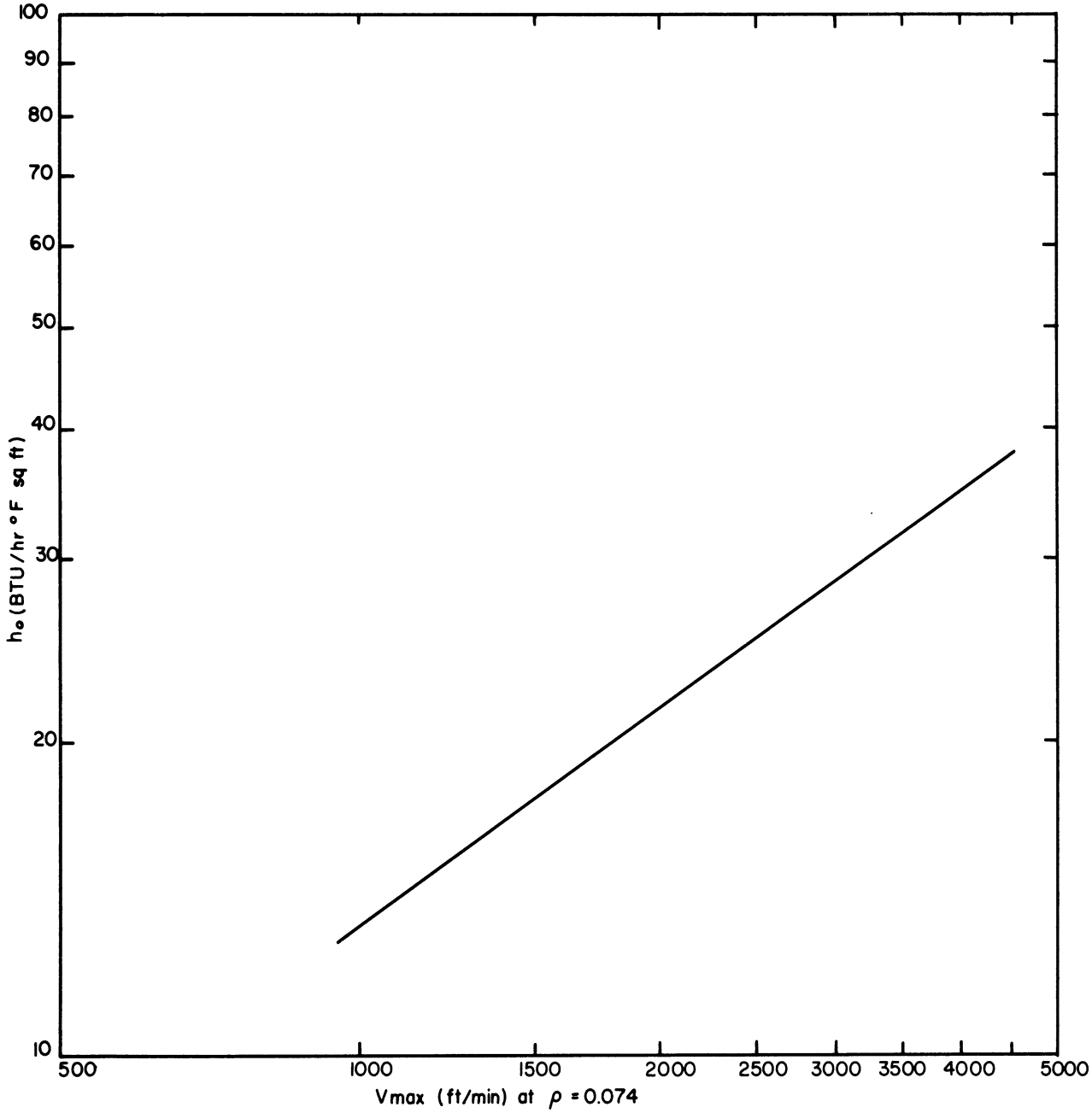

Figure 4. Heat Transfer Curve of Jameson[4], 3/4 inch Root Diameter Tube.

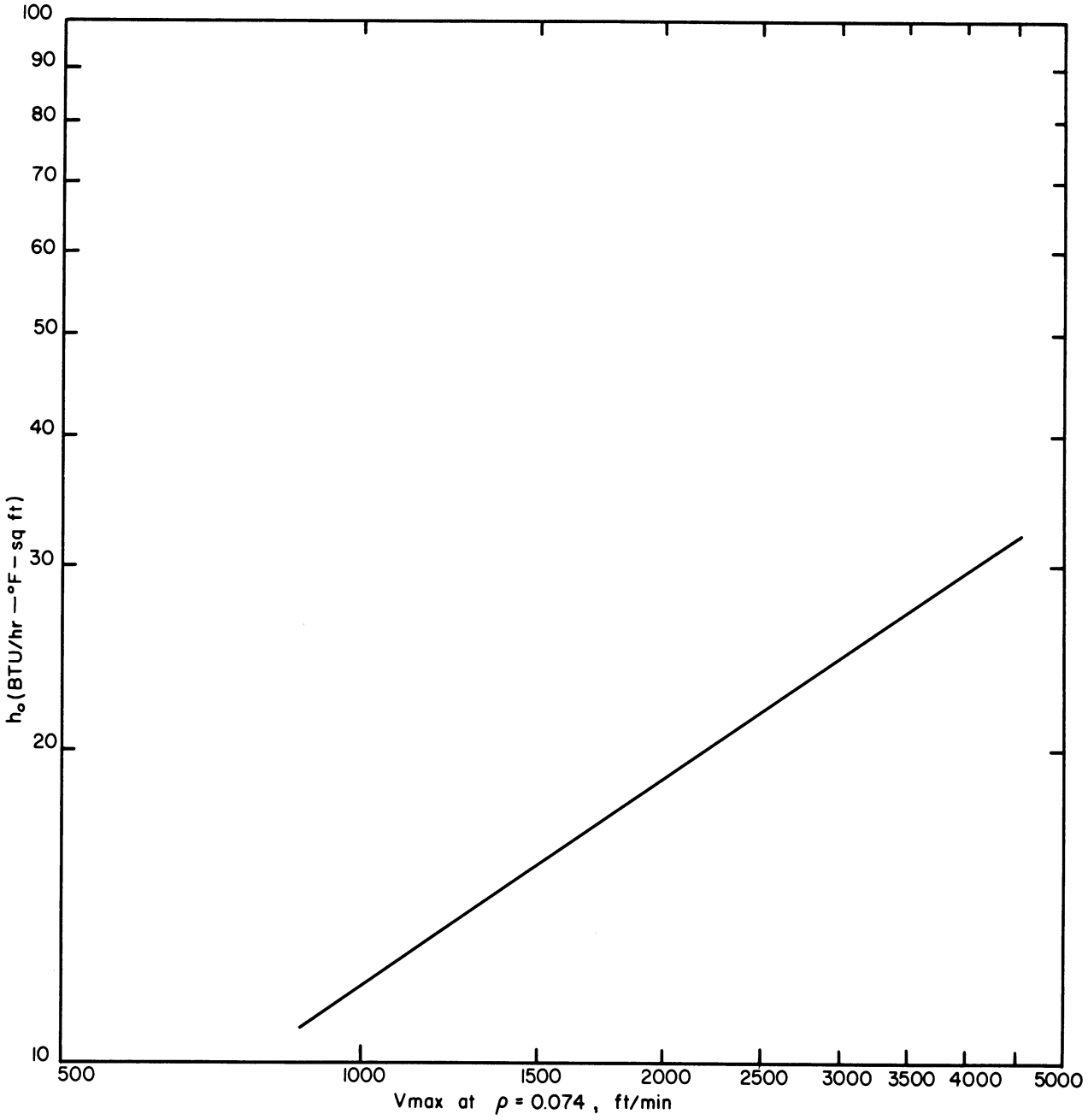

Figure 5. Heat Transfer Curve of Jameson[4], 1 inch Root Diameter Tube.

this tube bank was determined from results of heating air flowing in crossflow outside of the tubes with steam condensing inside of the tubes. The results of this investigation are shown in Figure 6.

Katz and co-workers[7] assembled the heat transfer and pressure drop results of thirty different tube banks from a variety of sources for correlation purposes. Six of the tube banks have already been discussed[5,6]. Of the remaining triangular pitch tube banks, only five units had more than three rows deep and contained monometallic tubes. The heat transfer and pressure drop performance of these five units are presented in Figures 7 and 8. Two monometallic in-line finned tube banks were also reported.

Schmidt[2] tested four triangular pitch finned tube banks. He studied the effect of different longitudinal spacings between the tubes on the tube bank performance. The type of tube used in this investigation was not reported. Schmidt noticed no effect of longitudinal spacing on the heat transfer performance. The variation in pressure drop performance was about the same as that noted by Jameson[4]. The performance curves of the individual rows of tubes were reported along with the overall heat transfer performance of the tube banks. These results will be further discussed in a later section. The heat transfer and pressure drop curves reported by Schmidt are give in Figures 9 and 10.

C. Local Rates of Heat Transfer to Finned Surfaces

Two investigations have appeared in the literature dealing with local rates of heat transfer to finned surfaces. M. L. Ghai[18] reported local heat transfer coefficients for two parallel straight fins which

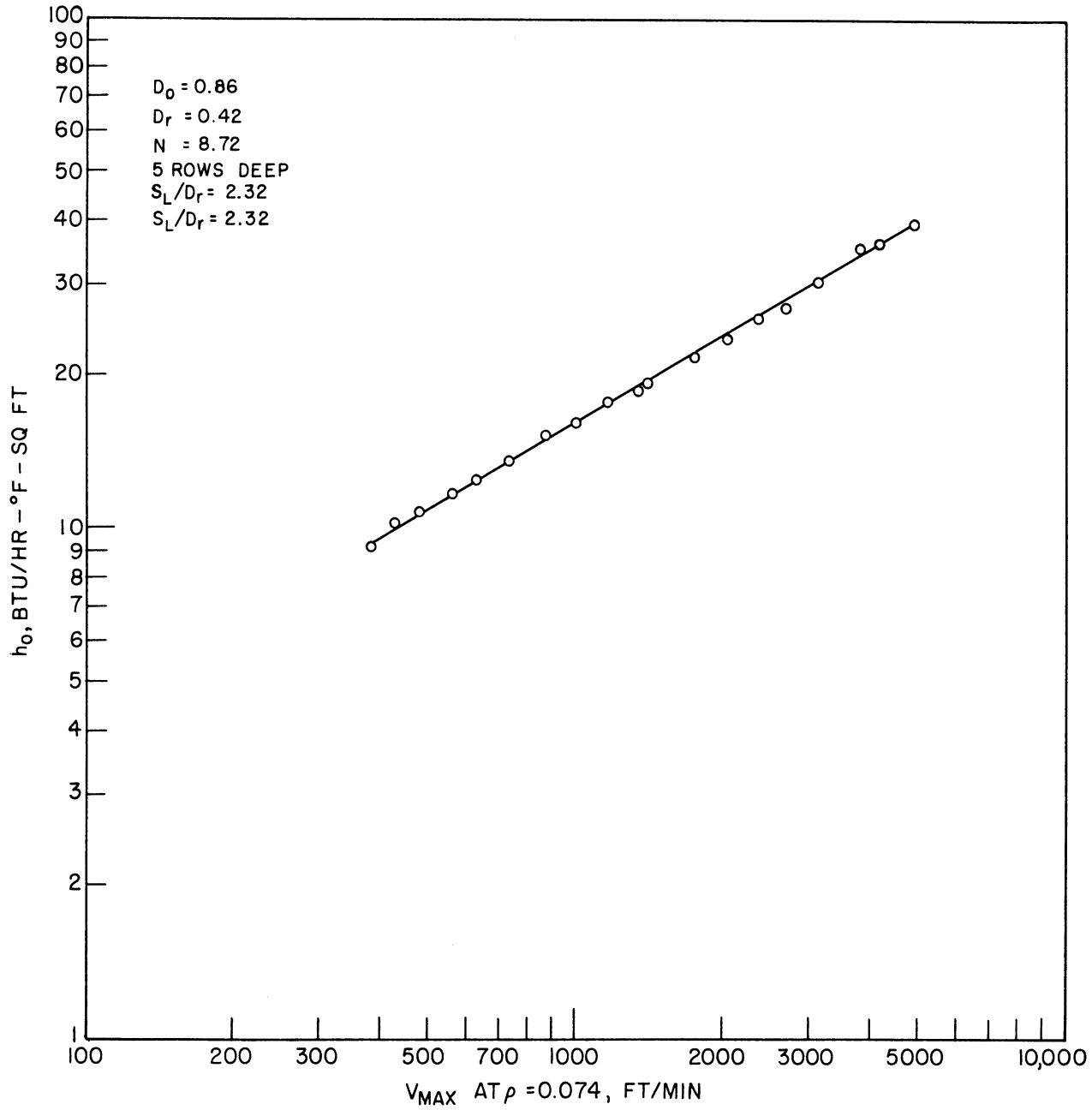

Figure 6. Heat Transfer Curve of London, Kays, and Johnson[15].

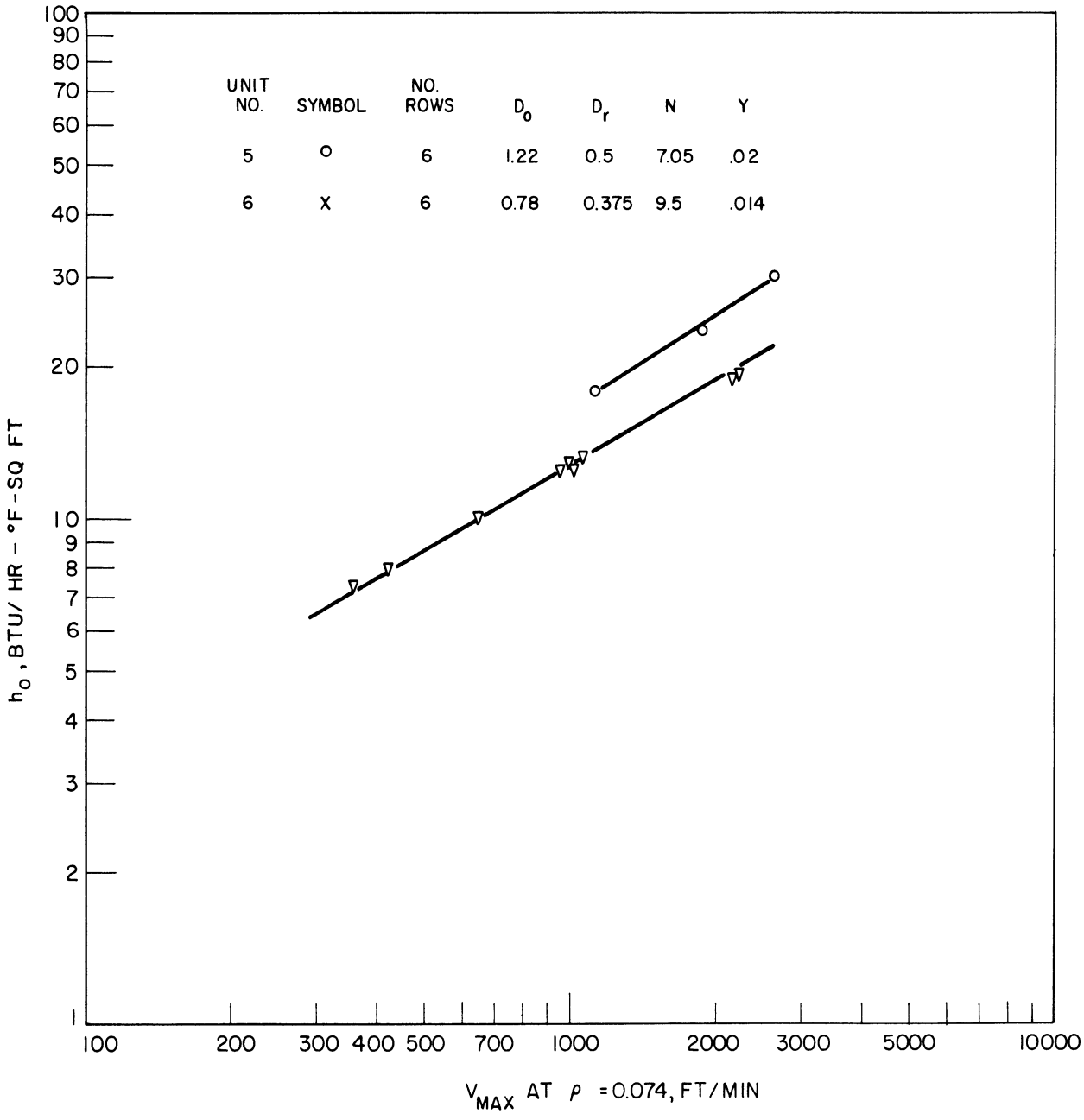

Figure 7. Heat Transfer Curves from Ref. 7, Units 5 and 6.

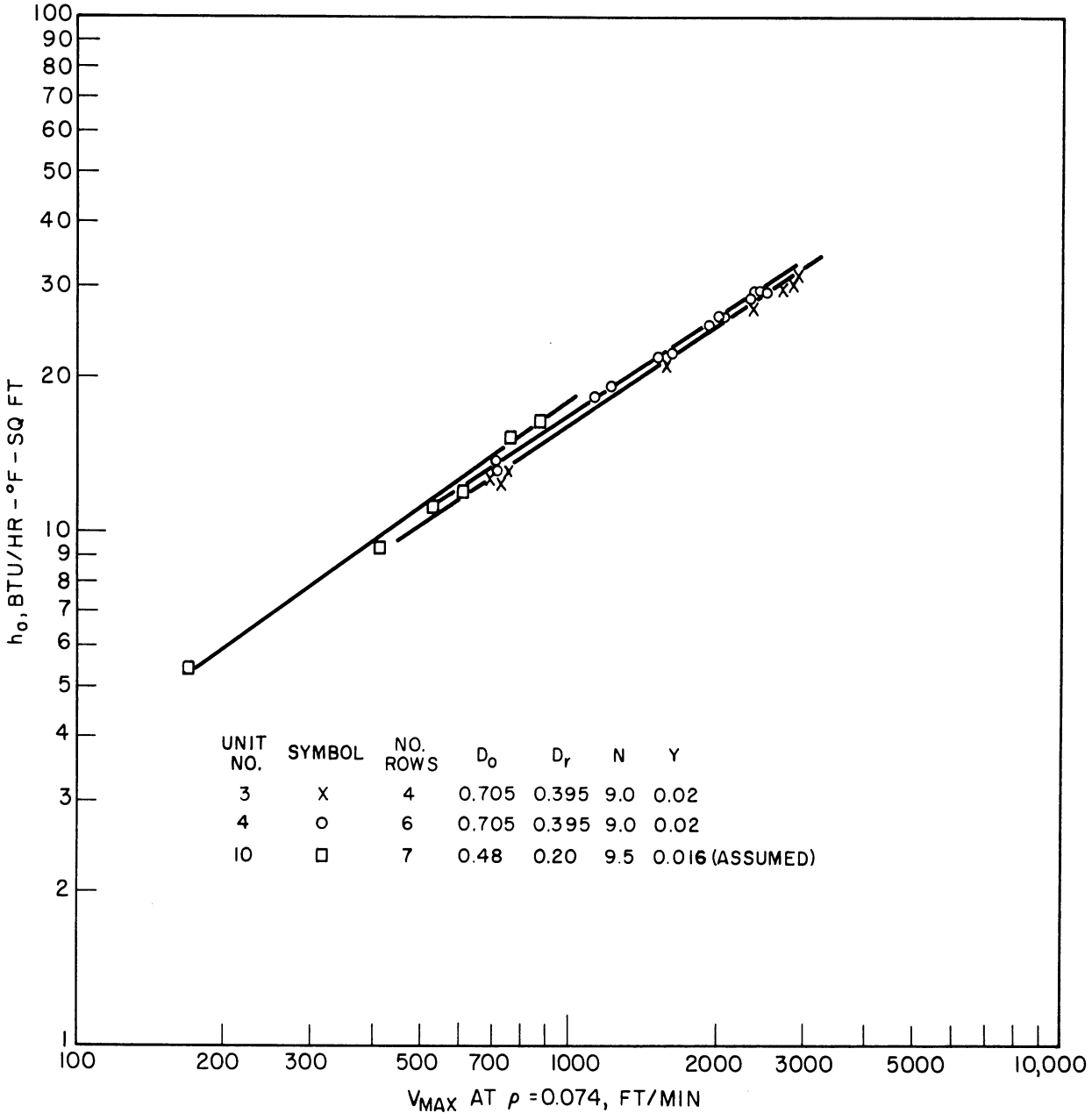

Figure 8. Heat Transfer Curves from Ref. 7, Units 3, 4 and 10.

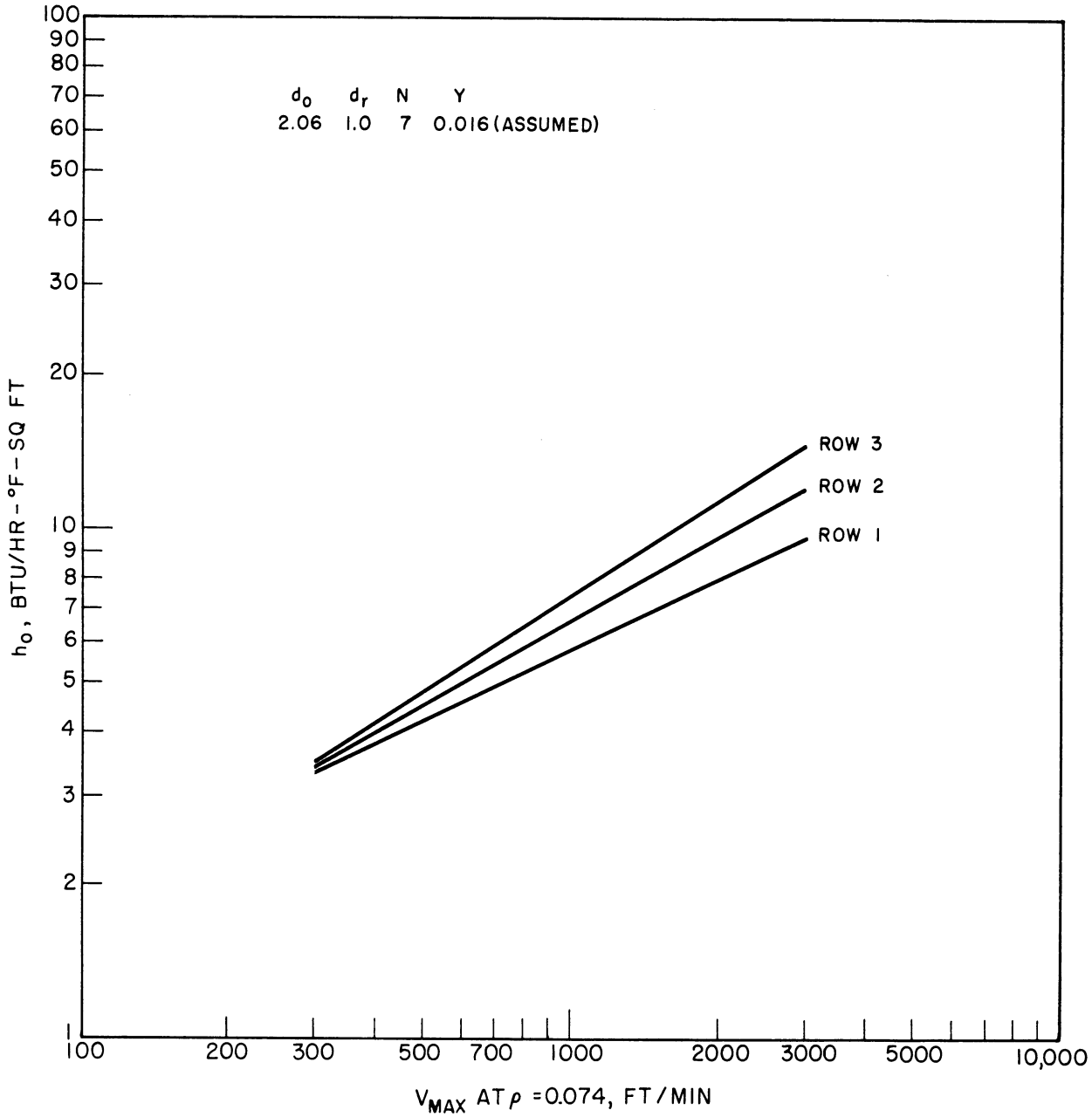

Figure 9. Heat Transfer Curves of T. E. Schmidt[2].

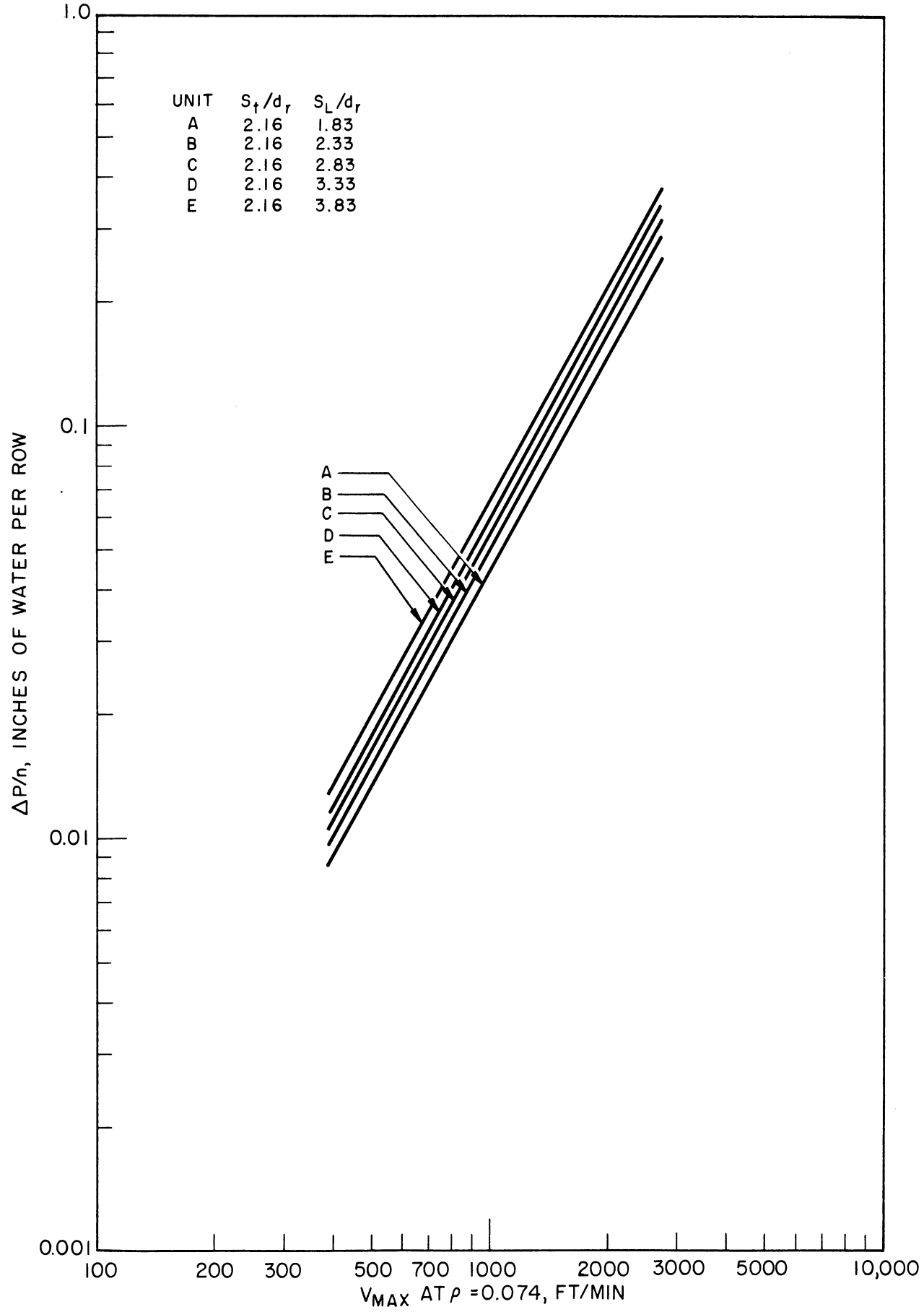

Figure 10. Pressure Drop Results of T. E. Schmidt[2].

were electrically heated at the base of the fins. The fins were attached to a non-conductive wall. The local heat transfer coefficient on the fin varied both with the angle from the leading edge of the fin and with the distance from the tip of the fin. The variation from the root to the tip of the fin was particularly large. This is indicated in Figure 11 for one of the tests. This figure indicates that the heat transfer coefficient at the tip of the fin is much greater than at the root.

Weiner, Gross and Paschkis[19] measured local rates of heat transfer on a single finned tube with water flowing perpendicular to the axis of the tube. The heat transfer coefficients for various areas on the fin were computed on the basis of the heat flux from the section under consideration to the ambient water. The difference between the skin temperature of the surface and the temperature of the water approaching the tube was used as the driving force.

The results were described by dividing the finned area into three sections; an active zone where the heat transfer coefficients were 50 per cent or more larger than the mean heat transfer coefficient; a recirculation zone where the heat transfer coefficients were less than half of the mean coefficient; and a mean zone where the coefficients were between 0.5 and 1.5 times the mean coefficient.

At the 90° position (90° from the leading edge) the heat transfer coefficient was found to be relatively constant and independent of the distance from the tip of the fin. This is contrary to the findings of Ghai for straight fins. This difference in findings can probably be attributed to the effect of the cylinder on the fluid flow over the finned area. This will be further discussed in a later section.

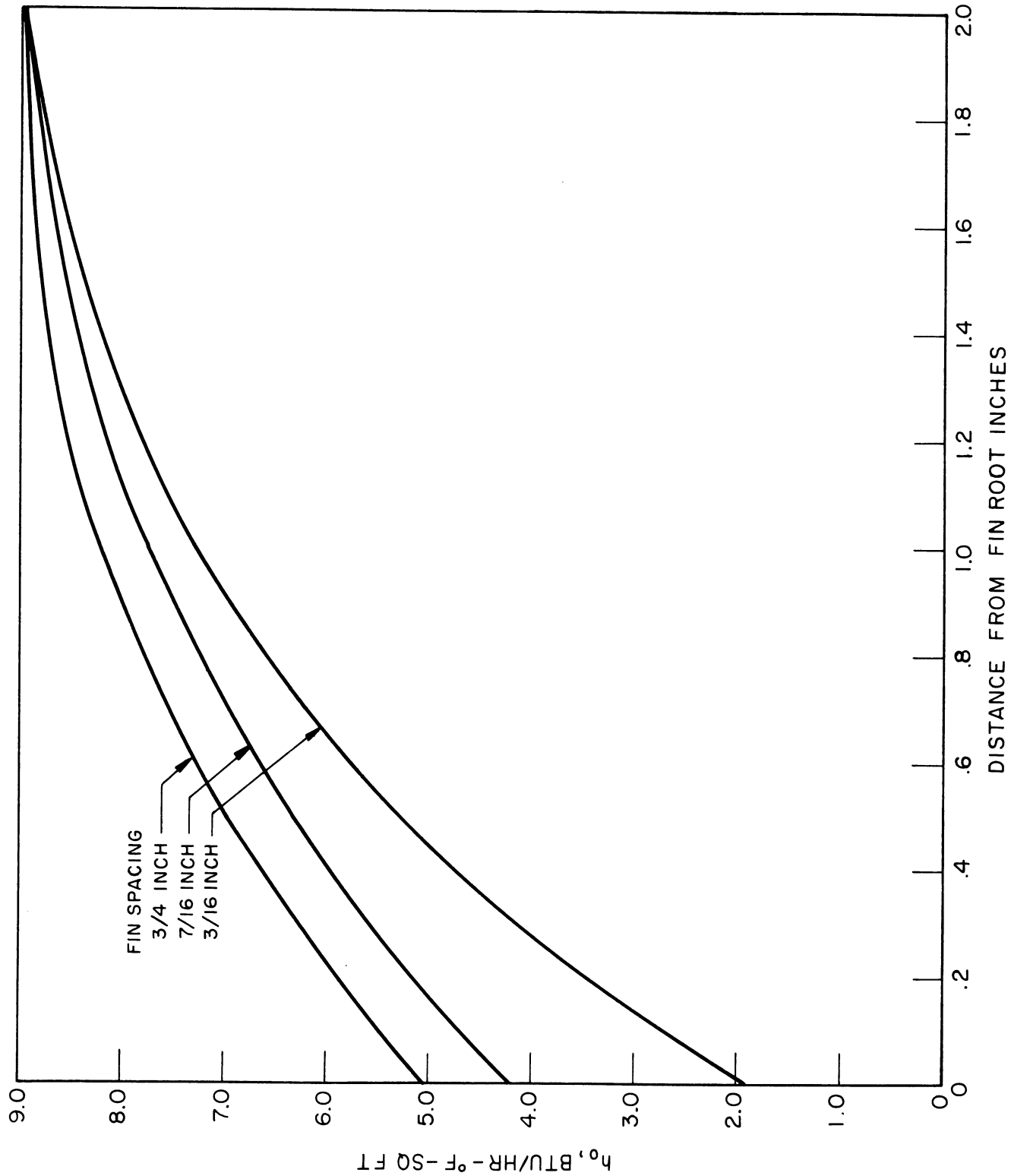

Figure 11. Variation in Heat Transfer Coefficient With Distance From Tip for a Longitudinal Fin, After Ghai.

The relative size of the "active" and "recirculation" zones on the fins were found to decrease with increasing flow rates.

D. Heat Transfer Correlations

Three heat transfer correlations for helically finned tubes have been presented in the literature. In chronological order they result from the work of Schmidt[2], and Katz and co-workers[3,7].

Schmidt's correlation, which appeared in a very brief article, was obtained from a comparison of the performance of single plain and finned tube data and the performance of a plain tube bank plus a laminated cooler. In his studies on single tubes, Schmidt observed that the ratio of the finned tube heat transfer coefficient to the plain tube heat transfer coefficient was a function of the fin height and fin spacing. Using the single tube data he obtained a relationship of the form:

$$\frac{h_o}{h_p} = 1 - 0.18\left[\frac{(d_o - d_r)N}{2}\right]^{0.63} \qquad (5)$$

where h_o = air film heat transfer coefficient for a finned tube bank and h_p = air film heat transfer coefficient for a plain tube bank. This relationship for single tubes gave good agreement with the experimental results obtained on a laminated cooler having five rows of in-line tubes. Substituting the following relationship for air flowing across triangular pitch plain tube banks which is recommended by McAdams[20]:

$$\frac{h_p D_r}{K_f} = 0.30\left(\frac{D_r G_m}{\mu_f}\right)^{0.6} \qquad (6)$$

into equation (5) gives:

$$\frac{h_o D_r}{K_f} = 0.30\left(\frac{D_r G_m}{\mu_f}\right)^{0.6}\left[1 - 0.18\left\{\frac{(d_o - d_r)}{2}\ N\right\}^{0.63}\right] \qquad (7)$$

Katz and co-workers studied the results of a number of investigations on heat transfer to finned tube banks. They presented two heat transfer correlations for air, which can be put in the following form:

$$h_o = B\ D_e^{\ m}\ V_m^{\ b} \qquad (8)$$

where the equivalent diameters of finned tubes, D_e, is defined as

$$(D_e)_1 = \left(\frac{S_A}{D_r}\right)^2 \left(\frac{ND_o}{12}\right) \qquad (9)$$

and

$$(D_e)_2 = S_A \left(\frac{N}{D_r}\right)^{0.3} \qquad (10)$$

The constant b, used in the above correlations, had a value of 0.56, and the constant m, had values of -0.5 and -1.0 for equations (9) and (10) respectively.

E. Pressure Drop Correlations

Four pressure drop correlations for finned tube banks have appeared in the literature. These correlations resulted from the work of Jameson[4], Katz and co-workers[7], and Gunter and Shaw[21]. These correlations will be discussed in the order given above.

Jameson[4] correlated the pressure drop data from a number of tube banks and obtained the following correlation for air near atmospheric pressure:

$$\frac{\Delta p}{n} = 4.25 \times 10^{-9}\ D_e^{-0.25}\ V_m^{1.75} \qquad (11)$$

where

$$D_e = \frac{D_{wh}}{\left[\left(\frac{H}{\frac{1}{N}-Y}\right)^{0.4}\left(\frac{1}{2\sqrt{\frac{S_t}{d_r}-1}}+\frac{1}{2\sqrt{\frac{S_\ell}{d_r}-1}}\right)^4\right]} \qquad (12)$$

Jameson stated that this equation fairly well correlated the data for tube banks in which the free area in an individual row of tubes is less than that in the diagonal openings between two successive rows of tubes.

Katz and co-workers[7] presented two correlations for the pressure drop of air flowing across triangular pitch finned tube banks. The first correlation can be reduced to

$$\frac{\Delta p}{n} = 1.52 \times 10^{-7} \frac{(ND_o)^{0.5} D_r^{0.3}}{S_A^{0.6}} V_m^{1.70} \qquad (13)$$

The second correlation is shown on Figure 12.

Gunter and Shaw[21] presented a general correlation for pressure drop across various surfaces with fluids in crossflow. The proposed relationship for flow in the turbulent region (Re > 200) is given by:

$$\frac{\Delta P g_c D_{vh} \rho}{G^2 L}\left(\frac{\mu}{\mu_w}\right)^{0.14} = 0.96\left(\frac{D_{vh}G}{\mu}\right)^{-0.145}\left(\frac{S_\ell}{S_t}\right)^{0.6}\left(\frac{D_{vh}}{S_t}\right)^{0.4} \qquad (14)$$

For air at 100°F this reduces to:

$$\frac{\Delta p}{n} = 5.85 \times 10^{-8} \frac{V_m^{1.855} S_\ell^{0.6}}{D_{vh}^{0.745}} \qquad (15)$$

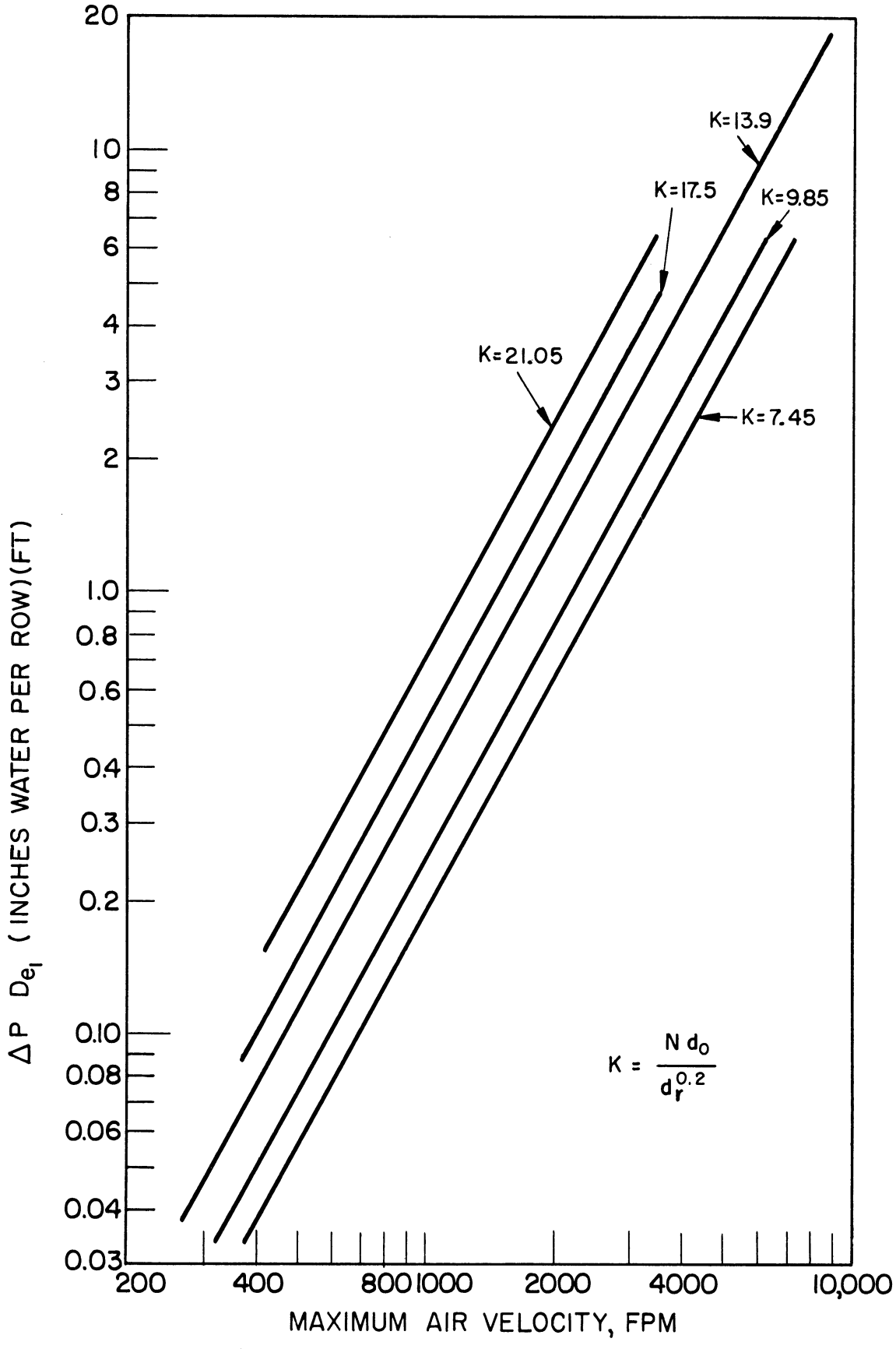

Figure 12. Finned Tube Pressure Drop Correlation of Katz, et al.

III. EXPERIMENTAL EQUIPMENT

The experimental equipment used in this investigation consisted of a twenty-six inch diameter wind tunnel designed in such a manner that a heat transfer unit could be placed between the entrance section of the wind tunnel and the wind tunnel itself. An overall view of the equipment is given in Figure 13. The equipment can be divided into the following sections:

1. The wind tunnel and auxiliary equipment
2. The tube banks.
3. Steam side equipment.
4. Instrumentation and measuring devices.

These are described in detail below. The equipment used to determine the performance of the tube banks was modified for several special tests. The modifications for these tests are described in the last part of this section.

A. Wind Tunnel and Auxiliary Equipment

The wind tunnel was composed of the following five sections:

a) Entrance section

b) Test section

c) Calming section

d) Blower

e) Exit section

The air traveled from the entrance section through the remaining sections in the order given above.

The entrance section was designed to give an essentially uniform velocity profile immediately prior to the test section. Frontal and side views are pictorially shown in Figures 14 and 15 respectively. As indicated in these figures, this section consisted of a sheet metal duct transcending smoothly from frontal dimensions of 32 inches by 48 inches to an 18 inch by 27 inch rectangular section. The duct was 19 inches long and was curved for approximately two-thirds of this distance. A rectangular angle iron frame riveted to the back of the entrance provided a flange for bolting to the test section, which was composed of one of the tube banks, and will be described below.

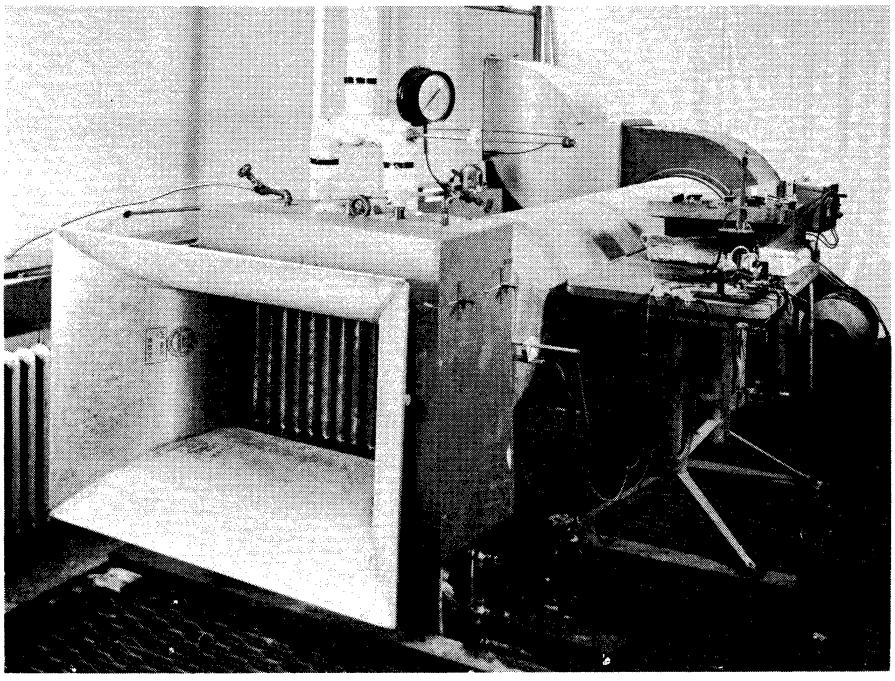

Figure 13. Overall View of Wind Tunnel With Tube Bank Installed.

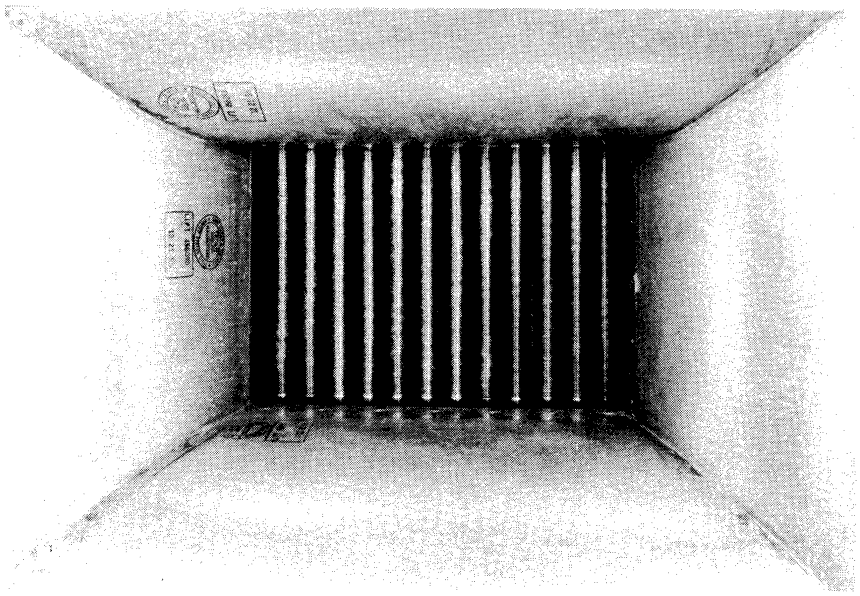

Figure 14. Frontal View of Entrance Section.

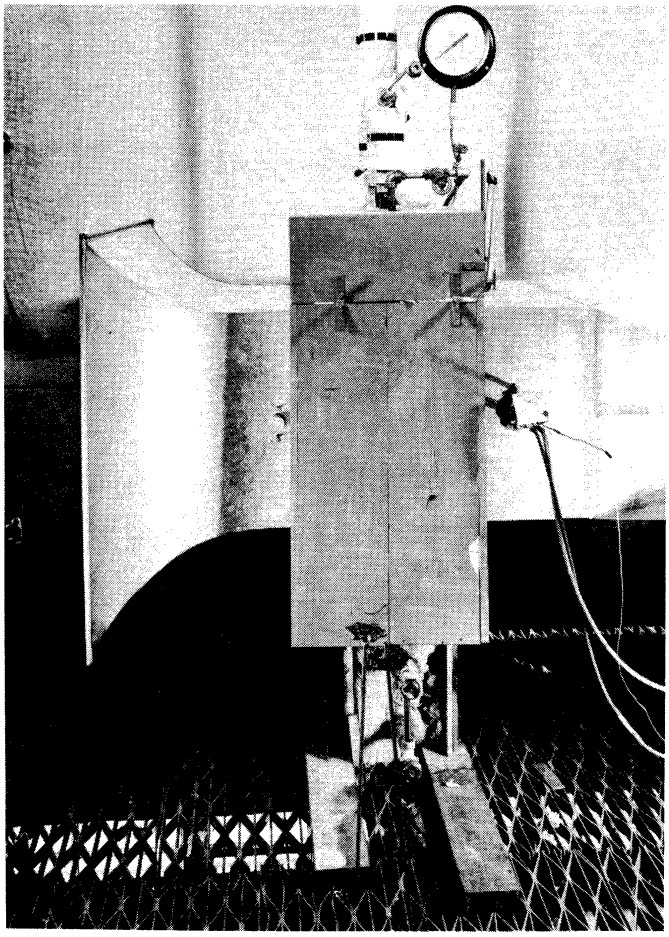

Figure 15. Side View of Entrance Section.

The calming section was composed of a hollow sheet metal tube interposed between the test section and the blower in order to keep any back mixing, which might occur due to the blower, from affecting the last rows of tubes. It consisted of a rectangular section, also 18 inches by 27 inches in cross section, 12 inches long followed by a hollow cylindrical section 112 inches long. The end of the cylindrical section was friction fitted to a flange on the blower.

The blower was a Number 4 Sirroco fan made by the American Blower Corporation. The fan is rated at 4000 cubic feet per minute of air at one inch of water pressure drop. The blower was powered by a five horsepower, shunt wound, D.C. motor. The speed of the motor was controlled by a system of variable resistors placed in the field and/or armature circuits of the motor. By placing additional resistance in the field circuit of the motor, the speed of the motor was increased. The motor speed was reduced by placing additional resistances in the armature circuit of the motor. The resistors in the armature circuit were connected by means of knife switches which allowed them to be placed in series or parallel operation. By means of this control, the motor speed could be varied between 150 and 1100 rpm. The normal speed of the motor was 800 rpm. An ammeter was also included in the control circuit to prevent an excessive overload of the motor at the higher speeds. The blower, motor, and speed control are pictorially shown in Figure 16.

The outlet section consisted of a rectangular sheet metal duct which allowed the air to pass out of the building. The section was

fastened on one end to the outlet of the blower and on the other end to a plywood board which replaced a window section having a rectangular hole the size of the duct opening. A rectangular steel plate hinged on the top served as a damper to further control the air velocity at the low speeds. This damper also served to protect the blower and exit section from the exterior weather elements.

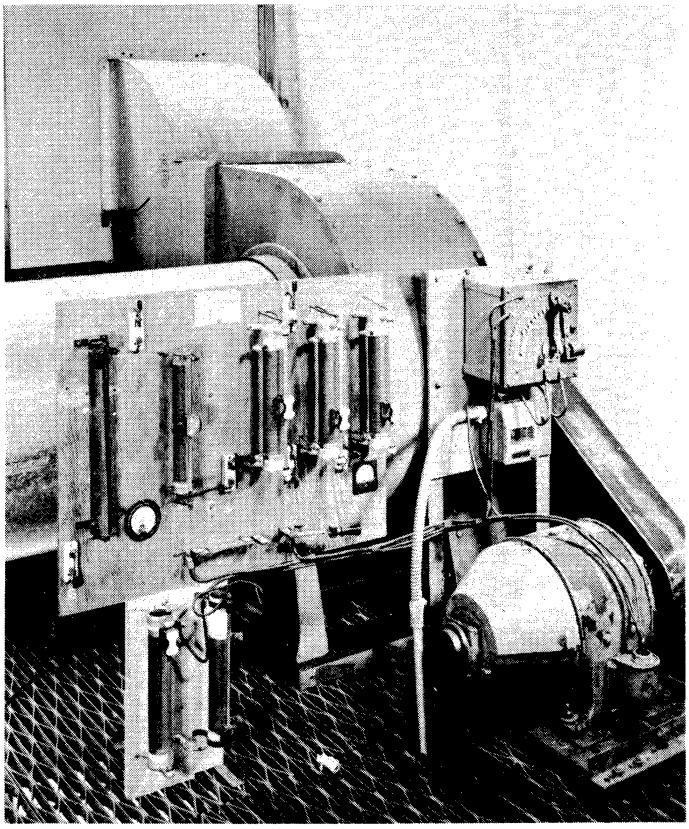

Figure 16. Blower, Motor and Speed Control System.

B. Tube Banks

Frontal views of the eight tube banks used in this investigation are shown in Figure 17 through 20. The dimensions of the tube banks are summarized in Table I. This table indicates the unit numbering system. This identification is adhered to throughout the remainder of this text.

Table I. Dimensions of Tube Banks Investigated

TUBE BANK	FRONTAL WIDTH, INCHES	FRONTAL HEIGHT, INCHES	NO. TUBES	NO. ROWS	TUBE SPACING	V_{in} V_{face}	ANGLE IRON SIZE	A_{total} ft^2	A_{min} (flow) ft^2
1	27	18	165	6	15/16"	4.63	3/4"x3/4"x1/8"	48.6	0.74
2	27	18	165	6	15/16"	3.30	3/4"x3/4"	128	1.02
3	27	18	165	6	15/16"	2.66	3/4"x3/4"	165	1.27
4	27	18	147	6	1-1/16"	2.43	3/4"x3/4"	147	1.39
5	27	18	147	6	1-1/16"	1.93	3/4"x3/4"	156	1.75
6	27	18	46	4	2-3/16"	2.33	1-1/2"x1-1/2"	159	1.45
7	27	18	46	4	2-3/16"	2.72	1-1/2"x1-1/2"	265	1.24
8	27	18	84	8	2-7/16"	1.96	1-1/4"x1-1/4"	572	1.72

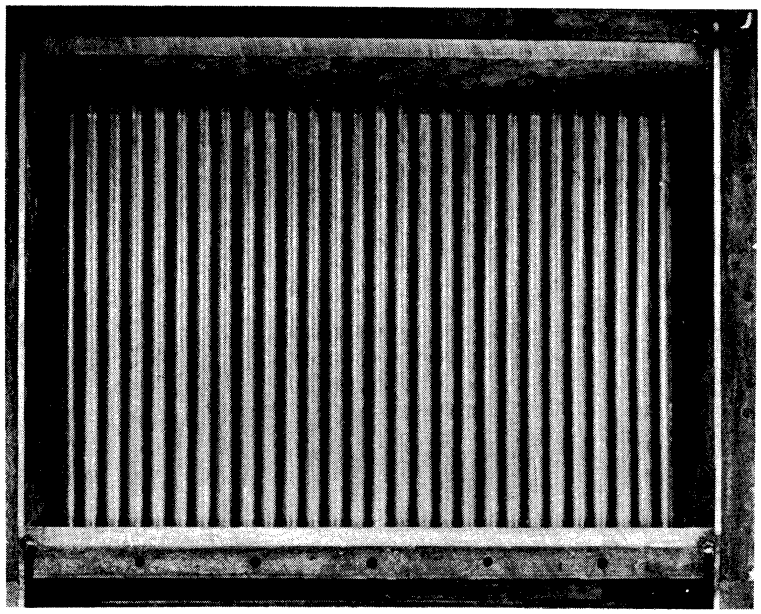

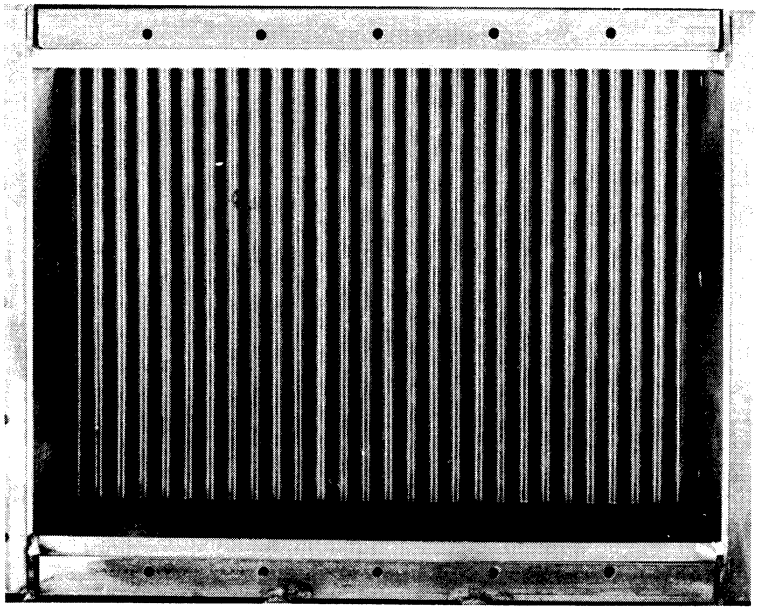

Figure 17. Frontal View of the Eight Tube Banks Investigated. Units 1 and 2.

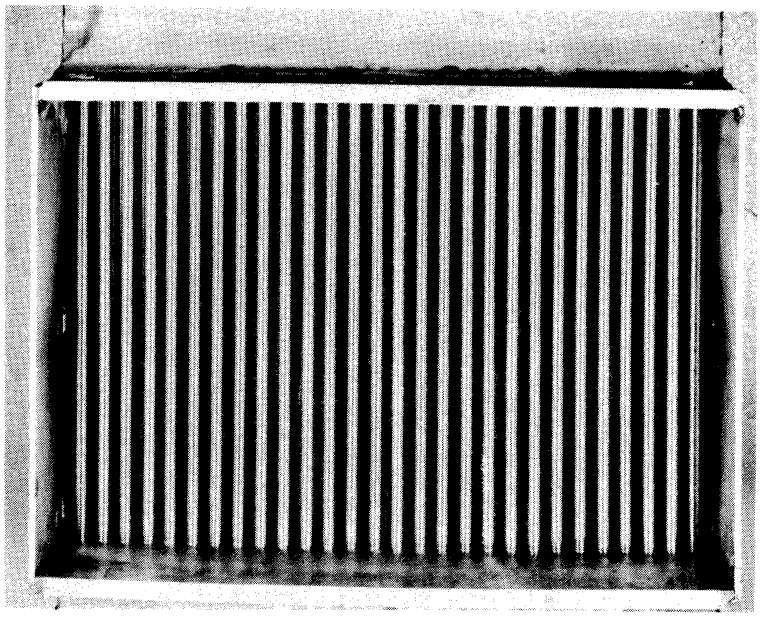

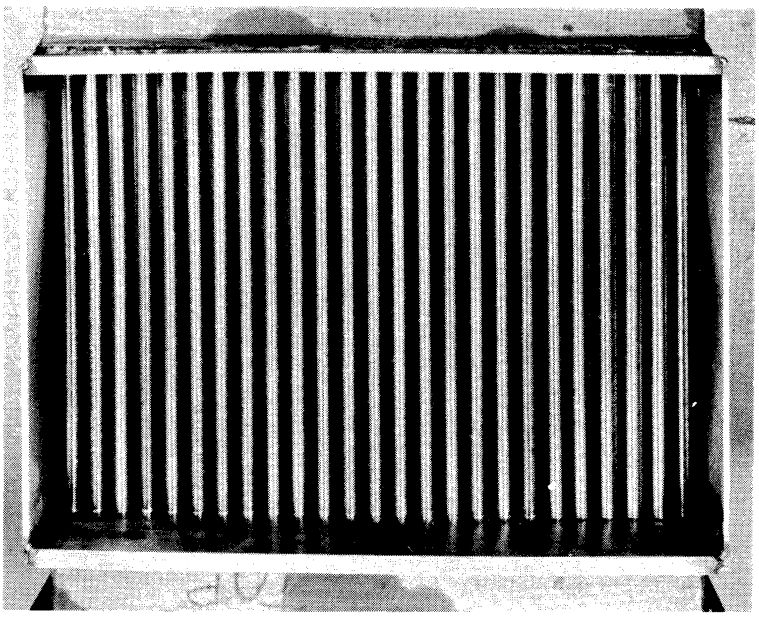

Figure 18. Frontal View of the Eight Tube Banks Investigated. Units 3 and 4.

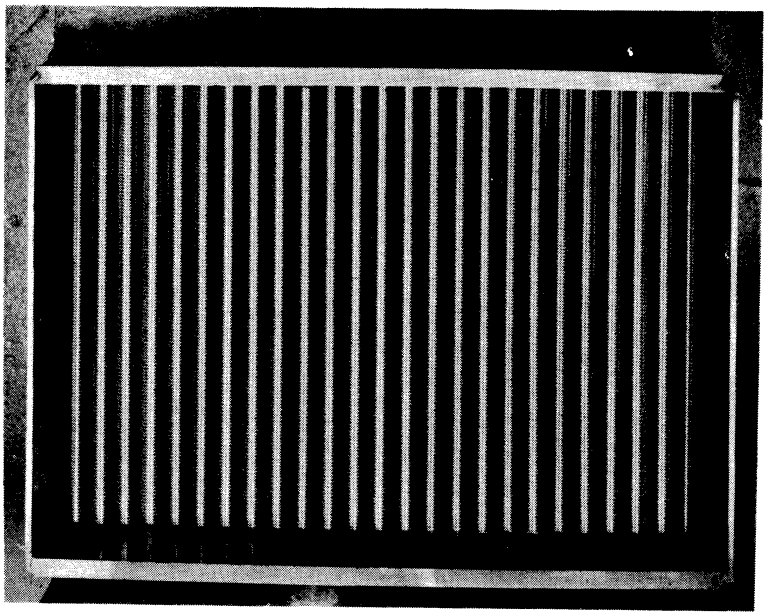

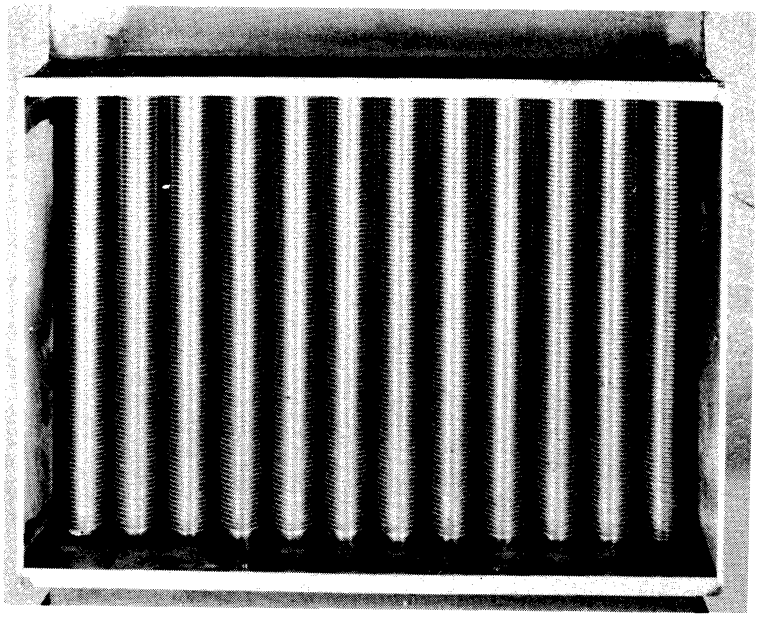

Figure 19. Frontal View of the Eight Tube Banks Investigated. Units 5 and 6.

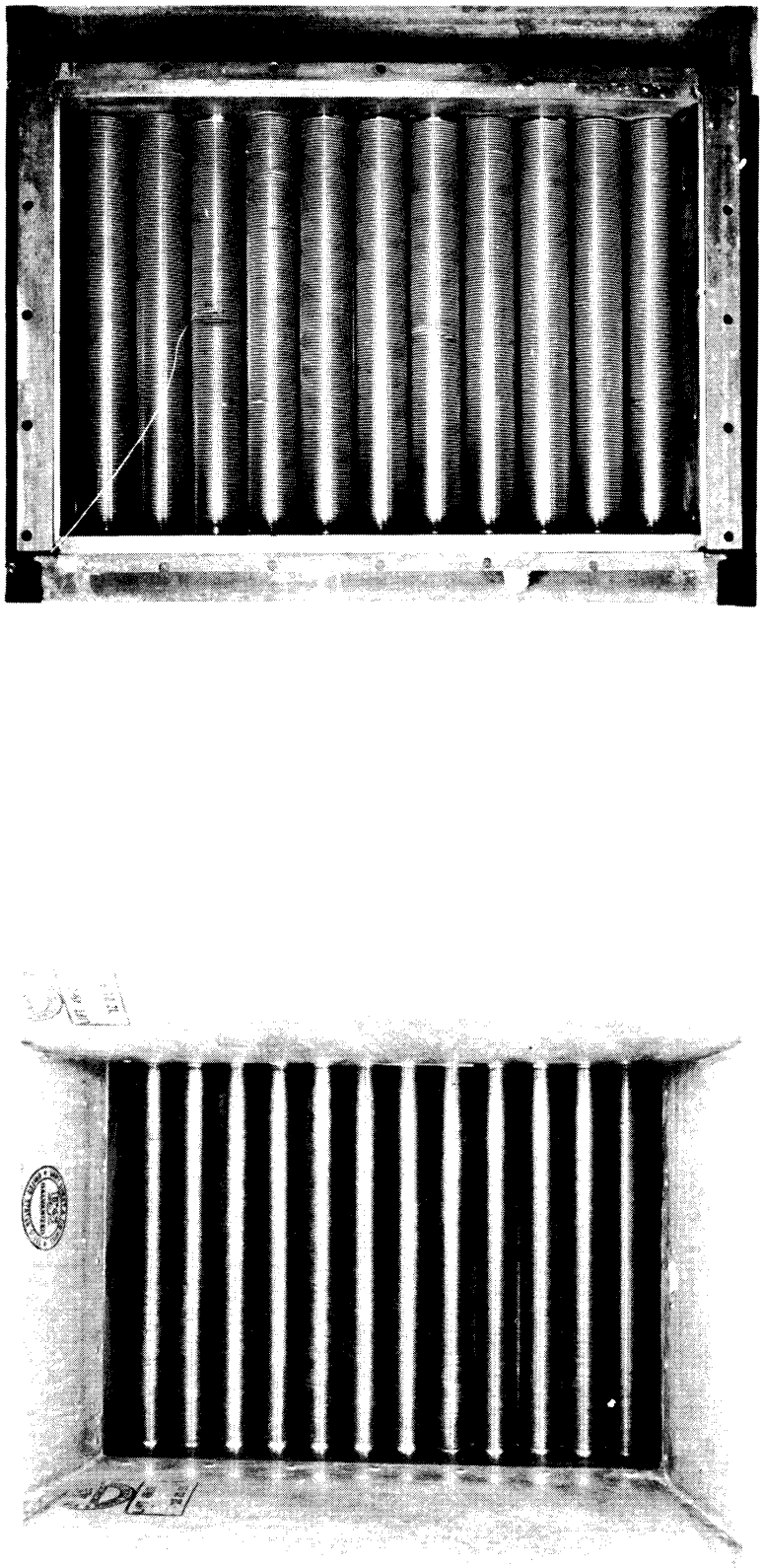

Figure 20. Frontal View of the Eight Tube Banks Investigated. Units 7 and 8.

The tube banks were each made up of three components: the tube sheets, the sides, and the tubes. The tube sheets were made from 3/4 inch thick hot rolled carbon steel plate with holes drilled through the plate on the tube pattern desired. All but two of the tube sheets were 27 inches long by 12 inches wide. The pair used for tube bank number 8 were 27 by 21 inches. The tube sheets were drilled in pairs in order to insure alignment of the holes for the ends of the tubes. The holes for the tubes were drilled 0.012 inches ($\pm$ 0.005 inches) larger than the outside diameter of the turned ends of the tubes. The diameter of the plain ends of the tubes and of the tube-sheet holes are given Table II. The holes were laid out on equilateral triangles with sides equal to the nominal outside diameter of the tube plus three sixteenths of an inch. A typical tube sheet layout is schematically shown in Figure 21 for tube bank number 8. A top view for one tube sheet for unit number 3 is given in Figure 22. As indicated in these figures, the odd number rows (commencing from the inlet end) contained one more tube than the even numbered rows.

The sides of the tube banks were made from 1/4 inch thick steel plate. The width was made equal to that of the companion tube sheets and the length was held constant at 19 1/2 inches. Lengths of angle iron were welded to both sides of each unit at distances corresponding to the even numbered rows in order to prevent the air from flowing between the outer tubes of the rows and the side panels. These strips were made 18 inches long and were placed with the right angle projecting into the tube bank. Different sizes of angle iron were used in the different tube banks. The positioning of the angle irons are indicated in Figure 21.

TABLE II

DIAMETER OF TUBE ENDS AND TUBE SHEET HOLE DRILL SIZES

Unit	Tube O.D. (turned ends) inches	Drill Size inches
1	0.750	0.762 ± 0.005
2	0.625	0.637 ± 0.005
3	0.525	0.537 ± 0.005
4	0.525	0.537 ± 0.005
5	0.405	0.417 ± 0.005
6	1.125	1.137 ± 0.005
7	1.125	1.137 ± 0.005
8	1.125	1.137 ± 0.005

The finned tubes used in the investigation were integral helically-finned tubes. The process used in forming these tubes consists of the cold extrusion of the fins from the walls of an initially plain cylindrical tube. The tubes produced in this manner are similar to hollow rods threaded over their entire length. Assuming constant fin thickness, the finned tubes can be described by the four dimensions, outside diameter, root diameter, fins per inch, and fin thickness, or d_o, d_r, N, and Y respectively. Four of the different finned tubes were made of aluminum while three were made

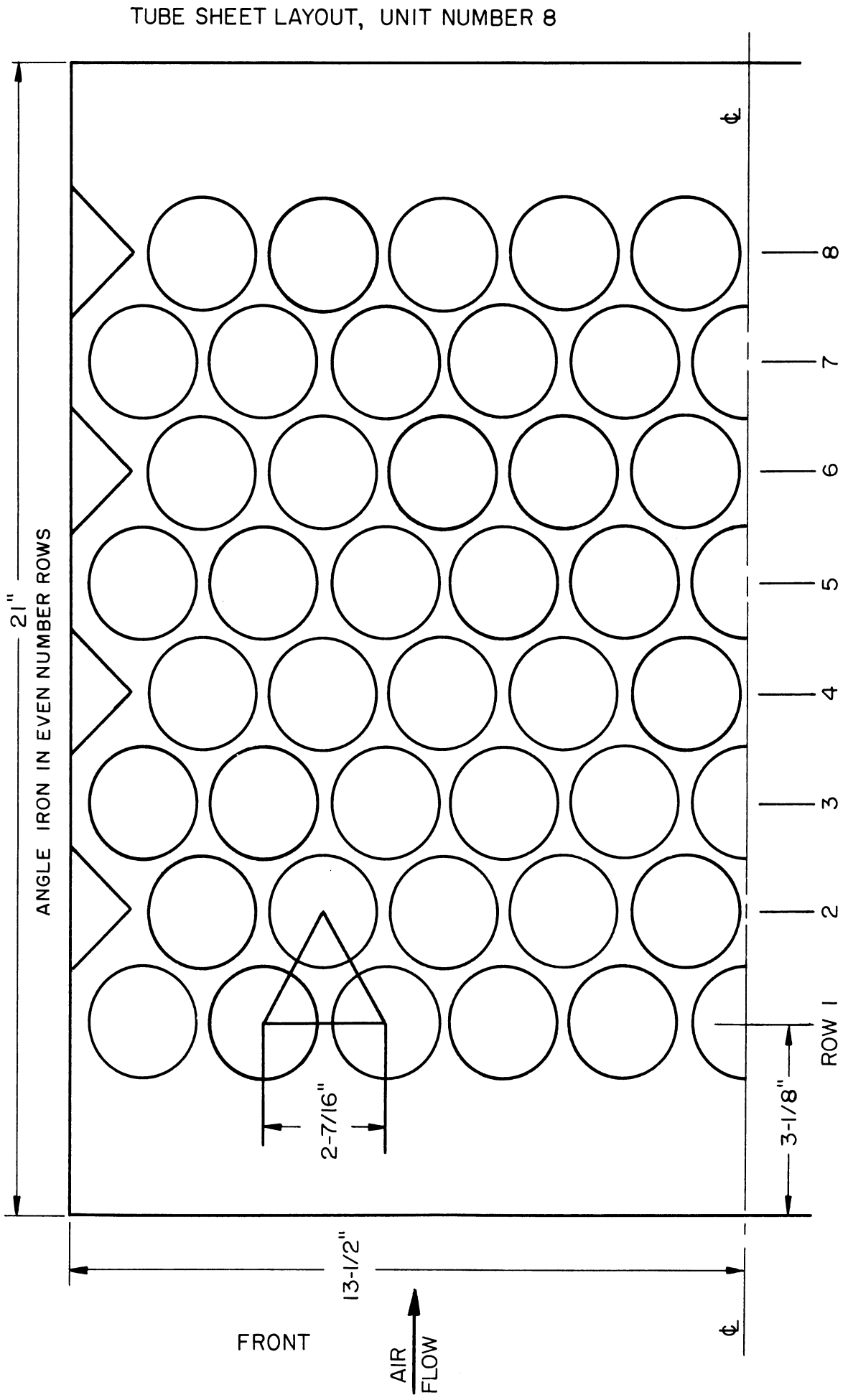

Figure 21. Tube Sheet Layout of Unit Number 8.

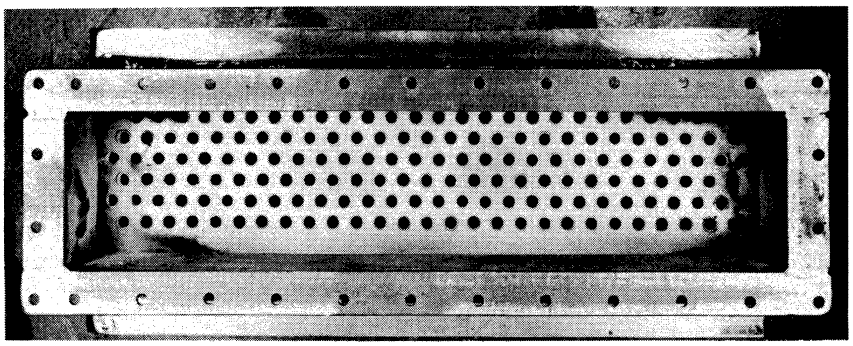

Figure 22. Top View of Unit Number 3.

of copper. The dimensions of the tubes are summarized in Table III. The tubes are pictorially compared in Figure 25.

The overall length of all tubes was constant at 19 1/2 inches, with a 3/4 inch long bare section on each end for insertion in the tube sheet. This left an 18 inch long section over which the tube was finned.

The tube bank was fabricated from the above three components by first inserting the ends of the tubes in the tube sheet holes, following which the sides were welded to the tube sheets. The tubes were then expanded against the tube sheet by means of a conventional tube expander powered by a quarter inch reversible electric drill. The tube expanders were designed to expand the walls of the tube approximately 0.035 inches. On some tube banks where a single expander could not provide a tight joint

Table III. Dimensions of Tubes Investigated

TUBE BANK	METAL	INCHES do	INCHES dr	FINS/INCH N	INCHES di	INCHES X_w	INCHES Y/fin	do/dr	Fin Resistance	A_o	A_o/A_i	Ar/Af
1	cu	0.750	0.750	--	--	--	--	1.0	0	0.196	1.15	
2	cu	0.737	0.625	19.5	0.489	0.0680	0.016	1.18	0.04	0.517	4.04	0.28
3	cu	0.762	0.546	11.33	0.444	0.0510	0.017	1.39	0.16	0.573	4.94	0.25
4	cu	0.894	0.554	11.22	0.454	0.0500	0.018	1.61	0.45	0.886	7.45	0.13
5	al	0.895	0.438	7.22	0.312	0.0630	0.022	2.04	1.35	0.709	8.68	0.16
6	al	1.960	1.140	5.13	1.0	0.0700	0.022	1.72	4.10	2.303	8.81	0.13
7	al	1.958	1.123	10.36	1.0	0.0615	0.021	1.74	4.80	3.84	14.60	0.064
8	al	2.303	1.147	8.0	1.0	0.0735	0.017	2.01	12.1	4.54	17.2	0.061

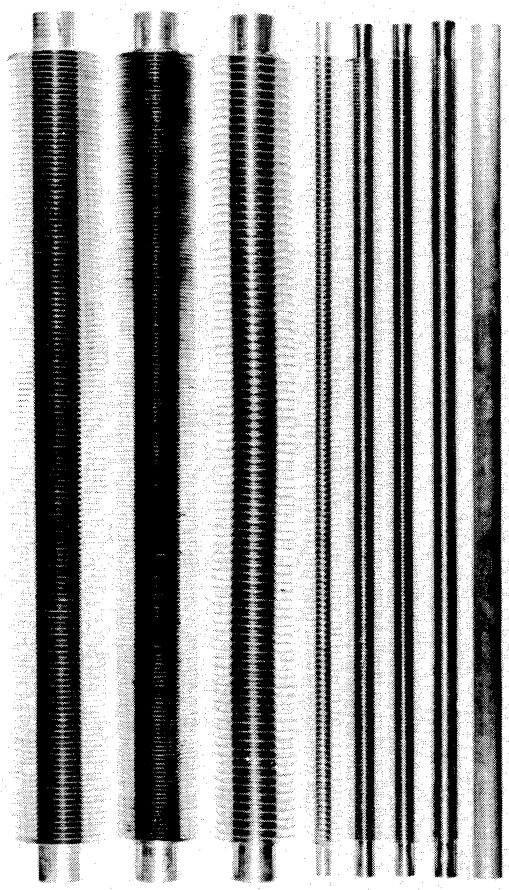

Figure 23. Comparison of the Tubes Used in the Investigation.

between the tube and tube sheet, a second expander was obtained and the tubes were expanded a second time with a larger expander.

The top and bottom steam chests were then welded in place, legs were attached and angle iron flanges were welded and drilled for attaching the unit to the adjacent sections of the wind tunnel. The unit was then ready for installation as the test section.

Frontal views of the eight test sections are given in Figures 17 through 20. A back view of unit number 6 showing the location of the angle iron on the even rows (row number 4 shown) is given in Figure 24. A top view of unit number 5 with the steam chest attached is given in Figure 22.

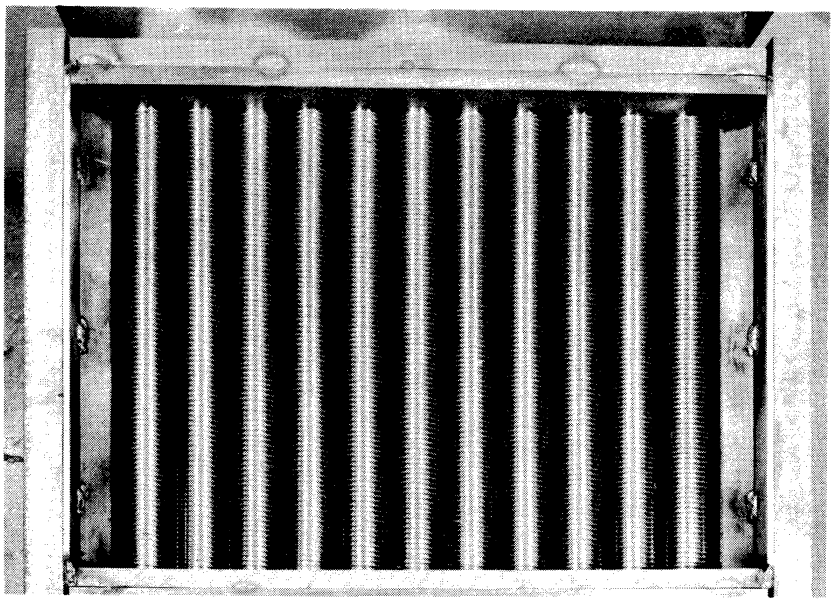

Figure 24. Rear View of Unit Number 6.

C. Steam Side Equipment

A schematic illustration of the steam side equipment employed is given in Figure 25. As shown in this figure, the steam came from the 60 psig service mains, was throttled to 3 psig by means of control valves A and B prior to entering the upper steam chest through twin supply lines in the top of the chest. The pressure of the steam was measured with a pressure gauge which, along with the thermometer shown on the figure, allowed the determination of the number of degrees of superheat of the incoming steam. Impingement baffles were provided in order to evenly dispurse the steam and prevent the in-rushing steam from affecting the

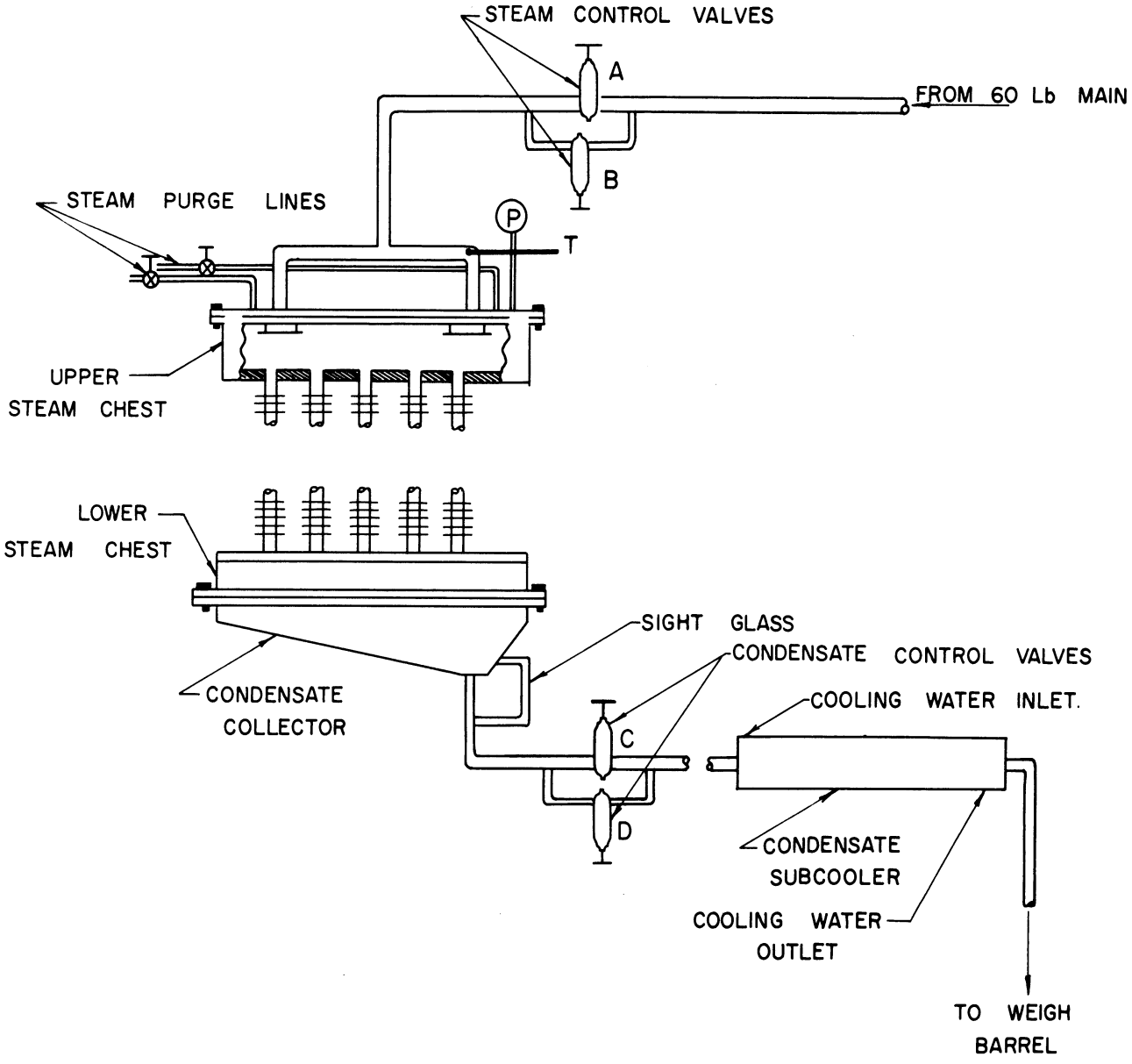

Figure 25. Flow Diagram of Stream.

steam condensing coefficient immediately below the openings. Two purge lines were also located on the top of the steam chest. The condensate was collected in the bottom steam chest. The condensate flow rate was controlled by means of valves C and D of Figure 25 from which it flowed by gravitational force through a sub-cooler to a weigh barrel.

One inch galvanized steel pipe was used the entire length of the steam supply line. The by-pass section, which included valve B of Figure 25, was made up of 1/4 inch pipe. The top of the steam chest was a rectangular section of 1/4 inch steel plate with holes drilled on the periphery about every four inches. These holes were used to bolt the top of the steam chest to the steam chest sides with twenty 3/8 inch bolts. A rubber gasket was used between the top and sides of the chest to prevent leaks. The sides of both the top steam chest and bottom steam chest were made from four inch channel iron welded to form a rectangular box. The bottom of the bottom steam chest was a rectangular shaped box having sloping sides as indicated in Figure 25. The sides reduced down to a two inch by three inch rectangular section on the bottom. A sight glass was located near the bottom of the section in order to see the condensate level. The condensate return lines were of 1/2 inch pipe with the exception of the by-pass line containing valve D which was of 1/8 inch pipe. The condensate sub-cooler was a double pipe heat exchanger made up from a three foot long section of 1 1/4 inch steel pipe for the outer shell and a 1/2 inch pipe for the inner section.

D. Instrumentation and Measuring Devices

The instruments and measuring devices employed on the steam side of the exchanger were: a pressure gauge, thermometer, sight glass, weigh barrel and timer. The pressure gauge used to measure the pressure difference between the steam in the steam chest and the atmospheric air was located on the top of the steam chest as indicated in Figure 25. The instrument was a standard bourdon-tube pressure gauge having a range of 0-5 psig with 0.1 psig graduations. The gauge was calibrated against a one-hundred-inch mercury column and was found to read correctly. This gauge was used throughout the investigation with the exception of the first tube bank (unit number 1) in which the steam pressure was measured (using the same pressure tap) by means of a water-filled manometer. The temperature of the incoming steam was measured by means of a mercury-in-glass thermometer located in an elbow of the incoming steam line about six inches above the steam chest also as shown in Figure 25. The thermometer had a range of 0-300°F with graduations of 2°F. The accuracy of the thermometer was checked against boiling distilled water (the pressure being noted) by means of which it was estimated to read not more than 0.5°F low. Due to the insensitive nature of the calculations on this reading it was deemed sufficiently accurate and no corrections were made to this reading. A sight glass, located adjacent to the bottom steam chest as previously described was used to maintain a constant level of the condensate in the steam chest.

The weigh barrel and timer were used to measure the rate of flow of the condensate. The weigh barrel, a standared fifty-five gallon drum containing an emptying valve and spigot on the bottom, was placed on a

platform type scale having a range of over 1000 pounds with graduations of 1 pound. The timer was a photographic type spring driven clock having individual minute and second hands. The accuracy of the timer was checked against an electric clock for two ten minute periods and was found to read correctly.

The air side of the exchanger required a number of instruments to determine the air pressure, humidity, temperatures, and flow rates. The barometric pressure of the ambient air was measured with a mercurial barometer having a Vernier scale by means of which the atmospheric pressure could be read to within 0.1 mm of mercury. A thermometer was attached to the barometer for ambient temperature measurements in order to make the standard corrections[22] for differences in the thermal expansion of the mercury and the glass. The air humidity was measured with a standard sling hydrometer operated before each series of runs immediately in front of the wind tunnel entrance. The pressure drop of the air flowing through the tube bank was measured by means of a micro-manometer attached to the static side of a pitot tube located in the main stream of air about six inches behind the last row of tubes. The micro-manometer, shown in Figure 26, was fabricated for this investigation. The inlet ambient air temperature was measured with a mercury-in-glass thermometer having gradiations of 0.1°C. The readings of this thermometer were compared with a U.S. Bureau of Standards calibrated thermometer in the range of 20°C to 30°C and were found to be in error by less than 0.1°C in this range. The outlet air temperature was measured by means of a copper-constantan thermocouple encased, except for the tip, in a three foot length of copper tubing. The tubing was inserted through a cork held

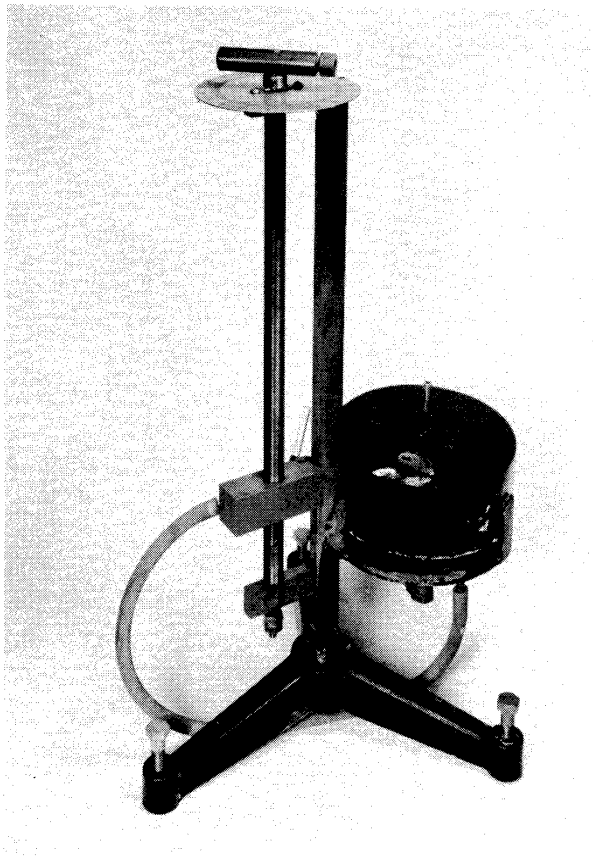

Figure 26. Micro-manometer Used in Investigation.

to the side of the wind tunnel approximately six inches behind the last row of tubes. The thermocouple tip was moved horizontally behind the tube bank at the centerline of the exchanger in order to make a traverse of the air temperature leaving the unit. The thermocouple tip was shielded from radiation by means of a short section of sterling silver tubing placed over and flattened against the junction. The thermocouple EMF was measured with a Leeds and Northrup precision potentiometer. The cold junction temperature was measured with a mercury-in-glass thermometer placed adjacent to this junction. This thermometer was also calibrated against a Bureau of Standards calibrated thermometer. The air velocity was obtained from a Biram's vane type anemometer. This unit,

shown in Figure 27, has a four inch diameter frame with three dials reading to 10,000 feet. The movement has jeweled bearings, a disconnector, and an automatic zero setting attachment and is delivered with calibration corrections obtained in wind-tunnel testing by the Taylor Instrument Co. The calibrations are made by comparative tests with standard instruments certified by the National Physical Laboratory (England) and the Bureau of Standards and are shown on Figure 28. The angular velocity of the vanes of this instrument is dependent on the square root of the inertia of the air approaching the vanes[23]. Since the square root of the inertia is proportional to the velocity, the angular velocity of the vanes is proportional to the air speed. The relative decrease of the frictional resistance of the moving parts

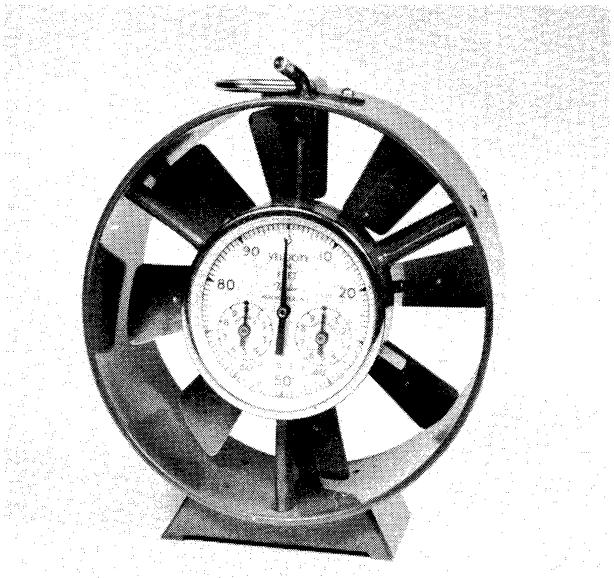

Figure 27. Vane-type Anemometer Used in Investigation.

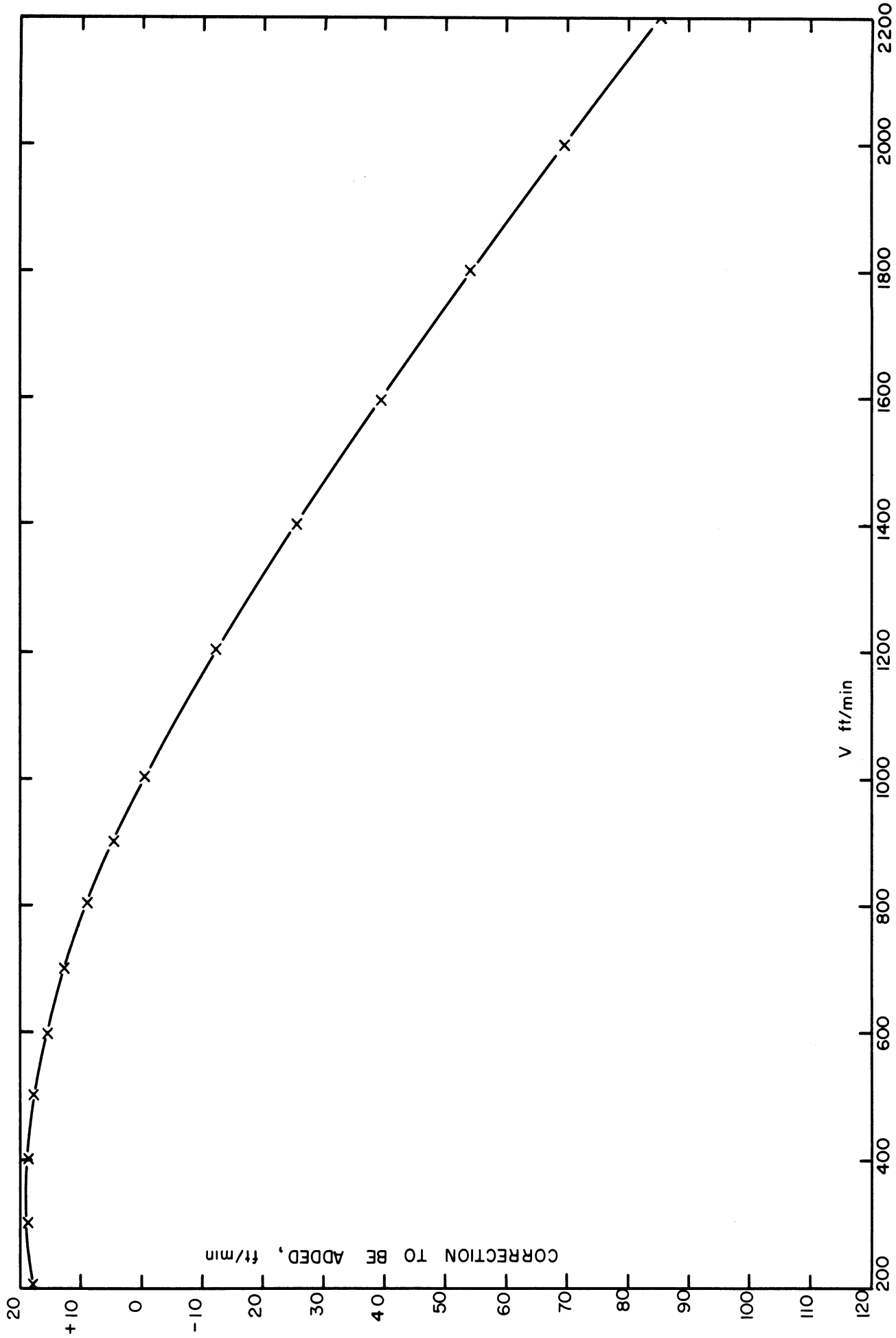

Figure 28. Calibration Correction of Anemometer (supplied by the Taylor Instrument Company).

of the instrument with increasing speed are taken into account by the calibration mentioned above. This type of instrument is generally considered accurate within ± 3%[24]. The particular instrument used in this study seemed to produce somewhat more consistant results than the figure generally quoted. The elapsed time for the anemometer was obtained with a stop watch which could be read to 0.1 seconds. The watch was calibrated against an electric clock and was found to give correct readings within 0.2 seconds in 5 minutes.

E. Modification Employed to Obtain Row-To-Row Performance Data

Tube bank number 8, containing eight rows of nominal 2 1/4 inch O.D., 1.1 inch root diameter tubes was modified in order to obtain the heat transfer performance of individual rows of tubes transverse to the air flow. Figure 21 schematically presents the tube sheet pattern of the tubes in this tube bank and indicates the numbering scheme used to denote the various rows. It will be noted that the numbering commences with the row nearest the air inlet and proceeds down the tube bank ending with the row nearest the outlet.

The steam side portion of this unit was modified in order to obtain the row to row performance of the tubes. Many types of modifications were attempted, however, only the one found successful will be described here.

The top cover and bottom collector of the steam chest were removed exposing the ends of the tubes to the atmosphere. In the row to be investigated the ends of the tubes were fitted with rubber stoppers containing one hole drilled in the center of the stopper and a second near the edge of the stopper. A rod, slightly longer than the tubes

(about 21 inches long) and threaded on each end was pushed through the center holes of the stoppers as shown in Figure 29. Nuts and washers were then placed on the threaded ends and tightened against the tube until the stoppers were sufficiently compressed to prevent any leakage of steam. A short 3-4 inch length of 1/4 inch copper tubing was placed in the second hole of each stopper.

In the tops of the tubes (steam inlet end) the copper tubing was directly connected to an inlet steam manifold by means of lengths of rubber tubing. The inlet steam manifold, consisted of two - one inch pipe nipples threaded into a pipe tee, closed on one end and containing a valve and tube assembly on the other in order to continuously purge steam from the system. The one inch pipe nipples were drilled and tapped for eleven - 3/8 inch pipe nipples on which one end of the rubber tubing was fitted. One of the rubber stoppers was fitted with a second section of copper tubing. This piece of copper tubing was connected to the steam pressure gauge in order to read the steam pressure within the finned tubes.

The copper tubing from the bottom of the finned tubes was connected to a manifold. The condensate manifold consisted of a 3/4 inch pipe drilled and tapped for 3/8 inch pipe nipples. The manifold was closed on one end and contained a globe valve in order to control the rate of flow of the steam condensate. Beyond the control valve was fitted a short length of nominal 2 1/4 inch O.D., 1.1 inch root diameter finned tubing in order to subcool the condensate and prevent serious flashing of the steam condensate.

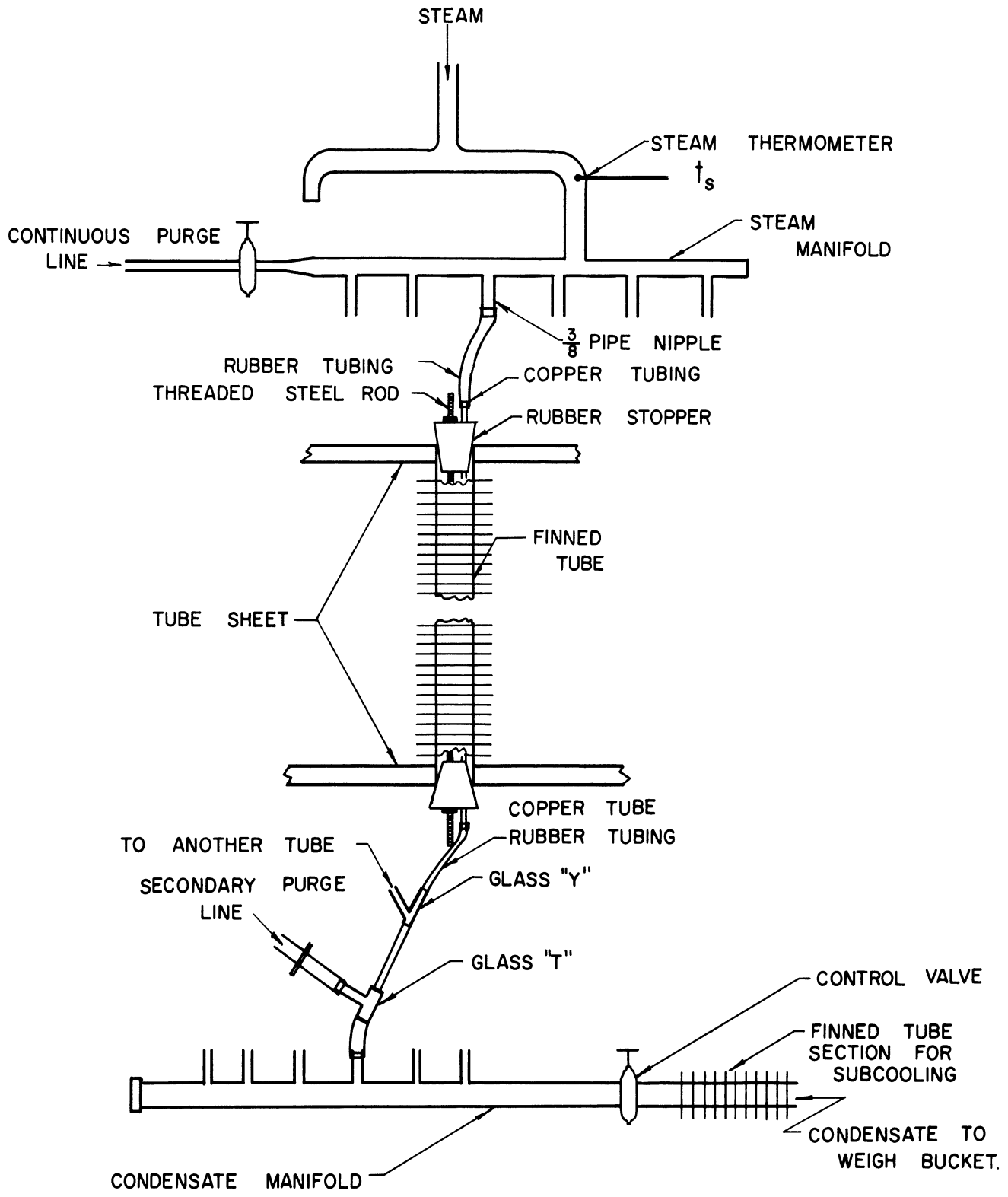

Figure 29. Modification of Steam Supply Used in Determining the Row to Row Performance.

Insulation was placed around the steam manifold and on both tube sheets. A series of runs were then taken and then the entire unit was moved to the succeeding row. In this manner, only a single row of tubes were heated for a series of runs in this study.

F. Modifications Employed to Obtain Steam Film Condensing Coefficients

In order to simultaneously determine the two film resistances governing the rate of heat transfer to the finned tube (air film resistance and steam film resistance) it is necessary to know an intermediate temperature, such as the wall of the tube. These date were obtained for two of the tubes included in unit number 8 by fastening copper-constantan thermocouples to the exterior of the tubes.

Thermocouples were attached to one of the tubes in the first row and one in the last row by holding the wire against the outside root portions of the tubes while placing a drop of thermosetting epoxy plastic over the tip and against the tube wall. The thermocouples were located approximately one foot down from the top of the tubes.

Since the resin used has a relatively low thermal conductivity, the above procedure insulates the thermocouple junction from the outside air.

G. Modifications Employed for Turbulence Measurements

A special test section used for measuring the degree of turbulence is described in Appendix C.

IV. EXPERIMENTAL PROCEDURE AND DATA

The techniques developed in obtaining the experimental data can be divided into four catagories. The four divisions listed below include: (1) the procedure used and data obtained for the performance characteristics of the tube banks; (2) the determination of the steam condensing coefficients; (3) the heat transfer coefficients of individual rows of tubes, and (4) the flow conditions of the air approaching the tube bank.

A. Experimental Procedure and Data for the Performance Characteristics of Tube Banks

The experimental technique developed for obtaining the performance characteristics of the tube banks is listed below in approximate chronological order. The blower motor was generally started with no external resistances in either the field or the armature circuits. The purge and outlet steam condensate valves were completely opened with no water flowing in the condensate sub-cooler. The steam valves were then opened sufficiently to produce a full scale reading on the steam pressure gauge (5 psig). This condition was maintained for about five minutes or until large quantities of steam were first seen to emerge from the condensate outlet line, following which the steam chest was deemed purged of air and the condensate control valves were closed and the steam throttled to produce 3 psig in the steam chest. Upon the appearance of condensate in the sight glass, the condensate control valves were adjusted so as to maintain the condensate level within the range of the sight glass which was about 5 inches in length. After making minor corrections to the steam pressure and condensate control

valves, the atmospheric pressure and humidity were obtained using the instruments described in the previous section.

A steady state condition of the heat transfer was checked with an uncalibrated mercury-in-glass thermometer placed in the exit air steam. Upon obtaining a constant reading of this thermometer over a five minute interval, a run was started.

The first step involved the simultaneous starting of the timer and collection of the condensate. Readings were taken of the outlet air pressure and inlet air and steam temperatures. The anemometer was placed in front of the tube bank and started simultaneously with the stop-watch. The outlet air temperature profile was then obtained using the thermocouple-potentiometer equipment previously described. Fourteen thermocouple readings were obtained during which time five anemometer and four inlet air temperature readings were recorded. The outlet air pressure was checked and the weight of condensate collected and time of collection were then recorded. A minimum of fifty pounds of condensate was collected. The duration of a run was about one half hour except for a few low air velocity runs where more time was required to collect the minimum amount of condensate. The heat gained by the air and the heat lost by the steam were then calculated from the data and, if the per cent discrepancy between these two quantities was below 5% the run was finished and a new run started.

For the second run of a series, the air velocity was changed by addition of resistances to either the armature or field circuits of the motor. Care was taken during the change in air velocity to maintain a minimum of 2 psig steam pressure in the steam chest. The general

procedure used was the same as for the first run except that the inlet air pressure and humidity were assumed constant over a maximum period of four hours. The data obtained for run number 709, unit number 7 are presented in Table IV.

For any individual run the heat lost by the steam is related to the condensate flow rate by:

$$Q_s = W_s (\Delta H) \qquad (16)$$

where: Q_s = heat released by the steam, Btu/hr

W_s = flow rate of condensate, Lb/hr.

and ΔH = difference in enthalpy between the incoming steam and exit condensate, Btu/lb.

Neglecting the sub-cooling of the condensate due to the temperature drop across the condensate film, the enthalpy difference is given by:

$$\Delta H = \lambda + (c_p)_s(\Delta t) \qquad (17)$$

in which:

λ = latent heat of vaporization of steam[25], Btu/lb.

$(c_p)_s$ = heat capacity of steam near atmospheric pressure, Btu/lb - °F

and Δt = degrees of superheat of the incoming steam, °F.

The error resulting from the neglection of the sub-cooling was estimated to be less than one-half of one per cent for the worst case, whereas the superheat energy generally amounted to slightly more than one per cent of the total energy released by the steam.

The energy gained by the air is given by:

TABLE IV

EXPERIMENTAL DATA OBTAINED FOR RUN 709

Barometer Reading = 742.2 mm Hg

Barometer Temperature = 22°C

Correction to be Added[22] = -2.8 mm Hg

Barometric Pressure = 739.4 mm Hg

Steam Pressure = 3 psig

Δp = 0.191 inches water

Steam Temperature = 234°F

Air Wet Bulb Temp. = 73°F

Air Dry Bulb Temp. = 70°F

Position*	M.V.	Amb. Temp. °F
26 1/2	2.320	79.0
25	2.176	
23	3.037	
21	3.038	
19	2.928	
17	2.932	
15	2.988	80.1
13	3.001	
11	3.009	
9	2.940	
7	2.819	
5	2.379	
3	1.820	
1	1.300	80.9
average	2.621	80.0

Inlet Air Temperature

Rdg.	°C
1	23.8
2	24.0
3	24.3
4	24.2
5	24.6
avg.	24.2

Anemometer Readings

Rdg. ft.	Time	Anemometer Velocity, ft/min
2404	10	240
1981	8	248
3217	13	247
2288	9	254
3040	12	253
	avg.	248

* Distance in inches from right wind tunnel wall, facing downstream

$$Q_a = W_a \, c_p \, (\Delta t)_m \qquad (18)$$

where: Q_a = thermal energy gained by the air, Btu/hr.

W_a = mass flow rate of air, Lb/hr.

c_p = heat capacity of inlet air at constant pressure, Btu/Lb °F

and Δt_m = mean temperature rise of air, °F

The mass flow rate of the air was calculated from:

$$W_{air} = V_f \times 60 \times A_f \times \rho \qquad (19)$$

where: V_f = velocity of air approaching the tube bank, ft/min.

A_f = flow area of duct at air velocity measurement position, a constant = 5.375 sq. ft.

and ρ = density of air approaching the tube bank, Lb/ft^3

The density of the air was computed for dry air from the perfect gas law[26], and then corrected for the amount of water vapor present (see Table V). The air velocity was obtained from the corrected anemometer reading. The fact that the anemometer was placed in a single location implies the assumption of a constant air velocity over the area immediately upstream from the tube bank. This assumption was checked without a tube bank in place and as will be shown later was found to be in error by less than 1.5%.

The heat capacity for air is given in Table V for various values of absolute humidity. These values were calculated from the equation:

$$c_p = 0.240 \left(\frac{1}{1 + H'}\right) + 0.44 \left(\frac{H'}{1 + H'}\right) \qquad (20)$$

TABLE V

EFFECT OF HUMIDITY ON THE PHYSICAL PROPERTIES OF DRY AIR

Absolute humidity Lbs H_2O/$lb_{dry\ air}$	Air heat capacity Btu/lb °F	Density of mixture / Density of dry air
0	0.240	1.000
0.002	0.240	0.999
0.004	0.241	0.998
0.006	0.241	0.997
0.008	0.242	0.996
0.010	0.242	0.995
0.012	0.242	0.993
0.014	0.243	0.992
0.016	0.243	0.990
0.018	0.244	0.989
0.020	0.244	0.988

where: 0.240 = heat capacity of dry air at 80°F and 1 atm. pressure[20], Btu/lb °F

0.44 = heat capacity of water vapor at 80°F and 1 atm. pressure,[20], Btu/lb °F

and H' = absolute humidity of the air, lbs of water vapor per pound of dry air.

The mean temperature rise of the air in flowing through the tube bank was calculated from the inlet and outlet air temperature measurements. The inlet air temperature used in these calculations was the average of five readings. The average outlet air temperature was computed from the average of fourteen thermocouple readings taken every two inches along the horizontal centerline behind the exchanger. The corresponding temperature profile for the exit air is given for run number 407 of unit number 4 in Figure 30 where the temperature rise of the air is plotted versus the distance from the vertical centerline of the unit. The general nature of this particular temperature profile was characteristic of the outlet air temperature measurements on this and the other tube banks investigated.

The variation between the measured temperature rises at various points is due to incomplete mixing of the air across the width of the exchanger. In order to verify the general accuracy of the procedure used in obtaining the mixed mean outlet air temperature, measurements were taken every 1/2 inch along the same centerline for two runs at low and high air velocities for unit number 7, a total of 53 points being required. A further check of the accuracy of the general procedure was made by obtaining a single air temperature measurement at a point approximately five feet down stream from the last row of tubes of the exchanger.

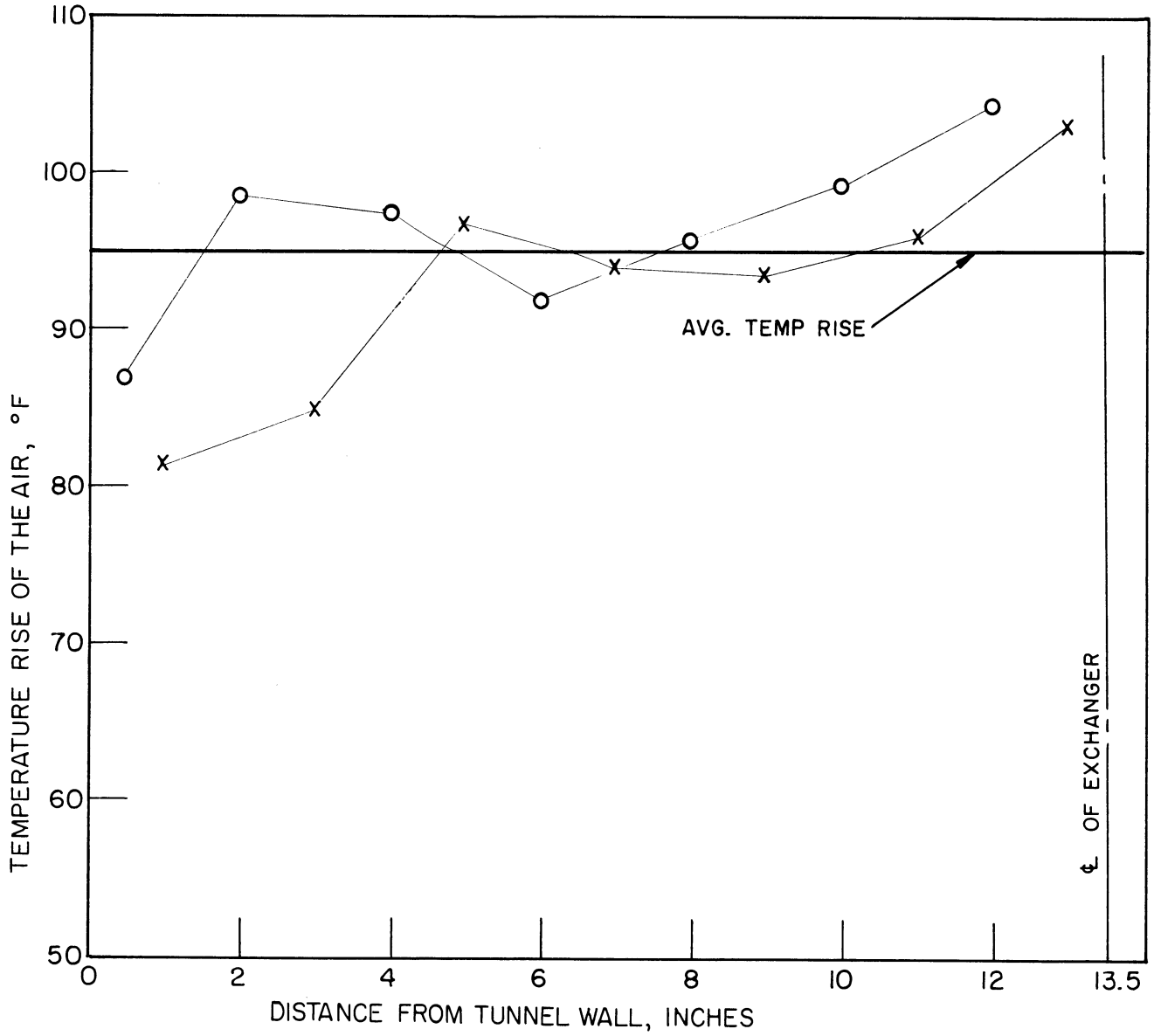

Figure 30. Temperature Profile of Exit Air for Run Number 407.

The three air temperature measurements and calculated heat transfer values are compared in Table VI for one of the runs.

TABLE VI

COMPARISON OF CALCULATED RESULTS FROM THREE DIFFERENT OUTLET AIR TEMPERATURE MEASURING TECHNIQUES

RUN NO. 708

Calculated Result	Average of 14 temperature measurements	Average of 53 temperature measurements	Single mixed mean measurement
Outlet air temperature, °F	162.2	161.2	160.8
Air side heat duty Btu/hr	288,000	285.000	284.000
Steam side heat duty, Btu/hr	282,000	282,000	282.000
Per cent discrepancy in Q's, %	2.1	1.0	0.7
Mean temperature difference ΔT_m, °F	93.5	93.9	94.1
U_o, Btu/hr - °F sq.ft.	11.55	11.40	11.34
h_o, Btu/hr - °F sq.ft.	15.0	14.8	14.7

The second run of this nature (Run 709) gave results comparible to those presented above on a percentage basis. Examination of Table VI indicates that the difference between the three measuring techniques is small and the average of the fourteen points (used in all experimental runs except two) yields reasonably accurate calculated results.

The overall coefficient of heat transfer is related to the heat duty by the relationship:

$$U_o = \frac{Q}{A_o (\Delta T_m)} \qquad (21)$$

The heat duty used in computing the overall coefficient was taken as the average of the steamside and airside heat duties. The heat transfer area was computed as the sum of the root and finned areas of the tubes plus the area of the tube sheets under the steam chests. The latter area was small compared to the area of the tubes, generally amounting to less than 5 per cent of the total. The mean temperature difference driving force is related to the saturated steam, inlet and outlet air temperature by:

$$\Delta T_m = \frac{(t_o - t_i)}{\ell n \left(\frac{t_{ss} - t_i}{t_{ss} - t_o} \right)} \qquad (22)$$

in which: t_o = mean outlet air temperature, °F

t_i = inlet air temperature, °F

t_{ss} = temperature of steam corresponding to the absolute pressure of steam in steam chest, °F (43)

The mean air film heat transfer coefficient is related to the overall coefficient and the other individual resistances to heat transfer by (assuming no fouling):

$$\frac{1}{h_o} = \frac{1}{U_o} - r_f - r_m - \frac{A_o}{A_i h_i} \qquad (23)$$

in which: r_f = resistance of the fin metal, hr-°F - sq.ft./Btu

r_m = resistance of the root metal, hr-°F - sq.ft./Btu

h_i = steam condensing coefficient, Btu/hr - °F-sq.ft.

and A_o/A_i = ratio of external to internal heat transfer area, dimensionless.

The fin resistance was computed from the relationship[17]:

$$r_f = \frac{\frac{2H^2}{3K_m Y}\sqrt{\frac{D_o}{D_r}}}{1 + \frac{A_r}{A_f}\left(1 + h_o \frac{2H^2}{3K_m Y}\sqrt{\frac{D_o}{D_r}}\right)} \qquad (24)$$

which is valid for fin efficiencies between 80 and 100 per cent[16,17].

The resistance of the root metal wall was computed using the relationship:

$$r_m = \frac{X A_o}{k_m A_m} \qquad (25)$$

The condensate film coefficient was calculated using the theoretical relationship of Nusselt for flow down a flat surface. The relationship, on a tube loading basis is[20]:

$$h_i = 0.826 \left(\frac{k_f^3 \rho_f^2 g_c \lambda}{\mu_f L}\right)^{1/3}\left(\frac{A}{Q}\right) \qquad (26)$$

However, since the physical properties and the condensing length of the steam are constant, equation 26 can be reduced to:

$$h_i = 36{,}000 \left(\frac{A}{Q}\right)^{1/3} \qquad (27)$$

where the area is the total inside area of the tubes.

The fin metal and root metal resistances are essentially constant as indicated in Table VII for the tubes used in unit number 7, therefore a plot can be calculated, a priori, for each unit giving the sum of the metal and steam resistances versus the rate of heat transfer, Q. Such a plot is given in Figure 31 for the tubes used in unit number 7.

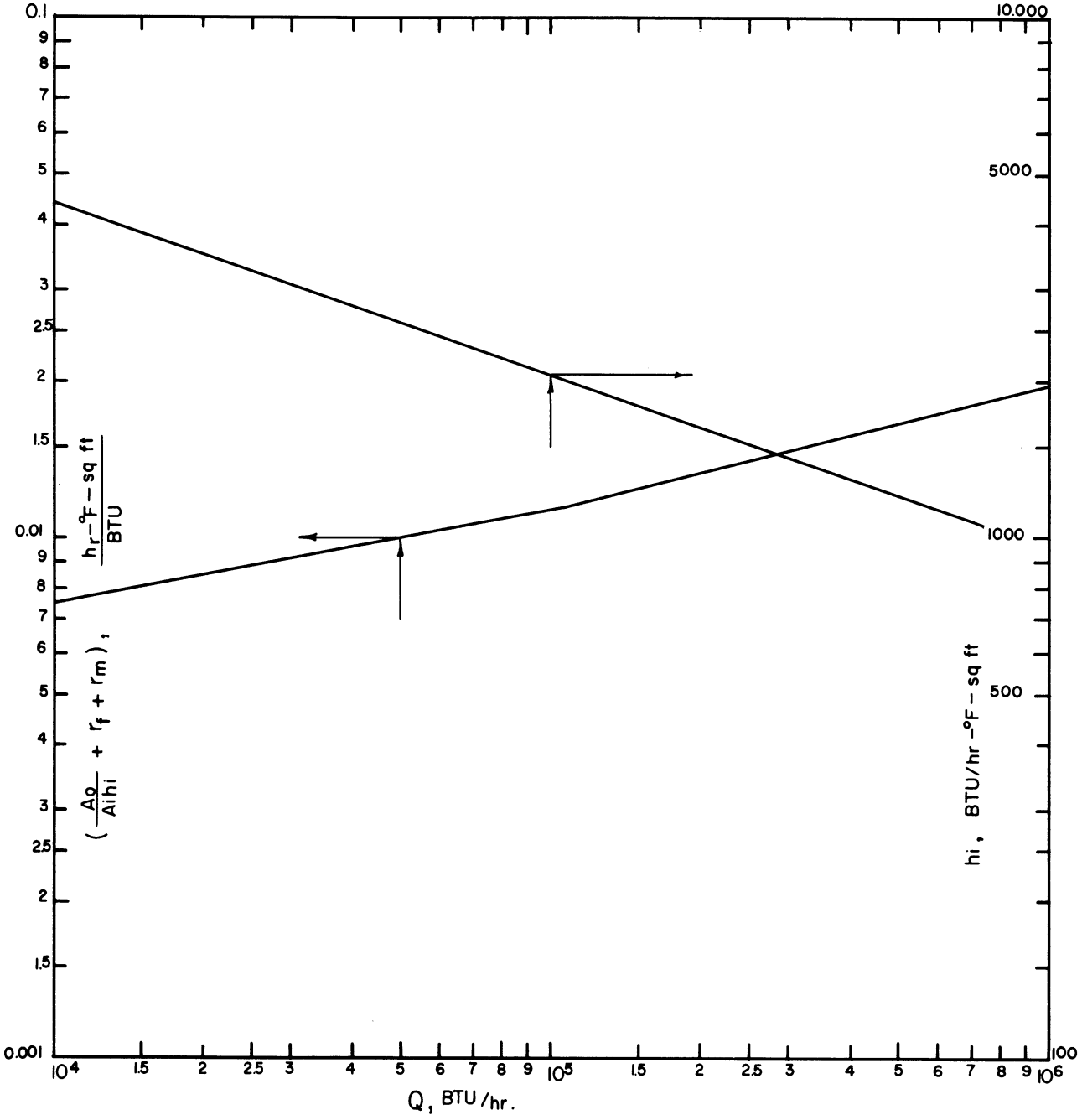

Figure 31. Sum of Steam and Metal Resistances of Tubes Used in Unit Number Seven versus Heat Duty.

TABLE VII

VARIATION OF FIN RESISTANCE WITH AIR FILM HEAT TRANSFER COEFFICIENT FOR THE TUBES USED IN UNIT NUMBER SEVEN

h_o	r_f
0	0.00367
10	0.00366
20	0.00365
30	0.00364
root metal resistance -	0.00052

The air film coefficient can be calculated by substituting the value of these resistances and the overall coefficient data into equation 23.

Tables VIII through XV summarize the heat transfer data obtained on the seven finned and one plain tube bank. Also included in these tables are the pressure drop data of the eight tube banks. The heat transfer coefficients for the seven finned tube banks are plotted on Figure 32 versus the maximum air velocities. This air velocity is defined as the average velocity that the air would have in passing through the minimum cross sectional area at a density of 0.074 pounds mass per cubic feet. This type of representation is equivalent to a plot of h_o versus G_{max}, the pounds per hour - sq.ft. cross sectional area, since:

$$G_m = V_m \rho 60 \qquad (28)$$

Table VIII. Original and Processed Data for Unit Number 1

RUN NO.	Q_s (STEAM) BTU/hr	Q_a (AIR) BTU/hr	W_{air} Lbs/hr	V_{max} ft/min at ρ=0.074	T_{steam} (Sat.) °F	t_{inlet} AIR °F	t_{outlet} AIR(MEAN) °F	ΔT_M °F	BTU/hr-°F-sq.ft U_o	BTU/hr-°F-sq.ft h_o	$\frac{h_o D_r}{k}/P_r^{1/3}$	$\frac{D_r G}{\mu}$	Δp INCHES OF WATER	$\Delta p/n$ INCHES OF WATER PER ROW
106	151000	154000	10950	3400	220.6	58.4	136.8	110.0	28.6	28.9	118.0	18950	1.85	0.308
107	144000	149000	10970	3410	220.6	79.1	135.6	107.5	27.9	28.2	115.0	18700	1.84	0.307
108	125000	127000	8550	2640	220.6	79.2	141.0	107.0	24.2	24.5	99.5	14600	1.19	0.195
109	125000	123000	8600	2660	220.6	79.5	138.7	108.3	23.5	23.7	96.0	14700	1.19	0.195
110	109000	107000	6540	2020	220.6	80.8	149.1	102.0	21.6	21.8	84.3	11200	0.78	0.130
111	100000	100000	6020	1860	220.2	81.7	151.2	100.0	20.6	20.8	84.0	10250	0.67	0.110
112	82800	84000	4890	1510	220.2	81.7	153.1	98.8	17.6	17.8	72.0	8350	0.47	0.078
113	82800	83800	4940	1525	220.2	81.7	152.1	100.0	17.1	17.3	70.0	8430	0.46	0.076
114	74400	74500	4210	1300	220.2	81.7	155.0	97.8	15.6	15.7	63.3	7170	0.37	0.061
115	53800	55500	2500	782	220.2	82.2	165.7	90.0	11.8	11.9	47.6	4300	0.15	0.025
116	54100	52600	2470	760	220.2	82.0	170.5	87.7	12.4	12.4	50.0	4160	0.15	0.025
117	36100	--*	1138*	462*	220.6	74.4	178.8	83.4	8.9	8.9	35.7	2530	0.056	0.0093
118	33300	--*	1262*	390*	220.6	74.7	180.8	81.6	8.1	8.2	32.6	2130	0.047	0.008
119	50400	--*	2220*	678*	220.6	74.5	170.0	90.3	11.6	11.7	47.1	3720	0.110	0.018
120	68000	70100	3290	1015	220.6	74.8	163.9	95.0	14.9	15.0	60.6	5600	0.235	0.039
121	62000	64500	2820	868	220.6	74.0	169.0	91.4	14.2	14.3	57.3	4750	0.180	0.030

*BEYOND LOWER RANGE OF ANEMOMETER
HEAT BALANCE ASSUMED

Table IX. Original and Processed Data for Unit Number 2

RUN NO.	Q_s (STEAM) BTU/hr	Q_a (AIR) BTU/hr	W_{air} Lbs/hr	V_{max} ft/min at ρ=0.074	T_{steam} (Sat.) °F	t_{inlet} AIR °F	t_{outlet} AIR(MEAN) °F	ΔT_M °F	BTU/hr-°F-sq.ft U_o	BTU/hr-°F-sq.ft h_o	$\frac{h_o D_r}{k}/P_r^{1/3}$	$\frac{D_r G}{\mu}$	Δp INCHES OF WATER	$\Delta p/n$ INCHES OF WATER PER ROW
201	247000	251000	12800	2830	219.8	80.5	163.0	91.6	21.2	22.9	89.0	13800	2.05	0.362
202	220000	226000	11120	2460	219.8	81.2	165.4	89.9	19.4	20.7	80.0	12000	1.53	0.255
203	186000	193000	9020	1990	220.0	78.8	167.6	89.3	16.6	17.5	68.6	9730	1.03	0.172
204	167000	173000	7720	1705	220.0	78.5	171.0	87.3	15.2	15.9	61.5	8300	0.804	0.134
205	151000	158000	6600	1470	220.7	73.8	171.0	88.3	13.6	14.2	55.5	7180	0.584	0.097
206	127000	129000	5330	1175	220.7	74.9	175.5	85.9	11.6	12.2	47.0	5750	0.428	0.071
207	100000	98000	3730	824	220.7	75.4	182.0	80.5	9.6	9.9	37.8	3980	0.252	0.042
208	49000	--*	1820*	402*	220.7	80.6	191.8	70.5	5.4	5.5	20.8	1930	0.076	0.013
209	60000	--*	2300*	508*	220.1	81.5	189.3	71.9	6.5	6.6	25.0	2430	0.098	0.016
210	72500	73000	2860	630	220.1	81.7	187.2	73.3	7.8	7.9	30.0	3030	0.153	0.0255
211	35400	--*	1292*	286*	220.1	82.8	195.8	65.4	4.2	4.2	16.1	1360	0.033	0.0056
212	69600	72600	2658	586	220.5	78.4	190.0	72.5	7.7	7.8	29.7	2810	0.126	0.021
213	90500	90500	3490	770	220.5	79.1	184.8	76.9	9.2	9.4	35.7	3700	0.205	0.0362
214	115000	114800	4600	1015	220.5	79.1	180.7	80.1	11.2	11.5	44.5	4890	0.346	0.0577
215	227000	230000	11050	2440	220.5	79.5	165.0	91.5	19.5	20.9	81.4	11900	1.72	0.287
216	239500	247000	11950	2640	220.5	79.0	163.8	93.3	20.4	21.8	84.5	12900	1.95	0.325
217	24100	--*	874*	181*	220.5	80.5	200.5	61.6	3.1	3.1	11.6	864	0.014	0.0024

*BEYOND LOWER RANGE OF ANEMOMETER
HEAT BALANCE ASSUMED

Table X. Original and Processed Data for Unit Number 3

RUN NO.	Q_s (STEAM) BTU/hr	Q_a (AIR) BTU/hr	W_{air} Lbs/hr	V_{max} ft/min at ρ=0.074	T_{steam} (Sat.) °F	t_{inlet} AIR °F	t_{outlet} AIR(MEAN) °F	ΔT_M °F	BTU/hr-°F-sq.ft U_o	BTU/hr-°F-sq.ft h_o	$\frac{h_o D_r}{k}/P_r^{1/3}$	$\frac{D_r G}{\mu}$	Δp INCHES OF WATER	$\Delta p/n$ INCHES OF WATER PER ROW
305	42500	--*	1440*	256*	220.3	83.7	204.0	56.5	5.3	5.3	17.6	1060	0.035	0.0058
306	65000	64000	2280	404	220.3	84.4	199.6	61.2	7.1	7.2	23.7	1680	0.070	0.0117
307	93000	93000	3540	630	220.3	85.6	193.0	67.4	9.7	10.0	33.1	2630	0.150	0.025
308	134000	132000	5380	954	220.3	86.0	185.2	73.8	12.7	13.3	44.3	4000	0.330	0.055
309	180000	185000	8110	1440	220.3	86.4	179.5	78.1	16.4	17.6	59.0	6050	0.660	0.110
310	240000	241000	11680	2065	220.3	87.8	172.1	83.5	20.3	22.1	73.9	8720	1.30	0.216

*BEYOND LOWER RANGE OF ANEMOMETER
HEAT BALANCE ASSUMED

Table XI. Original and Processed Data for Unit Number 4

401	221000	219000	9350	1510	220.3	89.1	184.5	73.5	15.5	17.2	52.4	6430	0.80	0.133
402	177000	181000	7460	1210	220.3	89.6	188.8	69.7	13.3	14.4	44.5	5110	0.51	0.85
403	133000	133000	5240	849	220.3	89.8	193.4	65.6	10.5	11.1	35.0	3580	0.30	0.050
404	108000	106000	3780	614	220.3	84.2	197.8	63.1	8.8	9.3	29.3	2600	0.175	0.029
405	85000	82000	2860	463	220.3	85.8	202.4	57.7	7.5	7.8	25.0	2070	0.10	0.017
406	59000	--*	2030*	330*	220.3	87.4	205.5	54.0	5.5	5.6	18.2	1380	0.042	0.007
407	256000	255000	11200	1810	220.3	87.6	180.6	77.1	17.1	19.4	57.8	7750	1.08	0.180

*BEYOND LOWER RANGE OF ANEMOMETER
HEAT BALANCE ASSUMED

Table XII. Original and Processed Data for Unit Number 5

501	96500	98500	3570	477	220.4	80.0	192.4	69.6	9.0	9.7	25.8	1610	0.0795	0.013
502	128500	131000	5190	693	220.4	80.8	184.3	76.6	10.8	12.0	32.0	2330	0.140	0.023
503	178000	178000	7360	985	220.3	79.3	177.9	82.0	13.9	15.9	43.0	3360	0.268	0.045
504	229000	234000	10280	1370	220.3	79.3	172.1	86.7	17.3	21.0	56.6	4670	0.500	0.083
505	283000	290000	13700	1830	220.3	79.8	165.9	91.0	20.3	25.8	70.0	6260	0.900	0.150
506	255000	253000	11850	1580	220.3	82.0	169.3	87.7	18.6	22.8	61.5	5390	0.68	0.113
507	200000	202000	8650	1170	220.3	81.0	175.0	83.3	15.4	18.0	48.5	3980	0.385	0.064
508	152000	150000	6180	827	220.3	84.0	182.5	77.0	12.4	14.0	37.2	2800	0.210	0.035

Table XIII. Original and Processed Data for Unit Number 6

RUN NO.	Q_s (STEAM) BTU/hr	Q_a (AIR) BTU/hr	W_{air} Lbs/hr	V_{max} ft/min at ρ=0.07	T_{steam} (Sat.) °F	t_{inlet} AIR °F	t_{outlet} AIR(MEAN) °F	ΔT_M °F	BTU/hr-°F-sq.ft U_o	BTU/hr-°F-sq.ft h_o	$\frac{h_o D_r}{k}/P_r^{1/3}$	$\frac{D_r G}{\mu}$	Δp INCHES OF WATER	$\Delta p/n$ INCHES OF WATER PER ROW
601	236500	243500	17700	2990	220.3	76.4	132.7	114.0	13.2	16.0	117.0	27300	1.46	0.365
602	194000	196000	13100	2210	220.3	78.1	140.2	108.0	11.3	13.2	95.8	20100	0.82	0.205
603	162000	162000	10100	1710	220.3	79.3	144.8	104.9	9.7	11.0	79.2	15500	0.53	0.132
604	114000	116500	6300	1063	220.3	80.0	155.4	97.9	7.4	8.1	58.0	9540	0.20	0.050
605	34500	--*	1890*	320*	219.6	84.6	193.8	66.0	3.3	3.4	23.4	2780	0.021	0.005
606	66000	65500	2890	600	219.6	84.2	176.7	80.4	5.1	5.4	37.9	5300	0.068	0.017
607	235000	233000	16850	2850	219.6	87.9	138.3	108.8	13.5	16.4	119.0	25800	1.42	0.355

*BEYOND LOWER RANGE OF ANEMOMETER
HEAT BALANCE ASSUMED

Table XIV. Original and Processed Data for Unit Number 7

701	214500	221000	10100	1830	220.0	81.8	171.4	85.6	9.6	11.7	81.0	16000	0.81	0.202
702	232000	243000	11320	2060	219.9	81.5	168.2	88.0	10.1	12.5	87.7	18100	1.03	0.257
703	179000	180000	7910	1440	219.9	81.9	175.3	82.5	8.2	9.6	67.0	12700	0.58	0.145
704	131000	129000	5290	960	219.9	83.0	182.3	76.9	6.4	7.1	49.2	8370	0.311	0.078
705	88000	86000	3280	597	219.9	84.2	190.8	69.1	4.9	5.1	35.6	5160	0.155	0.039
706	53500	--*	1610*	293*	219.9	84.6	203.9	55.8	3.4	3.5	23.6	2640	0.057	0.014
707	117000	117000	4640	844	219.9	82.8	185.6	74.1	6.0	6.6	45.1	7350	0.25	0.062
708	282000	288000	14300	2600	220.1	93.5	162.2	93.5	11.5	15.0	104.8	23400	2.10	0.350
709	113000	108500	3880	705	220.3	75.6	189.5	7 .0	5.6	6.0	41.9	6120	0.191	0.048

*BEYOND LOWER RANGE OF ANEMOMETER
HEAT BALANCE ASSUMED

Table XV. Original and Processed Data for Unit Number 8

801	334000	322000	11150	1460	219.7	81.0	199.4	60.9	9.4	12.6	87.5	12750	1.42	0.175
802	330000	327000	11380	1490	219.7	80.6	198.4	62.6	9.2	12.2	84.8	13000	1.42	0.175
803	410000	419000	14100	1840	219.7	74.7	196.5	66.5	10.7	15.2	105.5	16200	1.97	0.246
805	377000	377000	12900	1690	219.7	76.7	196.5	66.0	10.0	13.7	95.0	14800	1.85	0.231
806	283000	295000	9550	1250	219.7	77.7	202.4	59.1	8.5	10.9	75.5	10950	1.08	0.135
807	234000	233000	7250	950	220.3	75.2	207.5	54.5	7.5	9.2	65.5	8290	0.70	0.088
808	189000	185000	5860	770	220.3	77.9	207.0	50.5	6.5	7.7	53.4	6730	0.53	0.066
809	145000	138000	4350	570	220.3	80.5	210.2	43.0	5.9	6.7	39.5	4950	0.32	0.041

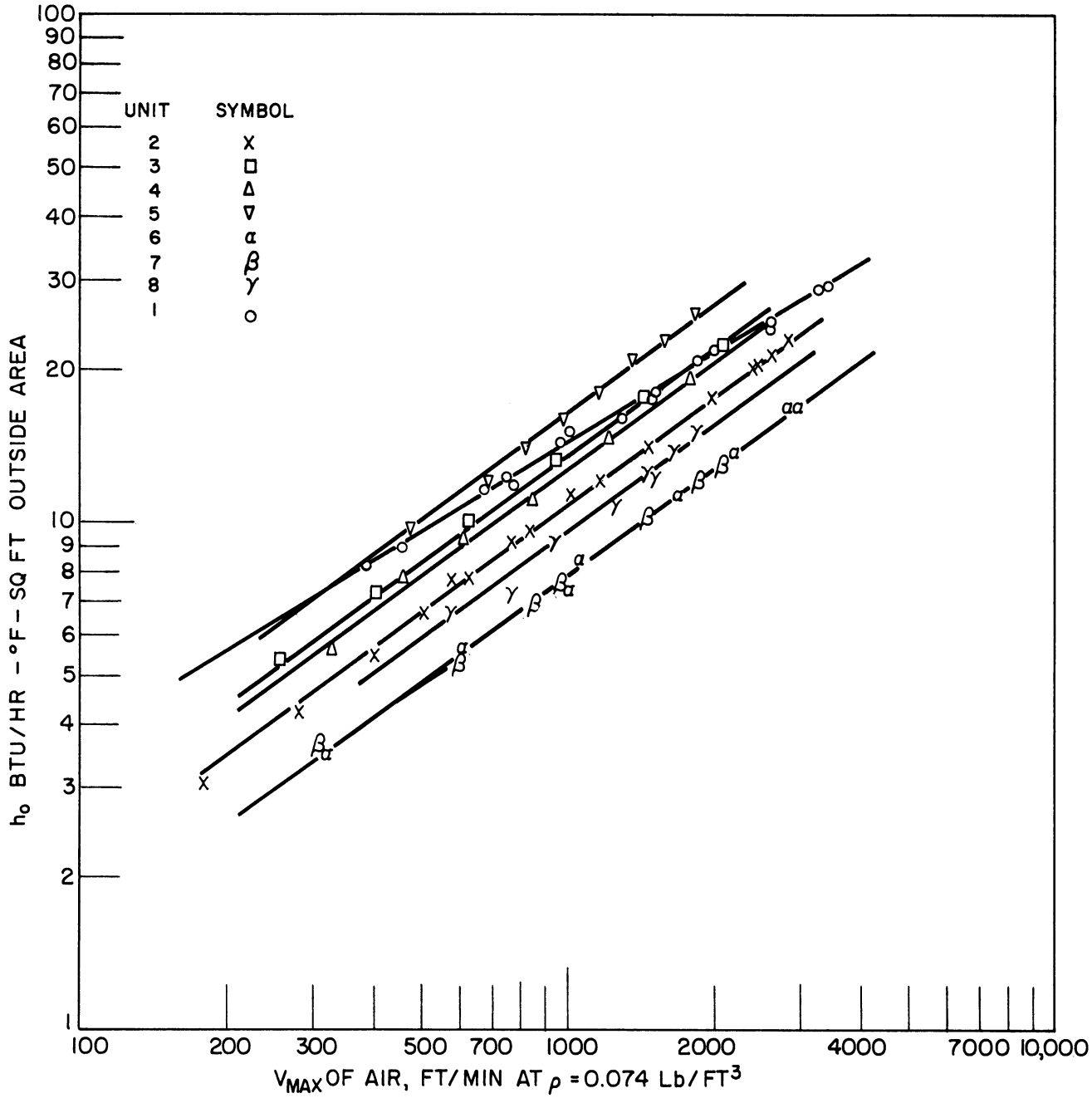

Figure 32. Heat Transfer Curves Obtained for the Seven Finned Tube Banks.

A sample calculation of an individual run is given in Appendix A.

The primary purpose of obtaining the data on the plain tube bank was not to question the validity of the existing data, but rather to provide a measure of the degree to which the data provided here can be compared with existing heat transfer data. The experimental heat transfer coefficients are plotted on Figure 33 and compared with two other sources of data for geometrically similar units on Figure 34[20,27]. Examination of Figure 34 indicates reasonable agreement between the data presented here for this unit and the data appearing in the literature.

B. Steam Condensing Coefficients

The steam condensing coefficients were calculated from wall temperatures obtained on one tube bank, unit number eight. Ignoring the small metal resistance of the root wall, a heat balance indicates that:

$$h_i A_i (t_{ss} - t_m) = U_o A_o (t_{ss} - t_o) \qquad (29)$$

in which: A_i = inside area of the tube, sq.ft./ft.

A_o = outside area of the tube, sq.ft./ft.

t_{ss} = temperature of saturated steam, °F.

t_m = metal temperature of the root wall, °F.

and t_o = mean outside air temperature, °F

Thus, from thermocouples attached to the root wall of the tubes, as described in the previous section, intermediate temperature measurements were made and the inside steam condensing coefficients calculated. The

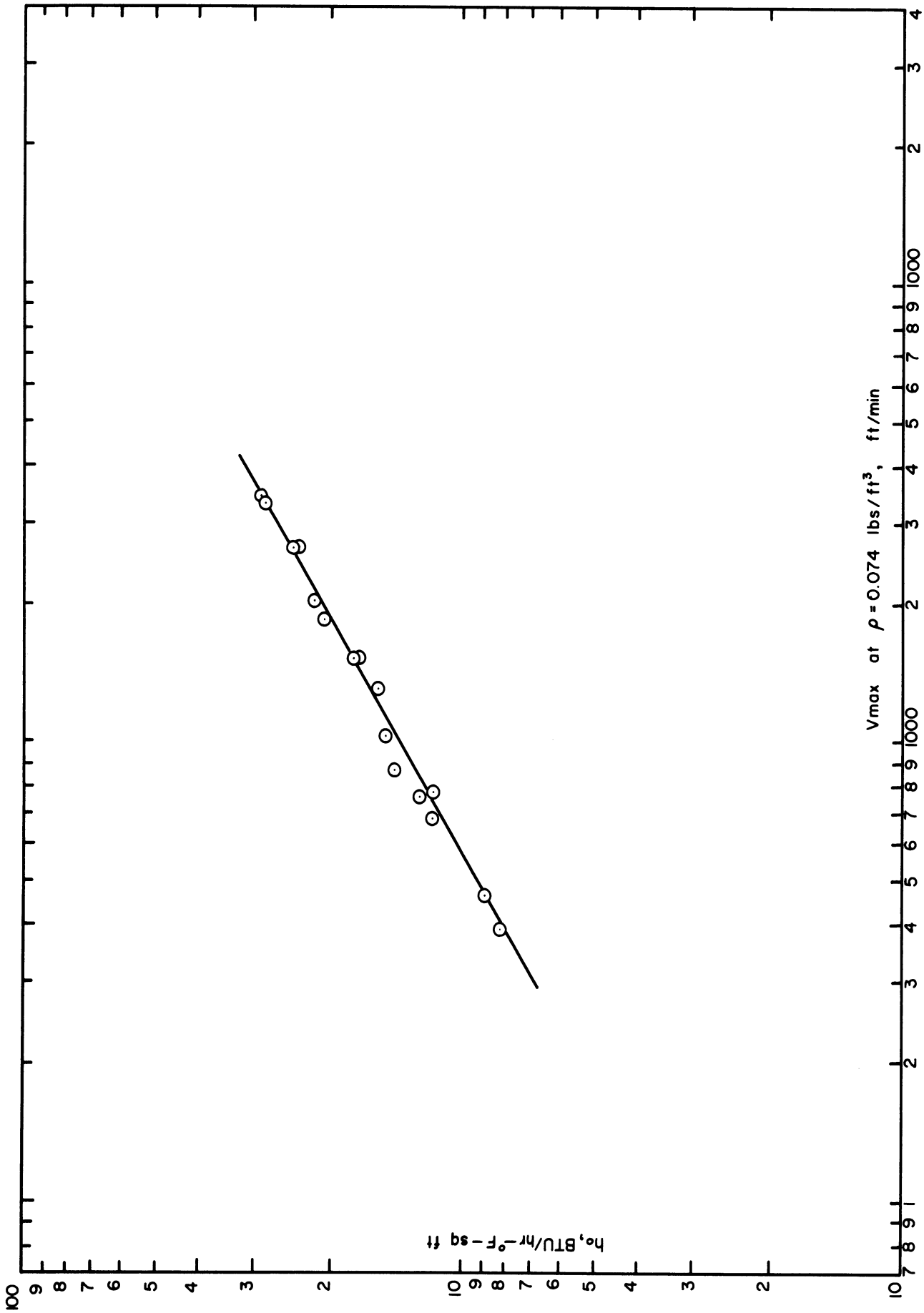

Figure 33. Summary of Heat Transfer Data of Plain Tube Bank.

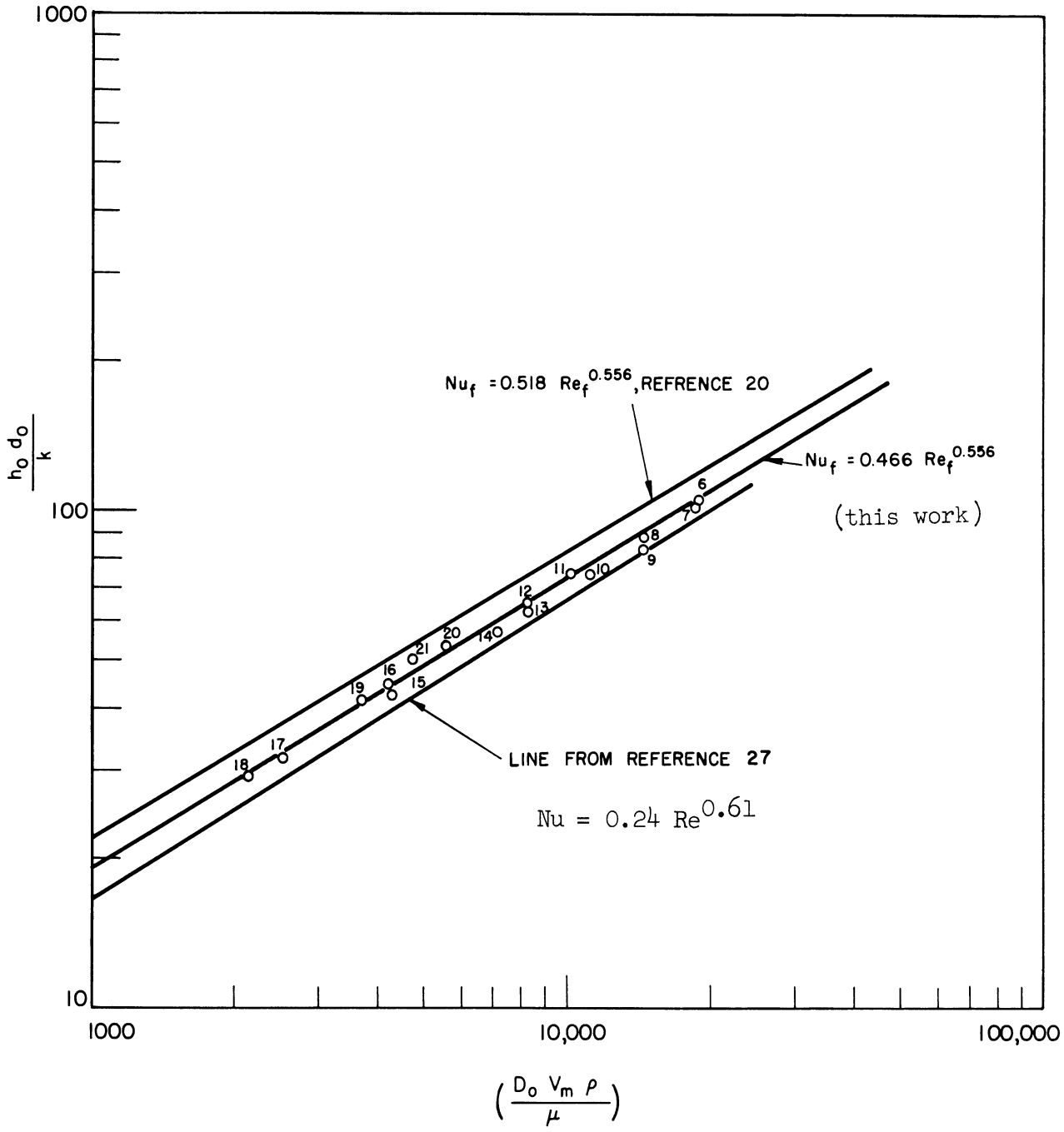

Figure 34. Comparison of Plain Tube Heat Transfer Results with Results on Geometrically Similar Units Available in the Literature.

coefficients thus calculated are point coefficients for the positions on the tubes where the thermocouples were attached. The relationship between the point coefficients and the temperature drop across the condensate film are derived in Appendix E, using Nusselt's condensing theory, while a sample calculation for one run is presented in Appendix A. The data obtained are summarized in Table XVI and Figure 35 where the point steam condensing coefficients are plotted versus the temperature drop across the condensate film. Also included on this figure is the line derived in Appendix E from Nusselt s condensing theory. As can be noted from this figure, the data fall about the theoretical

TABLE XVI

SUMMARY OF EXPERIMENTAL AND CALCULATED RESULTS - STEAM CONDENSING COEFFICIENTS

Run	Thermo-couple*	$t_{sat.\ steam}$ °F	t_{wall} °F	Δt_i °F	(h_i) experimental Btu/hr-°F-sq.ft.	(h_i) Nusselt Btu/hr-°F-sq.ft.
801	F	219.7	200.8	18.9	1190	1120
	B	219.7	218.7	1.0	3300	2160
802	F	219.7	197.7	22.0	1000	1090
	B	219.7	217.9	1.8	1870	1900
803	F	219.7	198.8	20.9	1195	1100
	B	219.7	216.1	3.6	1190	1620
805	F	219.7	200.8	18.9	1300	1120
	B	219.7	218.5	3.6	3300	2080
806	F	219.7	202.4	17.3	1180	1140
	B	219.7	219.0	0.7	3600	2350
807	F	220.3	206.4	13.9	1340	1210
	B	220.3	219.0	0.4	4100	2650
808	F	220.3	207.5	12.8	1250	1250
	B	220.3	220.0	0.3	4300	2800
809	F	220.3	209.6	10.7	1320	1300
	B	220.3	220.4	approx.-	-	-

* F = Front B = Back

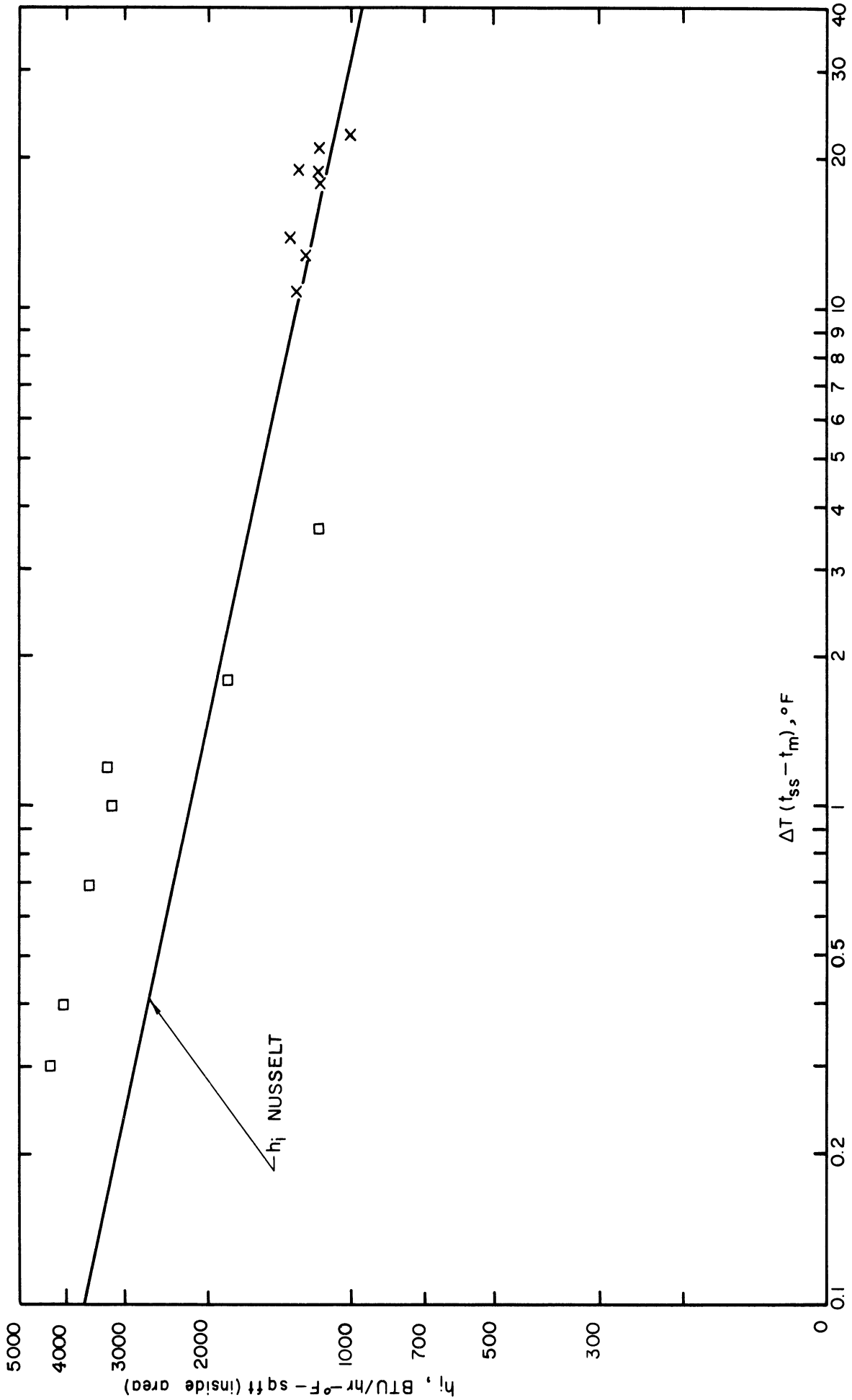

Figure 35. Summary of Steam Condensing Coefficient Data.

line except in the region of very low temperature differences. These deviations could be due to either experimental error in determining very small temperature differences or to some dropwise condensation at these small temperature differences. The principle conclusion drawn from these data is that for vertical tubes, the steam-side resistance can be predicted using Nusselt's theory with a reasonable degree of certainty.

C. Performance of Individual Rows of Tubes

The data in this series were obtained in the same manner as previously for the tube banks except that the condensate steam interface was maintained between the glass tee and glass Y indicated in Figure 29. The condensate was collected in a five gallon pail weighed before and after each run.

The data obtained in this portion of the investigation are summarized in Table XVII and Figure 36. The overall and air film heat transfer coefficients were calculated using the same procedures previously indicated. The total outside area used in these calculations was the outside area of the tubes in the heated row. No allowance was made for the fact that a portion of the tube-sheet immediately adjacent to the tube row being heated was hotter than the ambient air due to conduction; however, during the runs on the first row of tubes, the tube sheet adjacent to this row was felt with the hand. In this manner it was determined that the tube sheet temperature decreased rapidly, feeling relatively cool to the touch within a few inches. These data are compared with the data available in the literature in Figure 37. Examination of this figure indicates that the data obtained here has the

TABLE XVII. ORIGINAL AND PROCESSED DATA OBTAINED ON INDIVIDUAL ROWS OF TUBES (UNIT NUMBER 8).

RUN NO.	Q_s BTU/hr	Q_a BTU/hr	W_{air} Lbs/hr	V_{max} ft/min at ρ=0.074	T_{steam} (Sat.) °F	t_{inlet} AIR °F	t_{outlet} AIR °F	ΔT_M °F	A SQ.FT.	BTU/hr-°F-sq.ft U_o	BTU/hr-°F-sq.ft h_o	Δp INCHES OF WATER	$\Delta p/n$ INCHES OF WATER PER ROW
						FIRST ROW HEATED*							
11	72000	72000	11520	1510	220.2	77.7	103.3	129.5	75.0	7.35	9.35	1.40	0.175
12	66000	63000	8530	1118	220.2	77.9	108.1	127.0	75.0	6.75	8.30	0.83	0.104
13	54000	50000	5600	733	220.2	76.8	113.4	124.3	75.0	5.38	6.75	0.41	0.051
14	40000	37000	2190	381	220.2	79.8	131.2	112.1	75.0	4.35	4.87	0.15	0.019
						SECOND ROW HEATED*							
21	84000	84000	12200	1600	220.2	86.8	114.8	119.4	68.1	10.31	14.3	1.52	0.18
22	76000	75000	10000	1310	220.2	87.1	117.5	117.8	68.1	9.40	12.4	1.08	0.135
23	55000	52000	5440	713	220.2	87.8	126.5	111.5	68.1	6.85	8.26	0.39	0.049
24	43000	38000	3090	405	220.2	85.3	135.5	108.1	68.1	5.16	5.9	0.167	0.021
						THIRD ROW HEATED*							
31	60000	63000	5700	748	220.6	81.7	127.3	114.5	75.0	7.40	7.4	0.43	0.054
32	96000	97000	13000	1710	220.6	83.4	113.8	121.8	75.0	10.50	10.5	1.66	0.208
33	74000	78000	8650	1131	220.6	83.0	119.8	118.5	75.0	8.73	8.73	0.86	0.108
34	43000	41000	3360	400	220.6	84.0	139.3	106.6	75.0	5.15	5.15	0.19	0.024
						FOURTH ROW HEATED*							
41	90000	90000	12450	1630	220.3	77.9	107.5	127.6	68.1	10.38	10.38	1.53	0.190
42	78000	78000	9310	1220	220.3	78.1	112.1	125.0	68.1	9.1	9.1	0.93	0.116
43	61000	62000	6410	842	220.3	77.9	117.5	120.3	68.1	7.56	7.56	0.50	0.0625
44	41000	39000	3230	423	220.3	81.7	130.6	112.8	68.1	5.0	5.0	0.198	0.025
45	29000	30000	2040	268	220.3	81.9	142.4	105.0	68.1	4.22	4.22	0.10	0.0125

* Q_{air} USED IN CALCULATING U_o

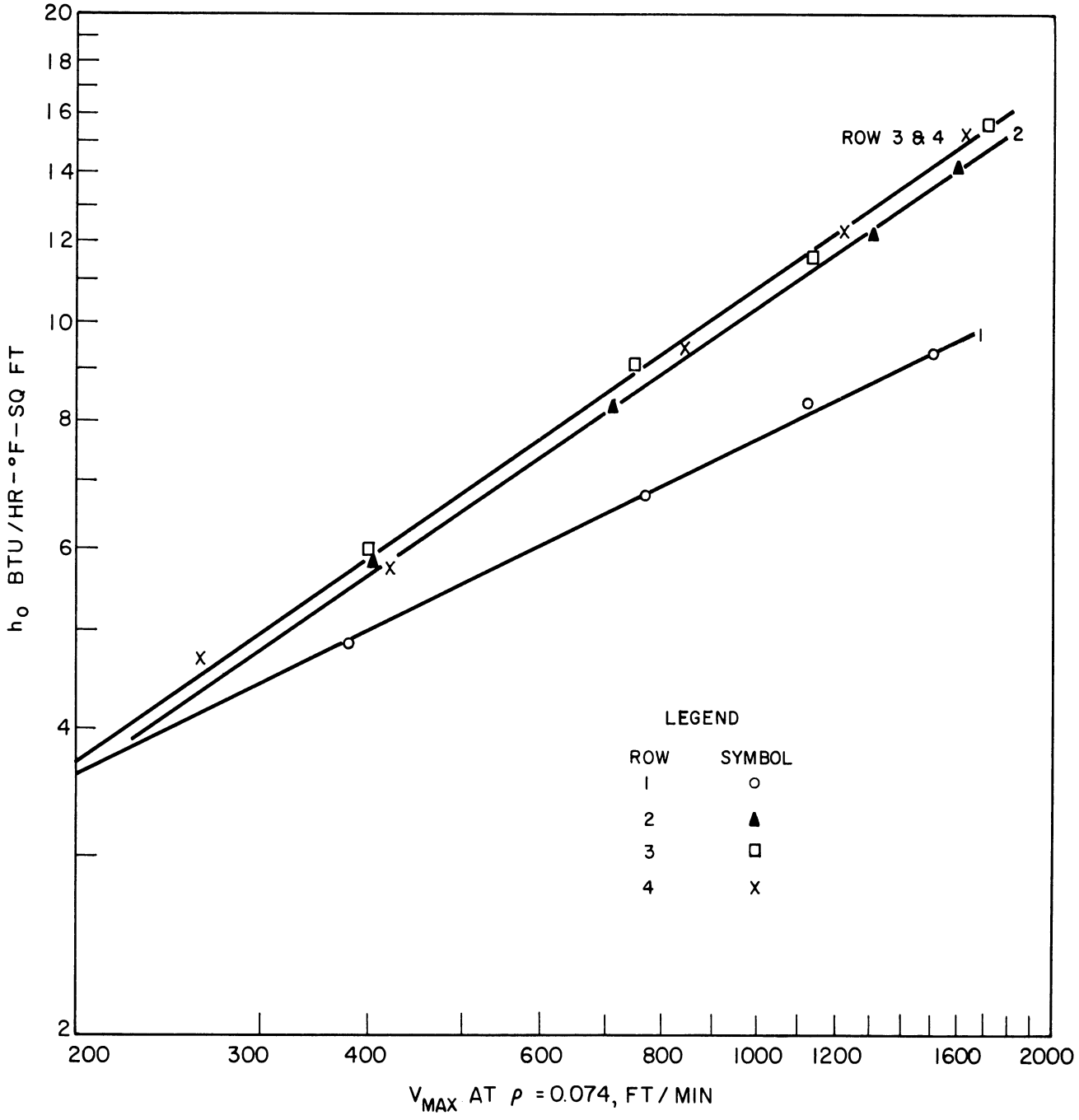

Figure 36. Heat Transfer Curves Obtained for the Individual Rows of Unit Number 8.

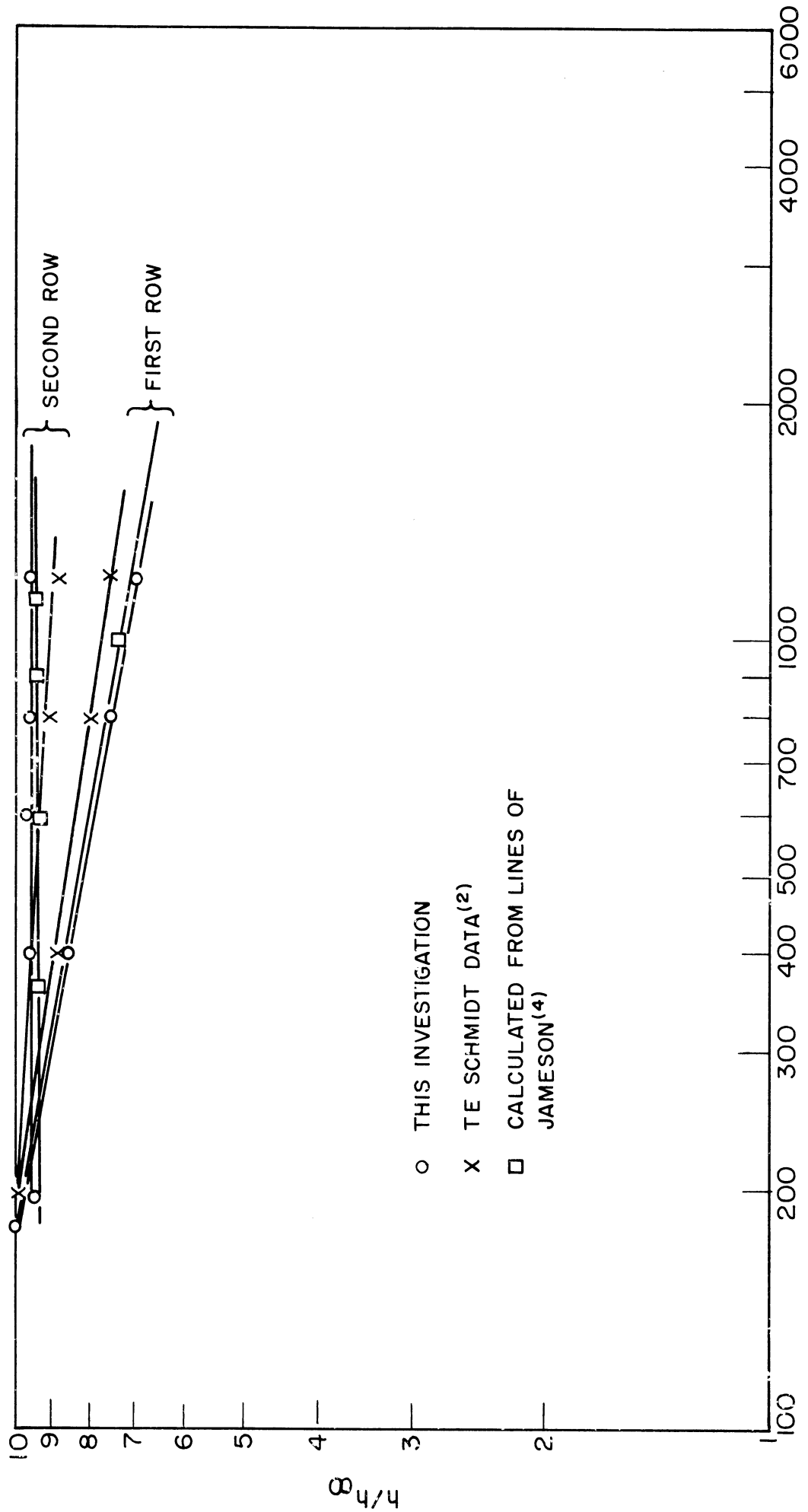

Figure 37. Comparison of Individual Row Heat Transfer Data with Data Appearing in the Literature.

same general trend as that determined by Schmidt and Jameson.

D. Flow Conditions of Air Approaching the Tube Banks

The conditions of the air approaching the tube banks are defined by the temperature, pressure and composition of the air and also by the velocity distribution and turbulence immediately upstream of the tube banks. The temperature, pressure and composition of the air were taken into account in each of the runs on all of the tube banks.

The velocity profiles or distributions were measured for two different air velocities at the outlet end of the entrance section. The measured velocity distributions, for mean air speeds of 2270 and 1000 feet per minute are presented on Figures 38 and 39. The data are presented in Table XVIII.

The lower velocity used for these measurements was near the limit of that which could be measured with any degree of precision. For example, an error in the setting of the micro-manometer of 0.002 inches results in more than a 2 per cent error in the computed air velocity, whereas, at the higher velocity, the same error in pressure measurement results in less than one half of one per cent error in velocity. Thus it is believed that a great deal of the scatter shown on Figure 39 is due to experimental measuring limitations.

Examination of the mean line for Figure 38 indicates that except in the neighborhood of the wind tunnel walls the velocity distribution varies less than one per cent from the integrated mean value.

The experimental procedure and data for the turbulence measurements are given in Appendix C.

TABLE XVIII

SUMMARY OF VELOCITY DISTRIBUTION DATA

High Velocity Run V_{avg} = 2270 ft/min

Position* X or Y, inches	(X/X)** or (Y/Y)	P inches water	V ft/min	V/V_{avg}
X - 1	0.074	0.302	2285	1.007
2	0.148	0.307	2310	1.018
4	0.296	0.303	2290	1.009
6	0.444	0.302	2285	1.007
8	0.592	0.301	2285	1.007
10	0.74	0.301	2285	1.007
12	0.89	0.293	2250	0.991
14	0.964	0.290	2245	0.989
15	0.89	0.295	2265	0.998
17	0.74	0.295	2265	0.998
19	0.592	0.300	2280	1.004
21	0.444	0.300	2280	1.004
23	0.296	0.302	2285	1.007
25	0.148	0.300	2265	0.998
26 1/2	0.030	0.25	2080	0.911
25	0.148	0.29	2245	0.989
23	0.296	0.306	2310	1.018
X - 1/8	0.01	0.048	913	0.868
2	0.15	0.063	1050	1.000
4	0.30	0.066	1070	1.020
6	0.44	0.063	1050	1.00
8	0.59	0.064	1058	1.008
10	0.74	0.066	1070	1.020
12	0.89	0.066	1070	1.020
13	0.96	0.065	1065	1.014
12	0.89	0.065	1065	1.014
10	0.74	0.062	1039	0.990
6	0.44	0.063	1050	1.000
4	0.30	0.061	1029	0.980
2	0.15	0.061	1029	0.980
1/2	0.04	0.054	1011	0.980
1/8	0.01	0.047	903	0.858
26 7/8	0.01	0.049	925	0.880
26	0.07	0.066	1070	1.020
25	0.15	0.068	1086	1.034
23	0.30	0.067	1078	1.026
21	0.44	0.066	1070	1.020
19	0.59	0.064	1058	1.008
17	0.74	0.064	1058	1.008
15	0.89	0.062	1038	0.990
13	0.96	0.062	1038	0.990

TABLE XVIII (CONT'D)

SUMMARY OF VELOCITY DISTRIBUTION DATA

Low Velocity Run V_{avg} = 1050 ft/min

Position X or Y, inches	(X/X) or (Y/Y)	P inches water	V ft/min	V/V_{avg}
Y - 14	0.44	0.064	1058	1.008
12	0.67	0.064	1058	1.008
10	0.89	0.062	1039	0.990
8	0.89	0.062	1039	0.990
6	0.67	0.064	1058	1.008
4	0.44	0.064	1058	1.008
1/4	0.03	0.051	941	0.895
1	0.11	0.060	1025	0.975
2	0.22	0.061	1032	0.983
4	0.44	0.062	1038	0.989
6	0.67	0.064	1058	1.008
8	0.89	0.062	1038	0.990
10	0.89	0.065	1065	1.014
12	0.67	0.062	1038	0.990
14	0.44	0.061	1032	0.983
16	0.22	0.060	1022	0.975
21	0.444	0.301	2290	1.009
19	0.592	0.302	2290	1.009
17	0.74	0.297	2270	1.000
15	0.89	0.290	2240	0.987
13	0.964	0.298	2275	1.002
13	0.964	0.298	2235	0.985
Y - 1/4	0.02	0.200	1860	0.820
3	0.33	0.292	2250	0.991
4	0.44	0.292	2250	0.991
6	0.67	0.288	2235	0.985
8	0.89	0.297	2275	1.002
10	0.89	0.304	2300	1.013

* The X positions represent the distance from the wind tunnel wall furthest from the windows, the Y's, distances from top wall, centerline values are X = 13.5 inches and Y = 9 inches.

** The dimensionless value represents the ratio of the distance of the measurement from the nearest wall to the centerline value.

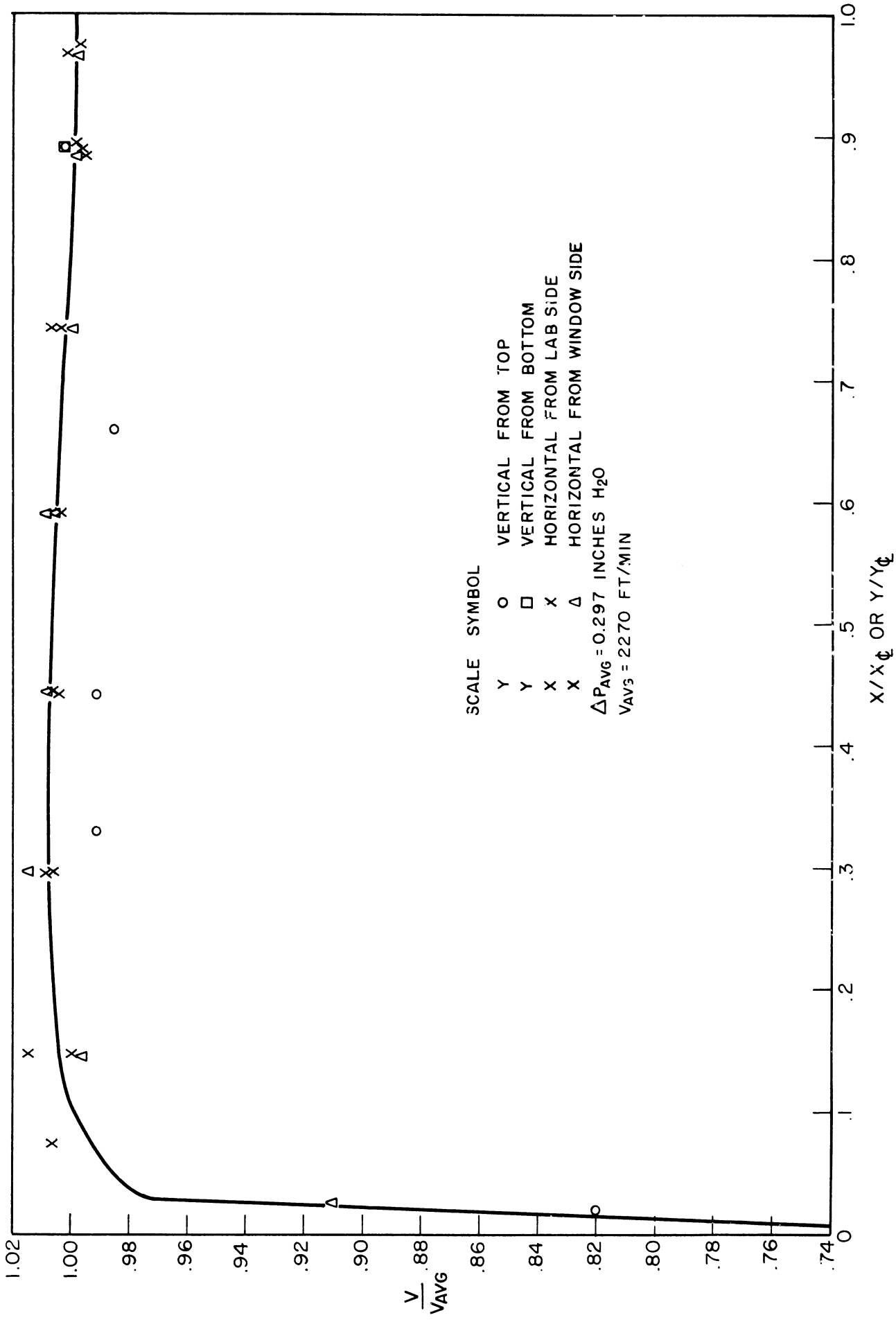

Figure 38. Velocity Distribution of Air at Entrance Section V_{avg} of 2270 ft. per min.

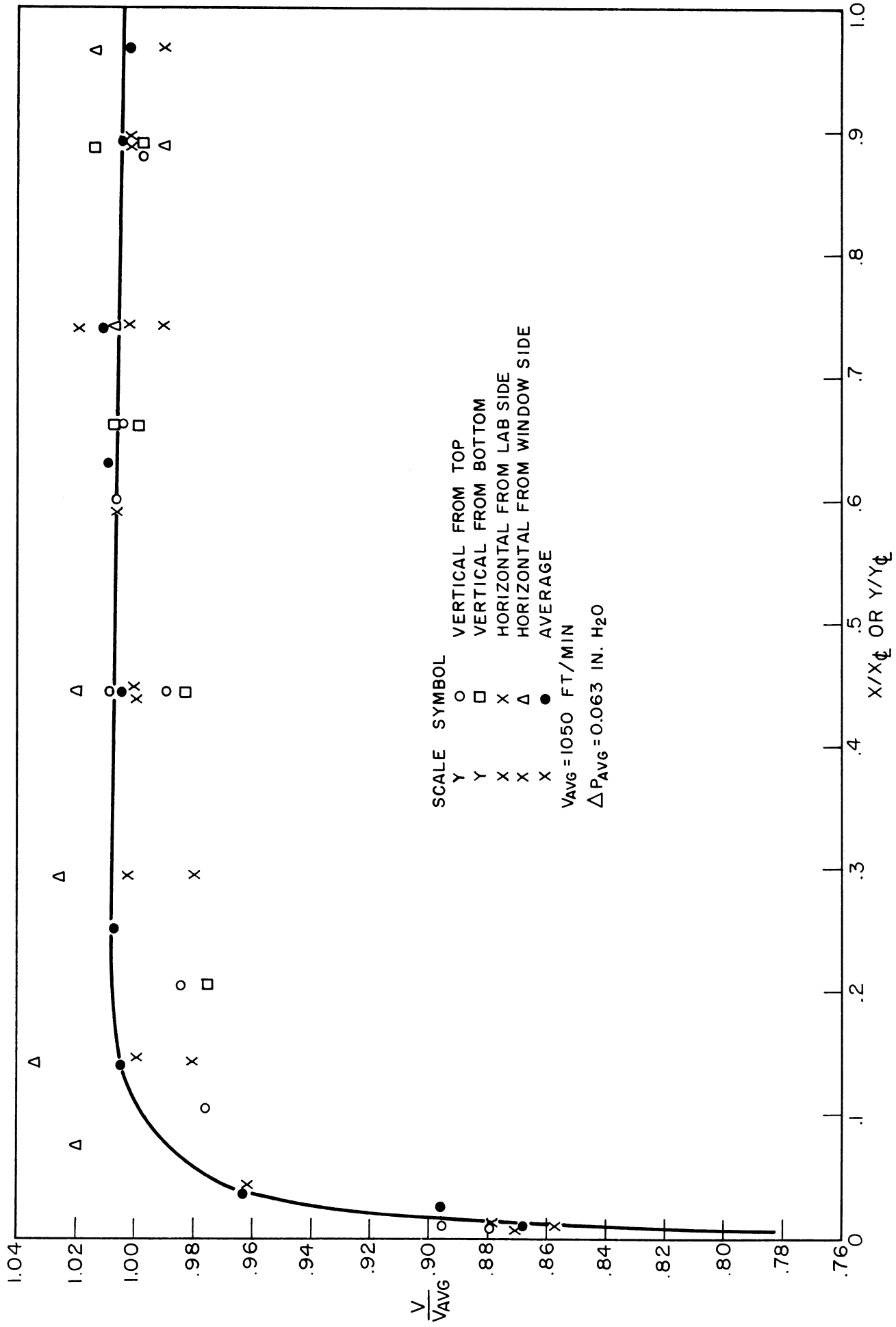

Figure 39. Velocity Distribution of Air at Entrance Section V_{avg} of 1060 ft. per min.

V. QUALITATIVE PREDICTION OF THE RELATIVE IMPORTANCE OF VARIOUS DIMENSIONS

The data for some of the tube banks and data appearing in the literature will be discussed and analysed in the following order:

(1) effect of number of tube rows on the heat transfer performance, and

(2) qualitative prediction of the effect of the tube and tube bank dimensions on the heat transfer performance of finned tube banks.

A. Effect of Number of Tube Rows on Heat Transfer Performance of Finned Tube Banks.

The individual-row heat transfer data given in the previous section for unit number 8, summarized on Figure 36, indicate the different heat transfer performances attained by the various rows of a bank of finned tubes. As indicated in this figure, the first row of tubes has a significantly different heat transfer coefficient than succeeding rows, which have essentially the same heat transfer coefficient. The heat transfer coefficient for the first row of tubes is related to the maximum air velocity by the equation:

$$(h_o)_1 = 0.30\ V_m^{0.47} \qquad (30)$$

as compared with the relationship for the remaining rows which is:

$$(h_o)_n = 0.09\ V_m^{0.70} \quad n > 1 \qquad (31)$$

This result is not surprising in view of the fact that at least a portion of the heat transfer for a bank of finned tubes is due to the jets and eddies caused by the upstream row(s) of tubes. The first row of tubes having, for this particular case, no large disturbances of the air upstream, it would be expected that this row would perform

differently than the succeeding rows where disturbances are present. The performance of the first row is dependent on the condition of the air approaching the tube bank. It might also be expected that the second and possibly later rows of tubes would also be dependent on the condition of the approaching air. The data shown in Figure 36 indicate that this is not the case and that the second and succeeding rows of tubes are virtually independent of air stream conditions approaching the first row.

Since the first row of tubes is affected by the air stream conditions it is necessary to define as completely as possible the conditions of the air approaching the tube bank in this investigation. The two principle properties which might affect the performance of the first row are the velocity profile and turbulence level of the air.

As previously mentioned, the air velocity profile was measured near the end of the inlet section for the two different air velocities of 2270 and 1050 feet per minute. The results are shown in Figures 38 and 39. As previously discussed, the air velocity of 1050 feet per minute was somewhat higher than experimentally attained with the tube banks in place and was near the lower limit of the air velocities which could be precisely measured with the pitot tube and micro-manometer. In fact, a great deal of the scatter which appears on Figure 39 is attributed to the experimental error encountered in attempting to measure a pressure difference of 0.063 inches of water. The average deviation for these two air velocities is less than 1.5 % from the mean air velocity values (except of course in the neighborhood of the entrance walls). The air velocity profile approaching the tube bank is believed

to be essentially constant.

It is a well known fact that the free stream turbulence of a fluid approaching a tube affects the heat transfer from that surface. This was experimentally shown by Comings[28] who varied the turbulence of a fluid immediately upstream from a cylinder transferring heat to air. The results of his study are shown on Figure 40 where the mean Nusselt number of the tube is plotted versus the turbulence of the air approaching the surface at a constant Reynolds number. As shown in this figure, increasing the turbulence increases the heat transfer coefficient. Unfortunately, no measurements have been made of the effect of the upstream turbulence level on the heat transfer performance of banks of tubes.

Measurements were made near the end of the inlet section of the wind tunnel using a turbulence measuring sphere in an attempt to determine the turbulence level of the air approaching the tube bank. The apparatus and procedure used, and the experimental results are summarized in Appendix C. Due to the air velocity limitations imposed by the motor-blower combination used, the precise level of the turbulence could not be measured. As is shown in Appendix C, however, the turbulence level must have been below a value of 2 per cent.

The performance data for the individual rows of tubes allows the calculation of a correction curve for the effect of the number of rows in a particular tube bank. The total rate of heat transfer to the air is equal to the sum of the rates of heat transfer of the individual rows, or:

$$Q_T = Q_1 + Q_2 + Q_3 + \text{-----} + Q_n \qquad (32)$$

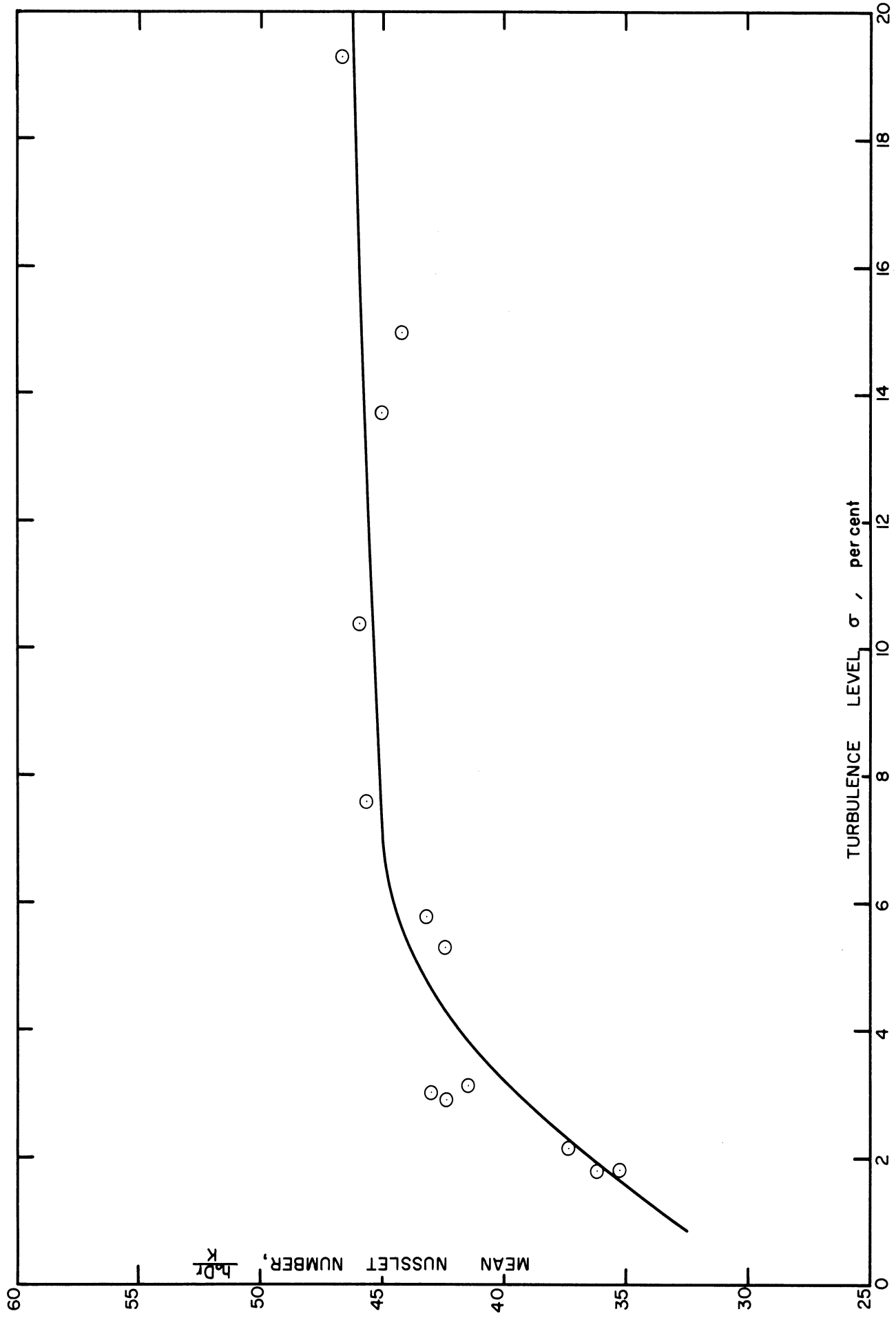

Figure 40. Effect of Turbulence Level on Heat Transfer From a Single Cylinder to Air at Re = 5800. (Ref. 28).

where: Q_T = total rate of heat transfer, Btu/hr

Q_1 = rate of heat transfer from the first row, Btu/hr

and Q_n = rate of heat transfer from the n^{th} row, Btu/hr

The rate of heat transfer is related to the mean heat transfer coefficient by:

$$Q = h_o A_o (\Delta T_M) \qquad (33)$$

where: Q = rate of heat transfer, Btu/hr

h_o = mean air film coefficient, Btu/hr - °F - sq.ft.

A_o = total exterior area of tubes, ft^2

and ΔT_M = mean temperature difference between the metal and air, °F.

Substituting the relationship for the heat transfer coefficient from equation 33 into equation 32 and simplifying (assuming equal area for all rows):

$$h_o(\Delta T_M) = \frac{(h_o)_1 \Delta T_1 + (h_o)_2 \Delta T_2 + \text{----} + (h_o)_n \Delta T_n}{n} \qquad (34)$$

The mean temperature difference driving force varies for the different rows, being highest at the inlet (first row of tubes) and lowest at the outlet (n^{th} row of tubes). For most practical applications however, the temperature differences can be cancelled to give:

$$(h_o)_{Mn} \cong \frac{(h_o)_1 + (h_o)_2 + (h_o)_3 + \text{-------} + (h_o)_n}{n} \qquad (35)$$

where: $(h_o)_{Mn}$ = mean heat transfer coefficient for a tube bank n rows deep

$(h_o)_1$ = mean heat transfer coefficient of the first row

and etc.

Since however, the heat transfer coefficients of the second and succeeding rows are constant, equation 36 can be written as:

$$(h_o)_{Mn} \cong \frac{(h_o)_1 + \sum_{i=2}^{n} (h_o)_i}{n} \qquad (36)$$

For a tube bank having a large number of rows, equation 36 can be reduced to:

$$(h_o)_{m\infty} = (h_o)_i \qquad i \geq 2 \qquad (37)$$

where: $(h_o)_{m\infty}$ = mean heat transfer coefficient for an infinite number of tube rows.

Taking the ratio of equations 36 and 37 the effect of number of rows on the mean heat transfer coefficient of a tube bank is:

$$\frac{(h_o)_{Mn}}{(h_o)_{M\infty}} \cong \frac{(h_o)_i + \sum_{i=2}^{n} (h_o)_i}{n(h_o)_i} \qquad i \geq 2 \qquad (38)$$

The heat transfer coefficient of the various rows at any particular air velocity can be substituted into equation 38 to give the ratio of the mean air film coefficient of a tube bank having n rows to the mean heat transfer coefficient of a tube bank of infinite extent. This is graphically illustrated in Figure 41 where this ratio is plotted versus the number of rows for various air velocities. Although these curves are actually discontinuous functions, since n must be an integer, they are shown as continuous curves for illustration purposes. Also included on this figure is the curve given by McAdams for triangular pitch bare tube banks[20]. This curve, although actually velocity dependent similar to the finned tube values, was taken as an average value for the usual range of velocities. The use of this figure is illustrated in an example found in Appendix D.

Two of the finned tube banks used in this investigation had four rows of tubes, one bank had eight rows, and four tube banks had six. In order to correlate the data, it is necessary to convert the results

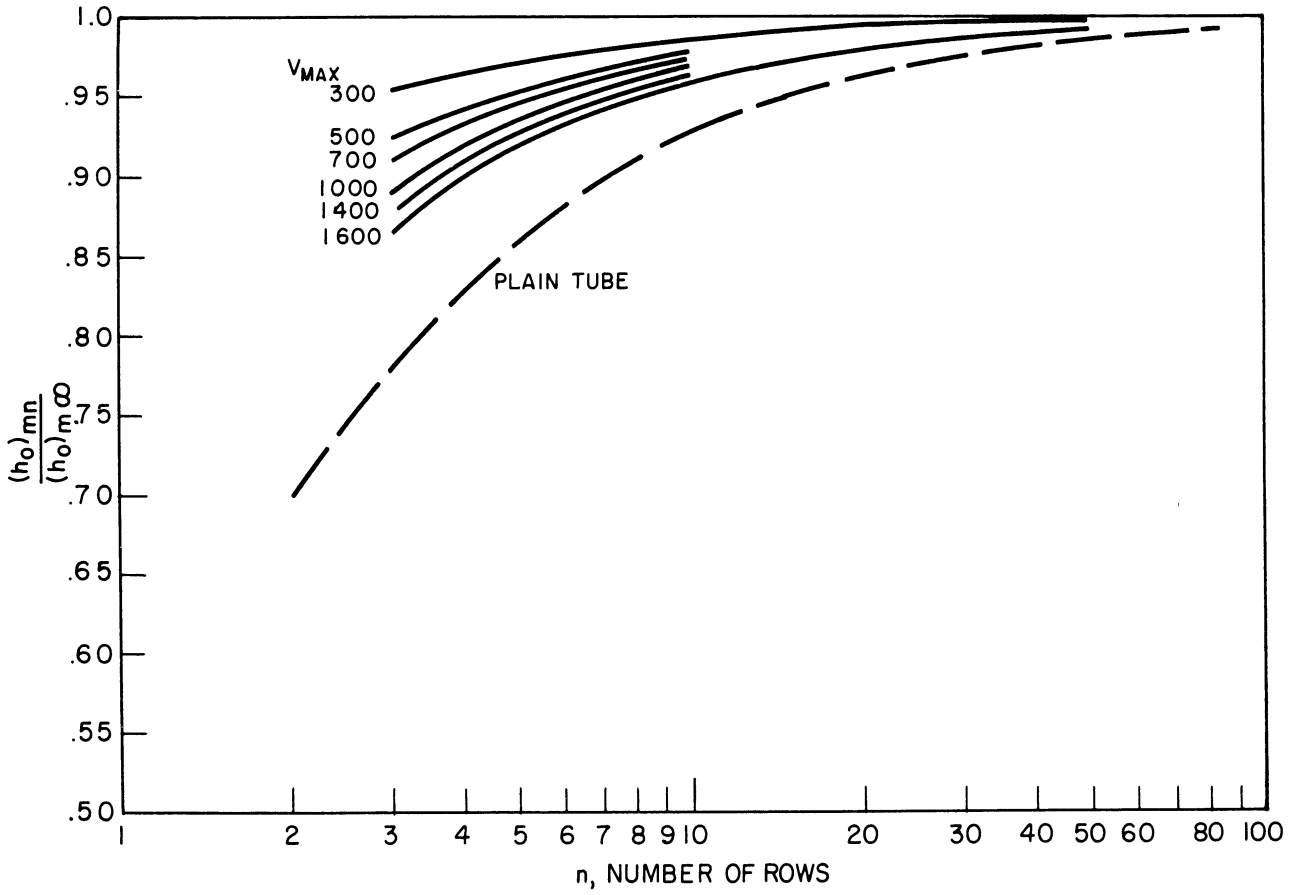

Figure 41. Effect of Number of Rows on Mean Heat Transfer Coefficient.

to a common basis, which for this particular case was arbitrarily chosen as a tube bank containing six rows of tubes. The corrections, based on the curves given in Figure 41 are given in Table XIX. As can be noted from this table, the corrections are very small; consequently an average value was taken to convert the heat transfer data.

TABLE XIX

CORRECTIONS USED TO CONVERT HEAT TRANSFER DATA TO SIX ROW DEEP BANK

Number of Rows	Correction at V_{max} = 400 ft/min	Correction at V_{max} = 1600 ft/min	Average Correction
4 rows	1.007	1.032	1.020
6 rows	1.000	1.000	1.00
8 rows	0.988	0.984	0.985

Similar computations can be made to convert the heat transfer coefficients computed from the correlations given later from the six row deep banks on which they are based to finned tube banks of any extent. However, two limitations of these curves should be pointed out. The first is the inherent assumption of a constant average mean temperature difference across various rows. This assumption is only approximately valid for moderate changes in mean temperature difference for the various rows. The second limitation is based on the fact that the effect of number of rows deep is almost entirely due to the first row.

B. Effect of Geometry on the Mechanisms of Heat Transfer.

The variations in the heat transfer performance between the tube banks investigated are due to the differences in geometry within the banks.

The geometry of banks can be described by the dimensions; S, tube spacing in the banks; N, number of fins per inch; D_o, outside diameter of the fin; D_r, root diameter of the fin; Y, fin thickness, and perhaps other variables generally not measured, such as, condition of the fin tip and roughness of the fin metal. What is desired is a correlation of the heat transfer data, i.e. a single functional relationship which would represent the data for all seven finned tube units.

The value of the mean heat transfer coefficient of air flowing through a bank of finned tubes is primarily dependent on the geometry of the bank. Since the above listed dimensions describe the geometry of the tube bank, they are the primary variables which are to be used to correlate the data. The relative importance of some of these variables can be determined from measurements of local coefficients of heat transfer over the surface of finned tubes and other data available in the literature. The finned surface of the finned tubes constitutes the majority of the external heat transfer area and the variation of the local heat transfer coefficients over the fin surface is of primary importance.

Effect of Tube Spacing

The spacing of the tubes used in this investigation was such that a 3/16 inch fin-tip-to-fin-tip clearance was maintained (on the nominal fin diameters) for all units. This results in an essentially constant tube spacing to fin diameter ratio. Neither this ratio nor any other single geometric ratio can be used to yield geometric similarity. The constancy of the tube pitch to fin diameter ratio does not necessarily imply that the variation in the heat transfer coefficients

obtained for the different banks of tubes is independent of the tube pitch.

The effect of the tube spacing can be qualitatively predicted from three investigations reported in the literature, the work of Grimison [29] on banks of plain tubes, and Schmidt[2] and Jameson[4] on banks of finned tubes. Grimison in reviewing the data of Huge[30] and Pierson[31] found that large variations in the transverse and longitudinal spacings of tubes in bare tube banks had little effect on the mean heat transfer coefficients at a given mass flow rate of air through the minimum free area. Although this work on plain tube banks would not preclude large effects of tube spacing in the heat transfer from banks of finned tubes, it would be expected that the finned tube heat transfer coefficients would not be particularly sensitive to this variable.

This conclusion is substantiated by the work of Jameson[4] who experimentally found no variation in the heat transfer coefficient for four different transverse and longitudinal spacings when compared at the same mass velocity of air through the minimum free area. Figures 3, 4 and 5 indicate the data of Jameson for the tube banks described in Table XX. Schmidt[2] varied the longitudinal pitch of one tube bank and also concluded that there was no effect of tube spacing in heat transfer to finned tube banks.

As mentioned earlier, the data of Jameson was obtained using banks of wrapped-on-finned tubing which has a inherent possibility of contact resistance between the root and fin portion of the tube. However, if a bond resistance was present in the tubes, it is unlikely that

TABLE XX

DIMENSIONS OF TUBE BANKS STUDIED BY JAMESON

	Tubes Studied (Tube No.)			
	1	2	3	4
d_r, inches	0.625	0.625	0.750	1.000
N , fins/inch	8.70	7.00	9.05	8.80
d_o, inches	1.121	1.121	1.463	1.737
Y , inches	0.010	0.010	0.012	0.012
A_o, sq.ft./ft.	1.138	0.946	2.049	2.560

Tube Banks Studied

Tube No.	S_T (in.)	S_L (in.)
1	1.232	1.35
1	1.848	1.35
2	1.232	1.35
3	1.557	1.75
3	1.982	1.75
3	2.725	1.75
3	2.725	0.80
3	1.982	1.375
4	1.959	2.063
4	3.079	2.063

this resistance, if any, varied in such a manner that it exactly cancelled any effects due to the variation in tube spacing. It can therefore be concluded that variation in the spacing of the tubes within reasonable limits (S/D_r ratios of 4/1 or less) play a minor role in heat transfer from banks of triangular-pitch-finned-tubes.

Effect of Fin Spacing

The effect, if any, of fin spacing could arise from the merging or interference of the fluid boundary layer on the top surface of one fin with the boundary layer of the succeeding fin. The mergence or interference of adjacent boundary layers could cause a considerable reduction in the air velocity in the areas where this occurred with a subsequent by-passing of the air around the heated surface resulting in a decrease in heat transfer coefficient. Three investigations involving this variable have been reported in the literature in addition to data presented here.

Ghai[18] measured local heat transfer coefficients on a long straight fin attached to a flat wall of the type shown in Figure 42. Included in his investigations were data for various fin spacings from 3/4 to 1/8 inch. In general the effect of the fin spacing was found to be very small for the area near the tip of the fin. There was a considerable decrease in the heat transfer coefficient near the root with decreasing fin spacing. This is shown in Figure 11. The eightfold variation in fin spacing caused an 18 per cent variation in the mean heat transfer coefficient.

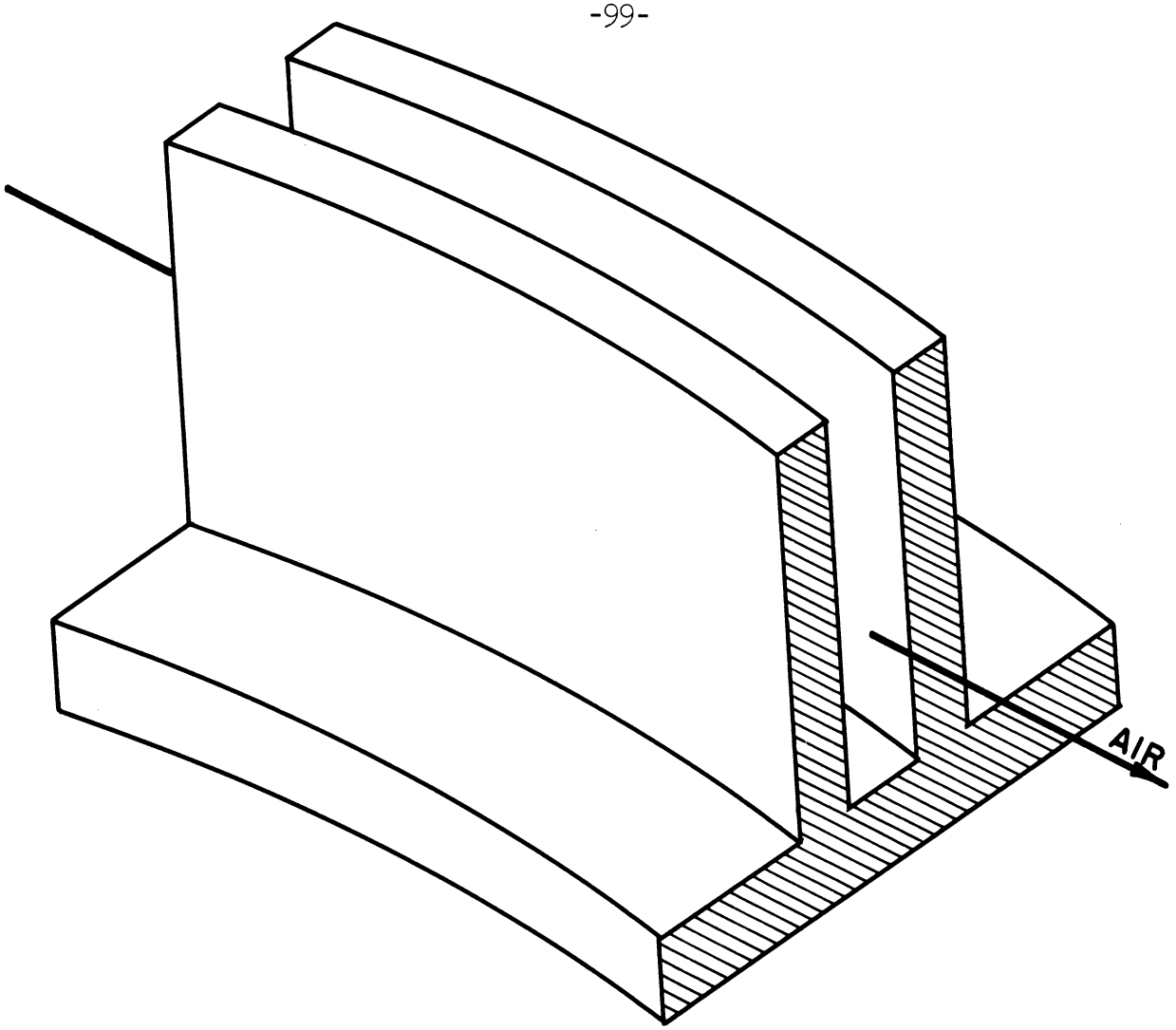

Figure 42. Type of Fin Studied by Ghai[18] and Wagener[36].

Wagener[32] also studied a number of straight finned surfaces of the same type as Ghai, primarily varying the air velocity and fin spacing. He concluded from his study that the most effective spacing for this type of fin was about 12 per cent greater than the thickness of one boundary layer. The effect of the fin spacing for spacing greater than the thickness of one boundary layer was small, whereas the effect of spacing below this thickness was quite pronounced. This is shown in Figure 43.

Jameson[4] in his studies included two finned tube banks containing tubes which were identical except for fin spacings of 0.133 and 0.105 inches between the sides of adjacent fins. The heat transfer performance of these units was found to be the same within experimental

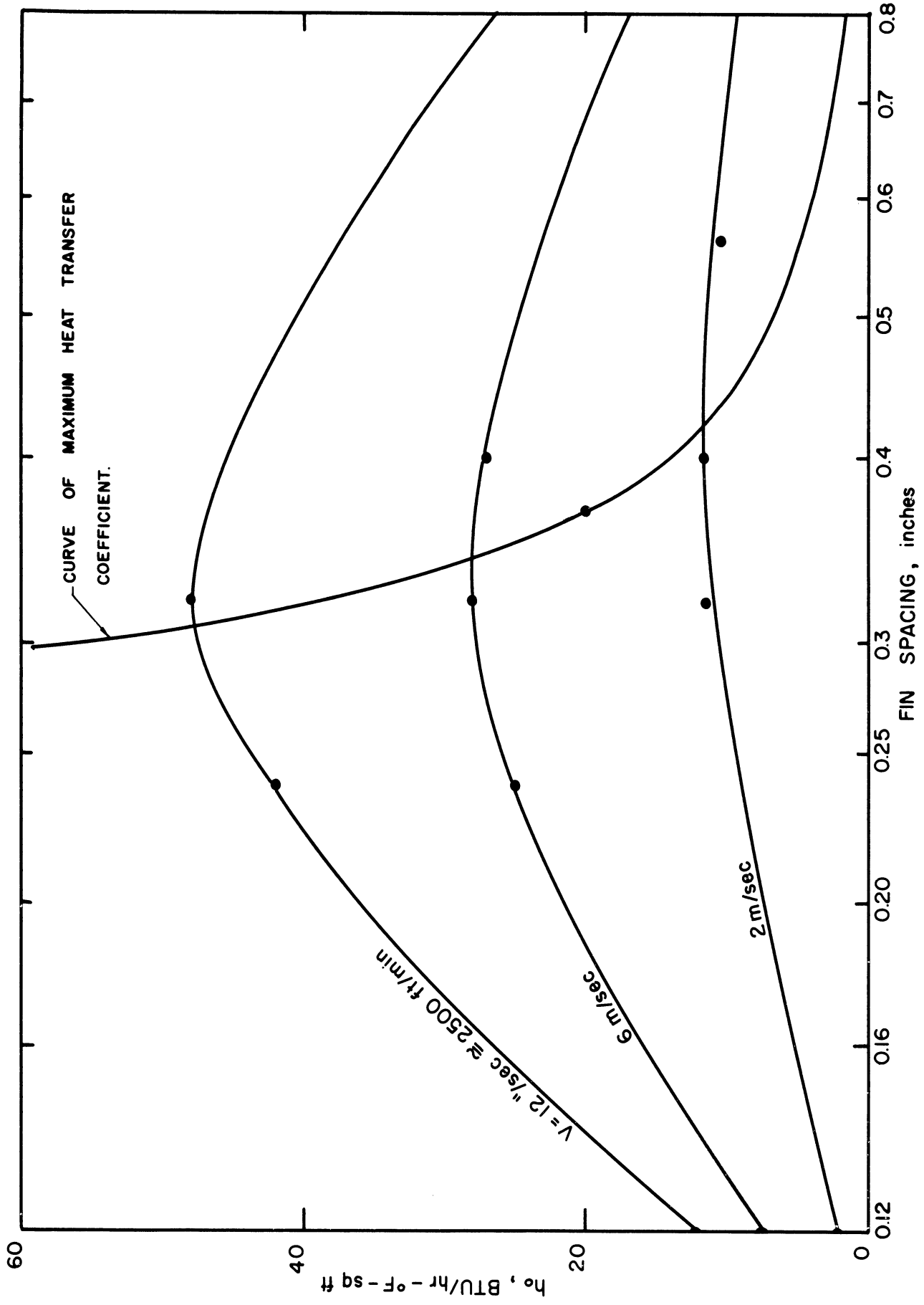

Figure 43. Effect of Fin Spacing for Longitudinal Fins After Wagener[36].

accuracy. These results are shown on Figure 3. Since the two fin spacings studied by Jameson differed by only 30 per cent, the apparent agreement between the heat transfer coefficients of this unit could have been due to small inaccuracies in the determination of air film coefficients.

Two tube banks included in this investigation, units number six and seven, contained tubes having the same dimensions except for the spacing of the fins. These units had identical heat transfer performance curves (well within experimental accuracy) as shown in Figure 44. Unit number six contained tubes having 5.13 fins-per-inch while the tubes in unit number seven had 10.36 fins-per-inch. The corresponding spacings between the fins are 0.173 and 0.0735 inches for the tubes in units six and seven respectively. Assuming that the mean air film heat transfer resistance is due entirely to a laminar boundary layer of thickness δ through which the heat is transferred by conduction, the mean thickness of this layer is given by:

$$\delta = \frac{k_{air}}{h_o} \times 12 = \left(\frac{0.187}{h_o} \right) \text{inches} \qquad (39)$$

If, in accordance with the results of Wagener[32], interference occurs starting when the spacing between the fins is in the order of one boundary layer thickness, the coefficient for these units at which this interference might occur would be: for unit number six:

$$(h_o)_c = \frac{0.187}{0.173} = 1.1 \text{ Btu/hr-°F-ft}^2$$

for unit number seven:

$$(h_o)_c = \frac{0.187}{0.0755} = 2.5 \text{ Btu/hr-°F-ft}^2$$

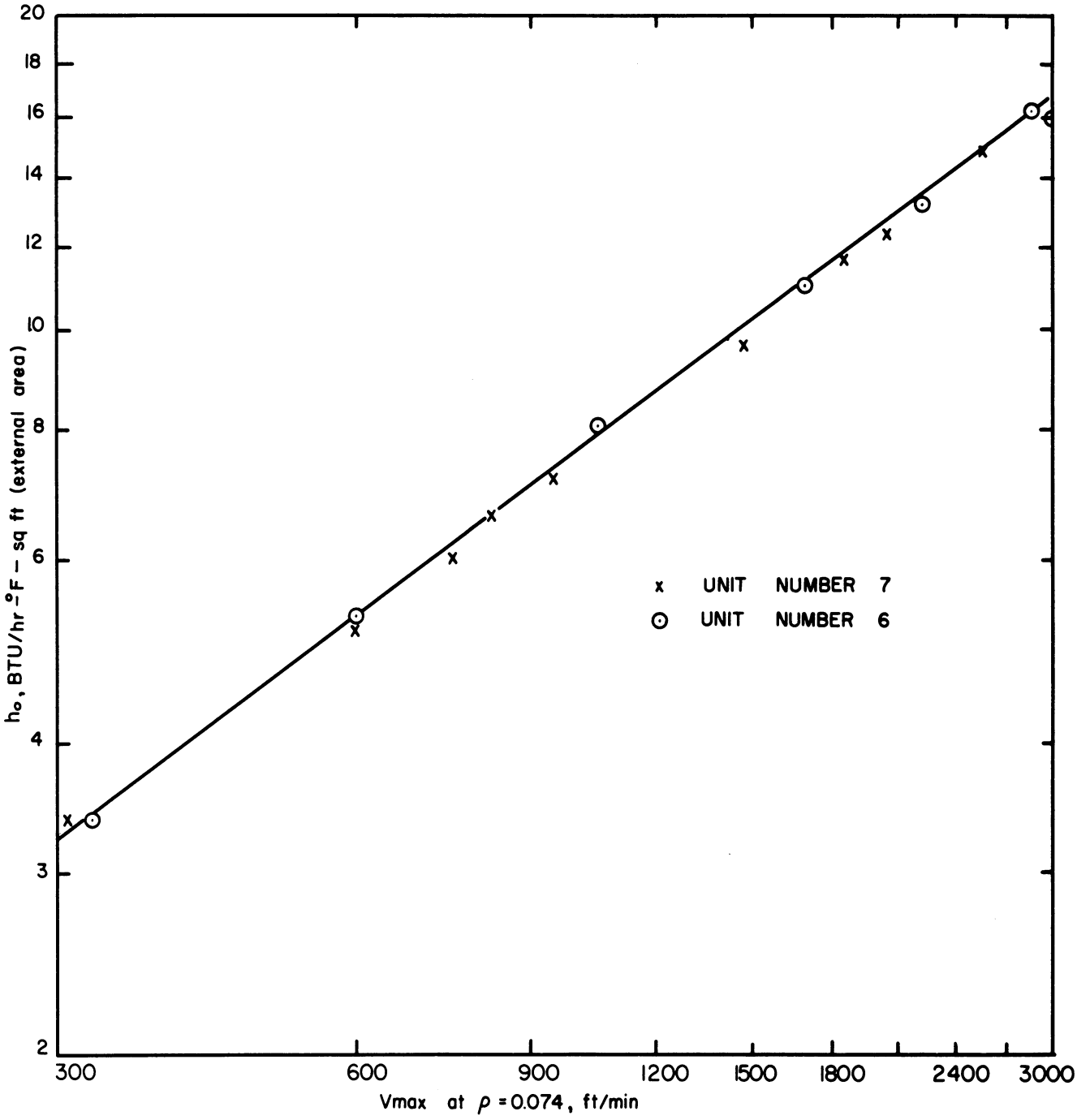

Figure 44. Comparison of Heat Transfer Data for Units Number 6 and 7.

where: $(h_o)_c$ = transitional value of the heat transfer coefficient, at which interference between adjacent boundary layers might occur.

Since all of the heat transfer coefficients measured for these units are appreciably above these values, it would be expected that there would be little or no effect of the different fin spacing on the heat transfer coefficients for these two units. Examination of the heat transfer curves (see Figure 44) indicates that the heat transfer data are well represented by a single line. The performance line of these units is supported by the data of one of the tube banks investigated by T. E. Schmidt. Figure 45 compares the heat transfer results obtained by T. E. Schmidt on a tube bank containing tubes with dimensions similar to units 6 and 7 except with 8 fins-per-inch. As indicated in this figure, the curve obtained by Schmidt is approximately the same as that representing units 6 and 7 with a slightly different slope.

It would be expected that if boundary layer interference occurred it would cause a change in the slope of the heat transfer coefficient-air velocity curve from the region where there was interference to the region where there was no interference. Unit number 2, containing tubes having 19.5 fins-per-inch, had a fin spacing of 0.035 inches. Substituting this value into equation 39, the transitional mean coefficient is predicted as:

$$(h_o)_c = \frac{0.187}{0.035} = 5.4 \text{ Btu/hr-°F-ft}^2$$

Two of the experimental heat transfer coefficients obtained on this unit fell well below the transitional value of 5.4. Since these two coefficients fall within the expected scatter of the data around the

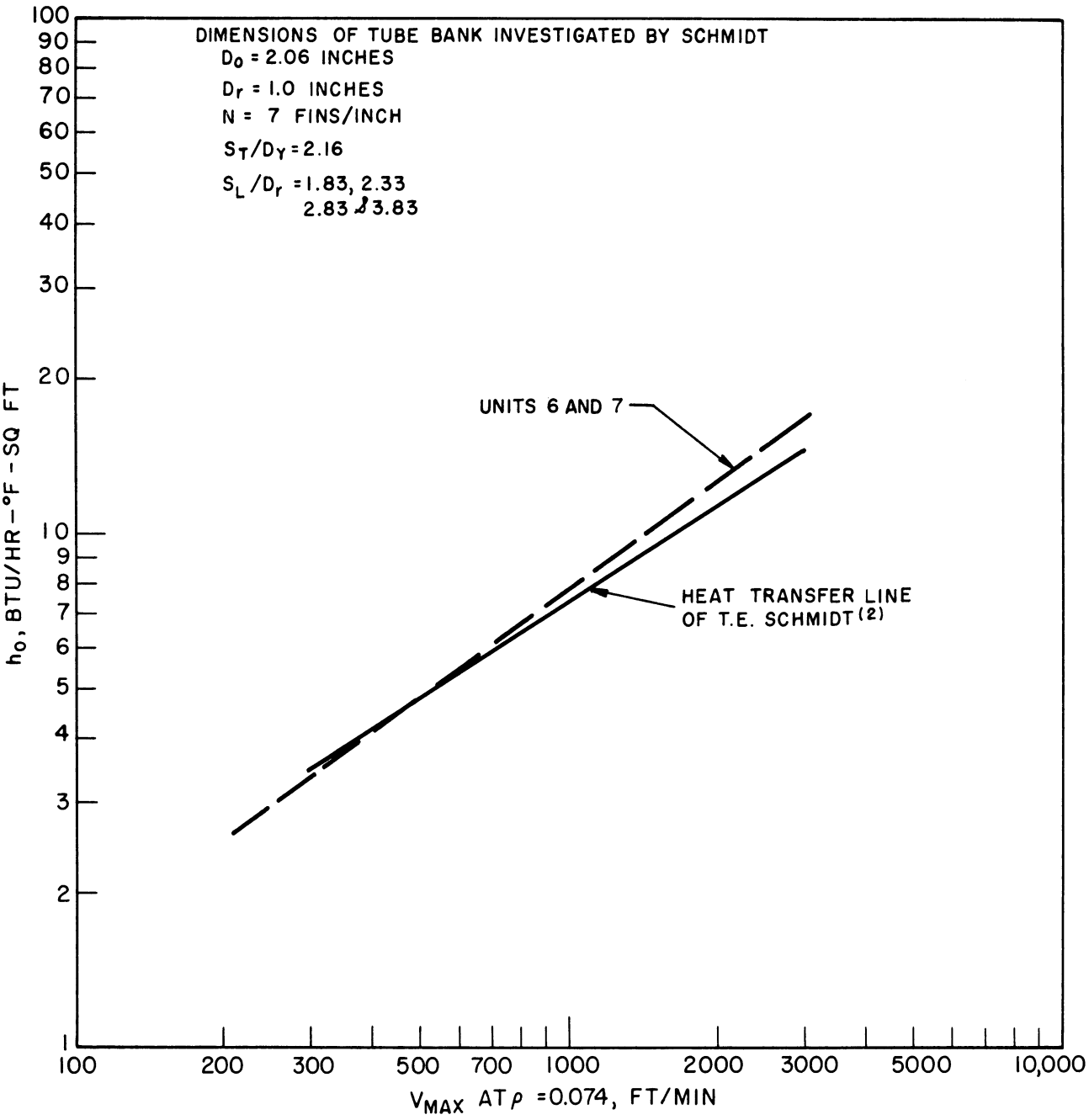

Figure 45. Comparison of Data of T. E. Schmidt with Heat Transfer Curves for Units 6 and 7.

mean line for the entire range of velocities it suggests that the effect of the fin spacing for finned tube heat transfer coefficients is less than the effect for longitudinal fins. Since the two data points below the predicted transitional value actually fall lower than the mean heat transfer curve, it is possible that a transition occurs, such as indicated in Figure 46. As indicated in this figure, the interference of adjacent boundary layers would probably cause a smooth rather than an abrupt change in the heat transfer-air velocity curve. As will be shown later, there is an area on the fin, in back of the tube which contributes little to the total heat transfer to the tube, consequently the thickness of the boundary layer over the active portion of the tube is less than that calculated by equation 39. This effect could be sufficient to cause a continued slope of 0.7 of the heat transfer curve below the calculated transitional coefficient.

One can conclude that for the range of fin spacings and air velocities included in this investigation, the effect of fins-per-inch on the heat transfer coefficient is probably negligible.

Effect of the Fin Diameter, Root Diameter, and Fin Thickness

The finned surface of a finned tube can be thought of as a series of circular flat plates, pierced by a cylindrical rod through the center. In order to determine the relative importance of the above three dimensional characteristics it is first necessary to examine the velocity and heat transfer characteristics of the combination of these two types of surfaces.

Assuming a constant air velocity approaching the tubes, the velocity profile of the air in passing over the fin can be deduced to

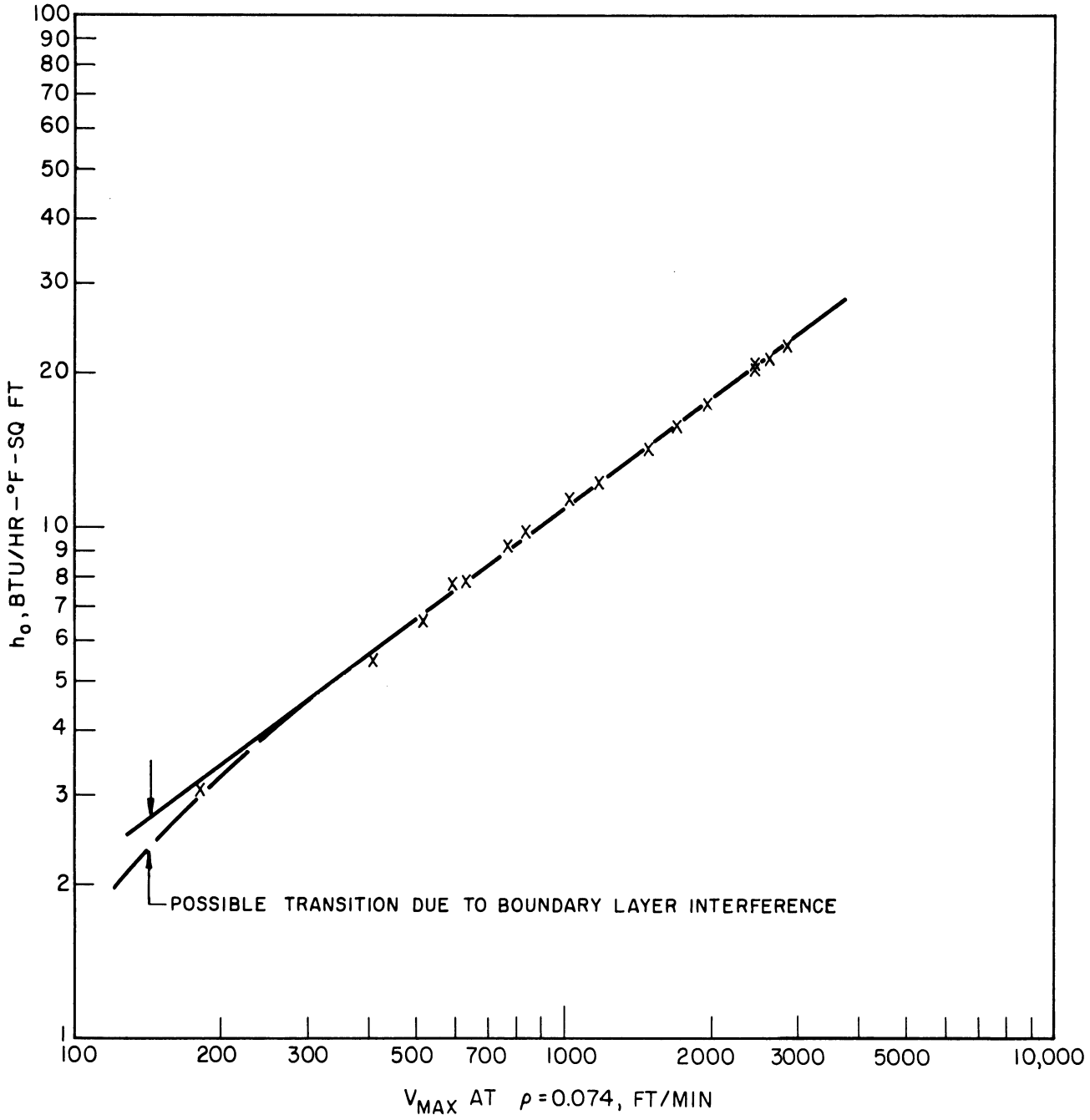

Figure 46. Data for Unit Number 2 Showing Possible Transition Due to Boundary Layer Interference.

have the shape schematically illustrated in Figure 47 for two positions on the tube. Near the front of the tube the velocity profile would be highest near the fin tip, steadily decreasing toward the center of the fin. The shape of this profile can be attributed to two augmenting effects. The first is the effect of the cylinder on the fluid flow upstream from the cylinder. It can be shown, from a study of the fluid dynamics, that the velocity profile for position such as A-A upstream of the cylinder is of the same general shape as shown in Figure 47[33]. The second mechanism tending to cause a velocity profile of this shape is that of skin friction. Comparing the length of the flow path over the fin in section A-A it is noted that this length increases from fin tip to centerline of the tube. Since the energy loss of the flowing fluid due to skin friction is proportional to length, there is a net mass flow of air toward the fin tip which produces a velocity profile of the same general shape as indicated in Figure 47.

The velocity profile at cross section B-B is due to the presence of the cylinder. The mass of air which upstream of the cylinder flowed between the root diameter and the centerline of the tube has to flow through the decreased cross sectional area between the root diameter and the fin tip at position B-B. Thus the velocity profile produces a maximum near the wall of the cylinder.

The velocity profile near the back of the cylinder is complicated by the presence of vortices. According to irrotational flow theory, the velocity distribution around a cylinder should be symmetrical around the 90° position of the tube. Experimentally, however, it has been shown that the flow in this region becomes rotational due to the formation of

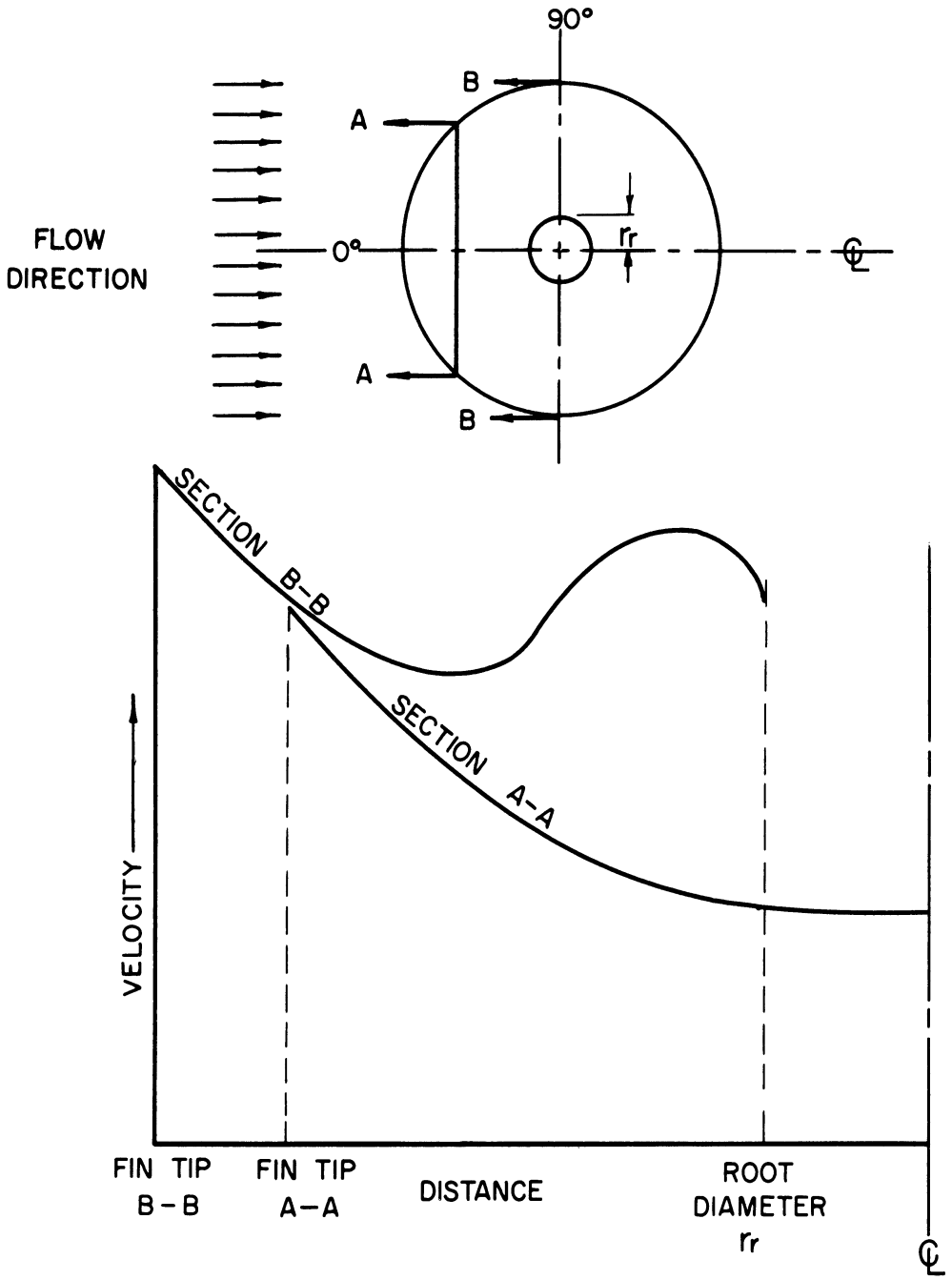

Figure 47. Schematic Illustration of Velocity Profiles Over a Fin Surface.

vortices starting near the 90° position of the tube. Although the vortices formed have in general large rotational velocities, the linear velocities in the general direction of flow are relatively small, creating a large residence time for the fluid in the rear of the cylinder.

The velocity profiles deduced above are partially substantiated by experimental measurements of heat fluxes on the fin of a finned cylinder. Figure 48 shows the radial variation in the heat transfer coefficient measured by Weiner and et al.[19], at the 90° position of the tube. Comparison of the shape of this curve with the section B-B velocity distribution curve in Figure 47 indicates that they are of the same general nature except in the region near the tip of the fin (which due to their method of measurement could be due to very small errors in heat flux). The heat transfer coefficients measured by Weiner and et al.[19] were defined by the relationship:

$$\frac{\Delta Q}{\Delta A} = h(t_m - t_i) \qquad (40)$$

where: ΔQ = the rate of heat transfer from a small section under consideration

ΔA = the heat transfer area between the fin and fluid for the section under consideration

t_m = mean metal temperature of the section

and t_i = inlet fluid temperature

The heat transfer coefficient thus defined does not take into account the temperature rise of the fluid in flowing over the metal surface.

Using the heat transfer coefficient defined above, Weiner and et al. presented the variation of the coefficient in the form of

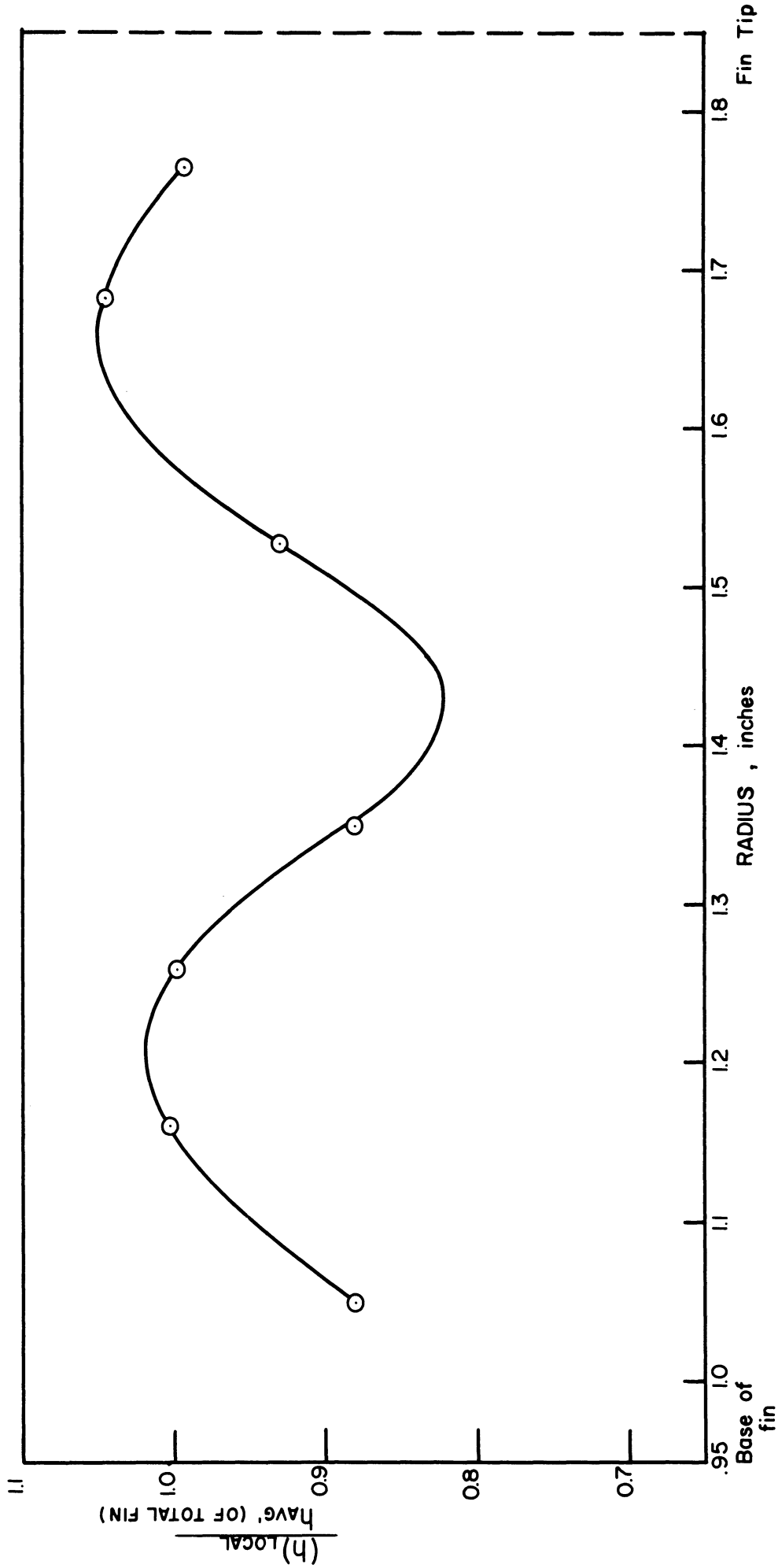

Figure 48. Radial Variation in Heat Transfer Coefficients After Weiner et al.

an active zone, a recirculating zone and a mean zone. The active zone was defined as the area over which the local coefficient was more than 50% greater than the mean coefficient for the entire fin. The recirculating zone was defined as the area over which the coefficient was less than half of the mean coefficient while the mean zone was defined as the area over which the coefficient was between the above values.

The location and extent of these zones are described in Figure 49 for an approaching water velocity of 0.5 feet-per-second (which, using a Reynolds number basis corresponds to a maximum air velocity of about 2000 feet per minute). The presence of these zones was explained in the following manner.

The active area was attributed to the flow pattern caused by the square edge on the tip of the fin. This edge caused a contraction of the fluid on entering the fin passage with a consequent impingement on the fin surface upstream from the cylinder. The fin thickness of the tube investigated was given as 0.188 inches.

The fins of most commercial finned tubing and those included in this investigation are about one tenth of that value (about 0.02 inches). It is possible that the frontal fin surface of the tube investigated here would not be as efficient as indicated by the active zone, unless the tip of the fins were rough or presented a relatively thick hydrodynamic section. It was noted that all of the tubes used in this investigation had smooth tips except unit number 8 which had a slightly wavy-broken surface. This roughness could cause a relatively high mean air film heat transfer coefficient for this bank.

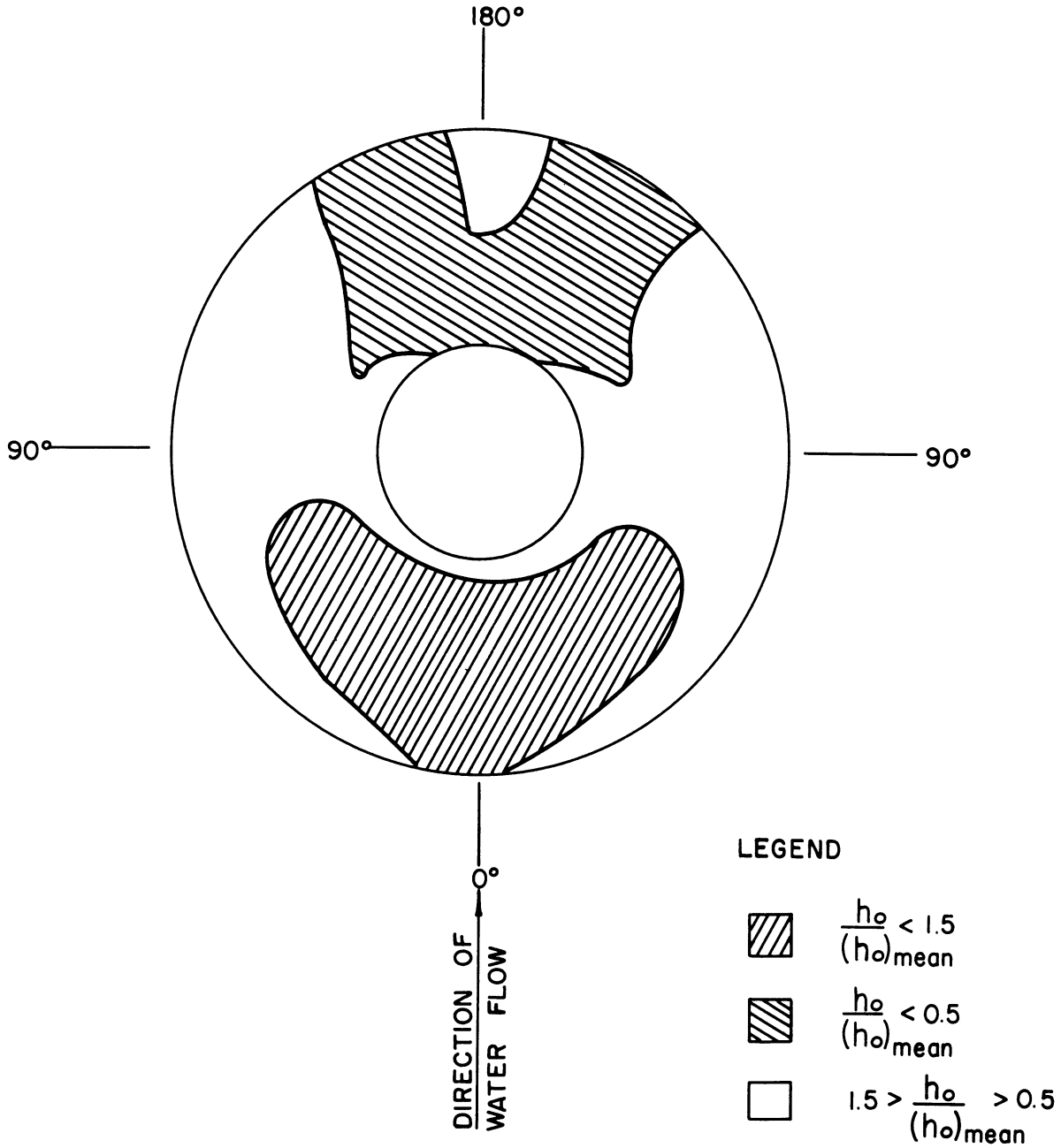

Figure 49. Local Heat Transfer Coefficients Over a Fin Surface After Weiner et al.

The recirculating zone on the fin surface was explained by the reversal of the fluid flow or vortice formation on the downstream side of the cylinder. As previously indicated, the formation of vortices reduces the mass flow rate of air in the area where they are present. It is believed that the low coefficients obtained in this area are due, not primarily to a decrease in the heat transfer coefficient for the recirculating zone, but are instead due to a loss in temperature difference driving force. The low mass flow rate of the fluid in the recirculating zone causes a relatively high temperature rise of the fluid in this area. Defining a point coefficient as:

$$\left(\frac{d\,Q}{d\,A}\right)_a = (h_o)_a\,(t_m - t_{bs})_a \qquad (41)$$

where: $\frac{dQ}{dA}$ = rate of heat flux through the fluid boundary layer at the point a

$(h_o)_a$ = fluid film heat transfer coefficient at point a

$(t_m)_a$ = metal skin temperature at point a

and t_{bs} = mean bulk stream fluid temperature at point a

$= t_i + (\Delta t)_a$

in which Δt_a = temperature rise of the fluid from the inlet to point a. Assuming that sufficiently small grids were taken over the fin surface, equations 40 and 41 can be equated to give:

$$(h_o)_a = (h)\,\frac{(t_m - t_i)}{[t_m - t_i - (\Delta t)_a]} = h\,\frac{(t_m - t_i)}{(t_m - t_{bs})} \qquad (42)$$

Which indicates that the fluid film heat transfer coefficient is always greater than the coefficient based on the inlet fluid temperature. The difference between the two coefficients is small unless the temperature

rise of the fluid approaches the value of $(t_m - t_i)$.

The temperature rise of the fluid in the wake of a heated cylinder was investigated by Berry and et al.[34] and by Billman and et al.[35]. They found that even for high velocities (of the order of 2000 feet per minute for air) the temperature rise of the fluid near the back of the cylinder approached the value of $(t_m - t_i)$. Figures 50 and 51 graphically present the ratios of $(t_m - t_{bs})/(t_m - t_i)$ determined by Billman for two different air velocities. The ratio $(t_m - t_{bs})/(t_m - t_i)$ represents the fraction of the initial temperature difference driving force which remains. Figure 50 contains a dotted line indicating the approximate location of the fin tips for units number 4, 5, 6, 7 and 8. As can be noted from this figure, (1) a substantial portion of the fin surface has a low temperature difference due to the temperature rise of the fluid and (2) the shape of the curves for $(t_m - t_{bs})/(t_m - t_i)$ near 0.5 are similar to the shape of the recirculating zone determined by Weiner[19] (see Figure 49). Corresponding effects can also be noted from the work of Lemmon[36] and McAdams[37].

It can therefore be concluded that the recirculating zone on the back portion of the fin is primarily due to a loss in temperature difference driving force. The effect of this phenomenon however, is the same as a decrease in the film heat transfer coefficient.

The fraction of the fin heat transfer area affected by this zone is dependent on the relative size of the fin and root diameters. With a constant fin diameter, as can be seen from Figure 50 the larger

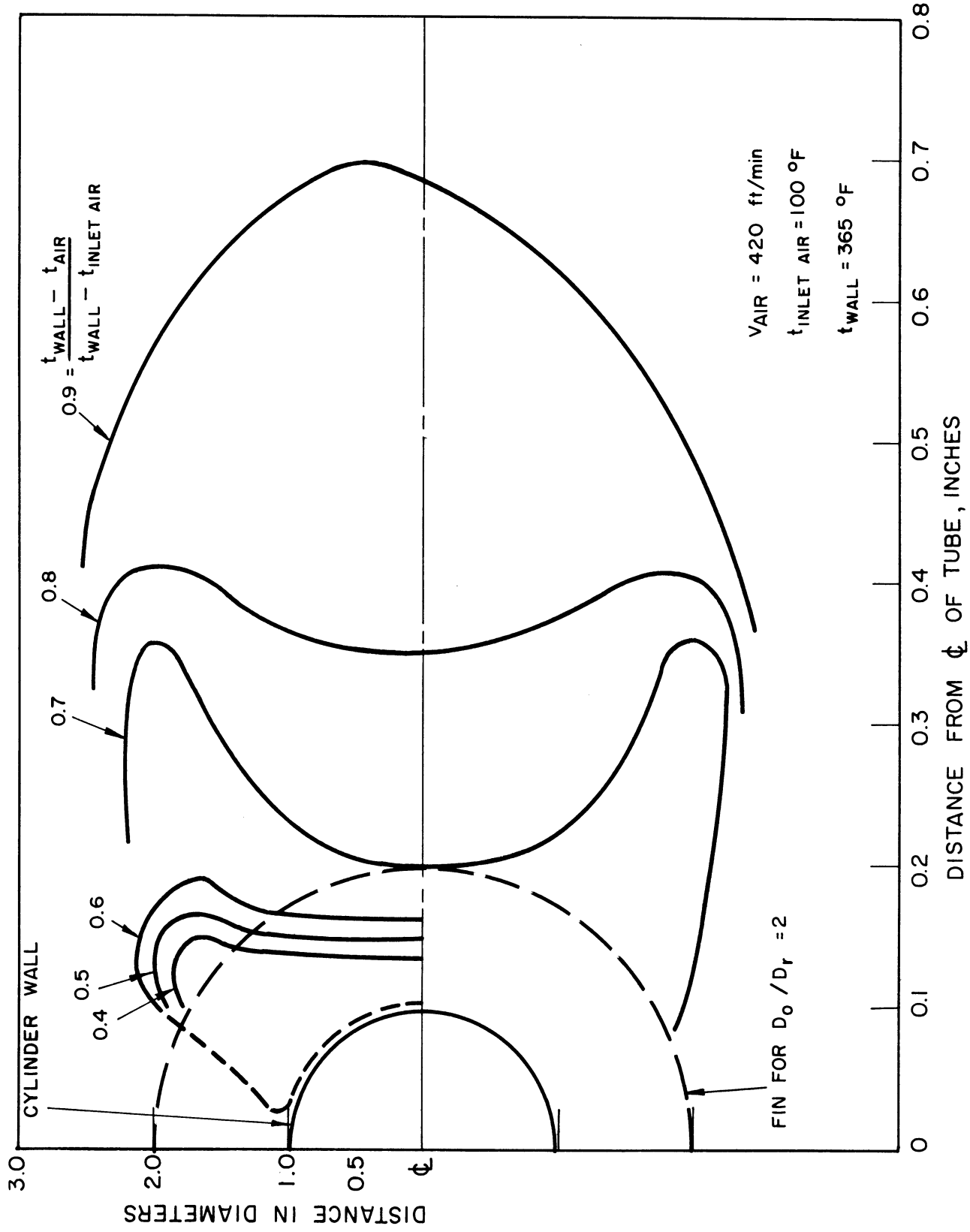

Figure 50. Temperature Differences in the Wake of a Heated Cylinder With an Air Velocity of 420 feet per minute After Billman[35].

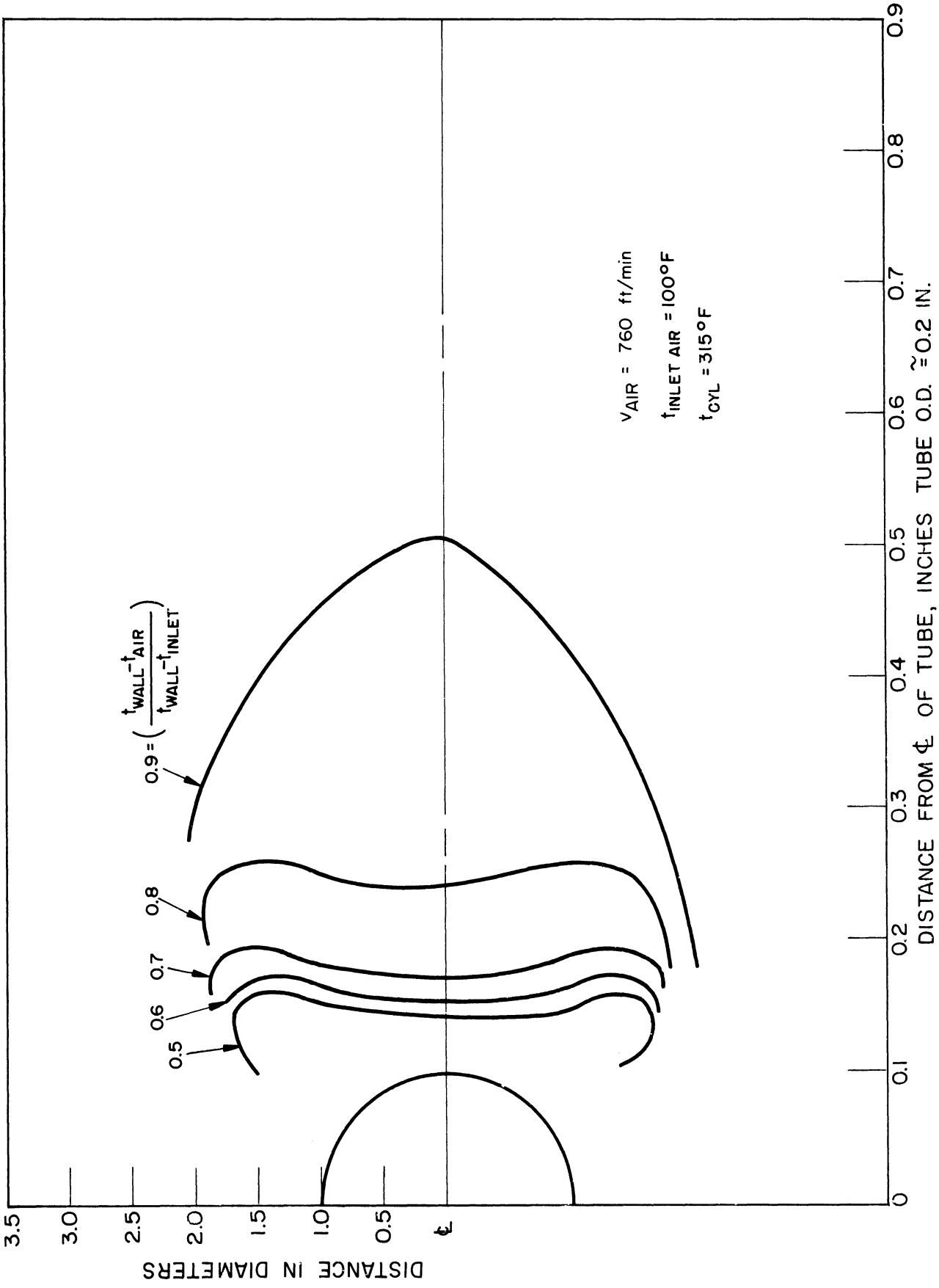

Figure 51. Temperature Differences in the Wake of a Heated Cylinder With an Air Velocity of 760 feet per minute After Billman[35].

the root diameter of the tube, the greater the fraction of fin area affected by the recirculation in back of the tube.

The heat transfer coefficients on the remainder of the fin surface depend on the air velocity and turbulence patterns over this area. The velocity profiles shown in Figure 47 indicate qualitatively the general trend which would be expected over the finned portion of a finned cylinder when the fluid velocity approaching the tube was uniform. In the center of a bank of cylinders, after the first row, the fluid stream approaching a tube would have a non-uniform velocity made up of jets and eddies due to the effects of the cylinder(s) upstream from the tube in question. This change in the fluid movement is schematically illustrated in Figure 52 by means of streamlines. The mass of fluid flowing between any two streamlines is a constant, since, by definition, the net mass transfer across any particular streamline is zero. Hence, comparison of the spacing between adjacent streamlines indicates the relative mass flow rates of the fluid, a wide spacing indicating a low mass flow rate in the direction of flow and a narrow spacing a high mass flow rate, etc. The local velocity over the various sections of the fin, however, is complicated by the possibility of vortices or rotational flow over large segments of the finned area. Thus, although the spacing between streamlines gives the mass flow rate of the fluid which (at constant density) is proportional to the net velocity in the principle direction of flow, the actual local velocity is dependent on both the net velocity and the presence and relative strength of any vortices in the area.

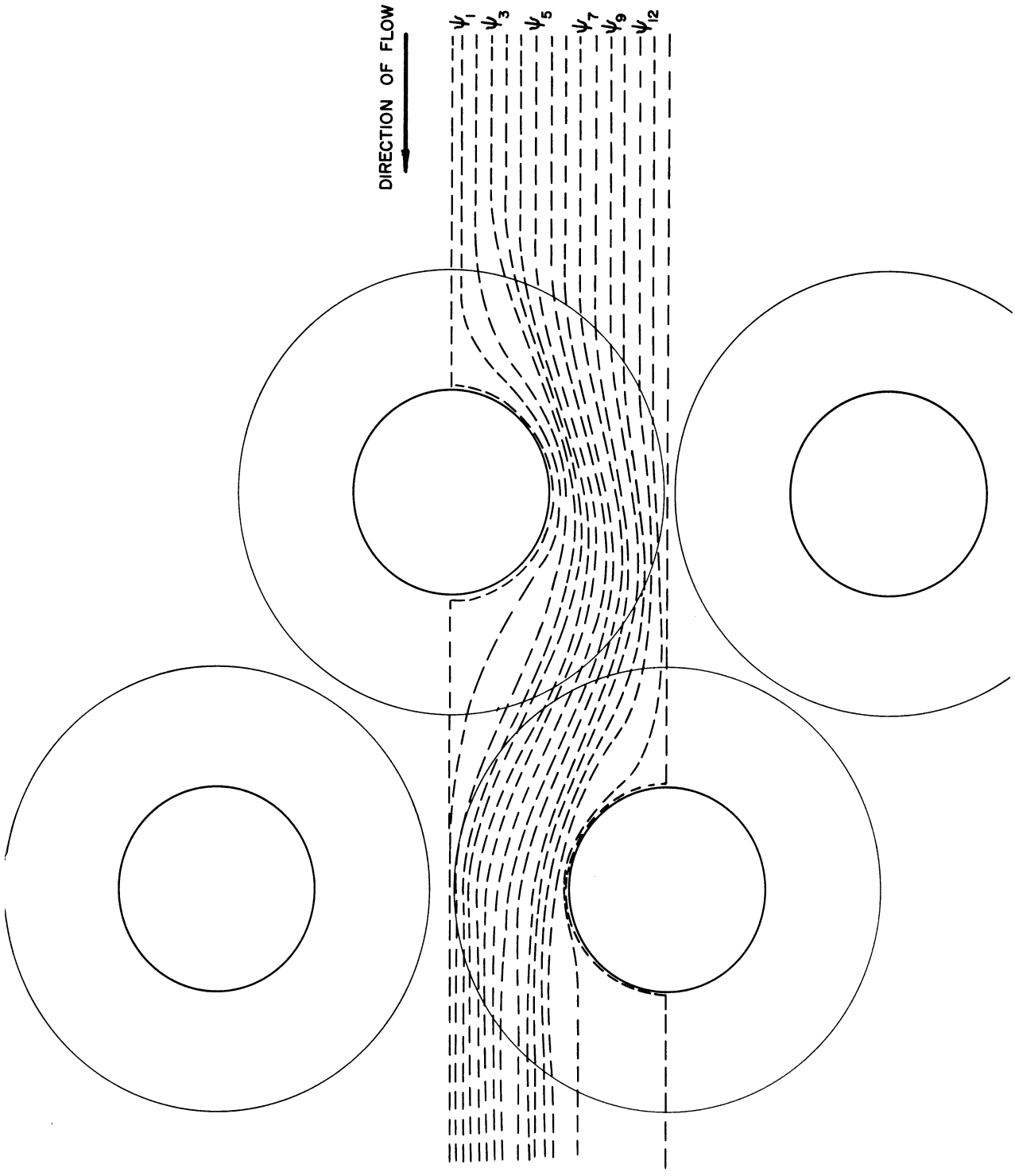

Figure 52. Schematic Illustration of Streamlines of the Air in Flow Through a Finned Tube Bank.

This point is illustrated by the following example. Assume that along a particular straight line, D-D, near the surface of a fin the net velocity in the principle direction of flow is denoted by the arrows shown below, the length representing the speed of the fluid.

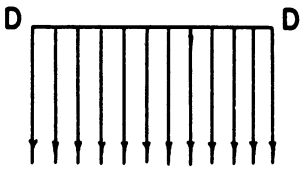

In the absence of forces tending to produce a vortice, the arrows denote the local velocities along the line D-D. If, however, due to pressure forces on the fluid, a vortex of the strength shown by the arrows below would be normally present,

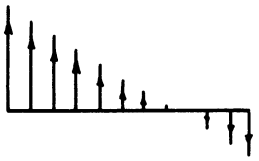

the local velocities along the line D-D would be obtained by addition of the velocity vectors contributed by the two types of flow. This results in a velocity distribution along the line D-D as schematically shown below.

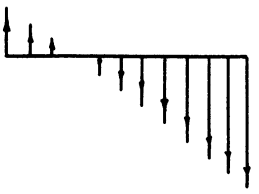

The local coefficients of heat transfer depend on the nature and thickness of the fluid layer immediately adjacent to the metal surface. A low velocity fluid boundary layer arises from the viscosity effects of

the fluid and the relative motion between the fluid and metal surface. The nature of this layer for a uniform flow of fluid over a flat plate has been well established and is known to develop in the manner indicated in Figure 53[38]. As indicated in this figure, the velocity of the air, at a given distance from the leading edge, depends on the distance from the metal surface. At a point O, for example, the velocity-distance curve might have the shape given by the curve I-I', which is a laminar type of boundary layer. The curve a-a' denotes the thickness of the boundary layer, δ, which is generally defined as the distance from the surface at which the velocity is 99 per cent of the main stream velocity. The boundary layer thickness starts at zero at the leading edge and continually increases in thickness until it becomes unstable and a transition commences such as at point c. The transition is followed by a new type of velocity profile called a turbulent boundary layer. As can be noted by the curve J-J', the velocity of the air increases rapidly with distance from the plate, with a fairly flat section with the boundary layer distance. The local heat transfer coefficients in these zones are schematically illustrated in Figure 54[38]. The change in the heat transfer coefficients are due to both the changes in the boundary layer thickness and the different mechanisms of heat transfer which occur in the various zones.

The heat transfer in the laminar zone is primarily by conduction, so that the local heat transfer coefficient is inversely proportional to the thickness of the boundary layer, or:

$$h \propto \frac{1}{\delta}$$

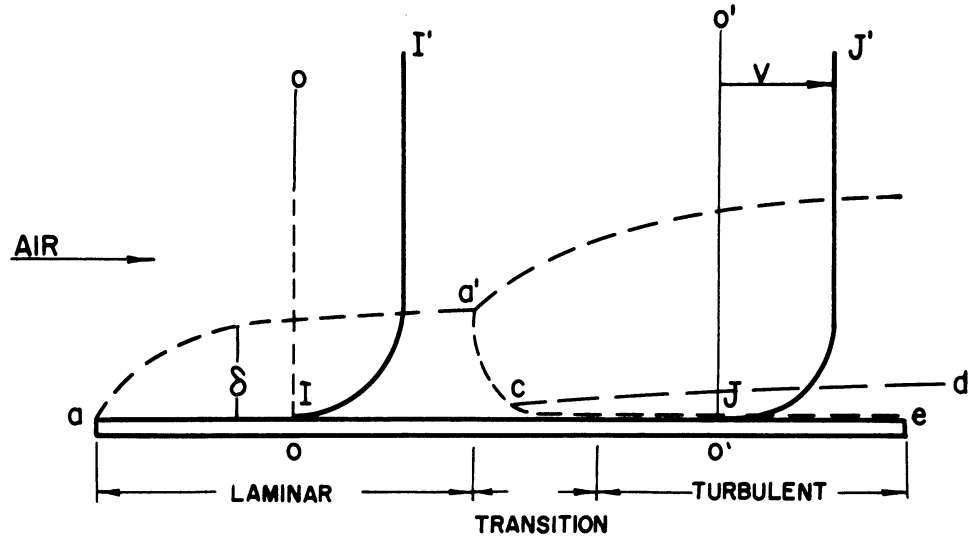

Figure 53. Laminar and Turbulent Boundary Layers on a Flat Plate.

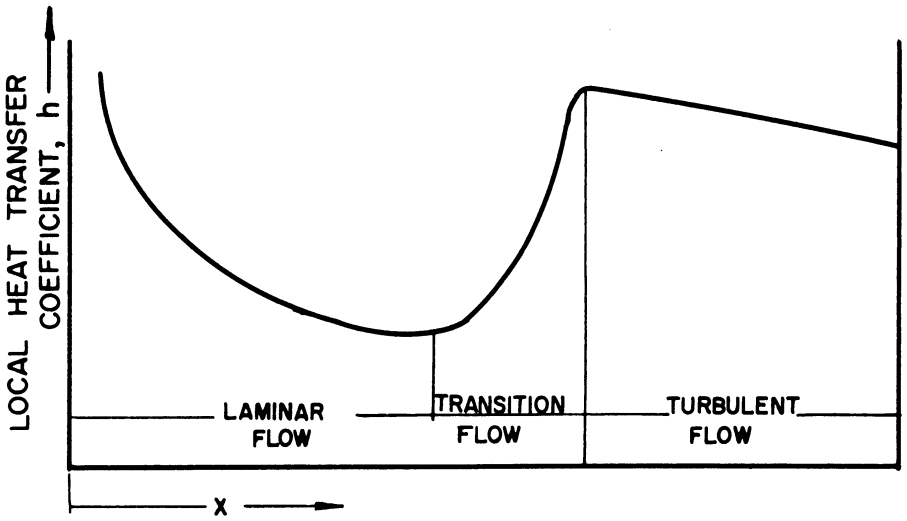

Figure 54. Local Heat Transfer Coefficients on a Flat Plate for Various Boundary Layer Zones.

In the turbulent zone, the heat transfer is by conduction through a "laminar sublayer", conduction and convection in a "buffer zone" and by convection in a "turbulent core". The mechanism occuring in the turbulent core is that vortices, formed in the area between the curves b and d which constantly introduce cool air from the main stream into this region. The mechanism in the buffer zone (region between d and e) is a mixture of the two adjoining regions because some of the cold molecules from the eddies penetrate into this area causing a higher rate of heat transfer than by conduction alone. A turbulent type of boundary layer always produces a higher heat transfer coefficient (at the same Reynolds number) than does a laminar.

Of importance here, is the type of boundary layer present over the fin surface. The Reynolds number at which the transition between the two types of flows occurs, as quoted by different investigators, varies from 20,000[39] to 500,000[40]. It is also known that the transition is dependent on both the free stream turbulence and the temperature difference between the metal and fluid stream[40], the transition Reynolds number decreasing with an increase in either of these factors. A third possible factor, not yet investigated, is the effect of the presence of the adjacent fin on the transition Reynolds number.

Table XXI, lists the range of Reynolds numbers, based on fin diameter and maximum air velocity, for the units investigated. Also included in this table is the percentage of the length of the fin that would have a turbulent boundary layer at the highest air velocity investigated assuming a transition Reynolds number of 20,000. As indicated in this table, the majority of the finned surfaces would be predicted to

have predominately laminar boundary layers for most of the air velocities investigated. If, however, the above factors affecting the transition Reynolds number sufficiently lower the transition Reynolds number value, the boundary layer on the finned surfaces could be predominately turbulent.

TABLE XXI

RANGE OF REYNOLDS NUMBERS INVESTIGATED
BASED ON FIN DIAMETER

Unit	Re Minimum	Re Maximum	Per cent of Fin Length in in Laminar Flow* Minimum Re	Maximum Re
2	1,020	16,300	100	100
3	1,470	12,100	100	100
4	2,220	12,500	100	100
5	3,280	12,800	100	100
6	4,800	34,600	100	58
7	4,600	31,600	100	63
8	10,000	32,600	100	61

*Based on Transitional Reynolds Number of 20,000

If the boundary layer over the finned surface is predominately laminar, then it would be expected that the length factor in both the Reynold's and Nusselt numbers would be the diameter over the fin. If, however, the boundary layer was predominately turbulent due to the main stream turbulence caused by the wake of the root portion of the tube, the root diameter might be expected to be the length factor best correlating the data. This can best be determined by experimental data.

The mean heat transfer coefficient over the fin surface is defined as:

$$h_o = \frac{Q}{A_o \left[t_m - (t_{air})\right]_{mean}} \qquad (43)$$

where: Q/A_o = heat flux from the metal surface to the ambient fluid, Btu/hr sq.ft.

and $[t_m-(t_{air})]_{mean}$ = mean temperature difference between the metal surface and the ambient air, °F

The temperature difference indicated above is an average both from the standpoint of the metal temperature and the ambient air. The variation in the metal temperature is taken into account by the incorporation of the fin metal resistance, whereas the mean air temperature is generally obtained from an average of the mixed mean inlet and outlet temperatures. Dividing the finned heat transfer area into "active" and recirculating sections, the majority of the heat transfer is accomplished by the active section of the fin. Thus, although the temperature rise of the air in the inactive or recirculating zone behind the cylinder is high, this air contributes but little to the mixed mean outlet temperature.

If the mean heat transfer coefficient over the fin surface is defined as:

$$(h_o)_{mean} = \frac{\int_0^A (h_o)_a \, d\,A}{A} \qquad (44)$$

where: $(h_o)_{mean}$ = mean air film heat transfer coefficient

and $(h_o)_a$ = point heat transfer coefficient on the air surface, defined by equation 41

The mean temperature must be given by:

$$(\Delta T)_M = \frac{\int \Delta T_a d\,A}{A} \qquad (45)$$

The measure of the correctness of the use of the logarithmic mean temperature difference would be by comparison of this temperature difference with that given by equation 22. Unfortunately, no data on the subject has appeared in the literature, however, a graphical integration of the temperature distribution illustrated in Figure 44, using the fin diameter indicated b, the dotted curve, indicates that the logarithmic mean temperature difference is probably within 10 per cent of the true value.

The mean air film heat transfer coefficient for air flowing over the surface of a flat plate is generally predicted from an equation of the form:

$$(h_o)_{mean} = C_1 \frac{V_m^{0.5}}{L^{0.5}} \qquad (46)$$

for a laminar boundary layer

and

$$(h_o)_{mean} = C_2 \frac{V_m^{0.8}}{L^{0.2}} \qquad (47)$$

for a turbulent boundary layer

where: C_1 and C_2 = constants slightly dependent on the air temperature

V_m = air velocity over the plate, ft/min.

L = length of the plate measured parallel to the direction of flow, ft.

The slope of the heat transfer-air velocity curves, for the tube banks investigated was found to be 0.7, i.e.

$$h_o = C\, V_m^{0.7} \qquad (48)$$

This value of the exponent, between those for laminar and turbulent flow over flat plates, could be due to:

(1) a turbulent boundary layer over the majority of the active portion of the fin combined with a lower exponent for the root portion of the tube.

(2) a turbulent boundary layer over the majority of the fin with a dependence of the fraction or the heat transfer rate of the recirculation area on the air velocity.

(3) a laminar boundary layer over part of the fin with a turbulent boundary layer over the remainder.

(4) the effect of the fin tip on the heat transfer coefficient on the front portion of the tube. Or any number of combinations of the above possible influences.

In summarizing the previous discussion on the effect of the fin diameter, root diameter and fin thickness it can be stated that:

(a) The effect of the fin thickness, if any, is probably due to an expansion and impingement of the fluid on the frontal portion of the fin.

(b) The effect of the fin diameter arises from two different mechanisms, (1) the larger the fin diameter, the smaller the fraction of fin area affected by the recirculation zone in the rear of the tube (and the higher the calculated mean heat transfer coefficient) and (2) the larger the fin diameter, the lower the mean heat transfer coefficient due to the build up of the laminar boundary layer, to the point where it becomes unstable and the boundary layer becomes turbulent. The dependence of the heat transfer coefficient on this variable is related to the relative strength of these two opposing mechanisms.

(c) The effect of the root diameter can arise from a number of different mechanisms, such as: the smaller the root diameter, the smaller the recirculation zone in the back of the tube, the root diameter affects the mean flow length of the air in flowing over the fin surface (the smaller the diameter, the longer the mean path); the size and degree of turbulence in the wake of a tube, which are dependent on the size of the root diameter, affect not only the heat transfer on the laminar boundary layer of the next tube downstream, but also could affect the position on this tube where the transition occurs.

The above discussions indicate that the most important variable is probably the root diameter, with the fin thickness and fin diameter having lesser effect on the mean heat transfer coefficient to banks of finned tubes. The quantitative dependence of the heat transfer coefficients on these variables, and the verification of the order of importance are discussed in the following section.

VI. CORRELATIONS OF EXPERIMENTAL HEAT TRANSFER DATA

A. Dimensional Analysis

A second approach, widely used in correlating heat transfer and fluid flow data is dimensional analysis. This method, more completely discussed by McAdams[20], consists of correlating the data in terms of dimensionless groups. For example, it is first assumed that the air film heat transfer coefficient for a finned tube bank is dependent on:

$$h_o = \varphi'(c_p, \mu, k, V_m, \rho, D_r, D_o, S, S_f, Y) \qquad (49)$$

where: φ' = a functional relationship (as yet unknown) between the heat transfer coefficient and the variables listed

Equation 49 can be grouped into dimensionless ratios by any of a number of methods[20] to yield:

$$\frac{h_o D_r}{k} = \varphi' \left(\frac{D_r V_m}{\mu}, \frac{c_p \mu}{k}, \frac{D_o}{D_r}, \frac{D_o}{S_f}, \frac{S_f}{Y}, \frac{S}{D_o} \right) \qquad (50)$$

Some of the groups listed above have been encountered numerous times in heat transfer work and have received special names and symbols, such as:

$$Nu = \frac{h_o D_r}{k} = \text{Nusselt number}$$

$$Re = \frac{D_r V_m \rho}{\mu} = \text{Reynolds number}$$

and $$Pr = \frac{c_p \mu}{k} = \text{Prandtl number,}$$

therefore equation 50 can be written in abbreviated form as:

$$Nu = \varphi' \left(Re, Pr, \frac{D_o}{D_r}, \frac{D_o}{S_f}, \frac{S_f}{Y}, \frac{S}{D_o} \right) \qquad (51)$$

The procedure used thus far has been rigorous to the extent that all of the variables which affect the mean heat transfer coefficient have been included in equation 49. Equation 51 denotes the fact that there is a relationship between the Nusselt number and the various dimensionless groups on the right hand side of the equation. In general the nature of this relationship must be obtained by a trial and error procedure with experimental data. By analogy with the results of studies of plain tube banks, it is <u>assumed</u> that the functional relationship denoted by φ' is of the form:

$$Nu = A\, Re^b\, Pr^c\, (D_o/D_r)^d (D_o/S_f)^e (S_f/Y)^f (S/D_o)^g \qquad (52)$$

where: A = a constant for all finned tube banks

b,c,d,e,f,g, = constant exponents.

The exponent b, on the Reynolds number can be determined from the slope of the heat transfer maximum air velocity lines of Figure 55.

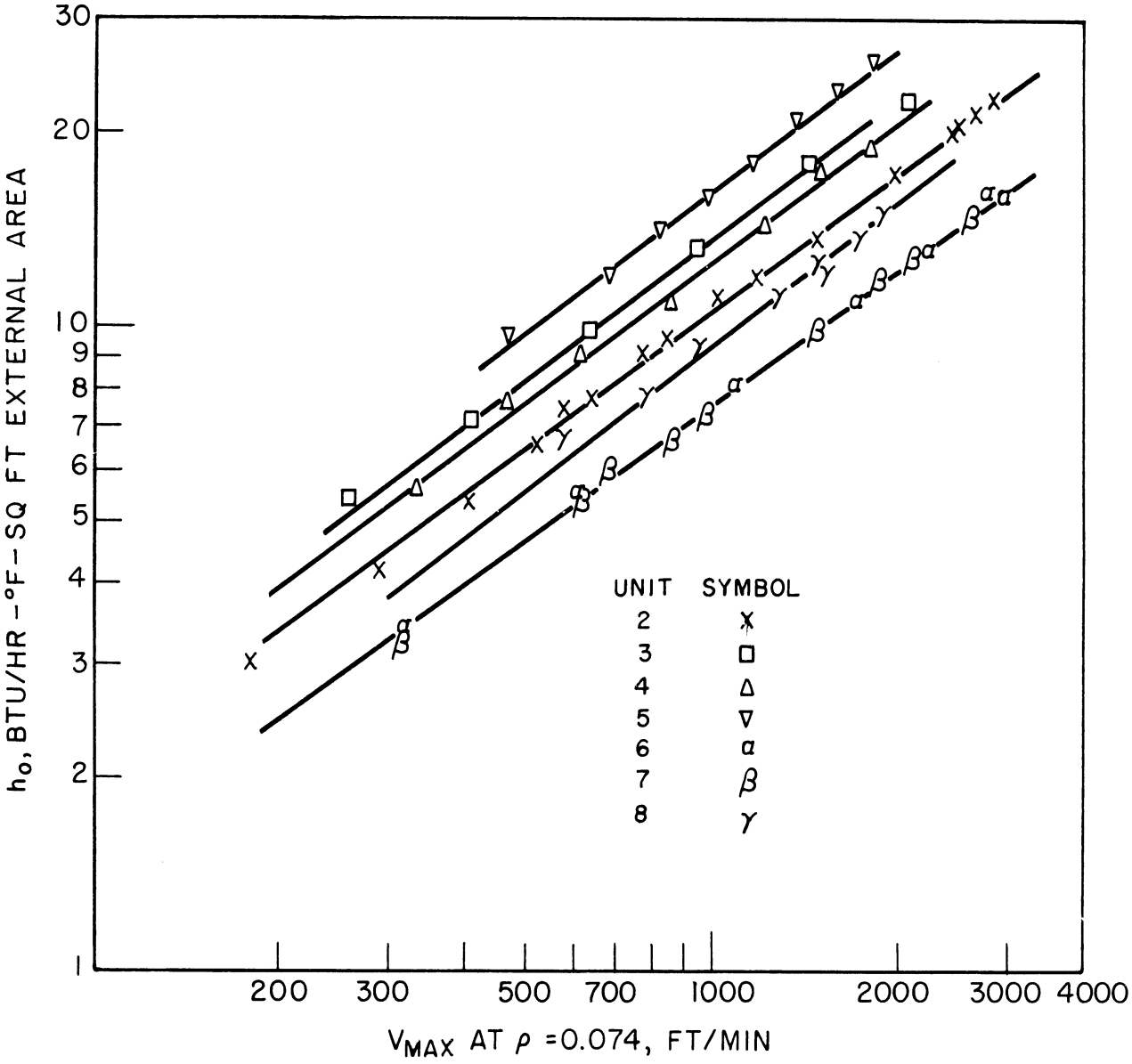

Figure 55. Experimental Heat Transfer Coefficients for the Seven Finned Tube Banks. Data for Units 6, 7 and 8 Corrected to Six Rows of Tubes.

The value obtained from these lines is 0.7.

The value of the exponent c, on the Prandtl group cannot be determined from the experimental data taken here due to the relative constancy of this value for air over wide ranges of temperature. The exponent assumed here is the value of one-third generally used for plain tube data.

The third group, the tube spacing over fin diameter ratio, also had little variation for the seven finned tube banks tested. The value of the exponent "g" has to be obtained from data in the literature. Fortunately, as previously discussed, Jameson[4] studied the effect of this ratio and found that the exponent "g" can be taken as zero for reasonably wide variations in this ratio.

In order to evaluate the exponents d,e, and f, given in equation 52, a least mean square fit was made on the experimental heat transfer data for the seven finned tube banks. Equation 52 was arranged in the form:

$$Nu = A\, Re^{b}\, (D_o/D_r)^{d}(D_o/S_f)^{e}(S_f/Y)^{f}\, Pr^{1/3} \qquad (53)$$

Taking logarithms of both sides of equation 53 yields:

$$\text{Log } Nu = \text{Log } A + b \text{ Log } Re + d \text{ Log } \frac{D_o}{D_r} + e \text{ Log } \frac{D_o}{S_f} + f \text{ Log } \frac{S_f}{Y} + 1/3 \text{ Log } Pr \qquad (54)$$

which is equivalent to:

$$Y = A' + bX_1 + dX_2 + eX_3 + fX_4 \qquad (55)$$

where: $Y = \text{Log } Nu$

$A' = \text{Log } A + 1/3 \text{ Log } Pr$

$X_1 = \text{Log } Re$

$X_2 = \text{Log } D_o/D_r$

$X_3 = \text{Log } D_o/S_f$

and $X_4 = \text{Log } S_f/Y$

which is a linear type equation involving four dependent variables.

A check of the value of the Reynolds number exponent was made by obtaining the value of b from the least-mean-square-fit of all of the data. A comparison of this value with the 0.7 value, obtained by eye, provides to a degree a measure of the validity of the resulting correlation. A check of the effect of the fin spacing was also included by including this variable in the heat transfer relationship. If the conclusions given in the preceeding discussions are correct, the variable should be dropped in the resulting correlation.

Due to the tedious and time consuming nature of the least-mean-square-fit type of calculations, the data were processed by means of a regression analysis program[41] on the University of Michigan Statistical Research Laboratory's IBM 650 digital computer. The program determined not only the best exponents for this type of correlation, but also a statistical measure of the significance of the geometrical groups used[42]. This was accomplished by means of the "F" factor which was set in the program to reject any variable (in this case dimensionless group) which had confidence limits of less than 97.5 per cent. This means that any group which would not improve the degree of correlation

for more than 97.5 per cent of the data points is automatically rejected from the correlation by the computer.

The constants determined by the program for six row deep finned tube banks are listed in Table XXII to three significant figures. Also included in this table are the rounded values of the constants to be used in the final correlation of the heat transfer data.

TABLE XXII

RESULTS OF LEAST-MEAN-SQUARE-FIT OF EXPERIMENTAL DATA

Constant	Constants From Computer	Rounded Off Constants
A	+ 0.364	+ 0.364
b	+ 0.685	+ 0.68
d	+ 0.468	+ 0.45
e	- 0.306	- 0.300
f	- 0.312	- 0.300

Using the rounded off values of the constants given in Table XXII, Equation 53 can be written as:

$$Nu = 0.364\, Re^{0.68} \left(\frac{D_o}{D_r}\right)^{0.45} \left(\frac{S_f}{D_o}\right)^{0.3} \left(\frac{Y}{S_f}\right)^{0.3} Pr^{1/3} \qquad (56)$$

which can be reduced to:

$$Nu = 0.364\, Re^{0.68} \left(\frac{D_o}{D_r}\right)^{0.45} \left(\frac{Y}{D_o}\right)^{0.3} Pr^{1/3} \qquad (57)$$

Equation 57 verifies the previously suspected fact that the heat transfer coefficient is independent of the spacing of

the fins. In the previous section, this conclusion was based on the results of two units, whereas the results given here were statistically derived from the heat transfer data on all of the units.

Equation 57 can be arranged in the following form:

$$h_o = \frac{0.364\ k\ V_m^{0.68} \rho^{0.68}}{\mu^{0.68}} Pr^{1/3} \left(\frac{1}{D_r}\right)^{0.77} (D_o)^{0.15} (Y)^{0.3} \qquad (58)$$

This form of the equation indicates the dependency of the heat transfer coefficient on the geometry of the finned tube.

As can be noted from this equation, the mean air film heat transfer coefficient is strongly dependent on the value of the root diameter, moderately dependent on the thickness of the fin, and practically independent of the fin diameter. This is in general accord with the conclusions reached from the mechanistic approach considered in the previous section.

B. Heat Transfer Correlations

The least-mean-square-fit of the data to the dimensionless equation given in the previous section provides the basic correlation of the heat transfer data. A comparison of the heat transfer data with equation 57 which resulted from the dimensional analysis is given on Figure 56. The data has a maximum spread of + 20% and -15% and an average deviation of $\pm$ 7 per cent from the correlating line. The data appearing in the literature are compared with this correlation on Figure 57. The spread of the data on this figure is greater than for Figure 56, but the degree of correlation is still relatively good, being of the order of + 25% to - 20%. This relationship is recommended for

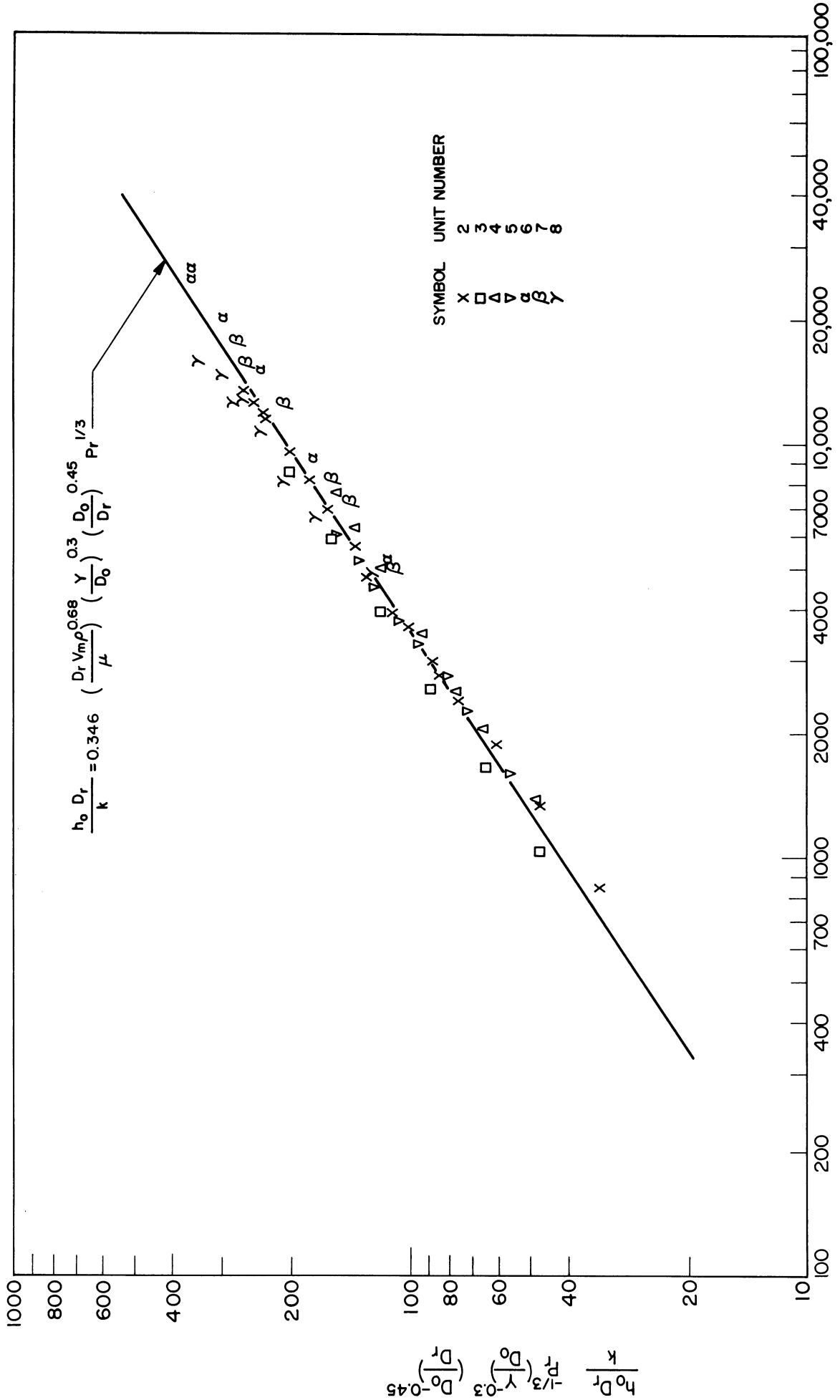

Figure 56. Comparison of Finned Tube Heat Transfer Data With Least Mean Square Fit Curve.

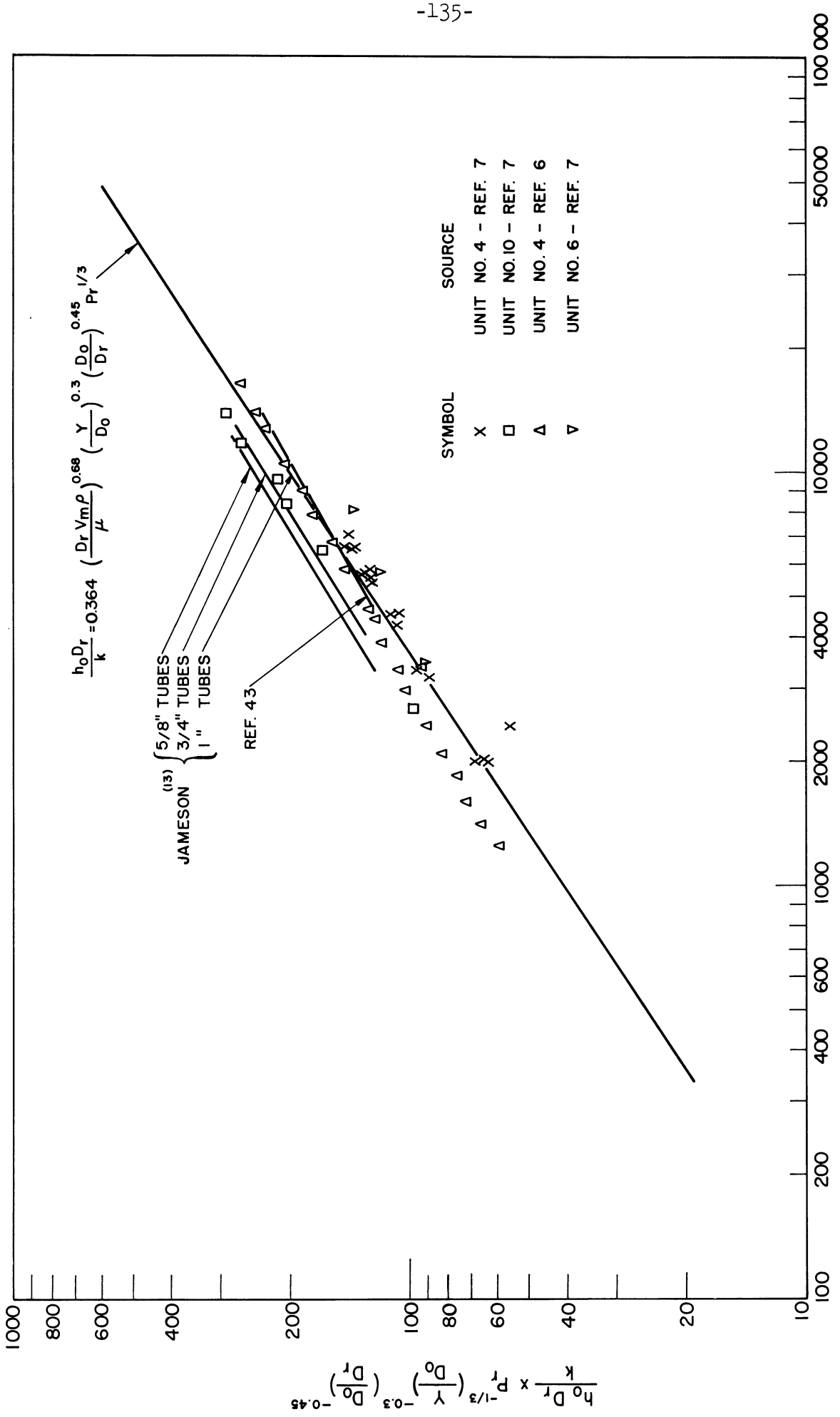

Figure 57. Comparison of Data Appearing in the Literature With Least Mean Square Fit Curve

predicting air film heat transfer coefficients within the range of variables included in the investigation as indicated in Table XXIII.

TABLE XXIII

RANGE OF VARIABLES INVESTIGATED

	Low	High
V_{max}, ft/min	181	2990
Q , Btu/hr	34,500	334,000
D_o, inches	0.737	2.303
D_r, inches	0.438	1.147
Y , inches	0.016	0.022
N , fins/inch	5.13	19.5
n , rows deep	4	8
h_o, Btu/hr-°F-sq.ft.	3.4	25.8
Δ p/n, in. H_2O/row	0.0052	0.365
(Y/D_o)	0.0074	0.0246
(D_o/D_r)	1.18	2.04
Re, $\frac{D_r G}{\mu}$	864	27,300
Nu, $\frac{h_o D_r}{k}$	10.3	106

A number of correlations were obtained using the tube bank dimensions and a trial and error procedure. Most of the resulting relationships provided very little degree of correlation. Two of the results are of interest here. The first of these is given by:

$$Nu = 0.036\ Re^{0.7}\ Pr^{1/3}\ (1/D_r)^{0.4} \qquad (59)$$

where: D_r = root diameter, feet.

This relationship is a dimensional equation, i.e. the constant is dependent on the units in which the root diameter is expressed. The heat transfer data for the seven finned tube banks are presented on Figure 58 in which the solid line through the data on this figure is given by equation 59. The plain tube data is also presented on this figure for comparison purposes. The correlation is compared with the data appearing in the literature on Figure 59. Equation 59 can be arranged in the form:

$$h_o = \frac{k\, V_m^{0.7} \rho^{0.7}}{\mu^{0.7}} Pr^{1/3} \left(\frac{1}{D_r}\right)^{0.7} \qquad (60)$$

Comparing this relationship with equation 58 it can be noted that they differ by only the exclusion of the terms $(D_o)^{0.15}$ and $(Y)^{0.3}$ in equation 58 and the power on the root diameter. Thus equation 60 can be viewed as a simplified form of equation 58. Although equation 60 has the disadvantage of being dimensional, it has the one advantage of remaining determinate for plain tube banks. This is not the case for equation 58.

A third correlation was obtained using the dimensionless relationship:

$$\frac{h_o D_r}{k} = 0.196 \left(\frac{D_r V_m \rho}{\mu}\right)^{0.7} \left[\left(\frac{H}{S_f}\right) \left(\frac{d_{wn}}{d_o - d_{wn}}\right)\right]^{0.25} Pr^{1/3} \qquad (61)$$

The relationship is compared with the finned tube data given here in Figure 60 and with the data from the literature in Figure 61. Examination of these figures indicates that while the equation satisfactorily correlates the data reported here, it does not satisfactorily correlate the data appearing in the literature. This equation is

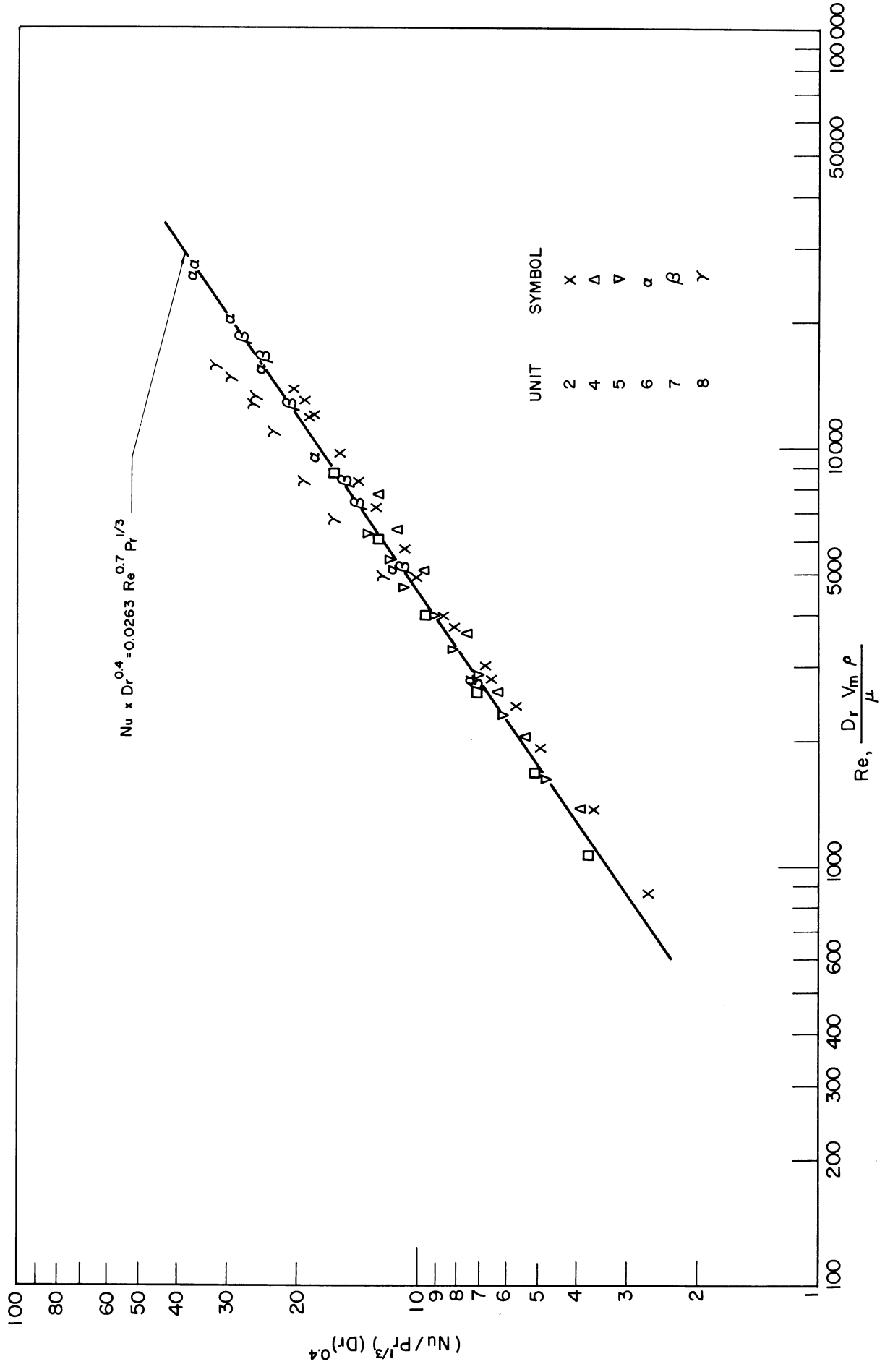

Figure 58. Comparison of Data with Empirical Dimensional Correlation.

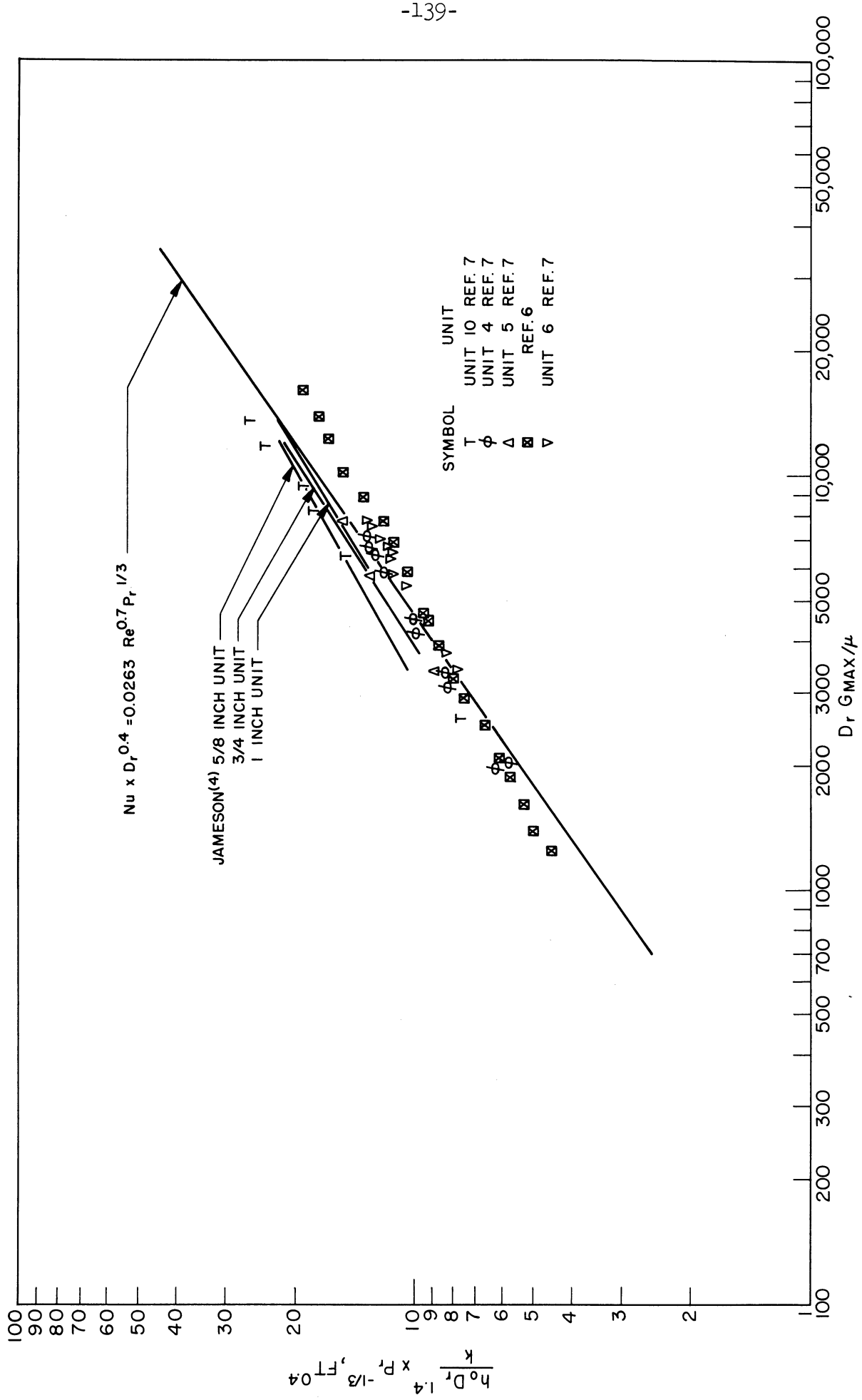

Figure 59. Comparison of Data From the Literature with Emperical-Dimensional Correlation.

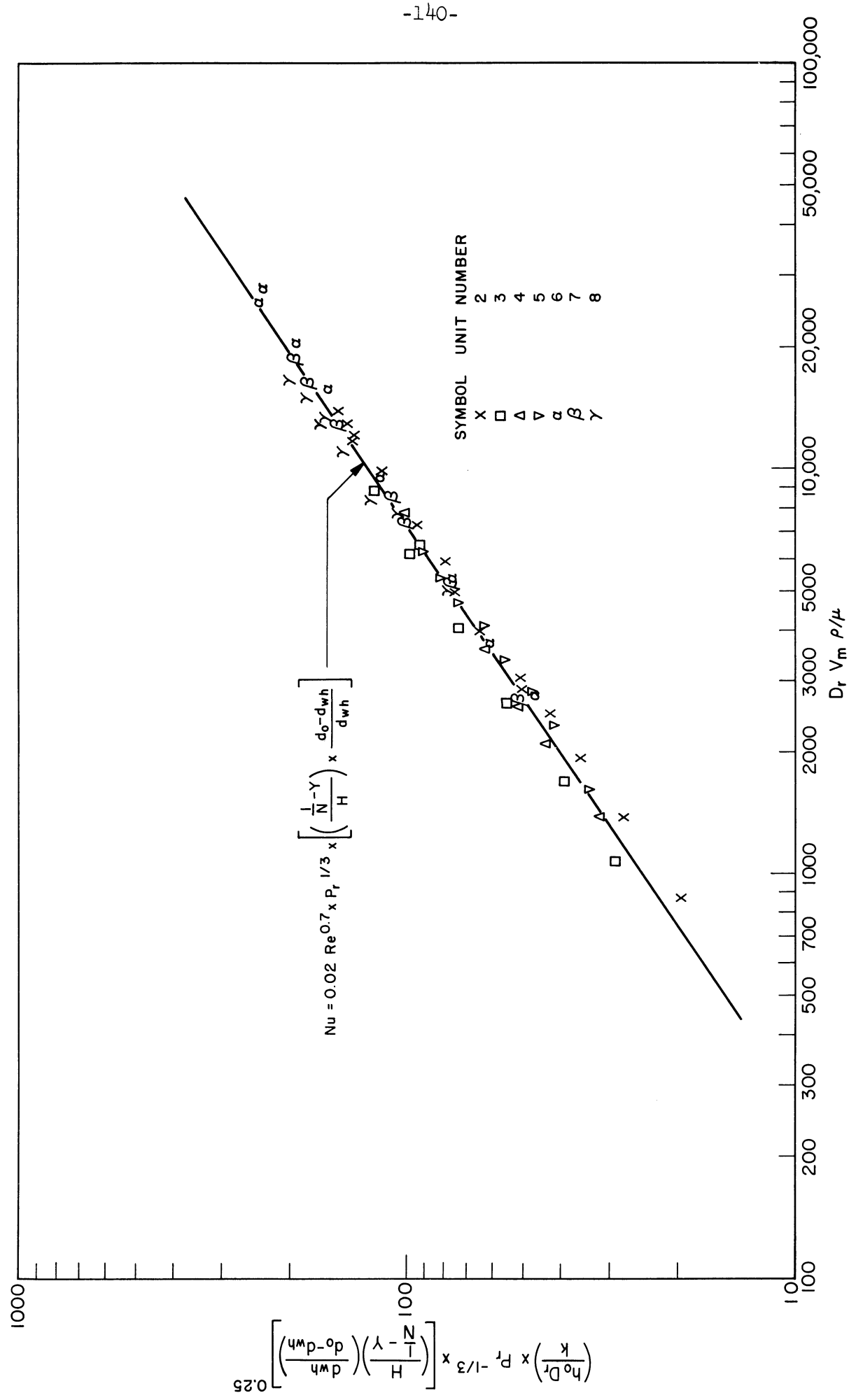

Figure 60. Comparison of Data with Emperical Dimensionless Correlation.

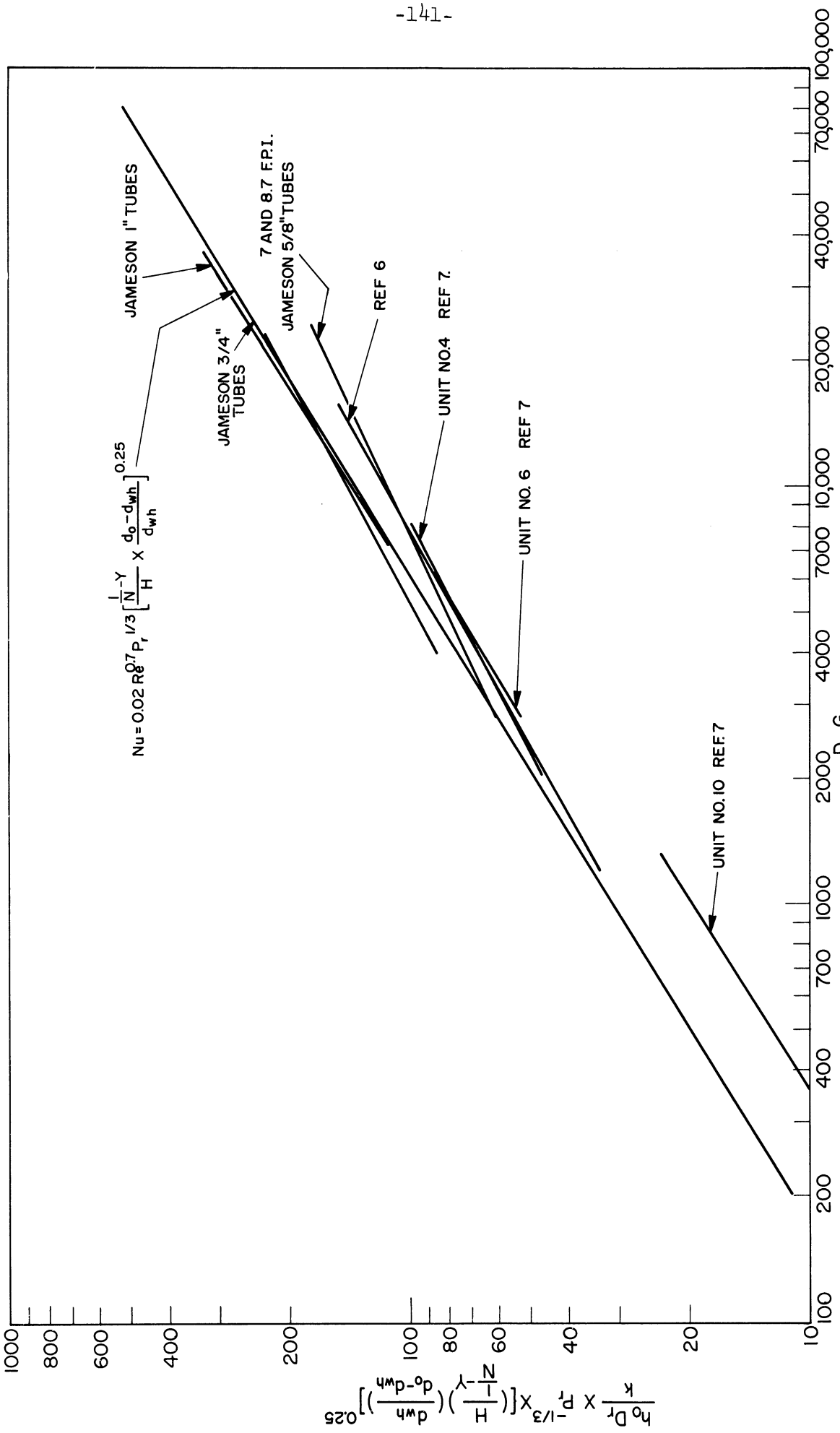

Figure 61. Comparison of Data From the Literature With Emperical-Dimensionless Correlation.

not recommended for general use.

The data reported here for the seven finned tube banks are compared with the correlations appearing in the literature in Figures 62, 63 and 64. Examination of these figures indicates that these relationships do not satisfactorily correlate the data.

It should be pointed out that the correlations represented by equations 57, 59, and 61 are for tube banks having six rows of tubes. In order to use these correlations for tube banks other than six rows deep the constants or the computed coefficients have to be corrected using Figure 41. This can be accomplished by using the relationship:

$$(h_o)_{mi} = (h_o)_{m6} \cdot \frac{(h_o)_{m\infty}}{(h_o)_{m6}} \cdot \frac{(h_o)_{mi}}{(h_o)_{m\infty}} \qquad (62)$$

where: $(h_o)_{mi}$ = mean air film heat transfer coefficient for a finned tube bank containing i rows of tubes

$(h_o)_{m6}$ = mean air film heat transfer coefficient for a six row bank of finned tubes (obtained from correlation)

and $\frac{(h_o)_{m\infty}}{(h_o)_{m6}} \cdot \frac{(h_o)_{mi}}{(h_o)_{m\infty}}$ = corrections for number of rows for a six row and an "i" row tube bank from Figure 41

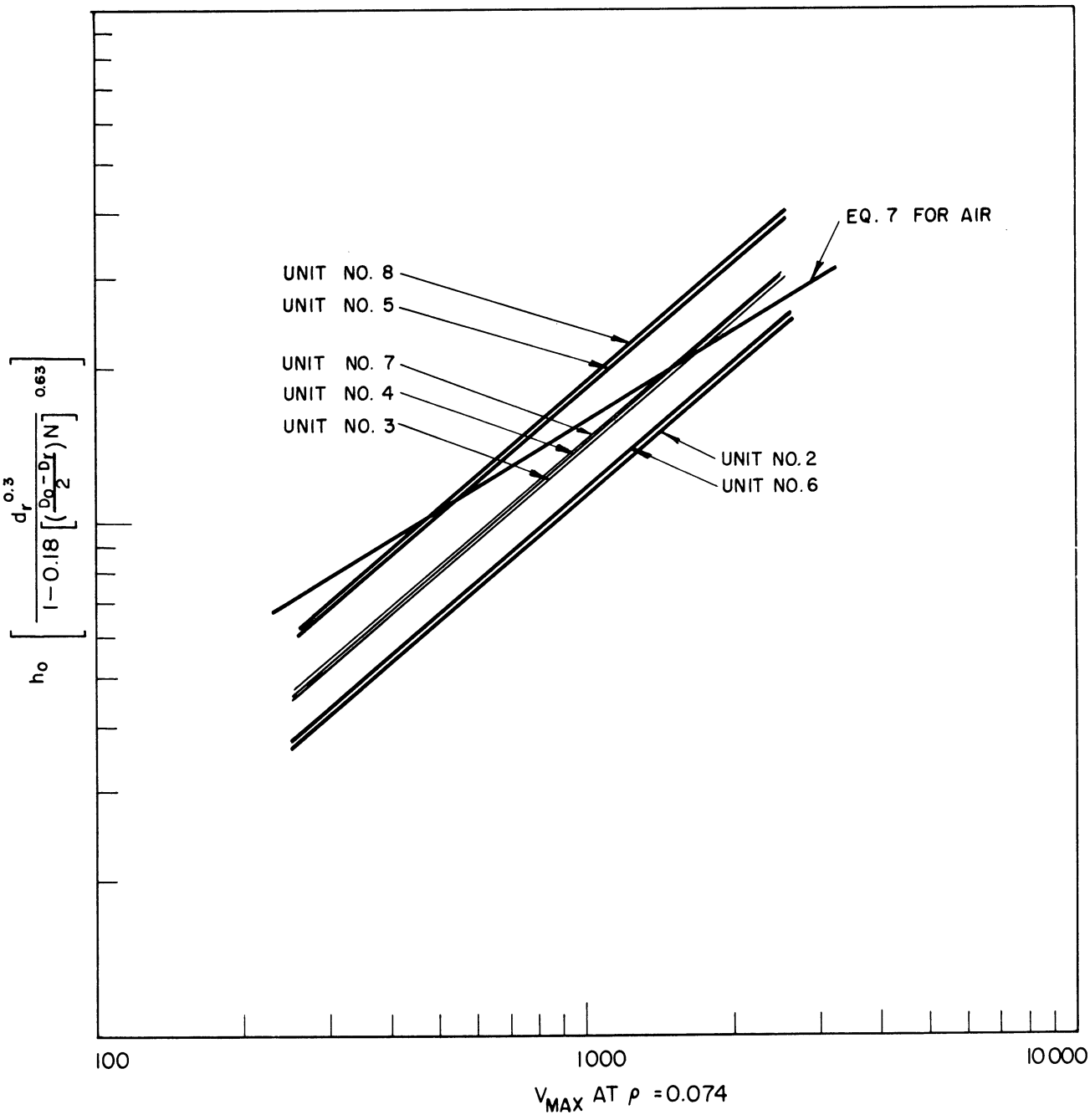

Figure 62. Comparison of Data With Correlation of T. E. Schmidt.

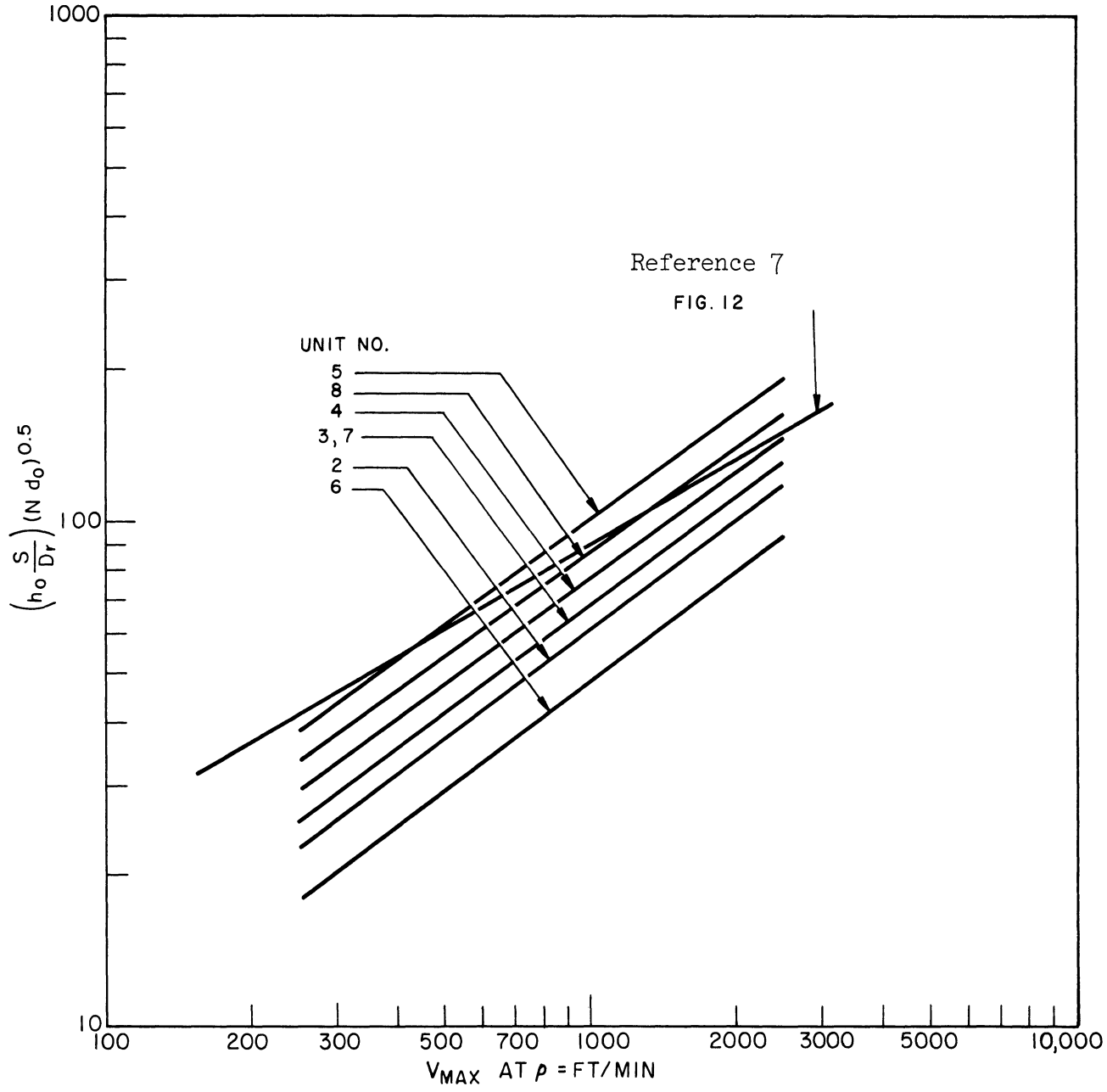

Figure 63. Comparison of Data with Dimensionless Correlation of Katz, et al.

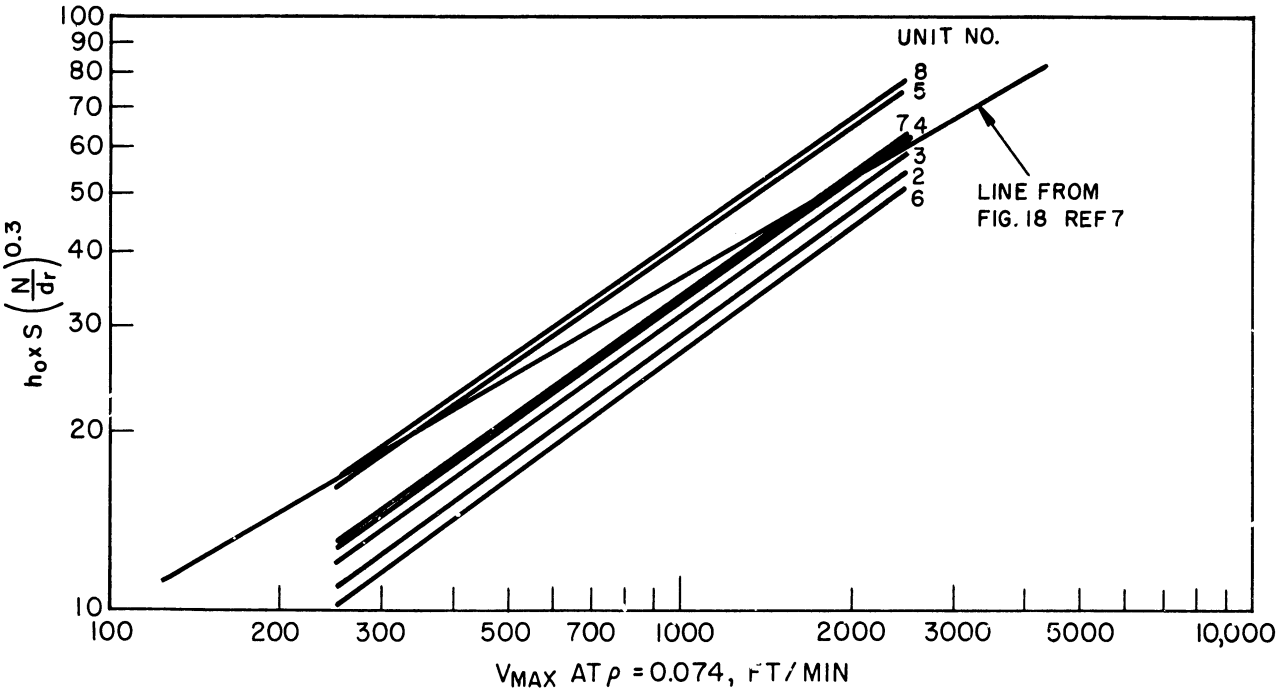

Figure 64. Comparison of Data with Dimensional Correlation of Katz, et al.

VII. ANALYSIS OF PRESSURE DROP DATA

Two different pressures can be properly defined for any moving fluid stream. The first pressure is the static pressure which is the pressure exerted by the molecules due to their random kinetic motion. A second is a velocity pressure which is the pressure exerted by the molecules due to their orientated motion, or speed in the direction of flow. Of principal interest here is the decrease in the static pressure encountered by the air in passing through the tube banks.

The difference between atmospheric pressure and the static pressure of the air measured immediately downstream of the tube banks can be divided into three principle effects; entrance pressure losses, tube bank pressure drop, and difference in velocity pressures of the air entering and leaving the tube banks. The static pressure immediately upstream from the tube bank is less than atmospheric because of the skin friction of the entrance section walls and the acceleration of the air to the face velocity in front of the tube banks. There is also a static pressure loss due to the increased air velocity leaving the tube banks caused by the increase in air temperature and subsequent decrease in air density. The total pressure difference between the atmosphere and the air leaving the tube banks can thus be written:

$$\Delta p_T = \Delta p_f + (1/2\ \rho\ V_f^2)_i + (\Delta \rho)_B + \Delta (1/2\ \Delta\ V^2) \qquad (63)$$

in which: Δp_T = total pressure difference between the atmosphere and air leaving the tube banks, inches of water

Δp_f = pressure loss due to skin friction of entrance section walls, inches water

$(1/2\rho V_f^2)_i$ = velocity pressure of air approaching the tube banks, inches of water

Δp_B = pressure drop of air in flowing through the tube bank, inches water

$\Delta(1/2\rho\Delta V^2)$ = difference in velocity pressure approaching and leaving tube banks, inches of water

where: $\Delta\, 1/2\ \rho\ \Delta\ V^2 = 1/2\ \rho\ (V_f)_o^2 - 1/2\ \rho\ (V_f)_i^2$

$(V_f)_i$ = inlet air face velocity

and $(V_f)_o$ = outlet air face velocity

which can be reduced to:

$$\Delta p_T = \Delta p_f + \Delta p_B + 1/2\ \rho(V_f)_o^2 \qquad (64)$$

Order of magnitude calculations of the entrance section skin friction losses indicate that it is several orders of magnitude smaller than the total pressure drop. This term can therefore be safely ommitted from the equation, leaving:

$$\Delta p_T = 1/2\ \rho(V_f)_o^2 + \Delta P_B \qquad (65)$$

Calculations of the magnitude of the velocity pressure term indicate that this term represents about two per cent of the total pressure drop. This was considered negligible compared with the total pressure drop so that equation 65 becomes:

$$\Delta p_T \cong \Delta p_B \qquad (66)$$

The pressure losses of the air in flowing through the exchanger are due to three mechanisms: skin friction, form drag, and expansion losses.

The skin friction pressure losses are attributed to the fluid boundary layers adjacent to the metal surface. As shown earlier, the

fluid molecules in the immediate neighborhood of the metal surface experience a decrease in their mean velocities in the direction of flow. These particles, upon again entering the main fluid stream at the end of the tube must again be accelerated to the main stream velocity. The energy necessary to accelerate these fluid molecules comes from a decrease in the static pressure of the entire fluid stream.

The form drag arises principly from the wake formed in the rear of the cylinder. The vortices formed in this wake, upon moving downstream decrease in size and dissipate their rotational energy in the form of heat. The fluid particles must then also be accelerated to the main stream velocity by means of a decrease in the static pressure of the main stream fluid.

The third cause of pressure loss arises from the expansion and contraction of the fluid flowing past the rows of tubes. The mean velocity of the air while flowing past the centerline of a row of tubes is approximately double the mean velocity immediately ahead of the row. The fluid particles upon passing past the row of tubes again revert to the mean velocity ahead of the row (neglecting the small change in density). This acceleration and deacceleration of the molecules is accomplished by a static pressure loss for acceleration and a static pressure gain in deacceleration, however, in the conversion of the static to velocity pressure and back, the gain in the static pressure never quite equals the loss due to the irreversible nature of the process. Thus there is a net loss in static pressure between the various rows due to expansion and contraction of the fluid.

Efforts to differentiate the total pressure drop data for flow through banks of tubes into the three mechanisms given above[6] have been generally unsuccessful. The best pressure drop correlations have been empirical and in terms of the total pressure drop of the units.

The pressure drop data for the eight tube banks tested was presented in Tables VIII through XV in tabular form. The same data is presented in graphical form in Figures 65 through 72 where the pressure drop per row of tubes is plotted versus the standard maximum air velocity, As indicated in these figures the data can be represented by straight lines on logarithmic paper, which is algebraically equivalent to equations of the form:

$$\frac{\Delta p}{n} = A V_m^{\,b} \qquad (67)$$

where: $\Delta p/n$ = pressure drop per row of tubes, inches of water per row

A = constant for any tube bank

V_m = standard maximum air velocity, ft/min at p = 0.074

and b = a constant which varied from 1.51 to 1.9 for various tube banks

In 1945, Gunter and Shaw[21] presented a correlation for predicting the pressure drop of fluids flowing in crossflow through plain and finned tube banks. The amount of data available on finned tube banks being very meager, the correlation was primarily based on data from plain tube banks. The small amount of data available on finned tube banks was fairly well correlated by their relationship, which for the turbulent region was given as:

$$\frac{\Delta p g_c D_{vn} \rho}{G_m^2 L}\left(\frac{\mu}{\mu_w}\right)^{0.14} = 0.96\left(\frac{D_{vn} G}{\mu}\right)^{-0.145}\left(\frac{S_\ell}{S_t}\right)^{0.6}\left(\frac{D_{vn}}{S_t}\right)^{0.4} \qquad (68)$$

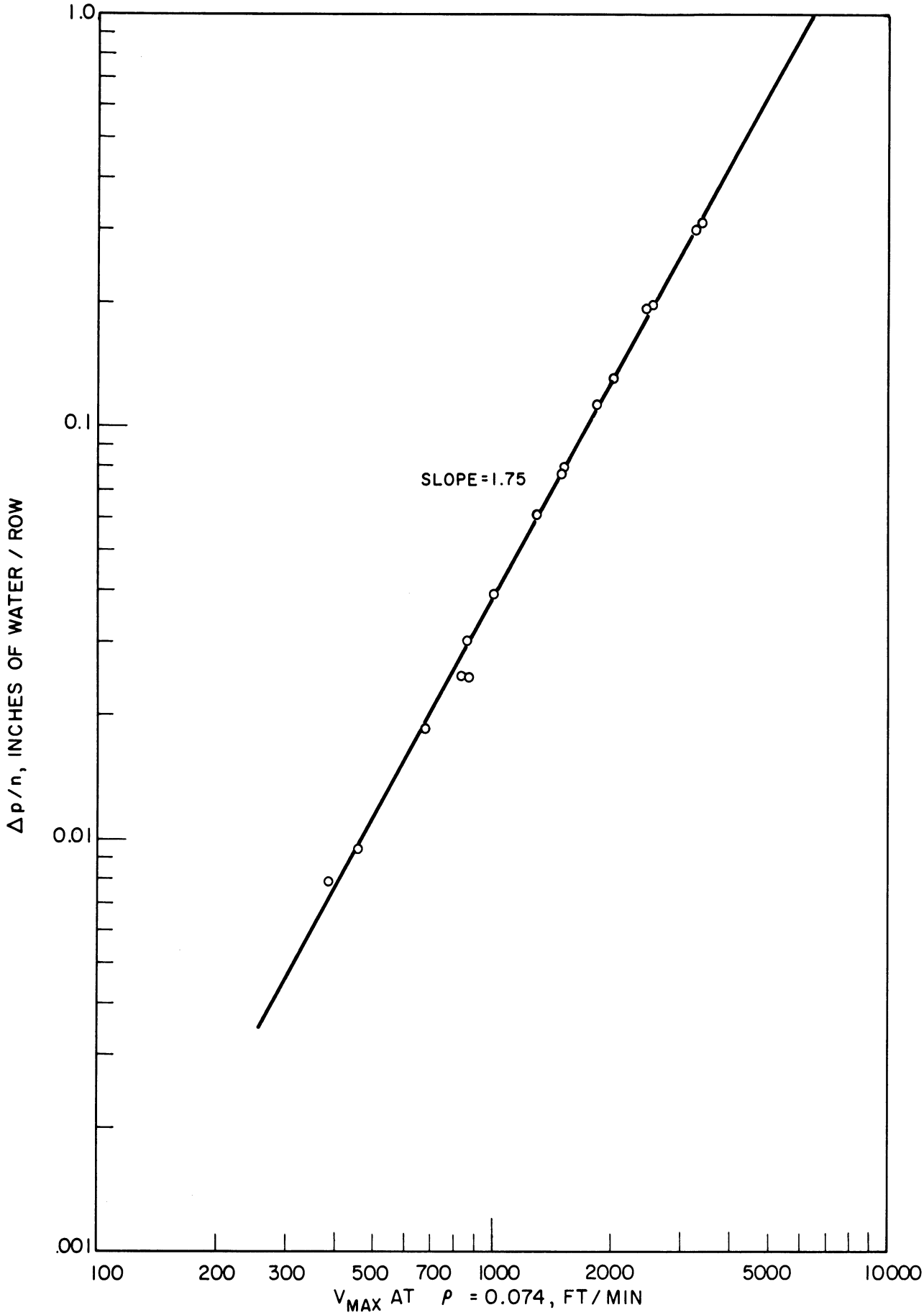

Figure 65. Pressure Drop Data of Unit Number 1.

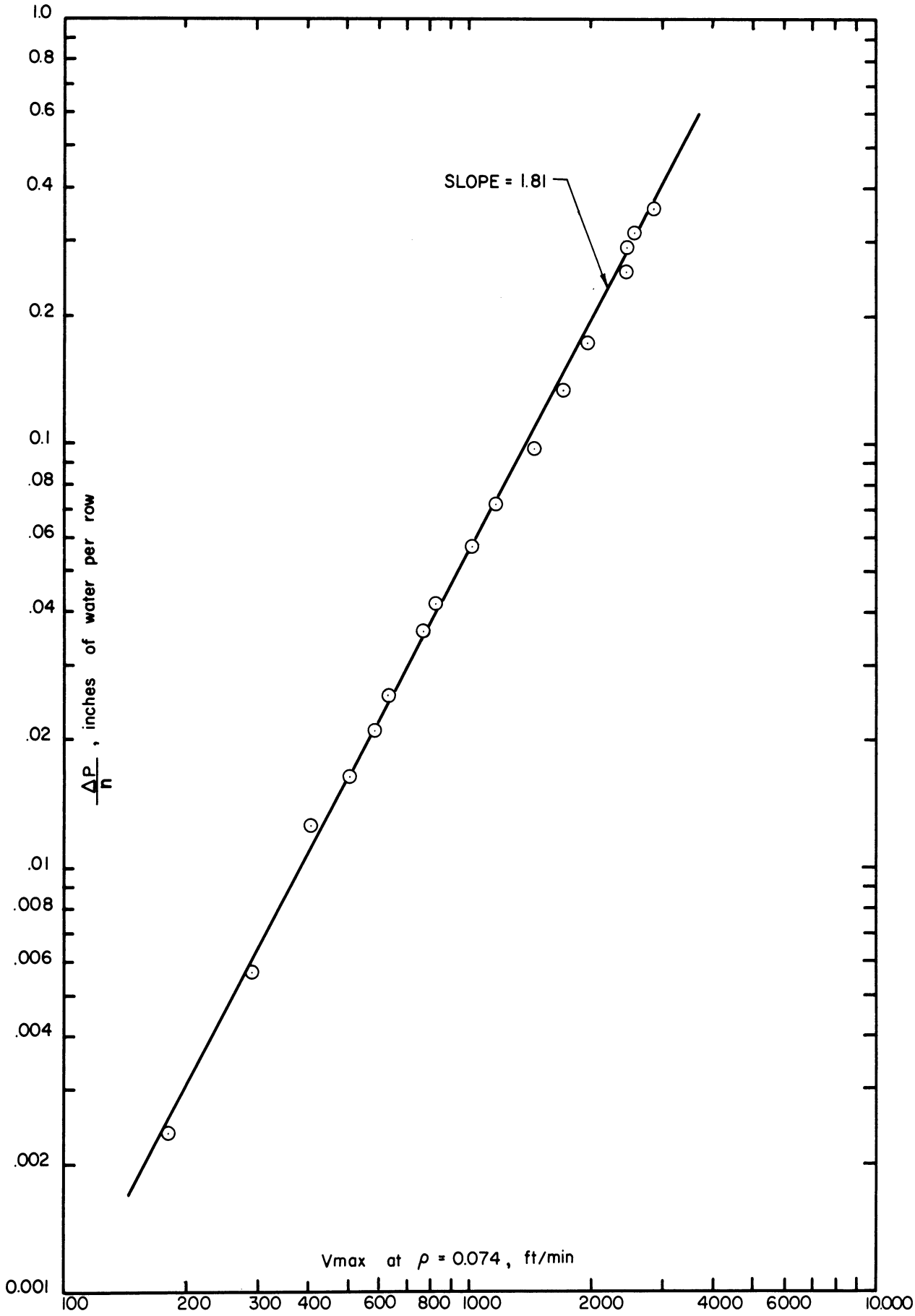

Figure 66. Pressure Drop Data of Unit Number 2.

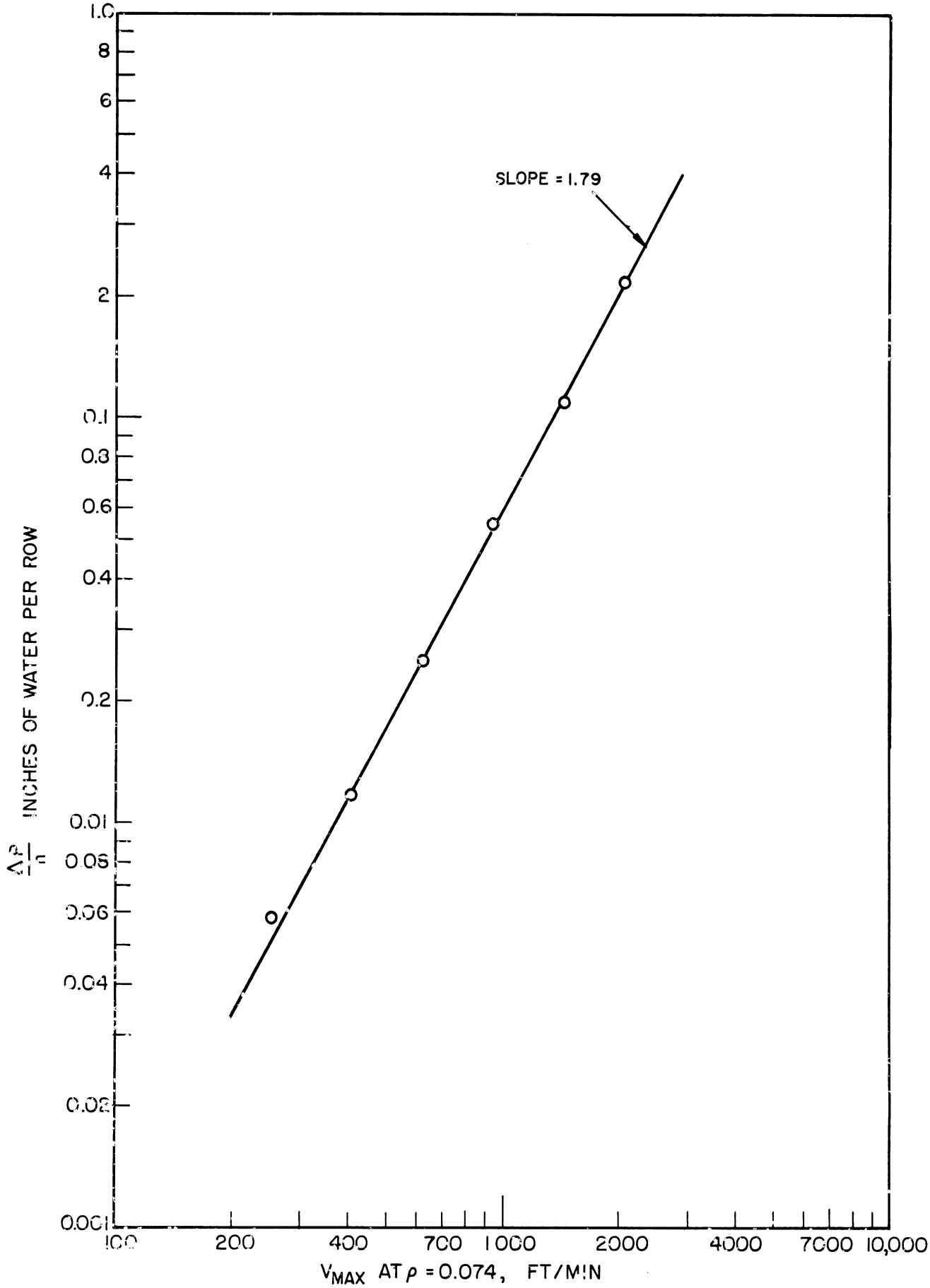

Figure 67. Pressure Drop Data of Unit Number 3.

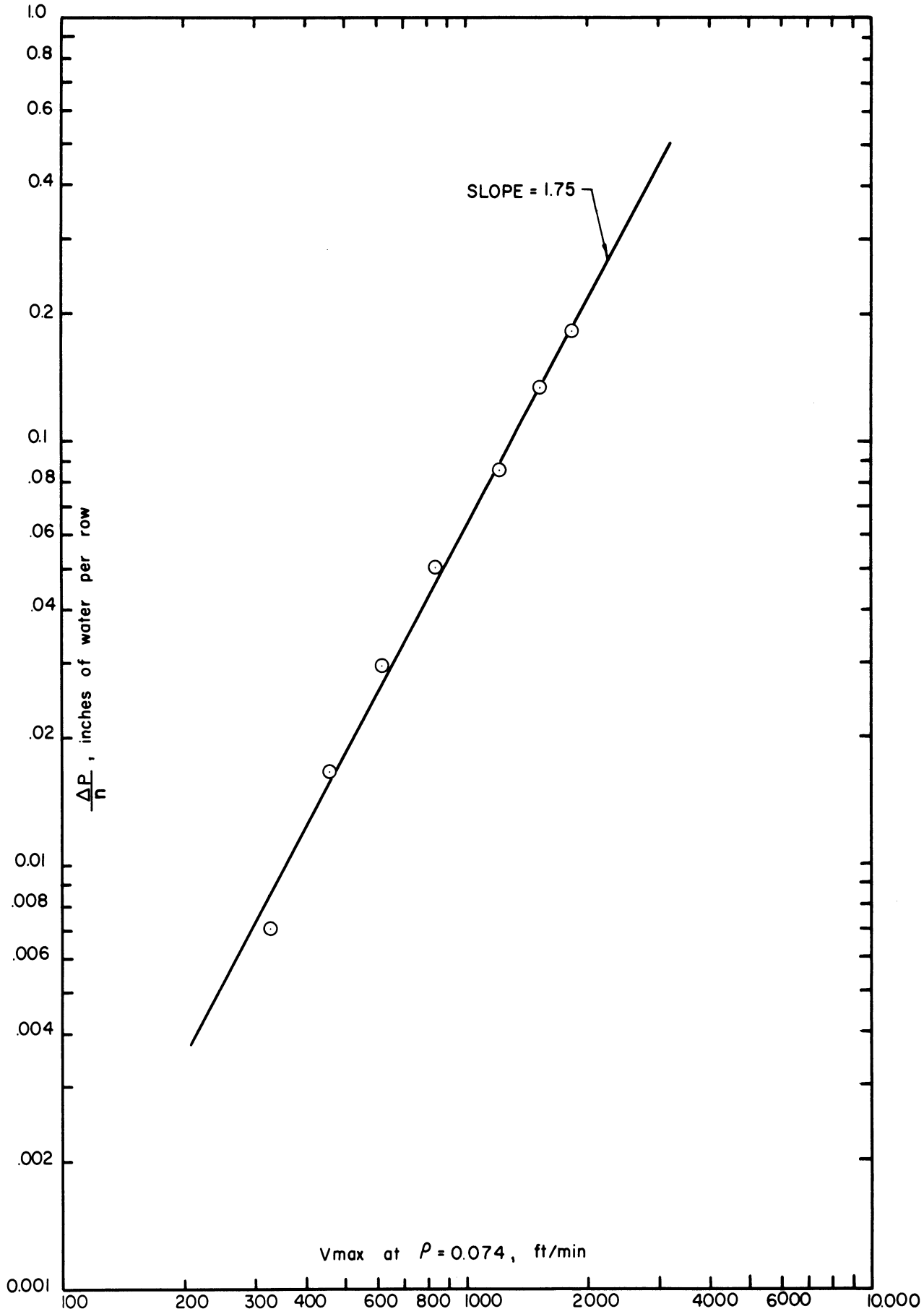

Figure 68. Pressure Drop Data of Unit Number 4.

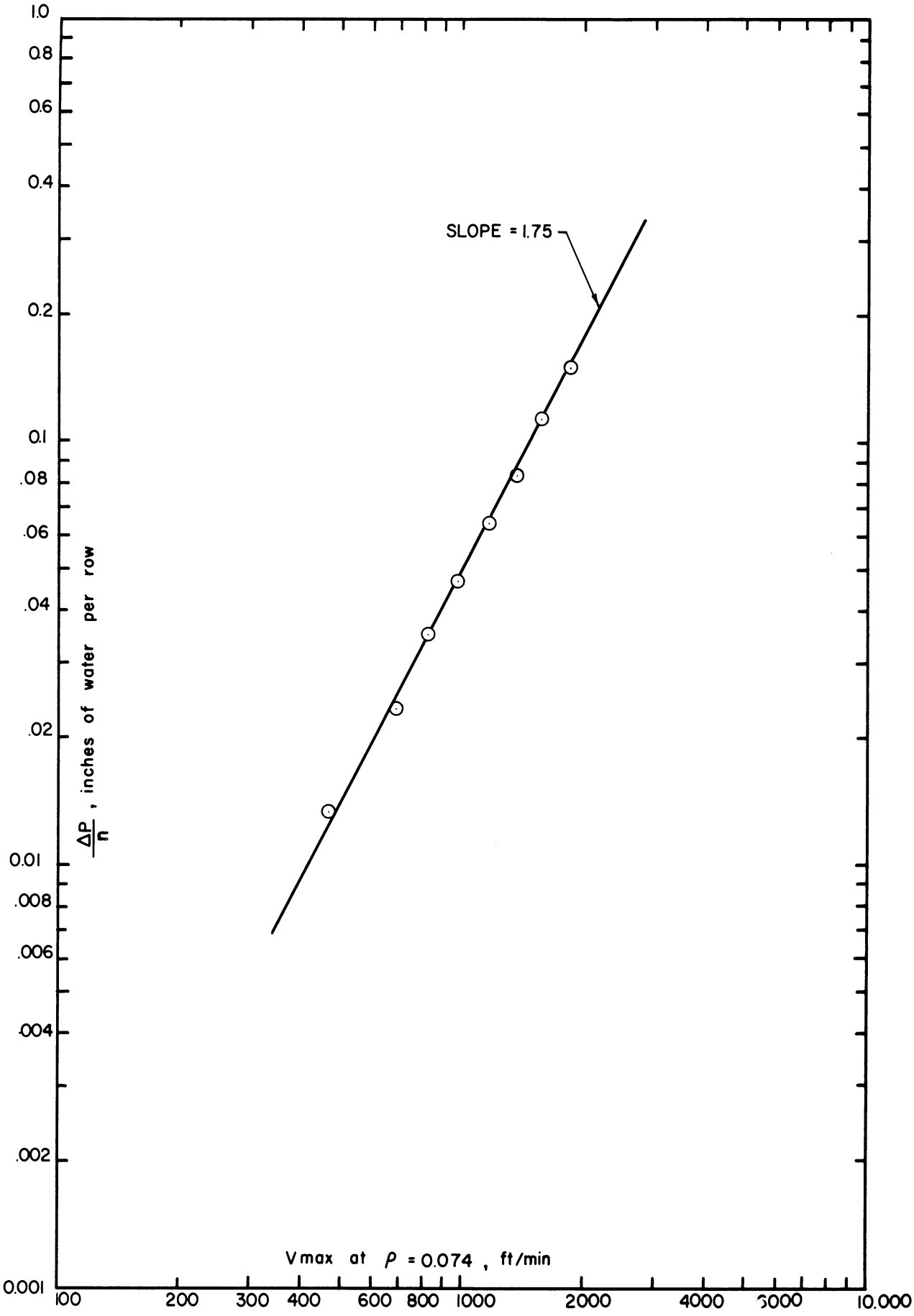

Figure 69. Pressure Drop Data of Unit Number 5.

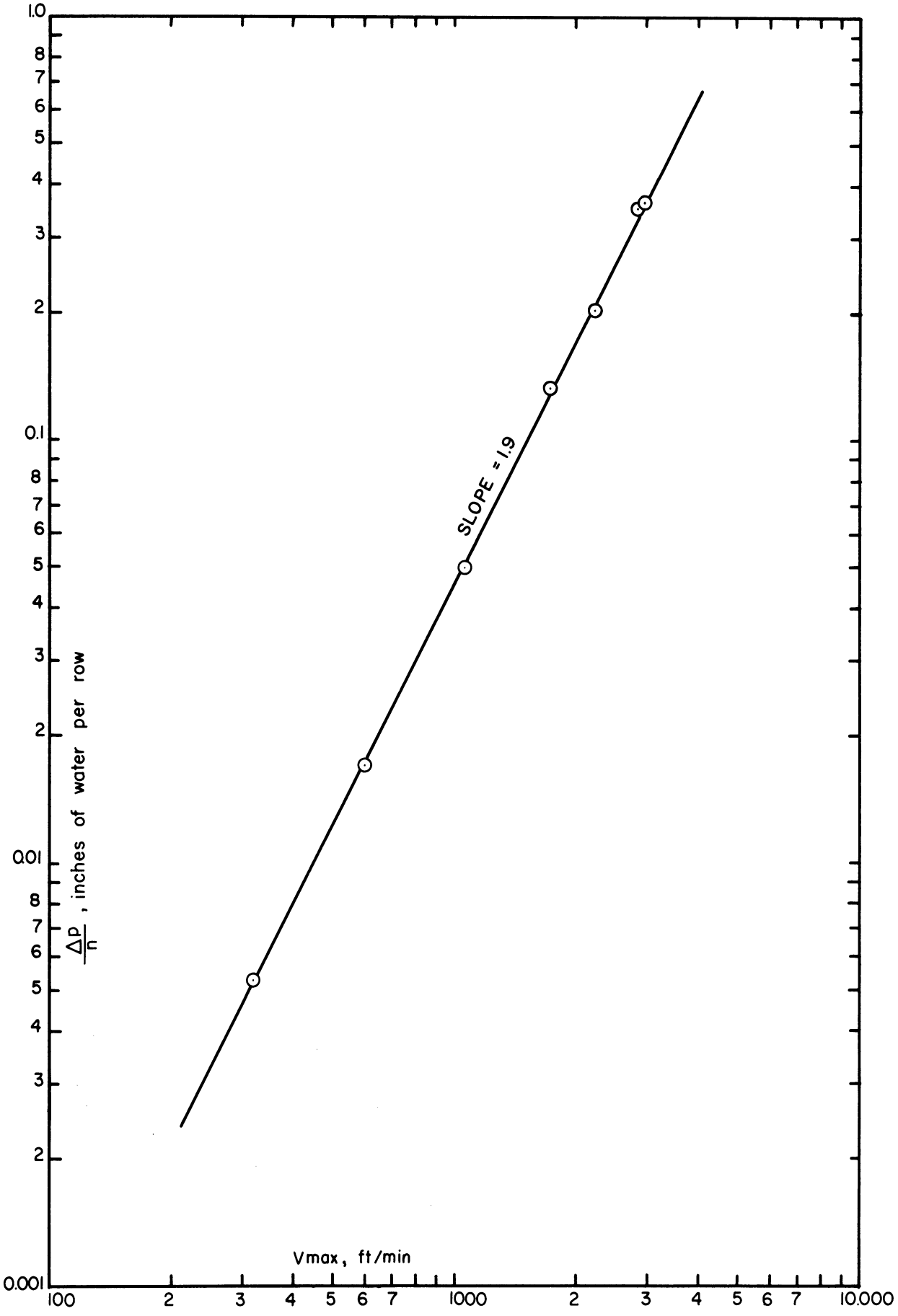

Figure 70. Pressure Drop Data of Unit Number 6.

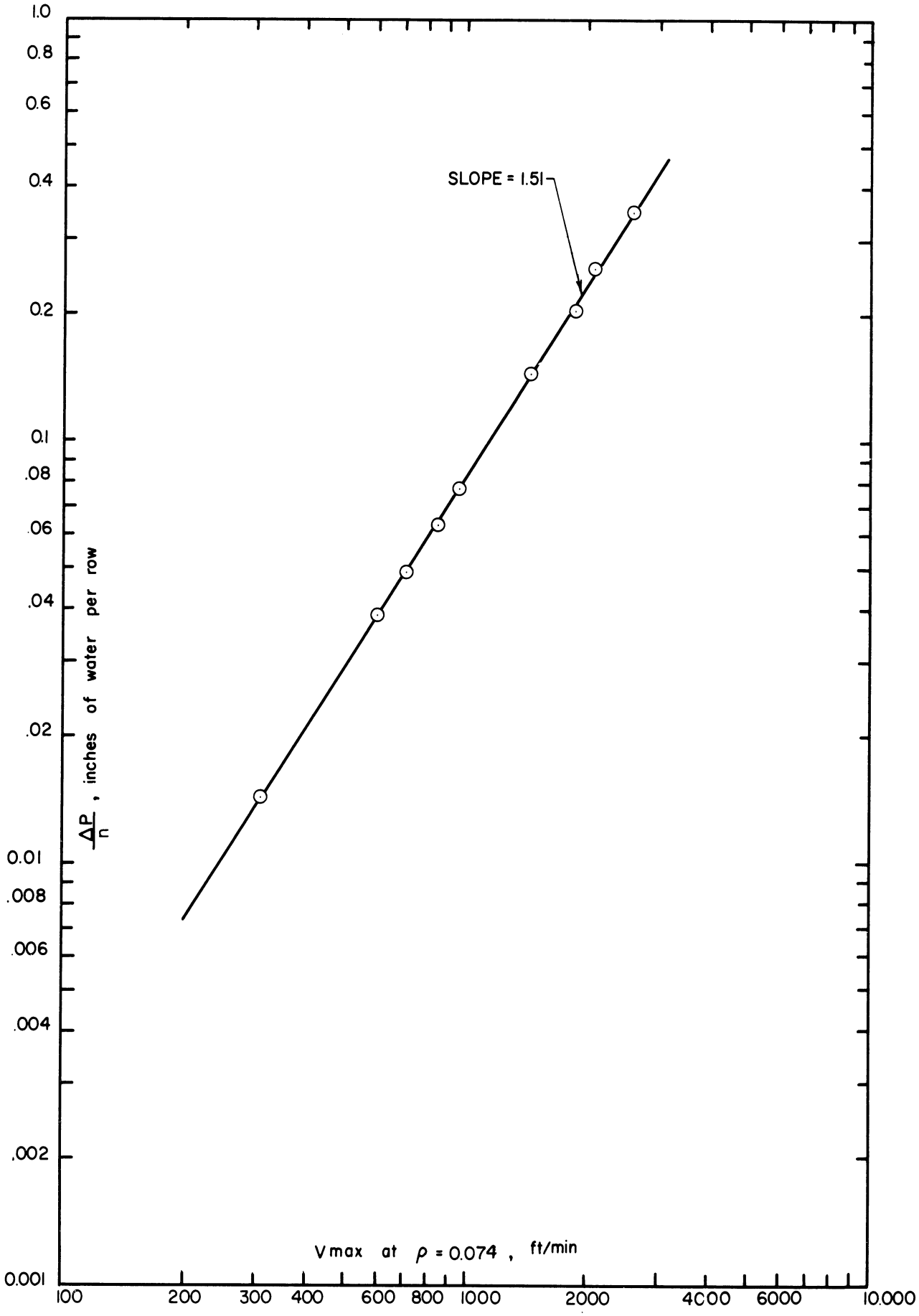

Figure 71. Pressure Drop Data of Unit Number 7.

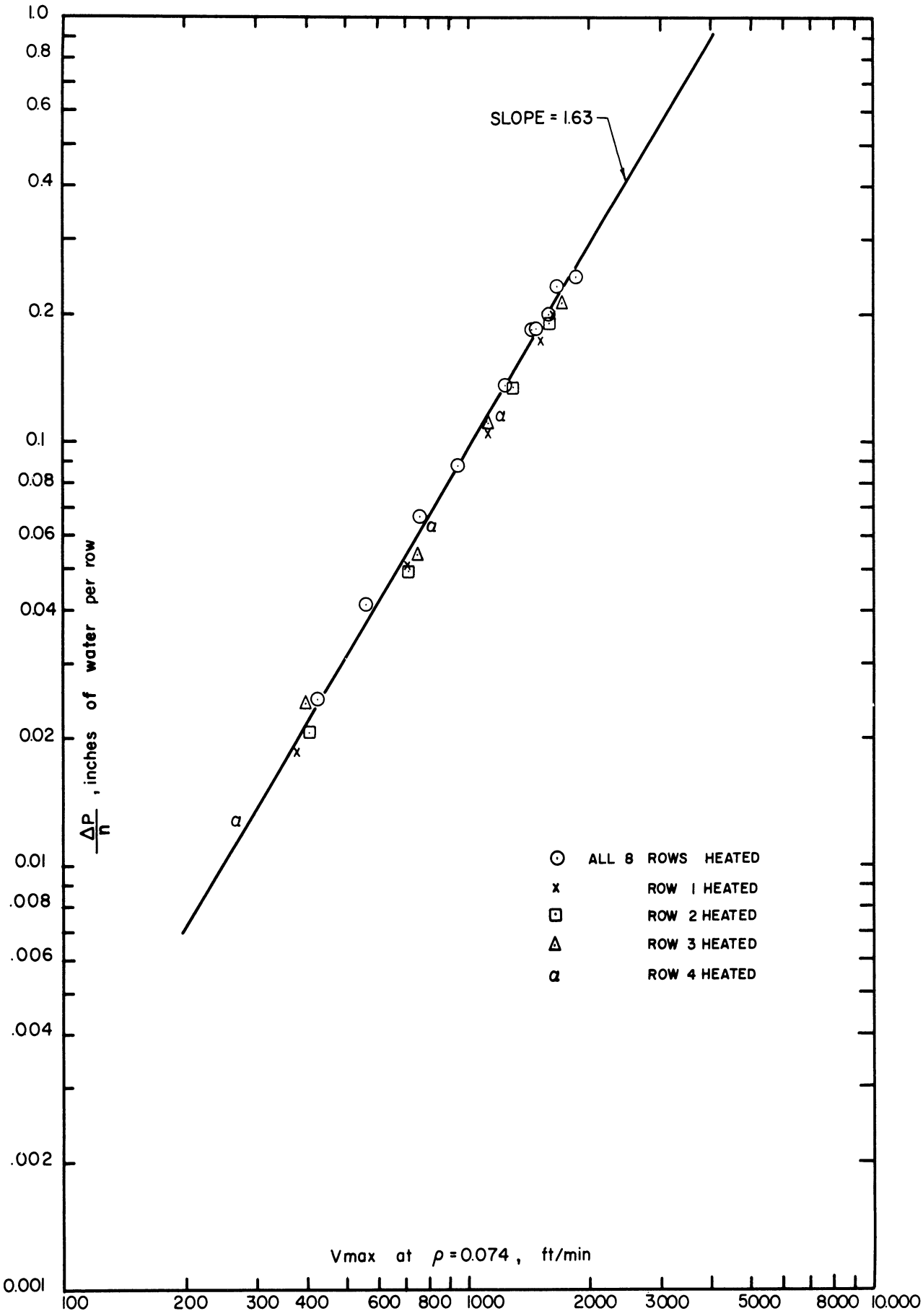

Figure 72. Pressure Drop Data of Unit Number 8.

which for air at 100°F reduces to:

$$\frac{\Delta p}{n} = 5.85 \times 10^{-8} \frac{V_m^{1.8555} \; S_\ell^{0.6}}{D_{vn}^{0.745}} \qquad (69)$$

The data for the eight tube banks are compared with equation 16 in Figure 73. Examination of this figure indicates a reasonable degree of correlation exists between the data and equation 16, with the line in this figure tending to be slightly higher and have a slightly higher slope than the majority of the data. This is better illustrated in Figure 74 where the data is compared with equation 68. As can be noted from this figure, the same discrepancy exists between the position and slope of the line and the experimental data. Examination of the original data shown in Figure 75 on which the correlation was based indicates that the slope of the line was primarily dictated by data with Reynolds numbers between 10^4 and 5×10^5. Thus the slope of the line in Figure 75 cannot be altered without appreciably affecting the original correlation. Examination of the original data indicates that the line can be lowered approximately 15 per cent without destroying the original plain tube correlation of Gunter and Shaw. The latter line is recommended for banks of finned tubes. The scatter of the data about the recommended mean line as shown in Figure 74 gives an average deviation of ± 15 per cent with maximum deviations of ± 26 per cent and - 31 per cent.

The pressure drop data is compared with other correlations available in the literature in Figures 76, 77, and 78, the lines from figures 66 through 72 being used to represent the data. Examination of these figures indicates that the degree of correlation of the data using these relationships is less than that obtained using equation 68 with a constant of 0.81.

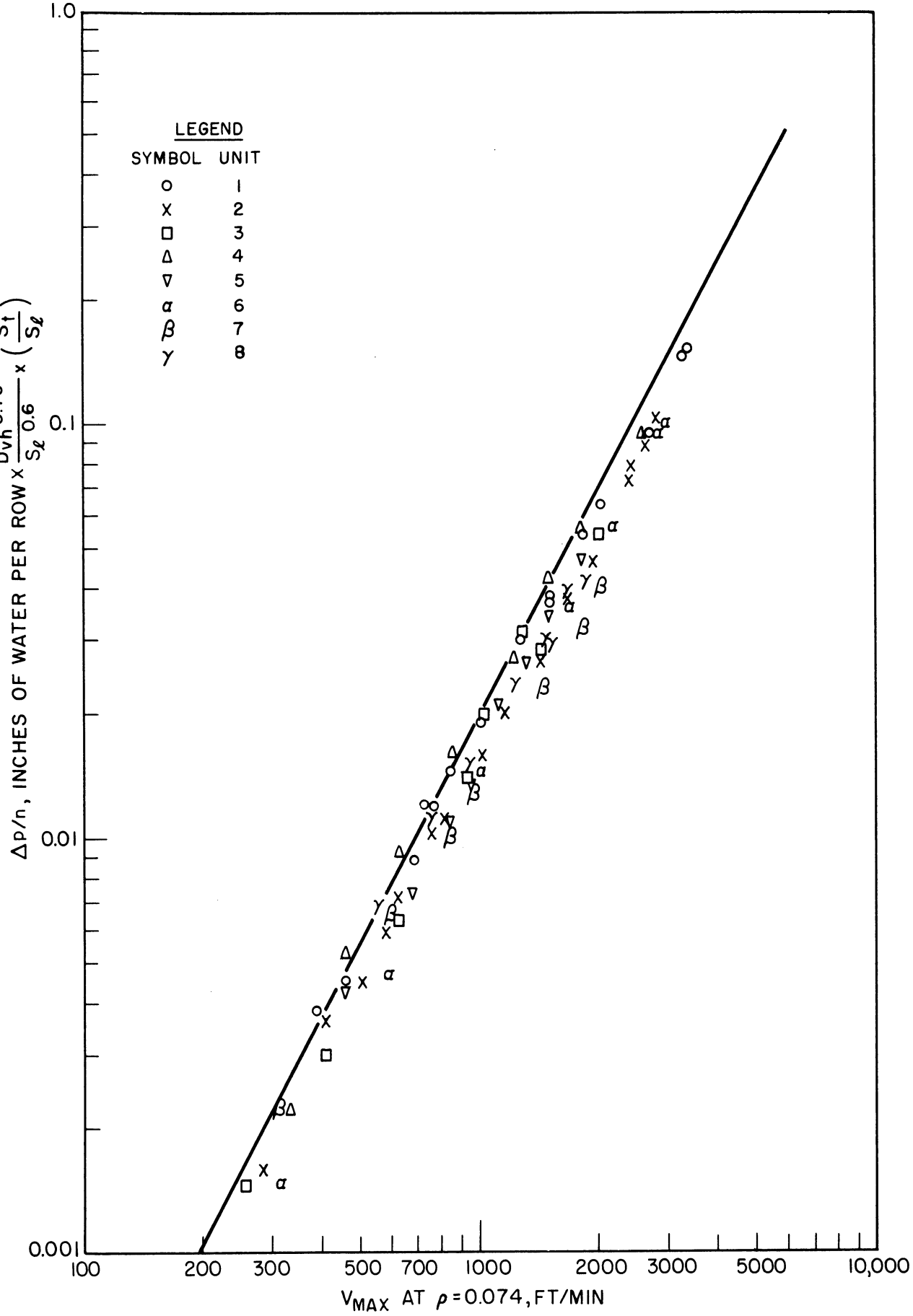

Figure 73. Comparison of Pressure Drop Data with Gunter-Shaw Correlation for Air at 100°F.

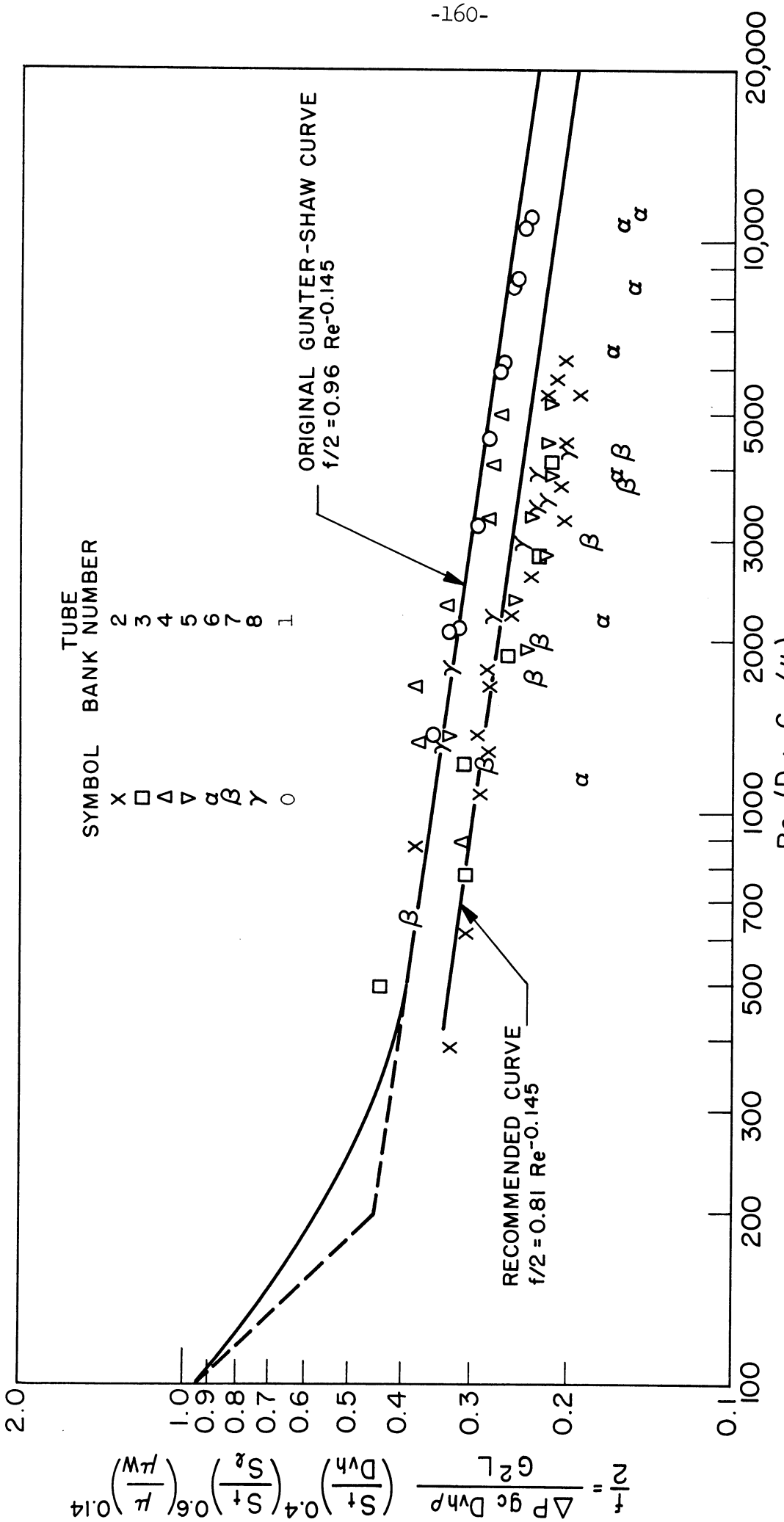

Figure 74. Comparison of Pressure Drop Data with Gunter-Shaw Correlation.

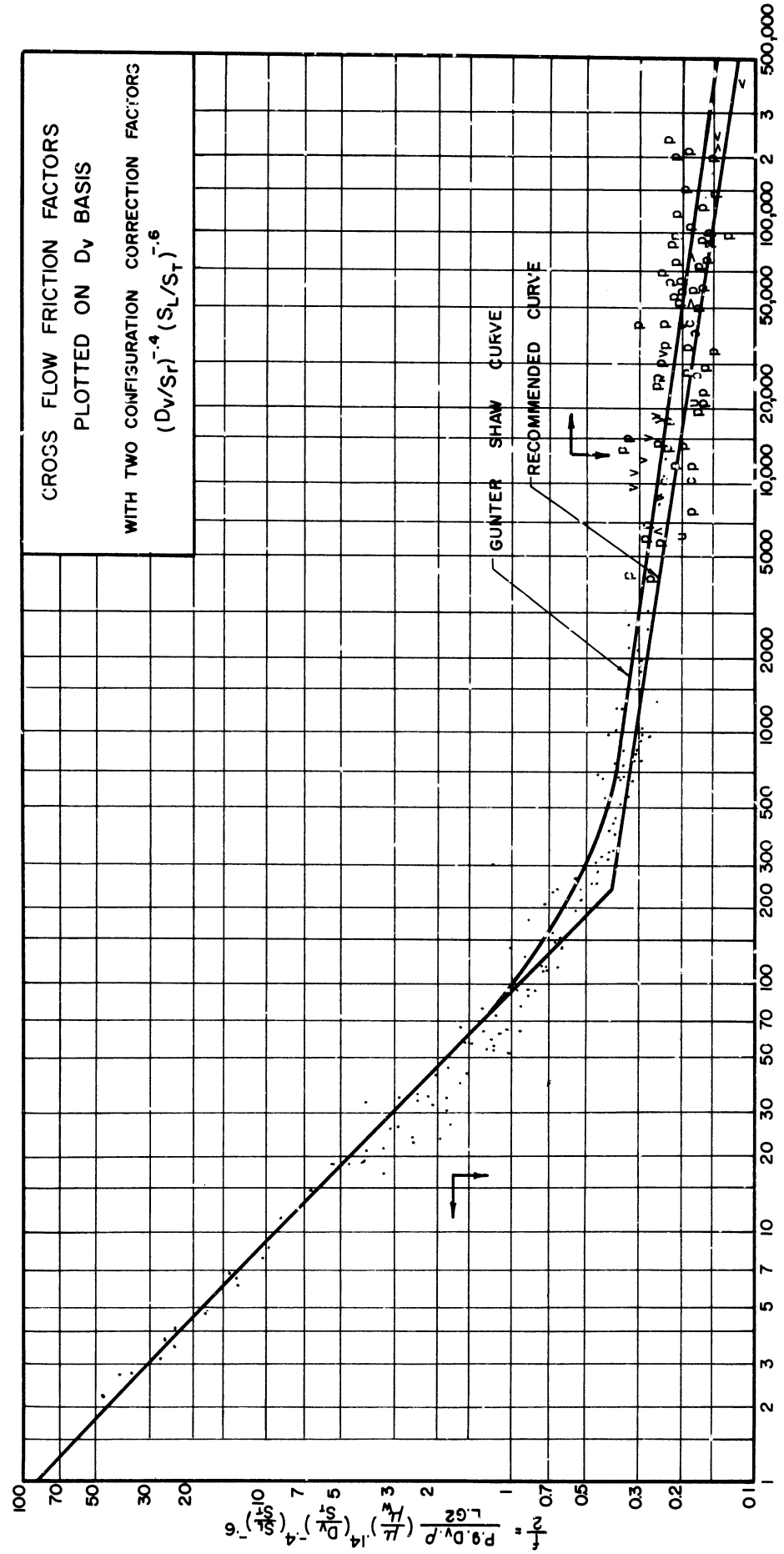

Figure 75. Original Data Used for Correlation by Gunter and Shaw Indicating Possible Lowering of Mean Curve

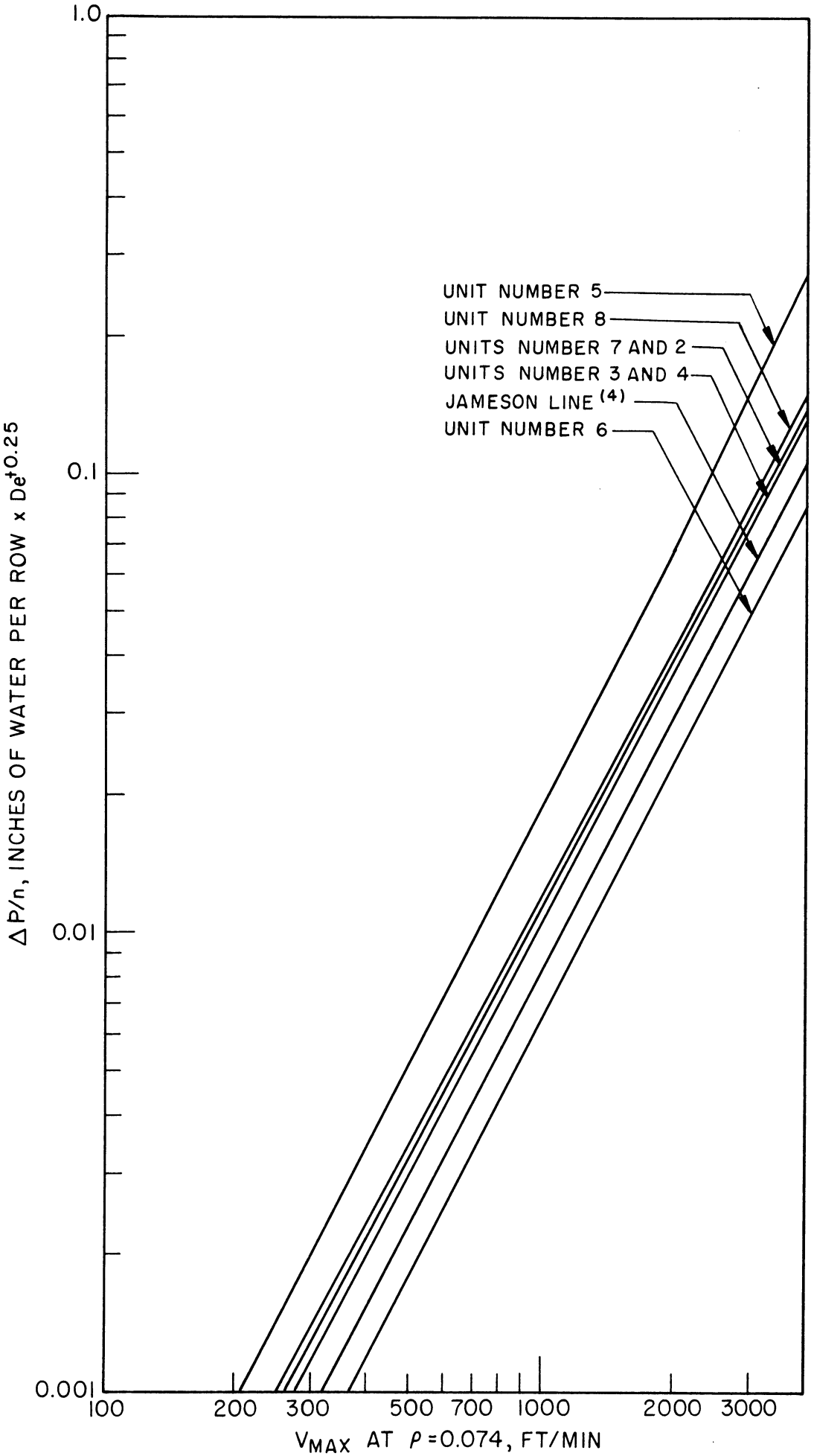

Figure 76. Comparison of Pressure Drop Data with Correlation of Jameson(4).

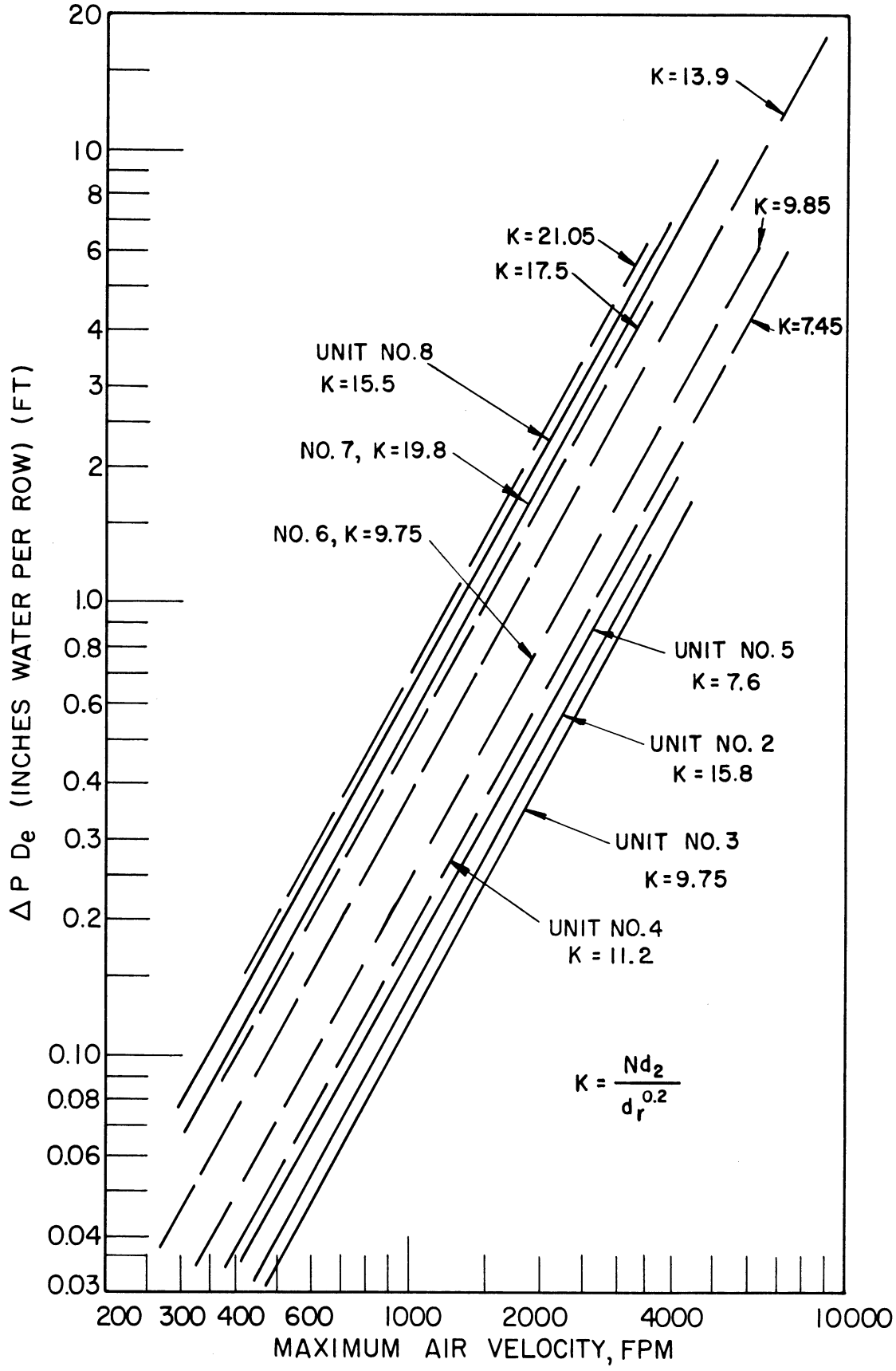

Figure 77. Comparison of Pressure Drop Data with Dimensionless Correlation of Katz, et al.(7).

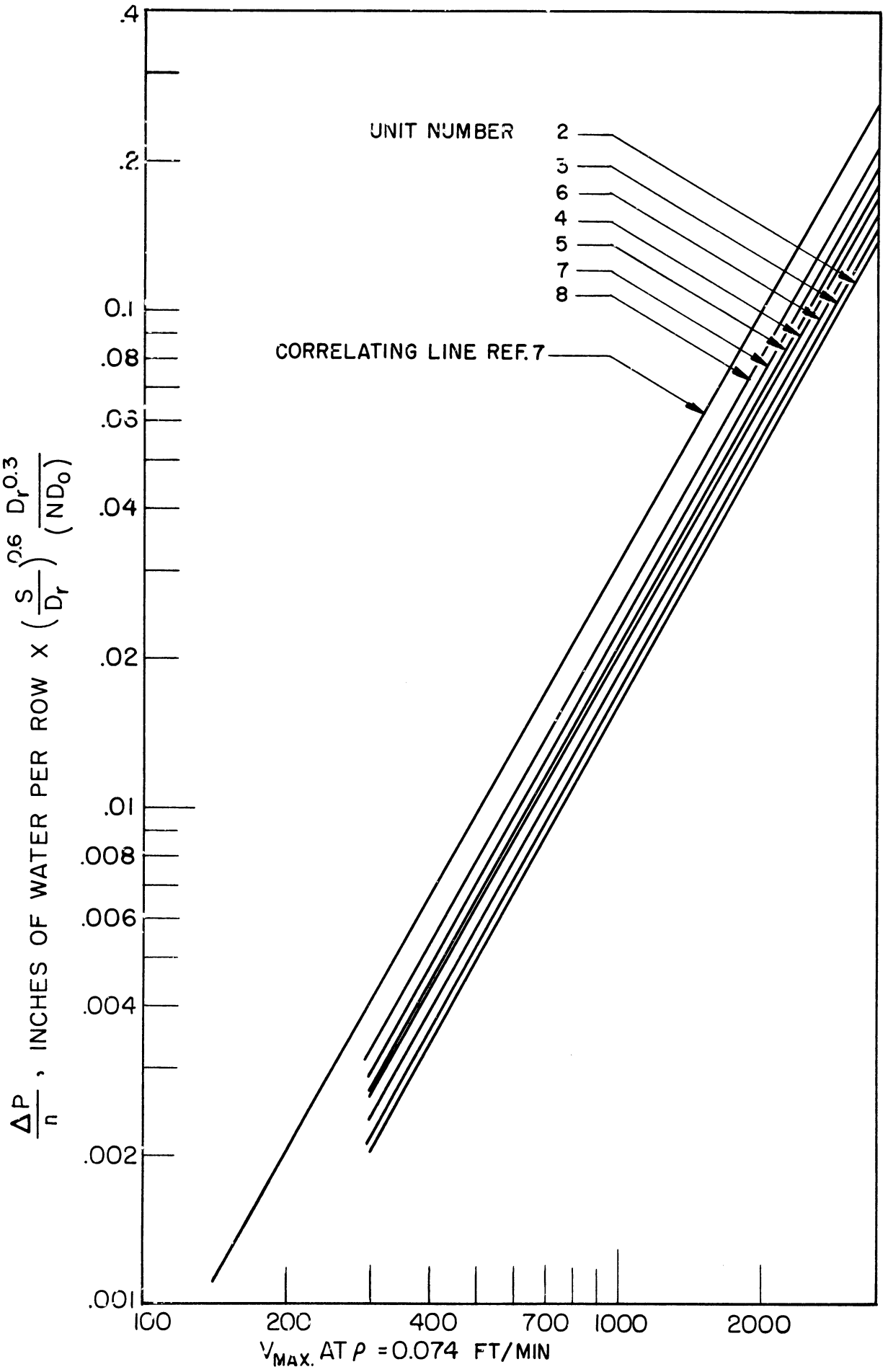

Figure 78. Comparison of Pressure Drop Data with Dimensional Correlation of Katz, et al.(7).

VIII. CONCLUSIONS

The following conclusions are made regarding the heat transfer and pressure drop characteristics of air flowing in crossflow by forced convection through banks of finned tubes laid out on equilateral triangular pitch arrangement.

1. The mean air film heat transfer coefficient for finned tube banks is dependent upon the number of rows of tubes normal to the direction of the air stream. This effect is primarily due to the fact that the first row of tubes has a different performance than succeeding rows.

2. The mean air film heat transfer coefficient for the finned tube banks studied can be described or correlated by the following relationship which is valid for tube banks having six rows of tubes:

$$\frac{h_o D_r}{K} = 0.364 \left(\frac{D_r G_{max}}{\mu}\right)^{0.68} \left(\frac{D_o}{D_r}\right)^{0.45} \left(\frac{Y}{D_o}\right)^{0.3} Pr^{1/3}$$

This correlation predicts air film coefficients with an average deviation of $\pm$ 7% for the experimental data.

3. The root diameter of the finned tubes is the most important single geometrical factor affecting the heat transfer to banks of finned tubes. The fin thickness and fin outside diameter are of lesser importance. The heat transfer coefficients of the finned tube banks investigated are independent of the spacing of the fins.

4. Applications of the existing heat transfer correlations available in the technical literature are generally limited to the dimensions of the tubes and tube banks used in establishing the correlations.

5. The pressure drop of the air flowing through the tube banks can be correlated by the following relationship:

$$\frac{\Delta p g_c D_{vn} \rho}{G_m^2 L} \left(\frac{\mu}{\mu_w}\right)^{0.14} = 0.81 \left(\frac{D_{vh} G}{\mu}\right)^{-0.145} \left(\frac{S_\ell}{S_t}\right)^{0.6} \left(\frac{D_{vh}}{S_t}\right)^{0.4}$$

The form of this relationship is based upon data originally obtained on banks of plain tubes. The equation predicts the pressure drop per row of tubes, within an average of $\pm 15\%$ for the experimental data.

IX. RECOMMENDATIONS FOR FUTURE WORK

The results obtained in this investigation indicate the need for additional work in two distinct areas. The first area involves the effects of the tube bank geometry on the mean heat transfer coefficients and pressure drop of the air flowing over the tubes. The second area involves a study of the local conditions on the fin surface.

The recommended heat transfer correlation presented here is an empirical relationship. Further study will be required to determine the range of tubes and tube bank arrangements over which the heat transfer correlation can be extrapolated. This study can be accomplished by investigating finned tube banks containing different tubes than those studied here. The tubes should also have different tube arrangements than reported in this investigation.

A study of the variation of the local heat transfer coefficints and temperature differences on the finned surfaces of finned tubes would be of great help in establishing the mechanisms of heat transfer. Such data would admittedly be very difficult to obtain.

APPENDICES

APPENDIX A

EXAMPLE CALCULATIONS

A. Example Calculation of the Mean Air Film Coefficient of a Finned Tube Bank.

An example calculation for Run Number 709 will be presented. The experimental data for this run is summerized in Table IV.

(1) Air Side Heat Duty

The air density of the inlet air is computed from the relationship[44]:

$$\rho_{air} = 29.2 \frac{P}{RT} \qquad (1\text{-A})$$

where: P = atmospheric pressure, atm.

T = temperature of air, °K

R = universal gas constant,[45] 1.314 atm. cu. ft./lb. mole °K

and ρ = density of dry air, lb./ft.^{3}

From Table IV

$$P = \frac{739.4}{760} = 0.972 \text{ atm.}$$

and $T = 273 + 24.2 = 297.2$ °K

Substituting these values into equation 1-A, the density is calculated as:

$$\rho_{air} = 29.2 \left(\frac{0.972}{297.2} \times 1.314\right) = 0.0726 \text{ lbs./ft.}^3$$

The absolute humidity of the air, using the wet and dry bulb temperature is[26]:

$$H' = 0.015 \text{ lbs./lb. dry air}$$

From Table V, the density correction is obtained as 0.99. The inlet air density is then:

$$\rho = 0.99\ \rho_{air} = 0.0719 \text{ lbs./ft.}^3$$

The average anemometer velocity is given in Table IV as:

$$V_{anem.} = 248 \text{ ft/min}$$

From Figure 28, the calibration correction is + 19 so that the face velocity of the inlet air is:

$$V_{face} = 248 + 19 = 267 \text{ ft/min}$$

The mass flow rate of the air is calculated from:

$$W = V_{face} \cdot \rho \cdot A_{face} \cdot 60 \qquad (2\text{-A})$$

Substituting the above values into equation 2-A the air flow rate is found to be:

$$W = (267)(0.0719)(3.375)(60) = 3880 \text{ lbs/hr}$$

The inlet air temperature is given as 24.2°C which is equivalent to 75.6°F. The mean outlet air temperature is obtained as follows:

cold junction temperature = 80°F = 1.072 mv*

average millivolt reading = 2.621

total millivolts = 3.693 mv*

the corresponding temperature is 189.5°F

The temperature rise of the air is:

$$\Delta t_{air} = 189.5 - 75.6 = 113.9°F$$

which gives a computed air side heat duty of:

$$Q_a = W\ c_p\ \Delta t_{air} = (3880)(0.245)(113.9) = 108{,}500 \text{ Btu/hr.}$$

(2) The steam side heat duty is computed from:

$$Q_s = W_s\ \Delta H \qquad (3\text{-A})$$

* referred to 32°F(46)

The change in enthalpy of the steam in condensing is[25]:

$$\Delta H = 970 \text{ Btu/lb}$$

The condensate flow rate is:

$$W_c = \frac{112}{57.5} \times 60 = 116.5 \text{ lbs/hr}$$

which yields a calculated steam side heat duty of:

$$Q_s = (116.5)(970) = 113{,}000 \text{ Btu/hr}$$

for a discrepancy of:

$$\text{discrepancy} = \frac{2(Q_s - Q_a)}{Q_s + Q_a} \times 100 = \frac{4{,}500}{110{,}700} = 4\%$$

which is within the 5% tolerance level used.

(3) Overall coefficient of heat transfer

The overall coefficient of heat transfer is computed from:

$$U_o = \frac{Q}{A \Delta T_m} \qquad (4\text{-A})$$

The rate of heat transfer given above is:

$$Q = 110{,}700 \text{ Btu/hr.}$$

The total external area for this unit from Table I is:

$$A = 265 \text{ sq. ft.}$$

The mean temperature difference driving force is computed from:

$$\Delta T_M = \frac{(\Delta t)_{air}}{\ln\left(\frac{t_s - t_i}{t_s - t_o}\right)} \qquad (5\text{-A})$$

in which: Δt_{air} = temperature rise of the air = $t_o - t_i$, °F

t_s = saturated steam temperature, °F

t_i = inlet air temperature, °F

and t_o = outlet air temperature, °F

The saturated steam temperature, obtained from the absolute steam pressure and steam tables[25] is:

$$t_s = 220.3\ ^\circ F$$

Therefore the mean temperature difference is:

$$\Delta T_M = \frac{113.9}{\ln\left(\frac{220.3 - 75.6}{220.3 - 189.5}\right)} = \frac{113.9}{1.54} = 74^\circ F$$

Substituting the above values into equation 4-A the overall coefficient is calculated as:

$$U_o = \frac{110,700}{(265)(74)} = 5.65 \text{ Btu/hr-}^\circ\text{F-sq.ft.}$$

(4) Air film coefficient and maximum air velocity

The air film heat transfer coefficient is related to the overall coefficient of heat transfer by:

$$\frac{1}{h_o} = \frac{1}{U_o} - r_f - r_m - \frac{A_o}{A_i h_i} \qquad (6\text{-A})$$

from Figure 51, for a heat duty of 110,700 But/hr, the metal and steam resistances are:

$$r_f + r_m + \frac{A_o}{A_i h_i} = 0.0115$$

Substituting these values in the above relationship, the air film resistances is computed as:

$$\frac{1}{h_o} = \frac{1}{5.65} - 0.0115 = 0.1655$$

or: $h_o = \frac{1}{0.1655} = 6.0$ Btu/hr-°F-sq.ft.

From Table I, the minimum flow area is:

$$A_{min} = 1.24 \text{ ft}^2$$

The maximum air velocity for an air density of 0.074 lbs/ft^{-3} is:

$$V_m = \frac{W}{(0.074)(60)A_{min}} = \frac{3880}{(0.074)(60)(1.24)} = 705 \text{ ft/min}$$

B. Example Calculation of Steam Condensing Coefficient

An example calculation for Run 803B is given below.

The experimental steam condensing film coefficient is calculated from the relationship:

$$h_i = \frac{U_o A_o \Delta T}{A_i \Delta t_i} = U_o\left(\frac{A_o}{A_i}\right)\frac{\Delta T_m}{\Delta T_i} \qquad (7\text{-A})$$

in which: ΔT_M = temperature difference between saturated steam and air leaving the heat exchanger, °F

the overall coefficient and temperature difference for this run are given in Table XV as:

$$U_o = 10.7 \text{ Btu/hr-°F-sq.ft.}$$

and $$\Delta T_M = 219.7 - 196.5 = 23.2 \text{ °F}$$

The ratio of outside to inside heat transfer area from Table III for this tube is:

$$A_o/A_i = 17.2$$

The temperature drop across the condensate film is given in Table XVI as: $\Delta t_i = 3.6$ °F

Substituting these values into equation 7-A, the experimental steam condensing coefficient is computed as:

$$h_i = 10.7\ (17.2)\left(\frac{23.2}{3.6}\right) = 1190 \text{ Btu/hr-°F-sq.ft.}$$

The theoretical condensing coefficient from the theory of Nusselt is obtained using equation 10-E derived in Appendix E.

$$(h_i) = 2160\ (1/\Delta t_i)^{2/9} \qquad (10\text{-E})$$

substituting for Δt_i:

$$h_i = 2160\ (1/3.6)^{2/9} = \frac{2160}{1.33} = 1620 \text{ Btu/hr-°F-sq.ft.}$$

APPENDIX B

DERIVATION OF THE FIN METAL RESISTANCE OF A FINNED TUBE

Two different fin resistances will be derived here, the first being the true fin resistance of a finned tube, and a second one, a pseudo resistance of more practical use in ordinary design procedures. The use of each in overall coefficient calculations will be illustrated.

Let the following sketch indicate the cross section of a finned tube with any given set of dimensions, D_o, D_r, N and Y. The temperature associated with the section of the tube indicated below are:

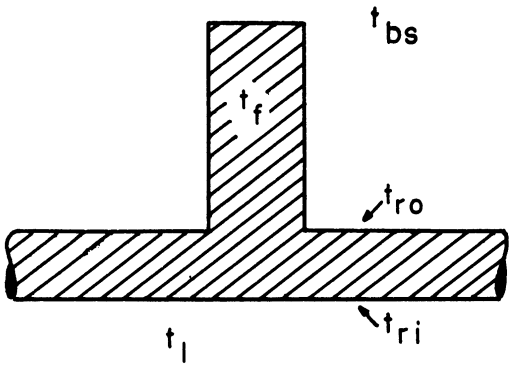

t_i = bulk stream temperature of fluid inside the tube

t_{ri} = temperature of metal on inside surface of the tube

t_{ro} = temperature of root metal on outside surface of the tube

t_f = average fin temperature

t_{bs} = bulk stream temperature of fluid outside of the tube.

A. Derivation of the True Fin Resistance of a Finned Tube

According to Newton's law of heating and cooling, the rate of heat transfer is considered to be proportional to an area through which

it is being transferred and the temperature difference driving force. The proportionality constant is considered either as a heat transfer coefficient or as the reciprocal of a heat transfer resistance. Considering the heat transferred through the finned section in the above diagram,

$$Q_f \propto A_f(t_f - t_{ro}). \tag{1-B}$$

Or, providing the proportionality constant in the form of the reciprocal of a resistance,

$$Q_f = \left(\frac{1}{r_f'}\right)(A_f)(t_f - t_{ro}) \tag{2-B}$$

In an analogous manner, the rate of heat transfer is related to the outside film resistances by:

$$Q_f = \left[\frac{1}{\frac{1}{h_o} + r_o}\right] A_f\,(t_{bs} - t_f) \tag{3-B}$$

Equating equations two and three and dividing both sides by A_f:

$$\left(\frac{1}{r_f'}\right)(t_f - t_{ro}) = \left[\frac{1}{\frac{1}{h_o} + r_o}\right](t_{bs} - t_f) \tag{4-B}$$

Solving for r_f';

$$r_f' = \left[\frac{1}{h_o} + r_o\right]\left(\frac{t_f - t_{ro}}{t_{bs} - t_f}\right) \tag{5-B}$$

or

$$r_f' = \left[\frac{1}{h_o} + r_o\right]\left[\frac{(t_{bs} - t_{ro}) - (t_{bs} - t_f)}{(t_{bs} - t_f)}\right] \tag{6-B}$$

Now defining the fin efficiency[14,17] as

$$\varphi = \left(\frac{t_{bs} - t_f}{t_{bs} - t_{ro}}\right)$$

and substituting this into equation 6-B gives,

$$r_f' = \left[\frac{1}{h_o} + r_o\right]\left[\frac{1}{\varphi} - 1\right] \qquad (7\text{-B})$$

or

$$r_f' = \left[\frac{1}{h_o} + r_o\right]\left[\frac{1 - \varphi}{\varphi}\right] \qquad (8\text{-B})$$

The above resistance can be used in the overall coefficient equation in the following manner.

The overall coefficient for the finned section is given by:

$$\frac{1}{U_f} = \frac{1}{h_o} + r_o + r_f' + \frac{XA_f}{K(A_m)_{fin}} + \frac{A_f}{(A_i)_{fin} r_i} + \frac{A_f}{(A_i)_{fin} h_i} \qquad (9\text{-B})$$

and the overall coefficient for the root section of the tube is given by:

$$\frac{1}{U_r} = \frac{1}{h_o} + r_o + \frac{XA_r}{K(A_m)_{root}} + \frac{A_r}{(A_i)_{root}} r_i + \frac{A_f}{(A_i)_{root} h_i} \qquad (10\text{-B})$$

The two overall coefficients U_f and U_r are related to the total overall coefficient by:

$$U_o A_o = U_r A_r + U_f A_f \qquad (11\text{-B})$$

B. Derivation of a Useful Pseudo Fin Resistance

The heat transferred through the exterior of the tube can be considered as the sum of that which is transferred through the finned and that which is transferred through root areas, or:

$$Q = Q_f + Q_r \qquad (12\text{-B})$$

The rate of heat transfer to the root section for a clean (unfouled) tube is also given by the expression:

$$Q_r = h_r A_r (t_{bs} - t_{ro}) \qquad (13\text{-B})$$

and correspondingly, the rate of heat transfer to the finned area is given by:

$$Q_f = h_f A_f (t_{bs} - t_f) \qquad (14\text{-B})$$

Now, defining a fin resistance in the following manner:

$$r_f = \frac{A_f(t_f - t_{ro})}{Q} \qquad (15\text{-B})$$

and substituting for Q from equations 12, 13 and 14 (and assuming $h_f = h_r = h_o$):

$$r_f = \frac{A_f\ (t_f - t_{ro})}{h_o\ [A_r(t_{bs} - t_{ro}) + A_f(t_{bs} - t_f)\ ]} \qquad (16\text{-B})$$

or

$$r_f = \frac{(t_{bs} - t_{ro}) \quad - \quad (t_{bs} - t_f)}{h_o\ [\frac{A_r}{A_f}\ (t_{bs} - t_{ro}) + (t_{bs} - t_f)\ ]} \qquad (17\text{-B})$$

The final result is obtained by dividing numerator and denominator by $(t_{bs} - t_{ro})$ and substituting for fin efficiency φ, to give:

$$r_f = (\frac{1}{h_o}) \left[\frac{1-\varphi}{\frac{A_r}{A_f} + \varphi}\right] \qquad (18\text{-B})$$

For a fouled tube the equation 18 becomes

$$r_f = \left[\frac{1}{h_o} + r_o\right] \left[\frac{1 - \varphi}{\frac{A_r}{A_f} + \varphi}\right] \qquad (19\text{-B})$$

The overall coefficient of heat transfer is given by:

$$\frac{1}{U_o} = \frac{1}{h_o} + r_o + r_f + \frac{XA_o}{KA_m} + \frac{A_o}{A_i}\ r_i + \frac{A_o}{A_i}\ \frac{1}{h_i} \qquad (20\text{-B})$$

Which is the form of the overall coefficient equation for bare tubes with the term "r_f" added.

APPENDIX C

MEASUREMENT OF DEGREE OF TURBULENCE

A. Theory

The turbulence level is a measure of the fluctuations of the velocity of a flowing stream of fluid about a mean value. Letting U, V, and W equal the mean velocities in the X,Y, and Z directions and $\overline{V}_1$, $\overline{U}_1$, and $\overline{W}_1$ the average fluctuations of the velocities denoted above (over a period of time), the turbulence number or per cent turbulence is defined as[40]:

$$\sigma = \frac{100}{V} \sqrt{\frac{\overline{V}_1^2 \quad \overline{U}_1^2 \quad \overline{W}_1^2}{3}} \qquad (1\text{-C})$$

In the main stream of a wind tunnel (outside of the boundary layer) the turbulence is generally close to isotropic,[40] i.e.:

$$\overline{V}_1^2 = \overline{U}_1^2 = \overline{W}_1^2 \qquad (2\text{-C})$$

so that equation 1-C can be reduced to,

$$\sigma = \frac{\sqrt{\overline{V}_1^2}}{V} \quad x \quad 100 \qquad (3\text{-C})$$

One novel method of measuring the turbulence level of a wind tunnel is that of the turbulence measuring sphere. This method, first suggested by Prandtl, was first studied by Dryden and Kuethe[47]. Additional studies were later made by Fage[48] and Dryden et al[49].

The turbulence measuring properties of the sphere are based on the experimentally observed fact that if the drag coefficient is plotted versus the Reynolds Number using logrithmic coordinates there occurs a smooth curve which has a sudden marked dip or decrease in the drag coefficient for Reynolds numbers in the neighborhood of 10^5. Figure 79, reproduced

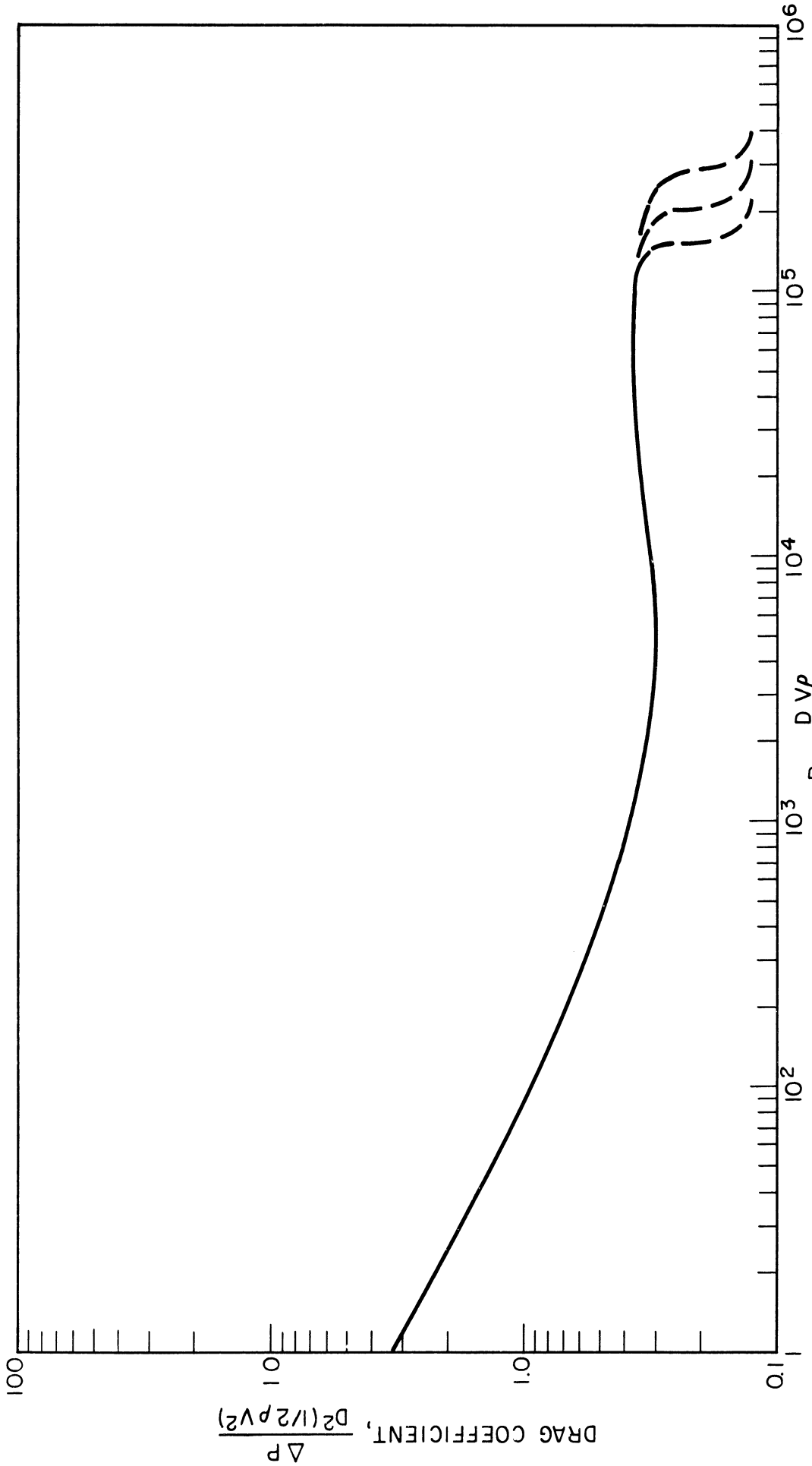

Figure 79. Drag Coefficient of Spheres as a Function of Reynolds Number.

from reference (40), indicates the shape of the curve. The dotted segments of the curve are included to indicate the fact that the Reynolds number at which the transition occurs is a function of the degree of turbulence of the fluid stream flowing around the sphere. Defining a critical Reynolds number as the Reynolds number at which the drag coefficient of a sphere equals 0.30 (the conventional friction factor has a value of 0.382, see Unit Operations[26]), the relationship between the turbulence level in a wind tunnel and the critical Reynolds number (for a 3 inch sphere is given in Figure 80.

The total drag of a sphere being difficult to measure, an alternate method of determining the critical Reynolds number has been devised[49,50]. This method uses a specially prepared sphere, generally a bowling ball, which has been standardized in the form indicated in Figure 81. It has been observed that a plot of the ratio of the pressure difference between the front and back openings on this sphere to the velocity pressure of the free stream versus the Reynolds number has the general shape indicated in Figure 82. Measurements on a number of spheres has indicated that a pressure coefficient of 1.22 is approximately equivalent to a drag coefficient of 0.3[49].

It should be mentioned here that the sphere method of measuring turbulence is not exact, the critical Reynolds number also being dependent on the scale or size of the turbulent eddies and possibly other factors which have not yet been investigated. In general, however, the degree of turbulence lies between the dotted curves indicated in Figure 80.

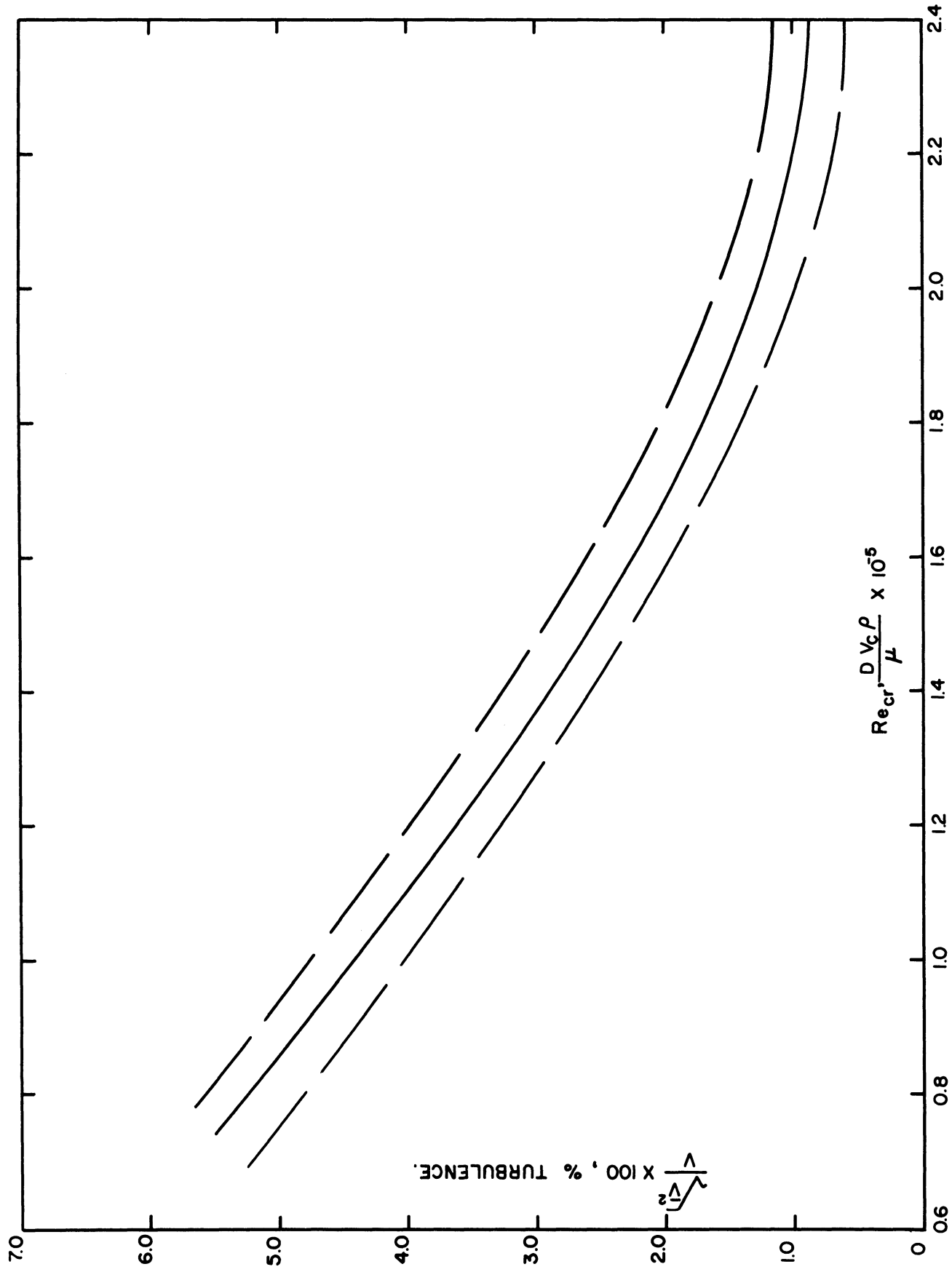

Figure 80. Per Cent Turbulence Versus Critical Reynolds Number for a 5 inch Sphere.

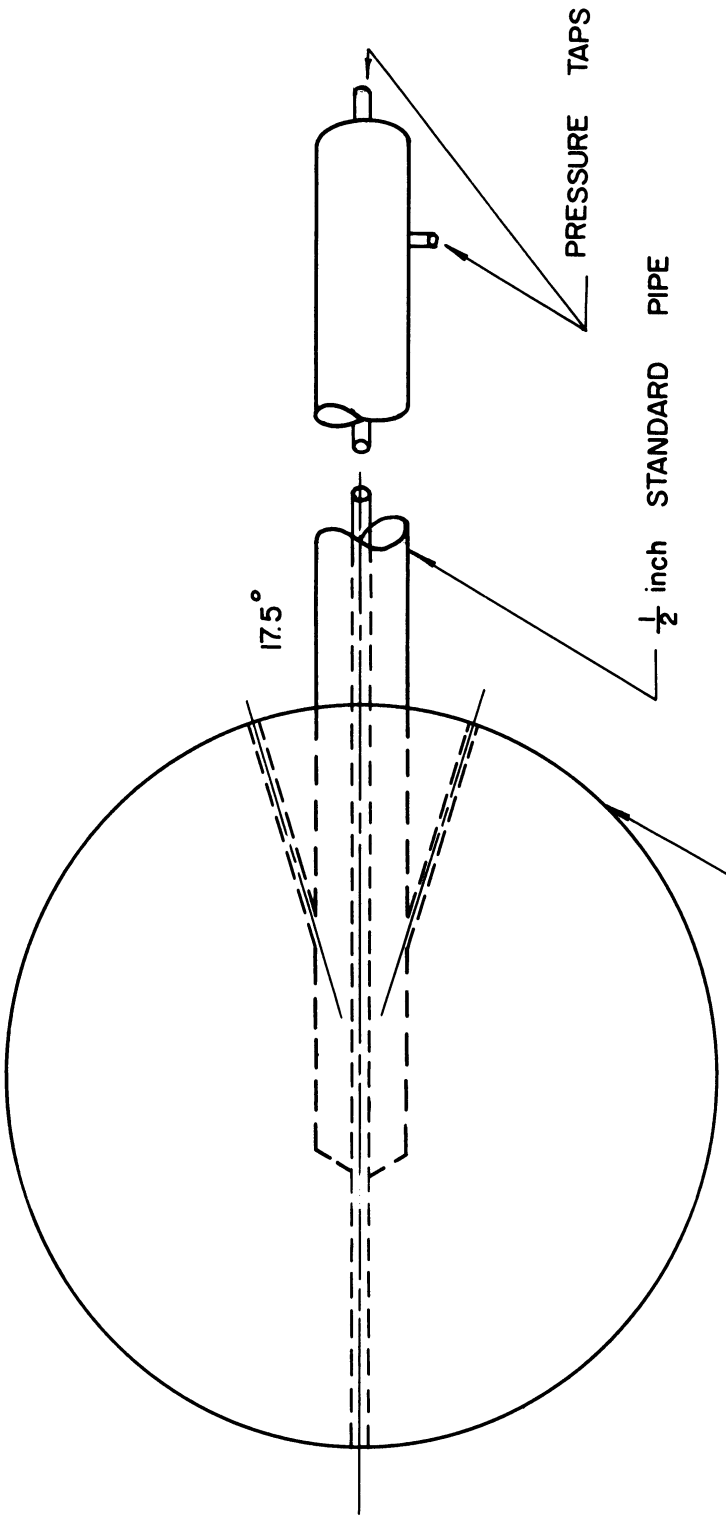

Figure 81. Details of Turbulence Measuring Sphere.

B. Apparatus

The apparatus consisted of a five inch "duck ball" prepared in the manner indicated in Figure 81. The tail spindel consisted of a standard one-half inch pipe which extended for twenty-three inches in behind the sphere. Four wires, approximately 0.06 inches in diameter were attached to the tail spindle 7 inches behind the ball and to the walls of the tunnel to provide the rigidity required.

A rectangular duct, 24 inches long with an opening of 18 by 27 inches was placed between the entrance and calming sections of the wind tunnel. The sphere was located at the center of the opening of this duct at approximately the same distance from the entrance as the tube banks.

The velocity pressure of the air was obtained by means of a pitot tube located in line with the center of the sphere and three inches from the wall of the tunnel (eight inches from the edge of the sphere).

The pressure difference on the sphere and the velocity pressure were measured with the micro-manometer previously described.

C. Experimental Data

As indicated by the experimental data, summarized in Table XXIV and Figure 82, the critical Reynolds number was not attained. This defect was due to the velocity limitations placed by the motor and blower used in this work. It was noted in the course of this investigation that for motor speeds greater than that occuring for the highest velocity reached, the air velocity would decrease rather than increase. It is therefore believed that the upper velocity attainable in this wind tunnel

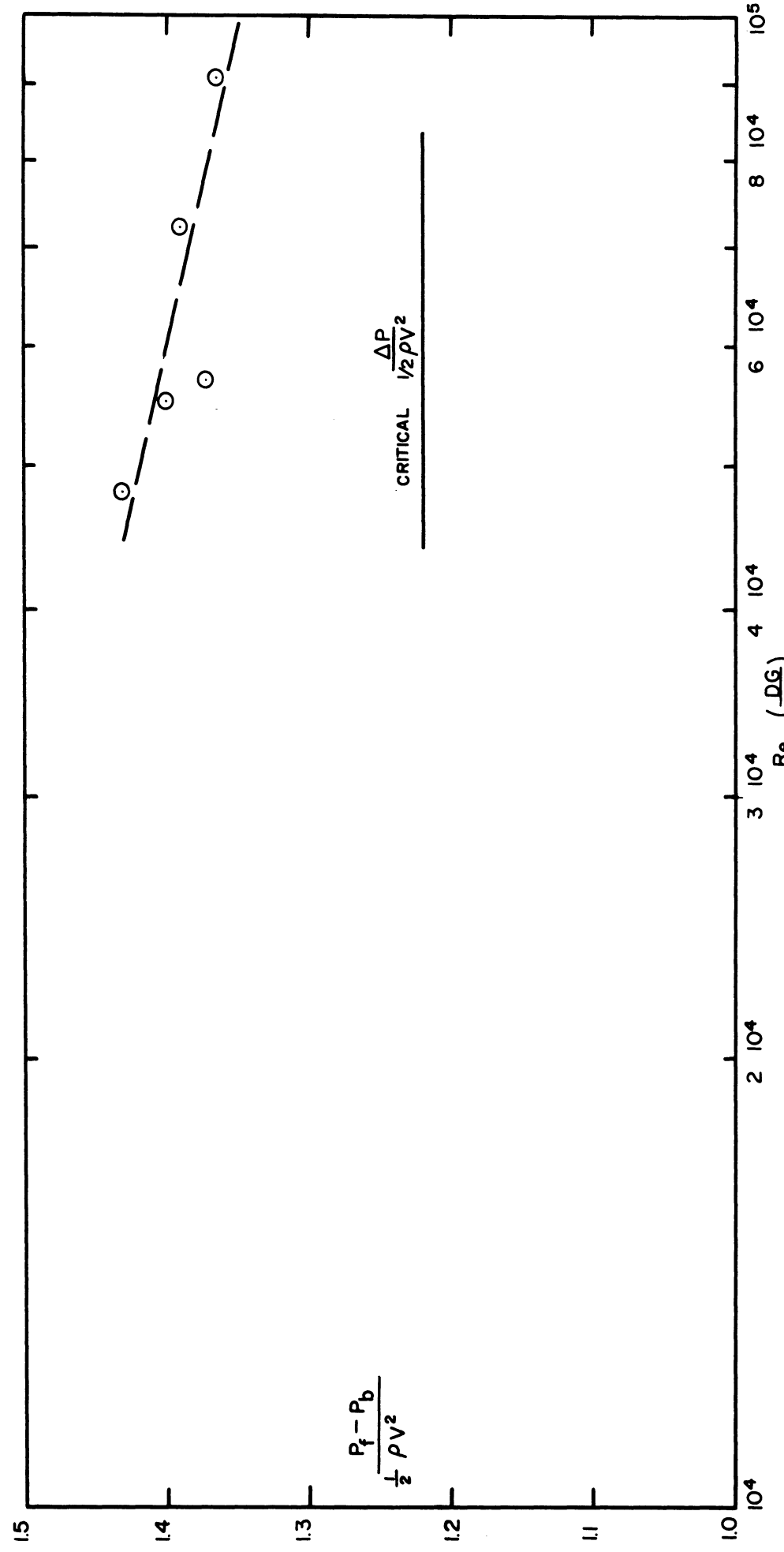

Figure 82. Experimental Pressure Ratios Versus Reynolds Number.

TABLE XXIV

SUMMARY OF AIR TURBULENCE DATA

Air Temp. = 29.9°C = 85.9°F Air Pressure = 733.7 mm Hg

Barometer Pressure = 737.5 mm Hg Wet Bulb Temperature = 79°F

Barometer Temperature = 30°C Dry Bulb Temperature = 88°F

Run	$1/2\,\rho V^2$ turns	$p_f - p_b$ in H_2O or turns	Δp in H_2O	$\sqrt{\Delta P}$	V ft/min	Re	$\frac{p_f - p_b}{1/2\,\rho V^2}$
1	4.2	6.0	0.0875	0.296	1200	48,000	1.43
2	5.48	7.67	0.114	0.338	1370	54,800	1.40
3	6.01	8.23	0.125	0.354	1440	57,600	1.37
4	14.98	20.48	0.312	0.56	2270	90.800	1.365
5	9.42	13.09	0.1962	0.444	1800	72,000	1.39

p_f = pressure of air on the front sphere

p_b = pressure of air on the back sphere

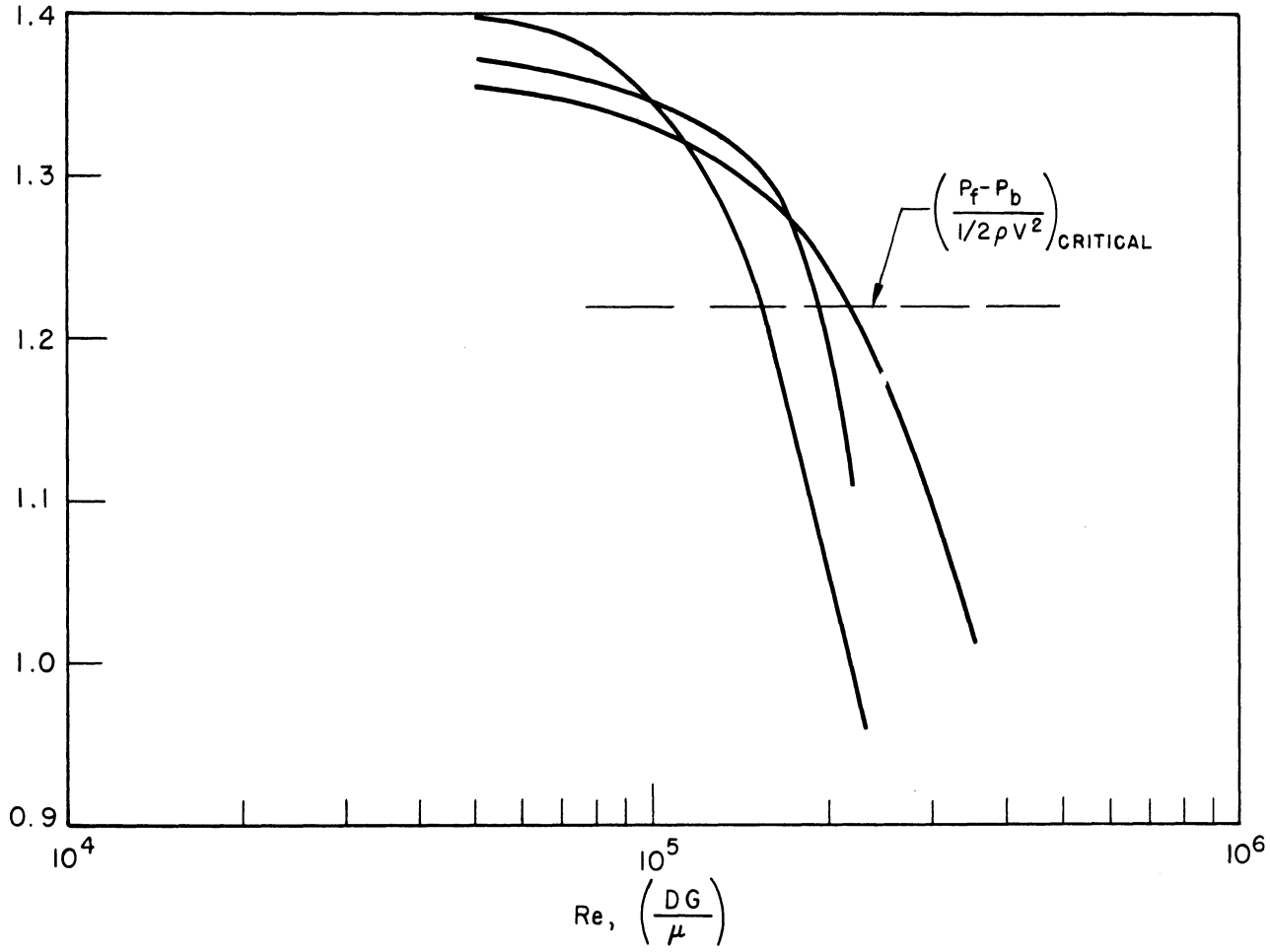

Figure 83. Typical Curves for Pressure Measuring Spheres for Three Turbulence Levels.

is limited by the blower used.

D. Analysis of Data

Due to the fact that the critical Reynolds number of the sphere was not reached, the turbulence level of the wind tunnel cannot be obtained from Figure 80. The data does allow, however, the determination of what the maximum turbulence level could be.

For a critical Reynolds number of 9.08×10^4, from Figure 80, the turbulence level is about 5% (using the solid line). Since the critical Reynolds number had not yet been reached, the turbulence level must have been below 5%.

Examination of Figure 83, however, indicates that a knee in the curve or transition starts to occur at Reynolds numbers well before the critical value. It can also be noted from this figure that the ratio of the critical Reynolds number to the Reynolds number at which the transition begins is approximately 1.8. Therefore, since (from the appearance of the curve on Figure 82) the transition had not started for the measurements given here, the critical Reynolds number for these measurements is probably greater than $1.8 \times 9.08 \times 10^4$ or 1.64×10^5. This indicates (from Figure 80) that the turbulence was probably below 2.1%.

APPENDIX D

EXAMPLE DESIGN INVOLVING AN APPLICATION OF THE CORRELATION

The following example involves the design of a forced air finned tube exchanger to cool 2000 gallons per minute of water used in the cooling jacket of a natural gas compressor from 161°F to 150°F. The heat transfer area and fan motor horsepower are required.

A. Heat Duty

The heat duty of the unit is obtained from the water-side as:

$$Q = W C_p \Delta t = 2000 \times 60 \times 8.3 \times (161 - 150)$$

$$= 10{,}950{,}000 \text{ Btu/hr.}$$

B. Design Conditions

The following design conditions will be assumed.

Air Side

Inlet air temperature	100	°F
Air velocity based on face area and density of 0.074 lbs/ft^3	600	ft/min

Water Side

Inlet water temperature	161	°F
Outlet water temperature	150	°F
Water flow rate	2000	gallons/min.

Tube and Tube Layout

Tube		
Fins/inch	10.36	fins/inch
O.D. Fins	1.958	inch
Root Diameter	1.123	inch
Fin Thickness, Y	0.021	inch
Fin Material	Aluminum	
Liner Material	Admiralty	
Liner I.D.	0.87	inches
Liner O.D.	1.00	inch

Outside area per ft. length	3.84	$ft.^2/ft.$
A_o/A_i	16.8	
Length of Tubes	24	feet

Tube Layout

Pitch Type	Equilateral Triangular	
Transverse Pitch	2.188	inches
Longitudinal Pitch (on diagonal)	2.188	inches
Number of Rows Deep	4	rows
V_{max}/V_{face}	2.52	
Number of Water Passes	2	

The determination of the required area and fan motor horsepower involve a trial and error procedure in which the required external area will first be assumed.

C. Trial Number 1

Assume an external heat transfer area of 41,400 square feet.

The number of tubes required is:

$$= \frac{41,400}{24 \times 3.84} = 448 \text{ tubes}$$

for a four row deep bank, the number of transverse rows is: $\frac{448}{4} = 112$ rows

for a total approximate width (ignoring end effects) of:

$$\text{Width} = \frac{112 \times 2.188}{12} = 20.4 \text{ ft.}$$

The total face area then is

$$A_{face} = 20.4 \times 24 = 490 \text{ sq. ft.}$$

Since a face velocity of 600 ft./min. was assumed, the flow rate of air is:

$$= 490 \times 600 = 294,000 \text{ standard cubic feet per minute}$$

or

$$W_{air} = 294,000 \times 0.074(lb/ft^3) \times 60 = 1,300,000 \text{ lbs/hr.}$$

The temperature rise of the air is computed from a heat balance as:

$$\Delta t_{air} = \frac{Q}{W_{air}(c_p)_{air}} = \frac{10,930,000}{1,300,000 \times 0.242} = 34.8°F$$

The mean temperature difference driving force between the water and the air is:

$$\Delta T_M = \frac{\Delta T_1 - \Delta T_2}{\ln \frac{\Delta T_1}{\Delta T_2}}$$

$$\Delta T_1 = 150 - 100 = 50°F$$

$$\Delta T_2 = 161 - 134.8 = 26.2°F$$

substituting

$$\Delta T_M = \frac{50 - 26.2}{\ln \frac{50}{26.2}} = \frac{23.8}{0.647} = 36.8°F$$

The correction to the logarithmic mean temperature difference is negligible[51].

To check the assumed area of 41,400 square feet, the area required will be calculated from $A = \frac{Q}{U_o \Delta T_M}$. The total resistance to heat transfer for a bimetallic tube is equal to the sum of the individual resistances or:

$$\frac{1}{U_o} = \frac{1}{h_o} + r_o + r_f + (r_m)_{al} + r_b \frac{A_o}{A_b} + (r_m)_{adm} + r_i \frac{A_o}{A_i} + \frac{A_o}{A_i h_i}$$

in which: U_o = overall coefficient of heat transfer

h_o = air film heat transfer coefficient

r_o = outside fouling resistance

r_f = fin resistance to heat transfer

$(r_m)_{al}$ = aluminum root resistance to heat transfer $= \frac{X_{al} A_o}{k_{al} (A_m)_{root}}$

where: X_{al} = root wall thickness

k_{al} = aluminum thermal conductivity

A_o = outside heat transfer area

$(A_m)_{root}$ = mean root metal heat transfer area

r_b = contact resistance between the root of the aluminum and the outside of the admiralty liner

A_o = outside heat transfer area per foot length

A_b = heat transfer area of bond

$(r_m)_{adm}$ = admiralty liner resistance to heat transfer = $\frac{X_{adm}\, A_o}{k_{adm}(A_m)_{adm}}$ [see $(r_m)_{al}$]

r_i = inside fouling resistance

A_i = inside heat transfer area per foot length

and h_i = inside water film coefficient

The individual heat transfer resistances are obtained as:

1. Air Film Resistance

The air film coefficient can be calculated from the dimensionless relationship:

$$\frac{h_o D_r}{k} = 0.364 \left(\frac{D_r G_{max}}{\mu}\right)^{0.68} \left(\frac{Y}{D_o}\right)^{0.3} \left(\frac{D_o}{D_r}\right)^{0.45} Pr^{1/3}$$

For the tube bank under consideration:

$$\left(\frac{Y}{D_o}\right)^{0.3} = \left(\frac{0.021}{1.958}\right)^{0.3} = (0.01072)^{0.3} = 0.256$$

$$\left(\frac{D_o}{D_r}\right)^{0.45} = \left(\frac{1.958}{1.123}\right)^{0.45} = (1.74)^{0.45} = 1.283$$

and $Pr^{1/3} = 0.89$

The Reynolds number is calculated as:

$$V_m = V_{face} \frac{A_f}{A_{min}} = (600)(2.52) = 1510 \text{ ft/min.}$$

$$G_{max} = V_m \cdot \rho \cdot 60 = (1510)(0.074)(60) = 6700 \frac{lb}{ft^2 hr}$$

μ = 0.0465 at 117.4 °F(20)

$$Re^{0.68} = \left(\frac{D_r G_{max}}{\mu}\right)^{0.68} = \left(\frac{1.123 \times 6700}{12 \times 0.0465}\right)^{0.68} = (13{,}500)^{0.68} = 640$$

therefore:

$$\frac{h_o D_r}{k} = 0.364\ (640)(0.256)(1.283)(0.89)$$

$$= 68.1$$

since $k_{air} = 0.015$ at 117.4 °F[20]

$$h_o = 10.8 \text{ Btu/hr-°F-sq.ft.}$$

which is the mean air film coefficient for a six row deep bank of finned tubes.

The mean air film coefficient for a four row deep bank is calculated using Equation 62 and Figure 41.

$$(h_o)_{m4} = (h_o)_{m6} \frac{(h_o)_{m\infty}}{(h_o)_{m6}} \frac{(h_o)_{m4}}{(h_o)_{m\infty}}$$

From Figure 41,

$$\frac{(h_o)_{m6}}{(h_o)_{m\infty}} = 0.936$$

and

$$\frac{(h_o)_{m4}}{(h_o)_{m\infty}} = .906$$

substituting:

$$(h_o)_{m4} = (10.8)\left(\frac{0.906}{0.936}\right) = 10.4$$

2. Outside Fouling Resistance

The outside fouling resistance is assumed negligible.

3. Fin Resistance Using Equation 24.

In the text, the fin resistance is computed as[17]:

$$r_f = \frac{\frac{2\,H^2}{3\,k_{al}\,Y}\sqrt{\frac{D_o}{D_r}}}{1 + \frac{A_r}{A_f}\left[1 + \frac{h_o \cdot 2H^2}{3\,k_{al}Y}\sqrt{\frac{D_o}{D_r}}\right]}$$

Letting

$$r_f' = \frac{2\,H^2}{3\,k_{al}\,Y}\sqrt{D_o/D_r}$$

(see Appendix B)

Then

$$r_f = \frac{r_f'}{1 + \frac{A_r}{A_f}\left[1 + h_o\, r_f'\right]}$$

Now;

$$H^2 = \left(\frac{0.418}{12}\right)^2 = 0.00122 \text{ ft}^2$$

$$k_{al} = 120 \text{ Btu/hr-°F-ft}$$

$$Y = \frac{0.021}{12} = 0.00175 \text{ ft}$$

$$\sqrt{D_o/D_r} = \left(\frac{1.958}{1.123}\right)^{1/2} = 1.32$$

Substituting into r_f'

$$r_f' = \frac{2 \times 0.00122 \times 1.32}{3 \times 120 \times 0.00175} = 0.0051$$

Now,

$$\frac{A_r}{A_f} = \frac{0.23}{3.61} = 0.064$$

and $h_o = 10.1$

subsituting into r_f:

$$r_f = \frac{0.0051}{1 + 0.064\,[1 + 0.0039 \times 10.1\,]} = \frac{0.0051}{1.066} \cong 0.0048$$

4. Aluminum Metal Resistance

$$(r_m)_{al} = \frac{X_{al}\, A_o}{k_{al}(A_m)_{al}}$$

For the tube under consideration:

$X_{al} = \frac{1.123 - 1.000}{2 \times 12} = 0.0051$ ft.

$A_o = 3.84$ sq.ft./ft.

$k_{al} = 120$ Btu/hr-°F-ft

$(A_m)_{al} = 0.278$ sq.ft./ft.

substituting

$$(r_m)_{al} = 0.00058$$

5. Bond Resistance

The bond resistance of this type of tube is of the order of 0.0005 or less[52]. The area of the bond is:

$$A_b = \pi D_{bond} = \frac{\pi}{12}(1) = 0.262 \text{ sq.ft./ft}$$

$$\therefore r_b \frac{A_o}{A_b} = 0.0005 \times \frac{3.84}{0.262} = 0.0073$$

6. Admiralty Metal Resistance

$$(r_m)_{adm} = \frac{X_{adm}\, A_o}{k_{adm}(A_m)_{adm}}$$

For the tube under consideration:

$X_{adm} = \frac{1.00 - 0.87}{2 \times 12} = 0.0054$ ft.

$A_o = 3.84$ sq.ft./ft

$k_{adm} = 64$ Btu/hr-°F-ft

substituting:

$$(r_m)_{adm} = 0.00132$$

7. Inside Fouling Resistance

The inside fouling resistance from T.E.M.A.[53] is

$$r_i = 0.001$$

or

$$r_i \frac{A_o}{A_i} = 0.001 \times 16.8 = 0.0168$$

8. Inside Water Coefficient

The inside coefficient can be predicted from the following dimensional relationship recommended by McAdams[20]:

$$h_i = 150\ (1 + 0.011\ t_w)\frac{V_t^{0.8}}{d_i^{0.2}}$$

in which: V_t = velocity of the water in the tubes, ft./sec.

t_w = average water temperature, °F

and d_i = inside diameter of the tube, inches

$$(d_i)^{0.2} = (0.87)^{0.2} = 0.973$$

$$(1 + 0.011\ t_w) = 1 + 0.011 \times 155.5 = 2.7$$

Using two passes on the water side:

$$V_t = \frac{2000 \times 8.3}{62.4 \times 60 \times 224 \times 0.0042} = 4.72 \text{ ft/min}$$

or: $V_t^{0.8} = (4.72)^{0.8} = 3.46$

substituting: $h_i = \frac{150 \times 2.7 \times 3.46}{0.973} = 1440$

or: $\frac{A_o}{A_i h_i} = \frac{16.8}{1440} = 0.0117$

The overall resistance to heat transfer is equal to the sum of the individual resistances given in sections 1 through 8 or:

$$\frac{1}{U_o} = 0.0961 + 0.0048 + 0.00058 + 0.0073 + 0.00132$$
$$+ 0.0168 + 0.0117 = 0.1386$$

or: $U_o = 1/\ 0.1386 = 7.2$

The required heat transfer area is:

$$A = \frac{Q}{U\Delta T_M} = \frac{10,950,000}{7.20 \times 36.8} = 41,300 \text{ sq.ft.}$$

which checks closely the assumed value of 41,400 sq.ft. Therefore no further trials will be required.

D. Pressure Drop and Fan Horsepower Requirements

The pressure drop per row of tubes of the air can be obtained directly from Figure 71 in the text as (for a $V_m = 1510$)

$$\frac{\Delta p}{n} = 0.16 \text{ inches of water/row}$$

for a four row deep bank:

$$\Delta p = 0.64 \text{ inches of water}$$

the required theoretical horsepower for air near atmospheric conditions is given by:

$$(H.P.)_T = W \times \Delta p \times M$$

where: $(H.P.)_T$ = theoretical horsepower required

W = lbs/hr of air

Δp = inches of water pressure drop

and M = conversion factor $= 3.5 \times 10^{-5} \ \frac{\text{H.P. - hour}}{\text{inches}_{H_2O}\ \text{lb}_M}$

The lbs/hr of air (given earlier) is:

$$W = 1.3 \times 10^6 \text{ lbs/hr.}$$

substituting

$$(H.P.)_T = (0.64)(1.3 \times 10^6)(3.5 \times 10^{-5}) = 29.2 \text{ H.P.}$$

Assuming a fan efficiency of 65% and a motor and gear box efficiency of 85%, the motor size is:

$$(H.P.)_{required} = \frac{29.2}{0.65 \times 0.85} = 53 \text{ horsepower.}$$

The unit designed above is of course not necessarily the optimum unit for this service. The selection of the optimum unit would involve designing a number of units varying: the number of rows deep, the air velocity, the tube pitch, and tube selected.

APPENDIX E

DERIVATION OF AN EQUATION TO PREDICT POINT CONDENSING COEFFICIENTS USING THEORY OF NUSSELT

The condensing coefficient at a point is defined as[20]:

$$(h_i)_p = \frac{k_f}{y} \qquad (1\text{-E})$$

in which: k_f = thermal conductivity of liquid film

and y = thickness of liquid film at point

but, from Nusselt's theory[20],

$$y^3 = \frac{3\,\Gamma_Z\,\mu_f}{\rho_f^2\,g_c} \qquad (2\text{-E})$$

where: $\Gamma_Z = W_Z/\pi D_i$

W_Z = lbs/hr of condensate flowing at point Z

and Z denotes the vertical distance down the tube, ft.

but, $$W_Z = \int_0^Z \frac{(h_i)_p\,\Delta t\,dA}{\lambda} \qquad (3\text{-E})$$

Assuming a constant heat flux to the tube inside surface and integrating equation 3-E:

$$W_Z = \frac{h_m\,\Delta t A}{\lambda} = \frac{h_m\,\Delta t \pi\,D_i Z}{\lambda} \qquad (4\text{-E})$$

where: h_m = the mean condensing coefficient from the top of the tube to the point Z.

Substituting from equations I-E and 4-E into equation 2-E yields:

$$\frac{k_f^3}{(h_i)_p^3} = \frac{3\mu_f h_m \Delta t\ \pi D_i\ Z}{\lambda \rho_f^2\ g_c \pi\ D_i} = \frac{3\mu_f h_m \Delta t\ Z}{p_f^2 g_c\ \lambda} \qquad (5\text{-E})$$

Simplifying equation 5-E gives:

$$(h_i)_p = \left(\frac{1}{3}\right)^{1/3} \left[\frac{k_f^3 \rho_f^2 g_c \lambda}{\mu_f}\right]^{1/3} Z^{1/3} \left(\frac{1}{h_m}\right)^{1/3} \left(\frac{1}{\Delta t}\right)^{1/3} \quad (6\text{-E})$$

For steam condensing near atmospheric pressure, McAdams[20] recommends the following relationship for the mean coefficient:

$$h_m = \frac{4000}{Z^{1/4} \Delta t^{1/3}} \quad (7\text{-E})$$

Substituting this into equation 6-E yields:

$$(h_i)_p = \left(\frac{1}{3}\right)^{1/3} \left[\frac{k_f^3 \rho_f^2 g_c \lambda}{\mu_f}\right]^{1/3} Z^{1/3} \left(\frac{Z^{1/4} \Delta t^{1/3}}{4000}\right)^{1/3} \left(\frac{1}{\Delta t}\right)^{1/3} \quad (8\text{-E})$$

$$= \left(\frac{1}{3}\right)^{1/3} \left[\frac{k_f^3 \rho_f^2 g_c \lambda}{\mu_f}\right]^{1/3} \frac{Z^{5/12}}{4000^{1/3}} \left(\frac{1}{\Delta t}\right)^{2/9} \quad (9\text{-E})$$

But for steam near atmospheric pressure[20]:

$$\left[\frac{k_f^3 \rho_f^2 g_c}{\mu_f}\right]^{1/3} = 5000$$

and $\lambda^{1/3} = 9.9$

For the particular installation under consideration, Z = 1.0 ft. Assuming that the point temperature difference measured at z is approximately equal to the mean temperature difference and substituting the above values into equation 9-E

$$(h_i)_p = 2160 \left(\frac{1}{\Delta t_i}\right)^{2/9} \quad (10\text{-E})$$

which is the equation of the line shown in Figure 35.

REFERENCES

1. Gupta, R. K., "Use of Flow Paterns in Predicting Shell Side Heat Transfer Coefficients for Baffled Shell and Tube Exchangers", Ph.D. Thesis, University of Michigan, September, 1956.

2. Schmidt, T. E., "Heat Transmission and Pressure Drop in Banks of Finned Tubes and in Laminated Coolers", Institute of Mechanical Engineering and A.S.M.E., Proc. of the General Discussion on Heat Transfer, Section II, 186-8, London, 1951.

3. Katz, D. L., Young, E. H., Williams, R. B. and Balekjian, G., "How to Design Finned Coils For Cooling" Petroleum Refiner, Vol. 33, No. 11, 1954.

4. Jameson, S. L., "Tube Spacing in Finned Tube Banks", Trans. A.S.M.E. 67, 633-42, 1945.

5. Katz, D. L. and Beatty, K. O. Jr. and Foust, A. S., "Heat Transfer Through Tubes With Integral Spiral Fins", Trans. A.S.M.E., 67, 665-74, 1945.

6. London, A. L., Kays, W. M., and Johnson, D. W., "Heat Transfer and Flow Friction Characteristics of Some Compact Heat Exchanger Surfaces, Part III - Design Data For Five Surfaces", Trans. A.S.M.E. 74, 1167-78, 1952.

7. Katz, D. L. and et al., "Correlation of Heat Transfer and Pressure Drop for Air Flowing Across Banks of Finned Tubes", Project 1592, Report No. 30, University of Michigan Engineering Research Institute, December, 1954.

8. Parsons, S. R. and Harper, D. R., "Radiators for Aircraft Engines", U.S. Bureau of Standards, Technical Paper No. 211, 1922, pp 327-330.

9. Harper, D. R. and Brown, W. B., N.A.C.A., Report No. 158, 1922.

10. Schmidt, T. E., "Die Warmeubertrugung durch Rippen", Zeit V.D.I., Vol. 70, 885-889 and 947-951, 1926.

11. Murray, W. M., "Heat Dissipation Through an Annular Disk or Fin of Uniform Thickness", Journal of Applied Mechanics, Trans. A.S.M.E. Vol. 60, pg. A-78, 1938.

12. Avrami, M. and Little, J. B., "Diffusion of Heat Through a Rectangular Bar and the Cooling and Insulating Effect of Fins, I The Steady State", Journal of Applied Physics, Vol. 13, pp. 255-264, 1942.

13. Carrier, W. H. and Anderson, S. W., "The Resistance to Heat Flow Through Finned Tubing" Heating, Piping, and Air Conditioning, Vol. 10, pp 304-320, 1944.

14. Gardner, K. A., "Efficiency of Extended Surface", Trans. A.S.M.E. Vol. 67, 621-631, 1945.

15. Kayan, C. F., "Fin Heat Transfer by Geometrical Electrical Analogy" Ind. Eng. Chem., 40, pp. 1044-49, 1948.

16. Dusinberre, G. M., "Fin Efficiency", Mechanical Engineering, 570, 1957.

17. Young, E. H. and Ward, D. J., "Fundamentals of Finned Tube Heat Transfer", Refining Engineer, Vol. 29, No. 11, October, 1957.

18. Ghai, M. L., "Heat Transfer in Straight Fins", Institute of Mechanical Engineering and A.S.M.E., Proc. of the General Discussion on Heat Transfer, Section II, 180-2, London, 1951.

19. Weiner, J. H., Gross, D. and Paschkis, V., "An Experimental Determination of Local Boundary Conductances For An Unbaffled Circular Finned Cylinder", Institute of Mechanical Engineering and A.S.M.E. Proc. of the General Discussion on Heat Transfer, Section II, 154-9, London, 1951.

20. McAdams, W. H., "Heat Transmission", McGraw-Hill Book Co., 3rd ed. 1954.

21. Gunter, A. Y. and Shaw, W. A., "General Correlation of Friction Factors for Surfaces in Crossflow", Trans. A.S.M.E., 67, 644-660.

22. Lange, N. A., Handbook of Chemistry, Handbook Publishing Co., Sandusky, Ohio, 1952.

23. Ower, E., Measurement of Air Flow, London; Chapman and Hall, Ltd., 1927.

24. Perry, J. H., Chemical Engineers' Handbook, pp. 398-9, 3rd ed., McGraw Hill Book Co. Inc., N.Y., 1950.

25. Keenan, J. H. and Keyes, F. G., Thermodynamic Properties of Steam, 1st ed., John Wiley and Sons, Inc., N.Y., 1952.

26. Brown, G. G. and associates, Unit Operations, John Wiley and Sons, Inc., pg. 76, 1951.

27. Kays, W. M., London, A. L. and Lo, R. K., " Heat Transfer and Friction Characteristics for Gas Flow Normal to Tube Banks - Use of a Transient - Test Technique" Trans. A.S.M.E., Vol. 76, pp. 387-96, 1954.

28. Comings, E. W., Chapp, J. T. and Taylor, J. F., "Air Turbulence and Transfer Processes; Flow Normal to Cylinders", Ind. and Eng. Chem., 40; 1076-82, June 1948.

29. Grimison, E. D., "Correlation and Utilization of New Data on Flow Resistance and Heat Transfer for Cross Flow of Gases Over Tube Banks", Trans. A.S.M.E., 59, 583-94, 1937 60,381-92, 1938.

30. Huge, E. C., "Experimental Investigation of Effects of Equipment Size on Convection Heat Transfer and Flow Resistance in Cross Flow of Gases Over Tube Banks," Trans. A.S.M.E., 59, 573-81, 1937.

31. Pierson, O. L., "Experimental Investigation of the Influence of Tube Arrangement on Convection Heat Transfer and Flow Resistance in Cross Flow of Gases Over Tube Banks," Trans. A.S.M.E., 59, 563-72, 1937.

32. Wagener, G., "Die Warmeuebergang an Kuhlrippen", Beihefte zum Gesundhuts Ingeniear, Reihe I, Heft 24, 1929.

33. Streeter, V. L., Fluid Dynamics, McGraw Hill Book Company, Inc. N. Y., 1952.

34. Berry, V. J., Mason, D. M. and Sage, B. H., "Temperature and Velocity Distribution in Wake of a Heated Cylinder," Chem. Engr. Prog., Symposium Series No. 5, Vol. 49, 1953.

35. Billman, G. W., Mason, D. M. and Sage, B. H., "Temperature and Velocity Distribution in Wake of a Heated Cylinder," Part I, Chem. Engr. Prog., Vol. 46, No. 12, Pg. 625-34.

36. Lemmon, A. W. Jr., Colburn, A. P. and Nottage, H. B., "Heat Transfer from a Baffled-Finned Cylinder to Air," Trans. A.S.M.E., 67, 601-12, 1945.

37. McAdams, W. H., Drexel, R. E. and Goldey, R. H., "Local Coefficients of Heat Transfer for Air Flowing Around a Finned Cylinder," Trans. A.S.M.E., 67, 613-20, 1945.

38. Knudsen, J. G. and Katz, D. L., Fluid Dynamics and Heat Transfer, Engineering Research Institute, University of Michigan, 1954.

39. Colburn, A. P., "A Method of Correlating Forced Convection Heat Transfer Data and a Comparison With Fluid Friction," Trans. A.I. Ch.E., 29, 174, 1933.

40. Kuethe, A. M. and Schetzer, J. D., Foundations of Aerodynamics, John Wiley and Sons, Pg. 290, 1950.

41. Statistical Research Lab., "University of Michigan, IBM 650 Regression Analysis Program."

42. Wall, J. R., Private Communications.

43. Aerofin Bulletin No. 0-53, Aerofin Corp., Syracuse 1, N. Y.

44. Dodge, B. F., Chemical Engineering Thermodynamics, McGraw Hill Book Co., N. Y., 1944.

45. Maxwell, J. B., Data Book on Hydrocarbons, D. VanNostrand Company Inc., N. Y., Pg. 137, 1950.

46. Wood, W. P. and Cook, J. M., Pyrometry, Pg. 254, McGraw Hill Book Co., N.Y., 1941.

47. Dryden, H. L. and Kuethe, A. M., "Effect of Turbulence in Wind Tunnel Measurements", N.A.C.A. Report No. 342, 1929.

48. Fage, A., "Experiments on a Sphere at Critical Reynolds Numbers", ARC Tech. Report 1776, 1937.

49. Dryden, H. L. and Schubauer, G. B., Mock, W. C. Jr. and Skramstad, H. K., "Measurement of Intensity and Scale of Wind Tunnel Turbulence and Their Relation to the Critical Reynolds Number of Spheres," N.A.C.A. Report No. 581, 1937.

50. Pope, A., Wind Tunnel Testing, Pgs. 105-108, 2nd ed., John Wiley and Sons, 1954.

51. Kern, D. Q., Process Heat Transfer, McGraw Hill Book Co, N. Y., 1st ed., 1950.

52. Young, E. H., Wall, J. R., Fleming, J. R. and Conroy, W. F., "Development of an Apparatus for the Measurement of Low Bond Resistances in Finned and Bare Duplex Tubes," University of Michigan, Engineering Research Institute Project 1592, Report No. 48, August, 1957.

53. Standards of the Tubular Exchanger Manufacturers Association, 3rd ed. TEMA, New York, 1952.